UCRL-MI-231267

IFE Science and Technology Strategic Planning Workshop - Part 5: Posters

To select an individual poster, click the table of contents entry on the next page (using the Hand Tool icon).

To save only a portion of this document, go to File/Print, select Adobe PDF as your printer, specify the desired range of pages, and save to a new file name.

Portions of this work performed under the auspices of the U. S. Department of Energy by University of California Lawrence Livermore National Laboratory under Contract W-7405-Eng-48.

Part 5 Contents

Posters

Layering Methods for Inertial Fusion Targets

Neil B. Alexander, D.T. Goodin, A.S. Bozek, D.T. Frey, K. J. Boehm

Inaugural IFE Science and Technology Strategic Planning Workshop:

Updates on Progress, Visions, and Near-Term Opportunities

San Ramon, CA
April 24-27, 2007

Work supported by Naval Research Laboratory thru contract N00173-06-C-60052 GENERAL ATOMICS

GA is developing Cryogenic Fluidized Beds for mass production of the fuel layering in IFE targets

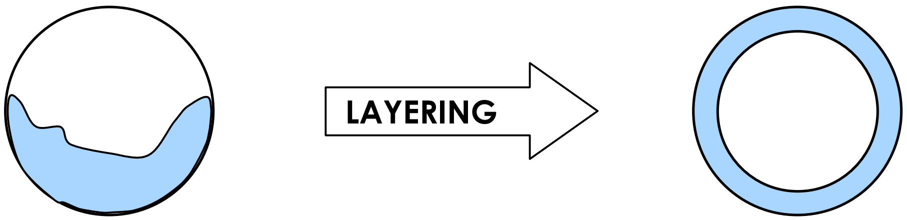

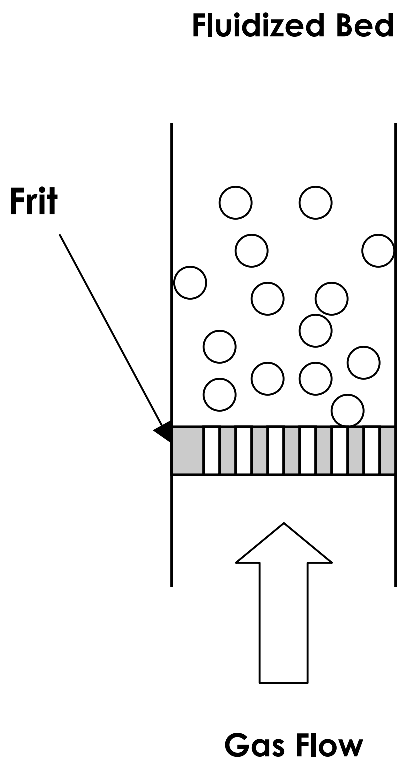

<u>Mass production layering must:</u>

- **Be reasonably fast**
- **Preserve other target properties**
  - Surface roughness
- **Be scalable to factory size**

In DT fuel layering, fuel moves until inner surface is isothermal

- **DT internal heating by betas allows sublimation until isothermal conditioı is reached**
  - Thicker layers hotter
  - Layering time is many hours
- **For D2 add heat to layer**
  - Infrared (IR) light, or other
- **Standard ICF method of holding targeı at center of isothermal cavity is inconvenient for IFE**
  - Too many cavities,
  - Too much precision centering

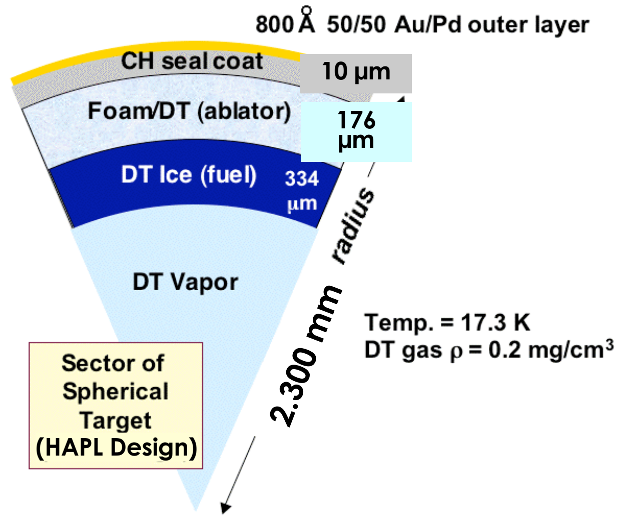

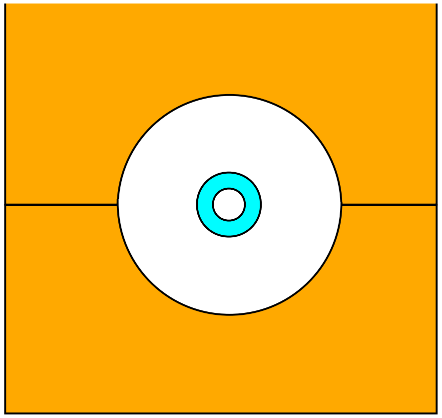

Fluidized beds scale well for IFE power plant

Portion of overall production plant conceptual layout

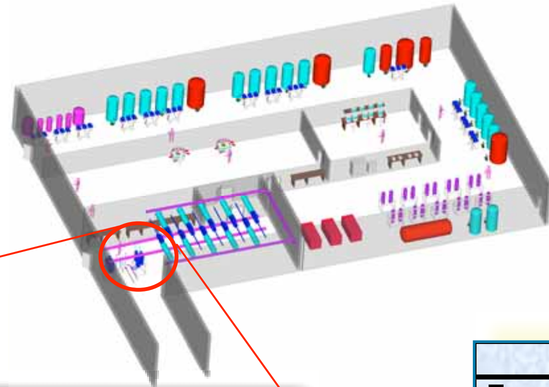

Approximately 100’ x 160’ facility for 1000 MW(e) plant

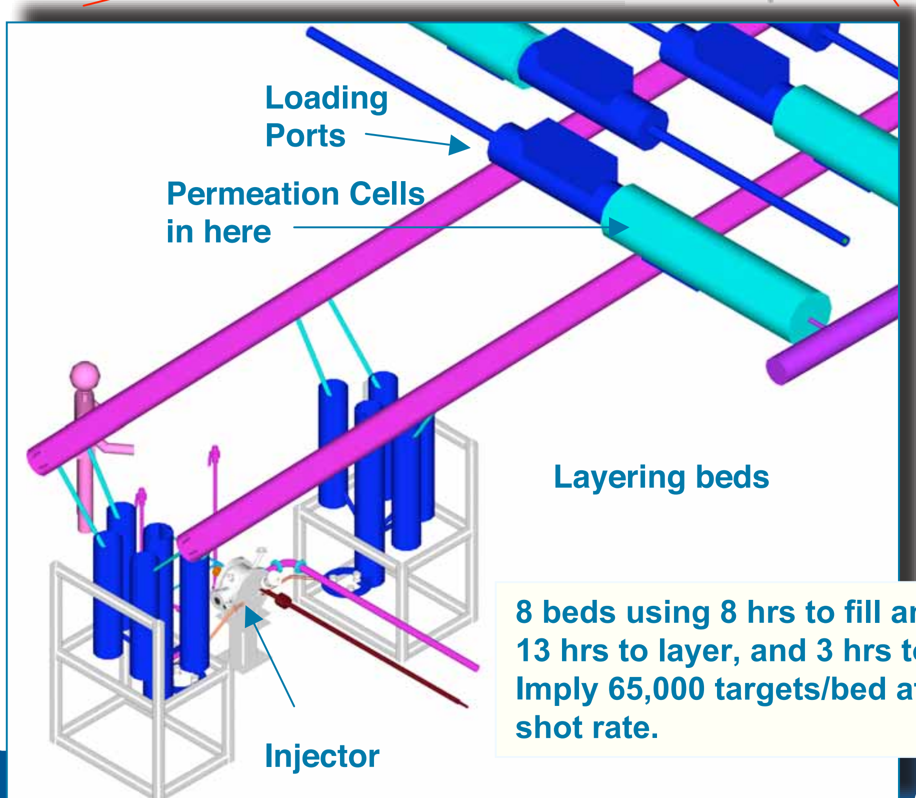

8 beds using 8 hrs to fill and cool, 13 hrs to layer, and 3 hrs to unload, Imply 65,000 targets/bed at 6 Hz shot rate.

Layering System Design Data

	Case A	Case B
Targets per bed	65,000	65,000
Diameter bed	200 mm	320 mm
Bed height, settled	112 mm	44 mm
Bed expansion	2	2
Bed height, operational	224 mm	88 mm
Operating temperature	18 to 19.7 K	18 to 19.6 K
Levitating fluid	Helium	Helium
Pressure of levitating fluid	380 torr	380 torr
Mass flow	55 gm/sec	140 gm/sec
Velocity of fluid	133 cm/sec	133 cm/sec
Pressure drop across bed	0.66 torr	0.26 torr
ΔT across bed (1 Q_{DT}; native betalayering)	0.134 K	0.054 K
Minumum fluidization velocity (U_{mf})	36 cm/sec	36 cm/sec
Ave. particle circulation time	0.70 sec	0.27 sec
Temperature change with time at inner surface of DT ice	<0.1 K	<0.003 K

Target motion in the cryogenic fluidized bed provides a time-averaged isothermal environment for uniform layers

- **Particles (targets) levitated by a gas stream**
- **Beta heat from DT causes temperature gradient in bed (69 mK nominal conditions)**
  - A de-layering influence
- **Random circulation and rotation eliminates effects of temperature gradient**

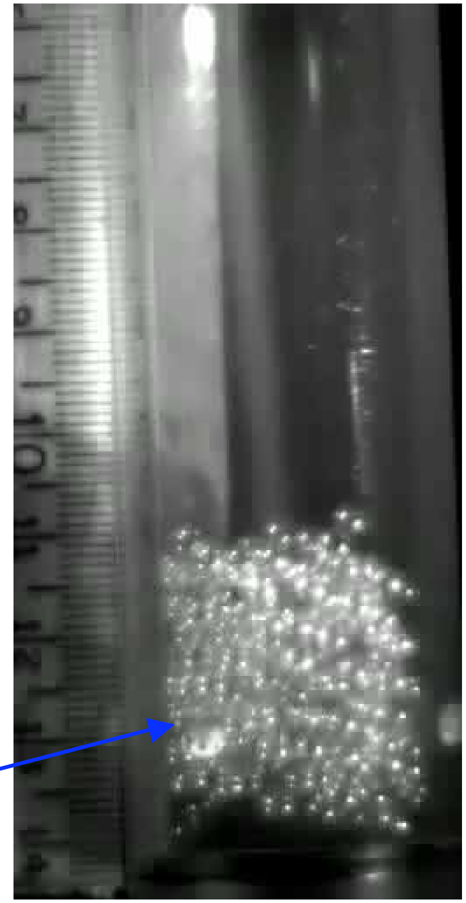

Fluidized Bed with Bed Expansion =2

Hotter

Cooler

When Beta-layering

Frit

Gas flow

Here: 1 atm N_2 at RT
Cryo: 0.5 atm He at 18K

Neopentyl alcohol as room temperature surrogate for DT

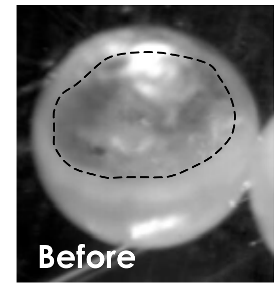

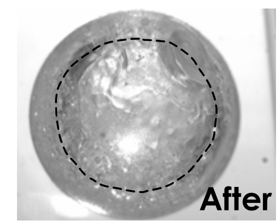

For uniform layers we want a small temperature gradient (ΔT) from bottom to top of bed

Baseline Operating Point:
0.5 atm,
χ=2,
ΔT=69 mK

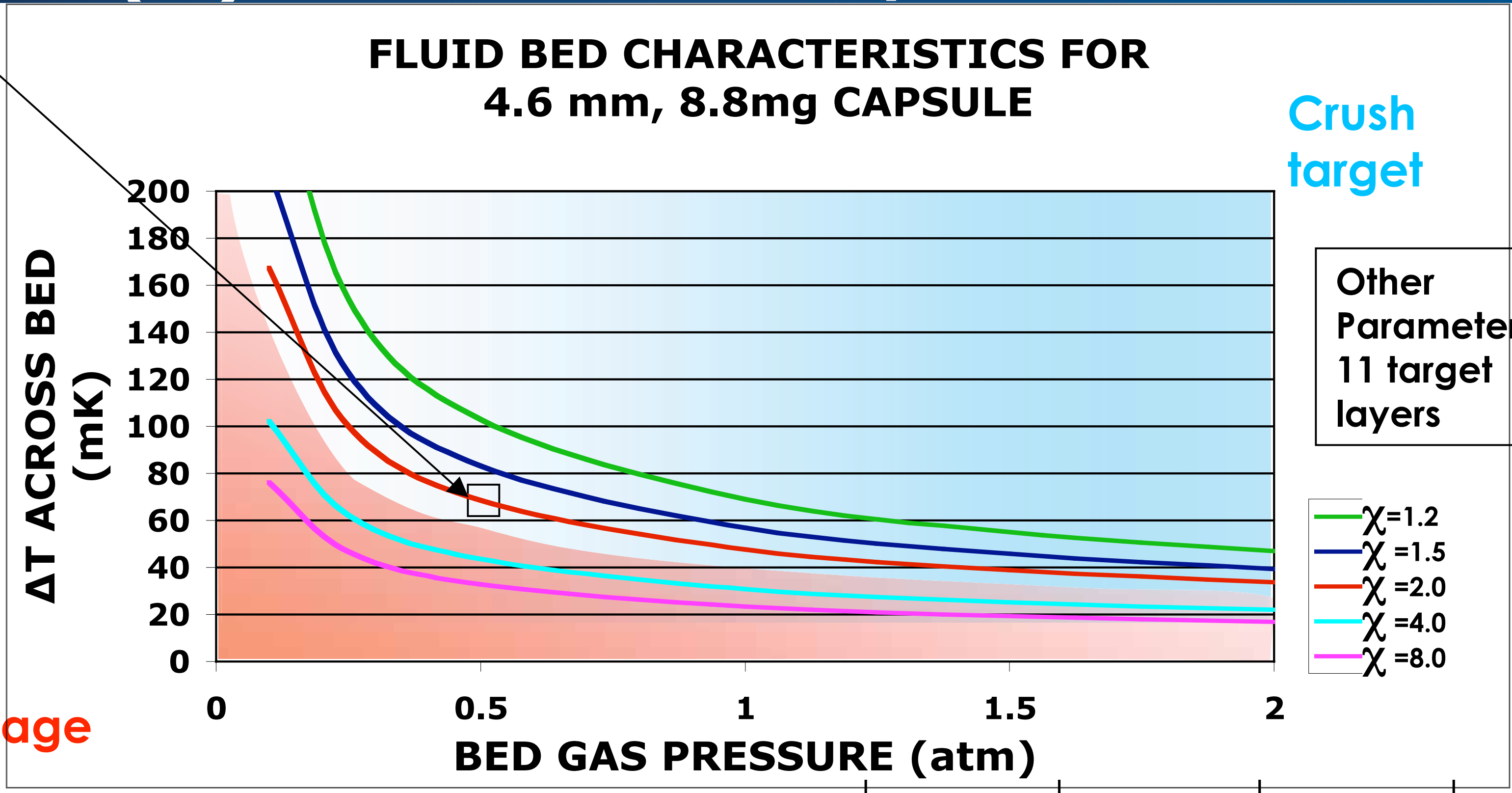

- $\chi \equiv$ Bed expansion ratio= h/h'
  - Function of mass gas mass flow

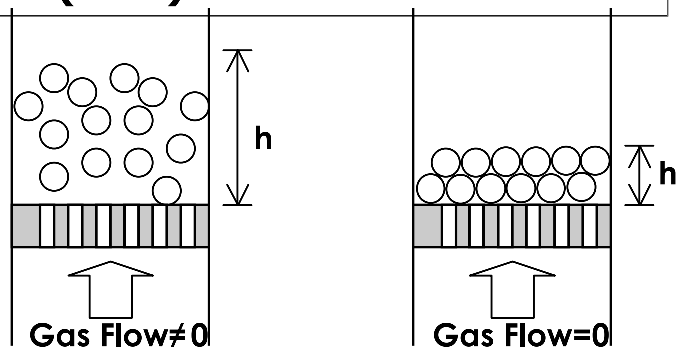

A fluidized bed test loop is being used to test bed configuration

- Room temperature, closed loop using cryo-helium blower
- Cryo compatible frit design verified to produce good fluidization (no channeling)
- Alternate bed frits tested to change: capsule spinning, circulation in bed, and interactions

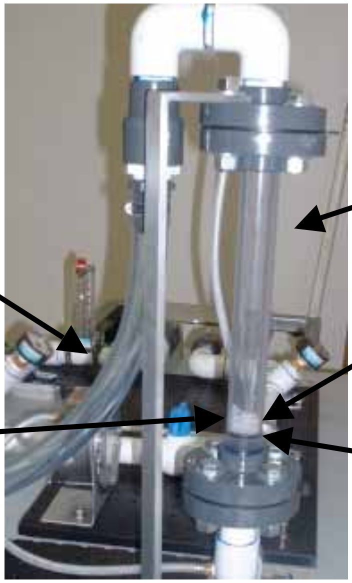

Successful Frit:
HCP array of Ø0.5 mm orifices
With 2 mm nearest neighbor spacing

Static cling of capsules controlled with Polonium strip on wall of bed
Without Polonium, fluidization only lasts 45 sec until capsules lock together

Whirling bed* enhances capsule spin and circulation within the bed

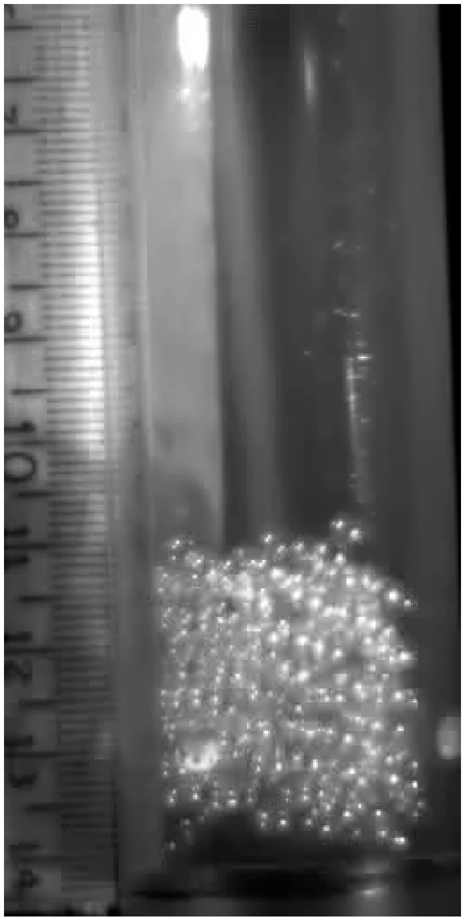

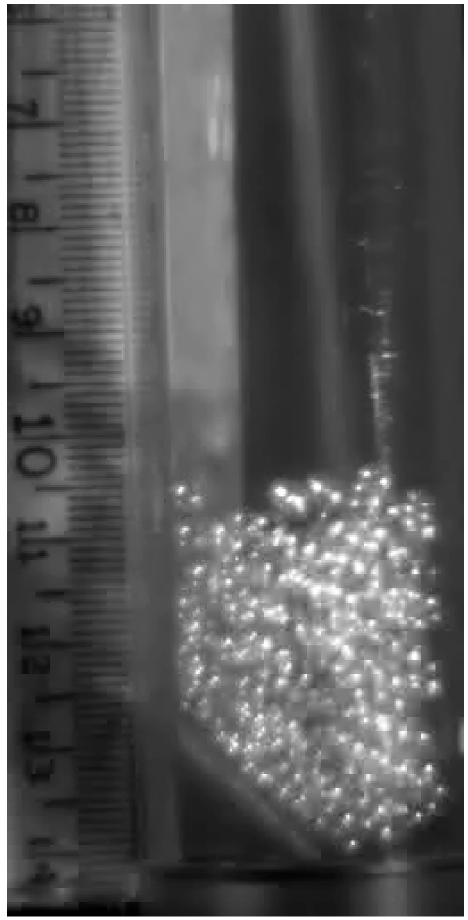

Slow Speed Video (x17)

Whirling bed frit

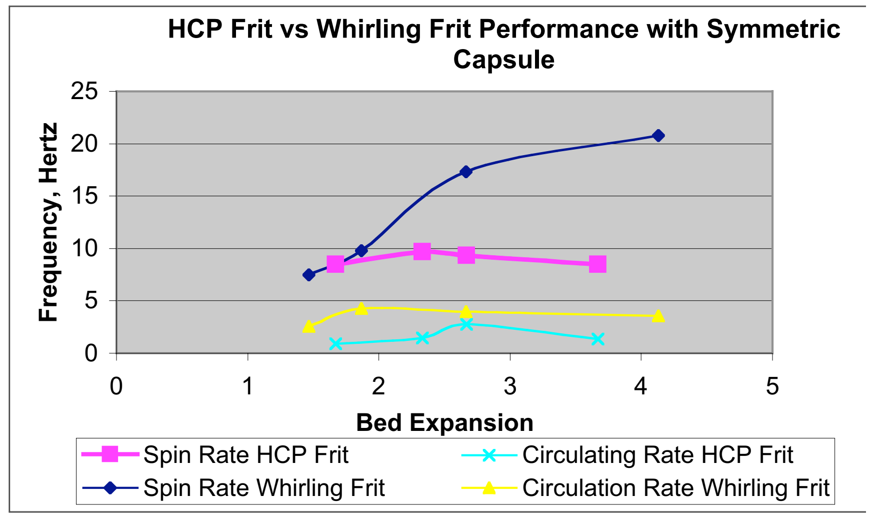

HCP frit

Whirling bed frit

- Nominal Bed Expansion (χ) of 2 has capsule spin rate = ~10 Hz

*Rios, G.M., Baxerras, J.L. and Gilbert, H., in *Fluidization*, Eds. Grace, J.R. and Madsen, J.M., 529, Plenum Press, New York (1980)

Temperature variations of helium gas are only slightly impressed onto fuel

- Differences in the thermal properties of fuel and helium gas lead to LARGE impedance mis-match at surface
  - Diffusivity, density, thermal conductivity, heat capacity, convection coefficient

3 mK local ΔT

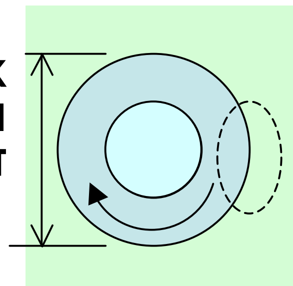

Capsule
Fuel

$$e_{par} := \sqrt{\frac{\left[k_{DT}\cdot 2\cdot \pi\cdot (\tau)^{-1}\cdot \rho c_{DT}\right]}{2\cdot h_{sphere}{}^{2}}}$$

$$e_{par} = 280$$

$$a := \sqrt{\frac{1}{2\cdot e_{par}{}^{2} + 2\cdot e_{par} + 1}}$$

$$a = 2.5\cdot 10^{-3}$$

Mis-match

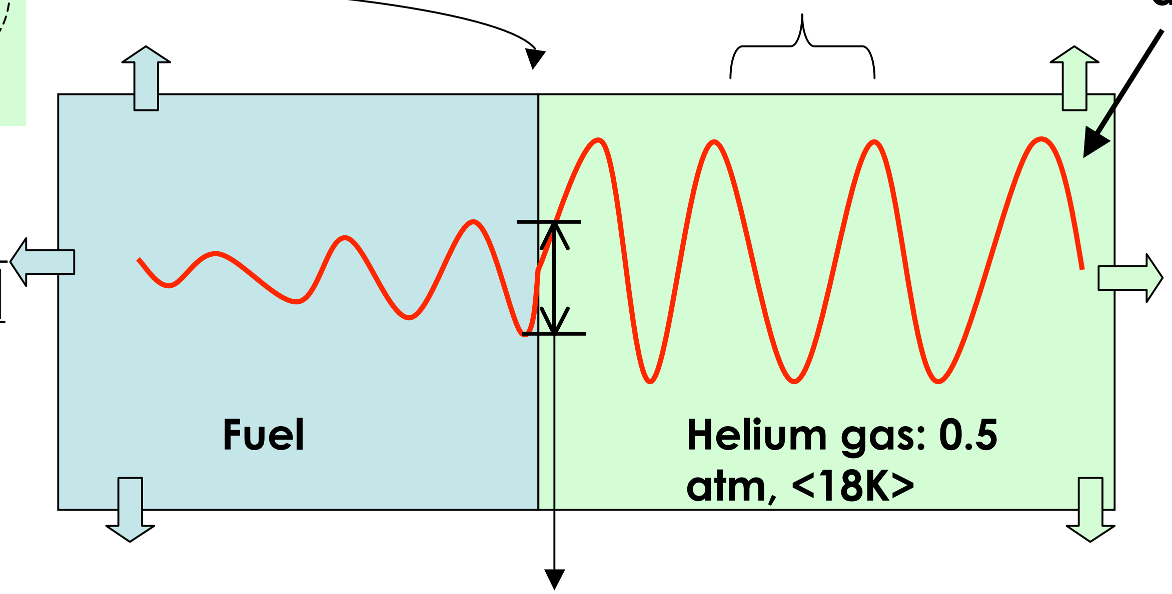

Fuel outer surface varies only 0.008mK

0.008mK temperature difference will yield 0.14 μm layer thickness difference to the beta-layer

- Apply dynamic ΔT to static model of fuel layer movement
- 1-D spherical model of beta-layering non-uniformities (from UR/LLE)

$$\Delta T = \frac{1}{6}\cdot\frac{qdot}{k_L}\left[\left[R_o^{\,2} - R_{i2}^{\,2} - 2\cdot R_{i2}^{\,3}\cdot\left(\frac{1}{R_{i2}} - \frac{1}{R_o}\right)\right] - \left[R_o^{\,2} - R_{i1}^{\,2} - 2\cdot R_{i1}^{\,3}\cdot\left(\frac{1}{R_{i1}} - \frac{1}{R_o}\right)\right]\right]$$

Ro = 2290 μm
(Ri1+Ri2)/2 = Ri=1780 μm

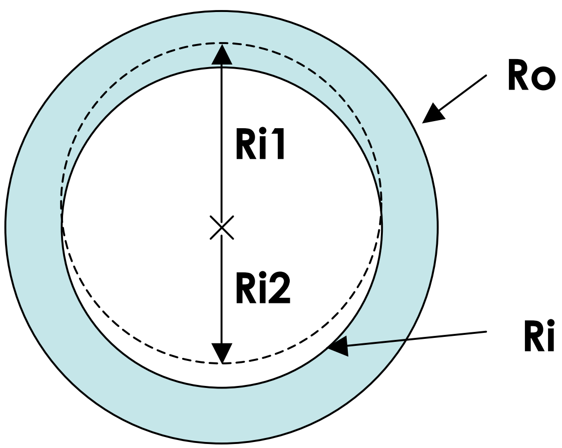

ΔT= 0.008 mK

(Ro-Ri2)-(Ro-Ri1) = Ri1-Ri2=0.14 μm

0.14 μm is below HAPL layer specification of 5 μm rms all modes; 0.5 μm rms high modes.

Gold coating stays 'smooth' for a long time in the fluidized bed

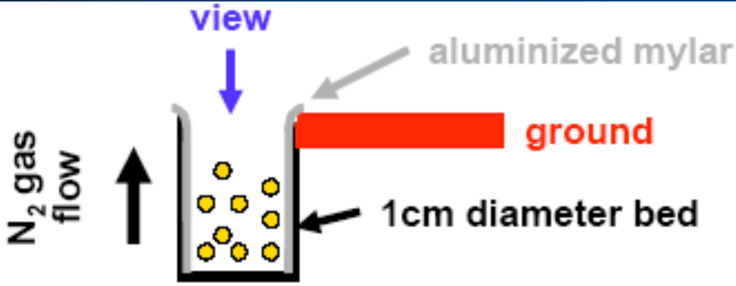

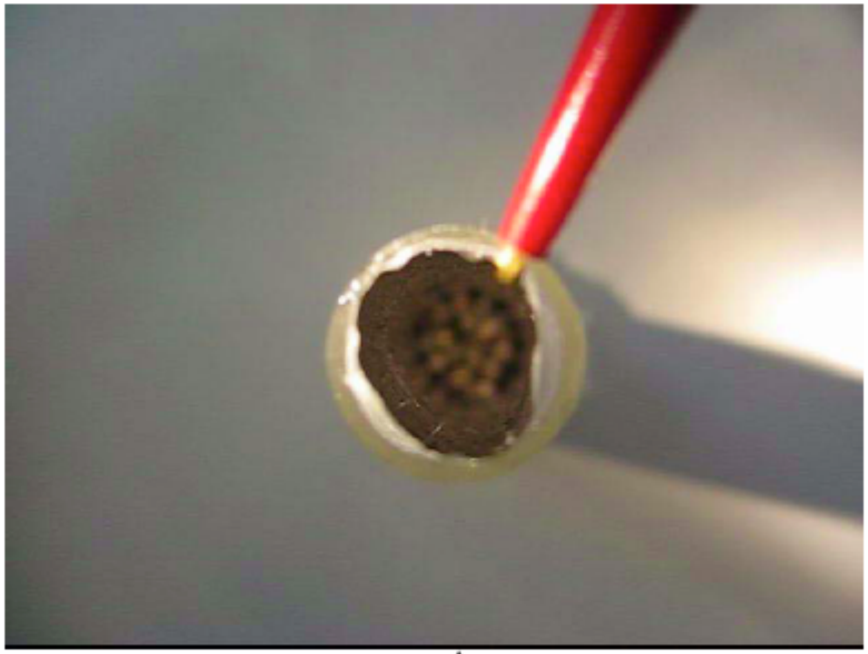

bed expansion = 2

- 2mm OD, 200 Å Au-coated shells
- Five shells pulled periodically
- Surface did not significantly roughen.

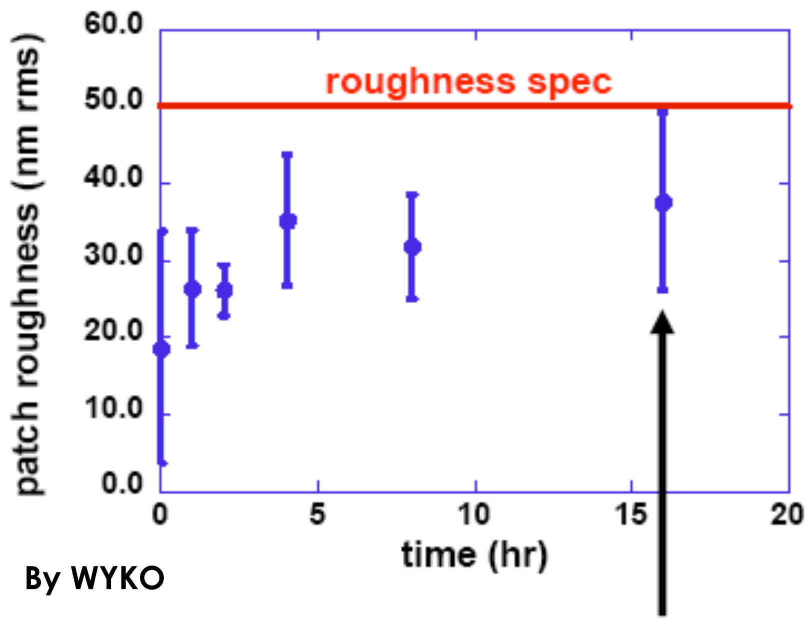

By WYKO

16 hr. estimated time in bed for power plant

Roughness ≈ Au layer thickness implies need to look for coating damage

Key MPLX scoping tests have been done

- **Static cling of capsules is controlled**
  - Polonium de-static strips

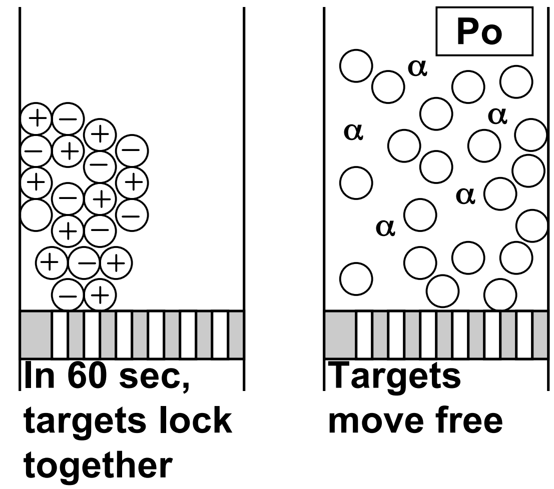

- **Surface of capsule remains 'smooth' on time scale of layering**
  - Need to look for damage to Au/Pd layer next

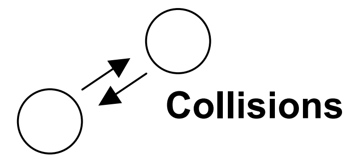

- **Circulation and spinning rates measured**
  - Rates fast enough for uniform DT layer at χ=2

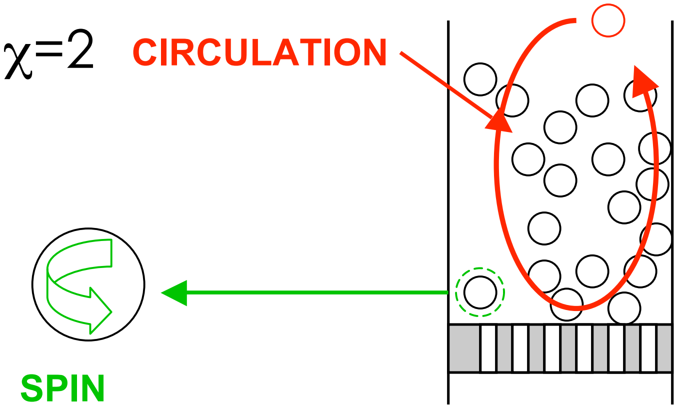

A cryogenic Mass Production Layering Experiment (MPLX) is being assembled

- For Deuterium Layers
- Permeation filled targets
- All Cryogenic circulation loop
- Allows reversed flow in bed
  - For initial freezing of layer without target motion

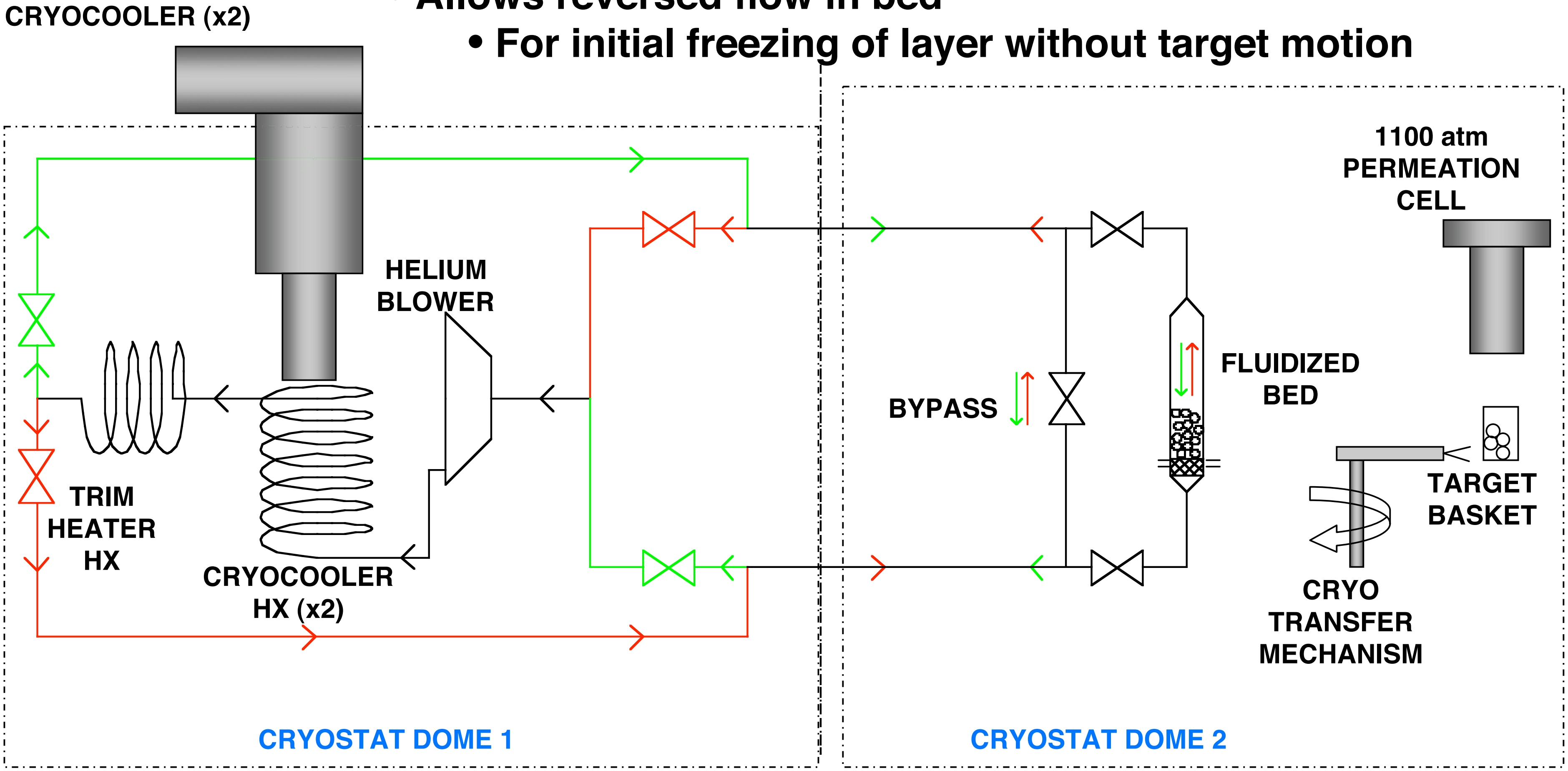

Design provides ~1Q_{DT} equivalent heating to 700 deuterium filled targets

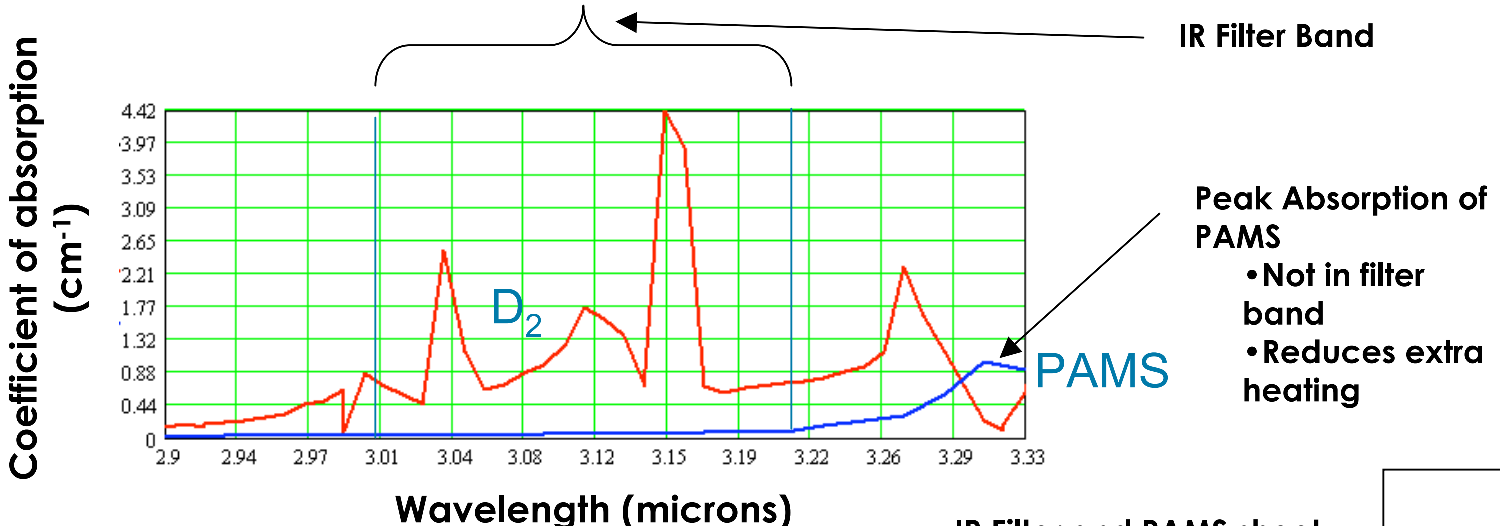

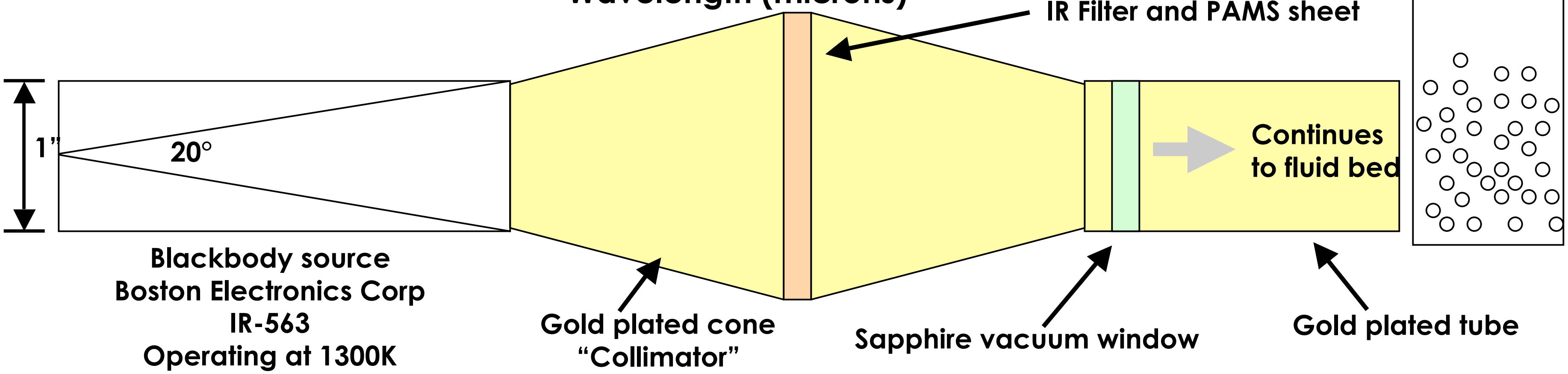

- Cone 'collimator' redirects rays to near normal for filter

Mass production layering experiment being brought online …

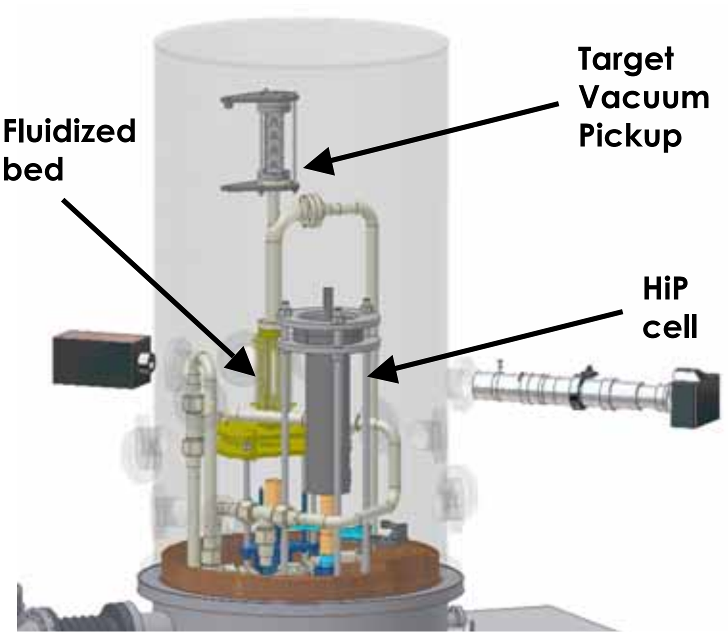

Hi-P cell (1100 bar)

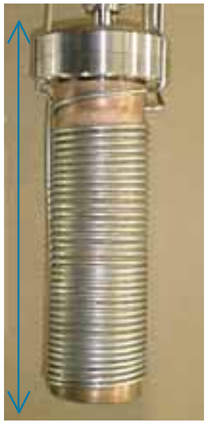

Includes filling with HD (via permeation thru overcoats)

SUMMARY

- **Fluid beds for layering scale nicely to power plant size**
- **Room temperature bed experiments show:**
  - Static cling of targets solved
  - Spin rates measured should allow highly uniform layers to be formed in cryo-bed
  - Targets spin with offset mass
  - Initial roughness experiments show outer Au/Pd coating stays smooth enough
    - More experiments planned on layer damage
- **Cryostat for layering deuterium in fluidized bed is in assembly**

Appendix

Mass flow required for given bed expansion is determined from generalized correlation

Pick bed expansion χ

$$\varepsilon = \frac{\chi - 1 + \varepsilon_0}{\chi - 1 + 1}$$

where is unexpanded bed void fraction

For spheres ε_0=0.4

$$\left(C_d \cdot \mathrm{Re}^2\right)^{\frac{1}{3}} = \left(\frac{4}{3} Ga\right)^{\frac{1}{3}} = d_p \Bigg/ \left(\frac{3\mu_{gas}^{\ 2}}{4\rho_{gas} g\left(\rho_p - \rho_{gas}\right)}\right)^{\frac{1}{3}}$$

These will determine $\left(\frac{\mathrm{Re}}{C_d}\right)^{\frac{1}{3}}$

Superficial gas velocity will be

$$v_{gas} = \left(\frac{\mathrm{Re}}{C_d}\right)^{\frac{1}{3}} \left(\frac{4\mu_{gas}\left(\rho_p - \rho_{gas}\right)g}{3\rho_{gas}^{\ 2}}\right)^{\frac{1}{3}}$$

Mass flow $\frac{dm_{gas}}{dt} = \frac{M_{gas} P v_{gas} Area_{bed}}{RT}$

Contours of Void fraction, ε

$\left(\frac{\mathrm{Re}}{C_d}\right)^{\frac{1}{3}}$

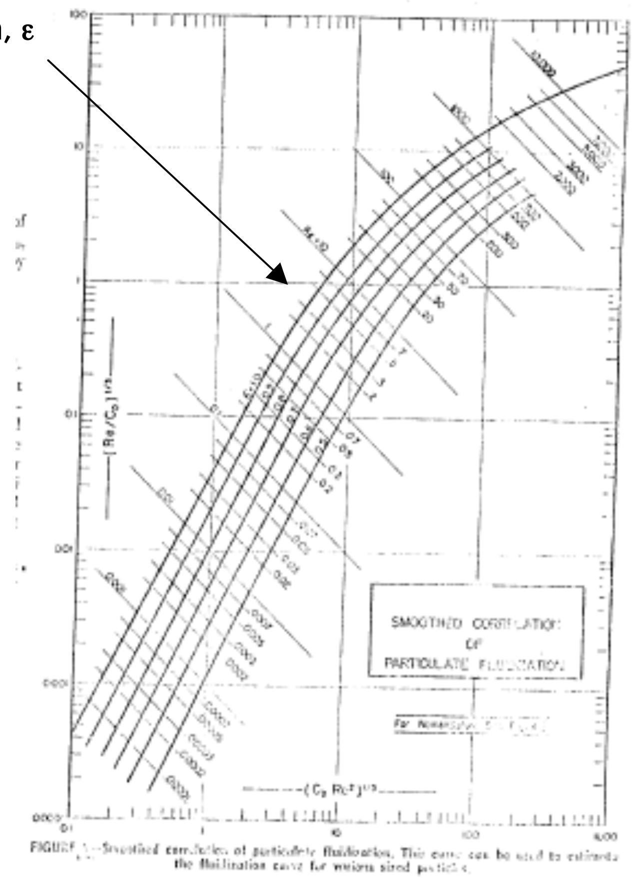

$\left(C_d \cdot \mathrm{Re}^2\right)^{\frac{1}{3}}$

F.A. Zenz, Fluid Bed Reactors Design, Scaleup, Problem Areas, AIChe Today Series, American Institute of Chemical Engineers, 1974, New York, pg 2-3

Beta or other heating warms bed from bottom to top

Heating rate/unit volume of target

$$\Delta T = \frac{h(1-\varepsilon)\dfrac{m_{DT\_p}\,q_{DT}}{Vol_p}}{\dfrac{dm_{gas}}{dt}\,\dfrac{C_p}{Area_{Bed}}}$$

Heat capacity of bed gas

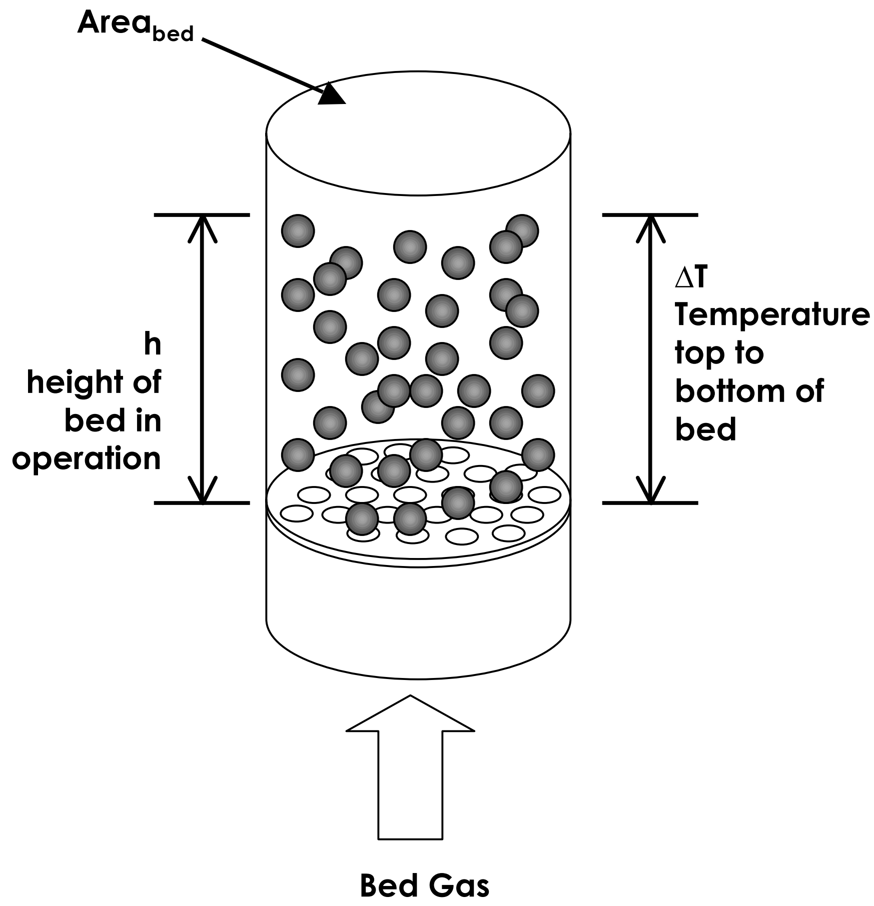

The circulation time of a target in the bed can be estimated

The circulation time of a particle in a fluidized bed is given by Rowe as

$$t_p = \frac{H_{mf}}{0.6\left(U - U_{mf}\right)\left[1 - \left(\frac{U - U_{mf}}{U_b}\right)\right]}$$

Where
H_{mf} is the height at minimum fluidization (~settled height),
U is the superficial velocity of the gas,
U_{mf} is the minimum velocity for fluidization,
U_b is the bubble (a void in particles) velocity.

Yates combines the Ergun equation with the empirical results of Wen and Yu for minimum fluidization voidage to obtain

$$U_{mf} = \frac{\mu}{d_p \rho_g}\left(\left\{33.7^2 + 0.0408\frac{d_p \rho_g \left(\rho_p - \rho_g\right) g}{\mu^2}\right\}^{1/2} - 33.7\right)$$

Where
μ is the viscosity,
d_p is the particle diameter,
ρ_g is the density of the gas,
ρ_p is the density of the particle,
g is the acceleration of gravity.

All inputs required come from bed design — except bubble velocity, U_b

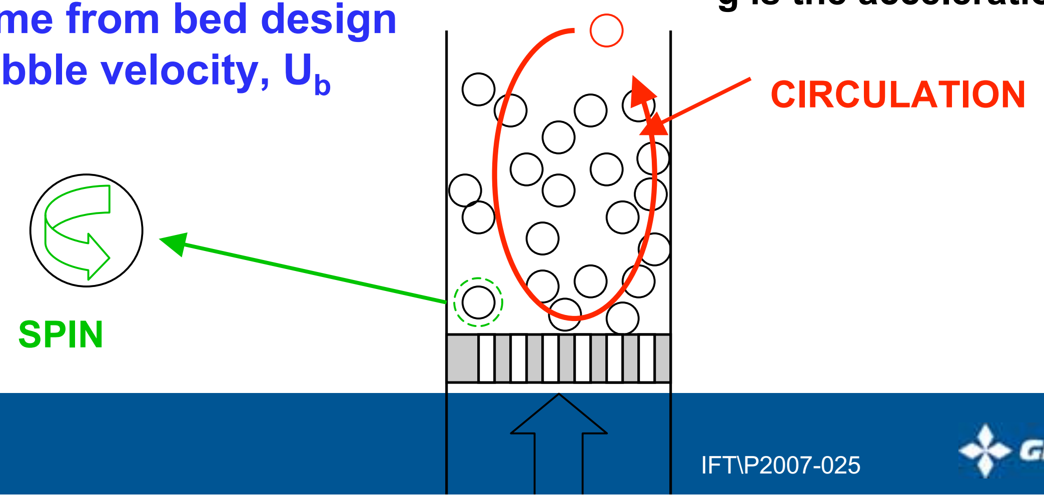

Expressions exist for bubble velocity

Davidson and Harrison give the average bubble velocity as

$$\overline{U}_b = \left(U - U_{mf}\right) + 0.711\left(g d_b\right)^{1/2}$$

Where
d_b is the bubble diameter.

Substitute into expression for t_p
Take integral average over all possible bubble diameters
0 to (bed diameter or bed height; whichever is smaller)

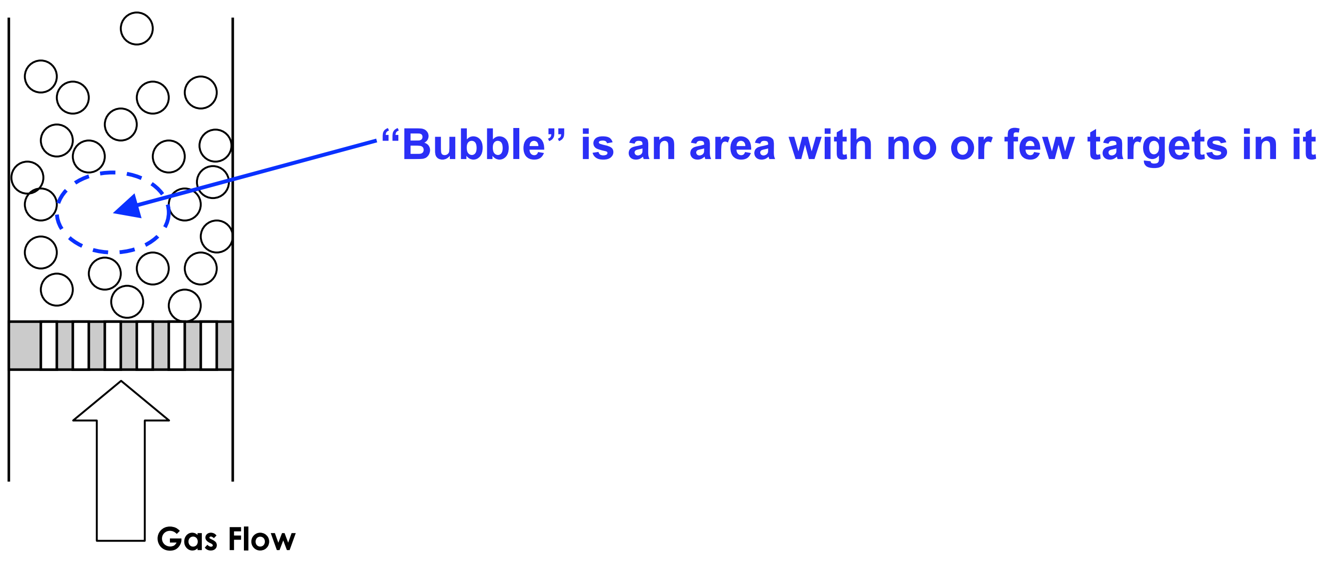

Circulation time of a target in the bed can be short

- Take an intregral average of t_p for all possible d_p's
  - 0 to bed diameter

	HAPL Target	Initial MPLX target	Room Temperature Experiment
Diameter (mm)	4.6	4.0	4.0
Mass (mg)	8.4	5.3	1.9
Fuel	DT	D2 (with 1Q_{DT})	Empty
Temperature (K)	~18	~18	300
Bed Pressure (atm)	0.5	0.5	1
Bed Gas	Helium	Helium	Air
H_{mf} (initial height; 11 layers) [mm]	51	44	44
Bed Expansion (χ)	2	2	2
U_{mf} (minimum fluidization) [cm/sec]	46	41	18
U (superficial gas velocity) [cm/sec]	160	150	62
ΔT across bed (mK)	69	66	NA
Target circulation Frequency ($1/t_p$) [Hz]	1.8	1.3	1.6

Theoretical estimates for circulation frequency for experiments

Different targets and setups expect similar frequency

Offset mass capsules also have significant spin rates

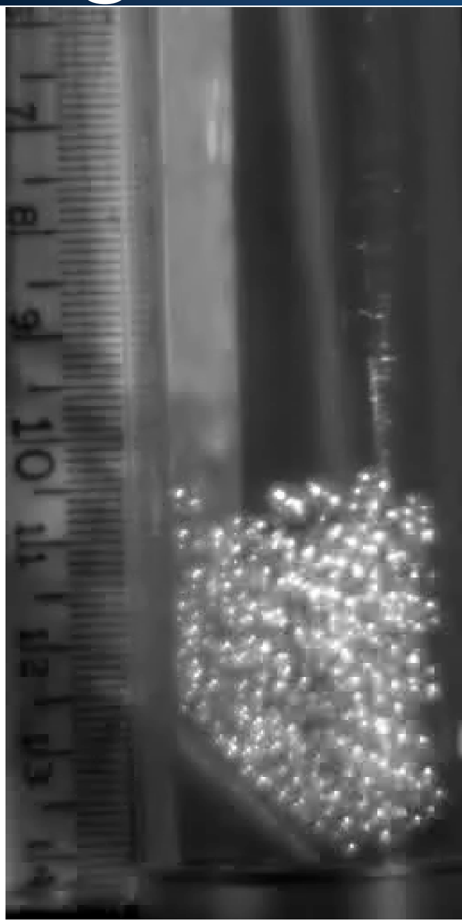

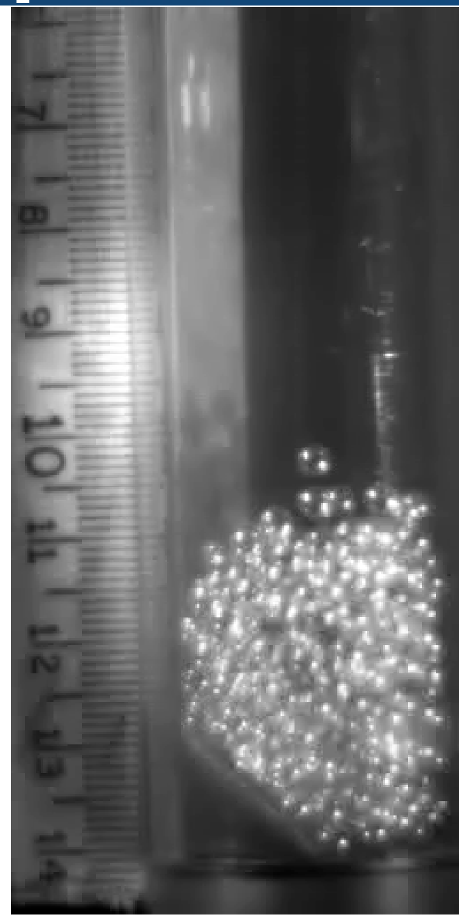

Slow Speed
Video (x17)

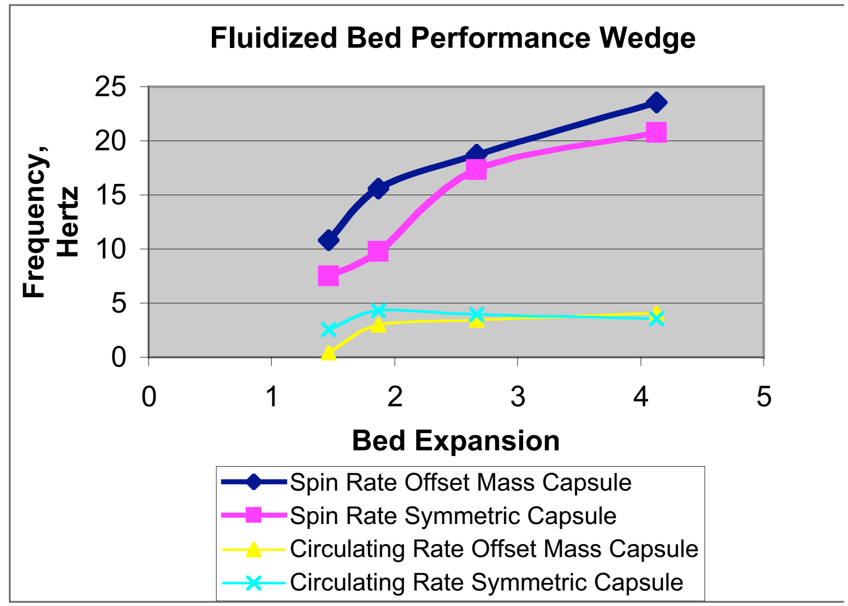

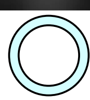

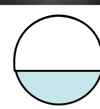 (1)

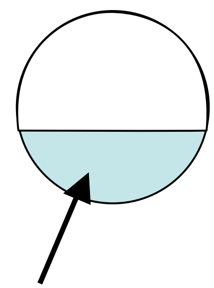

Injected White Paint

- **2 mg offset mass injected into capsule**
  - Similar to a starting condensed capsule

Faster layering is accomplished by adding heat to DT layer

- **Layering time constant is**
  - $\tau = H_{sublimation}/(Q_{DT} + Q_{added})$
  - Q_{DT} is heat of tritium beta's
  - Beta-layering has τ = 26 min = **1560 sec**
    - $Q_{added} = 0$
- **Adding heat flux through layer smoothes layer*†**

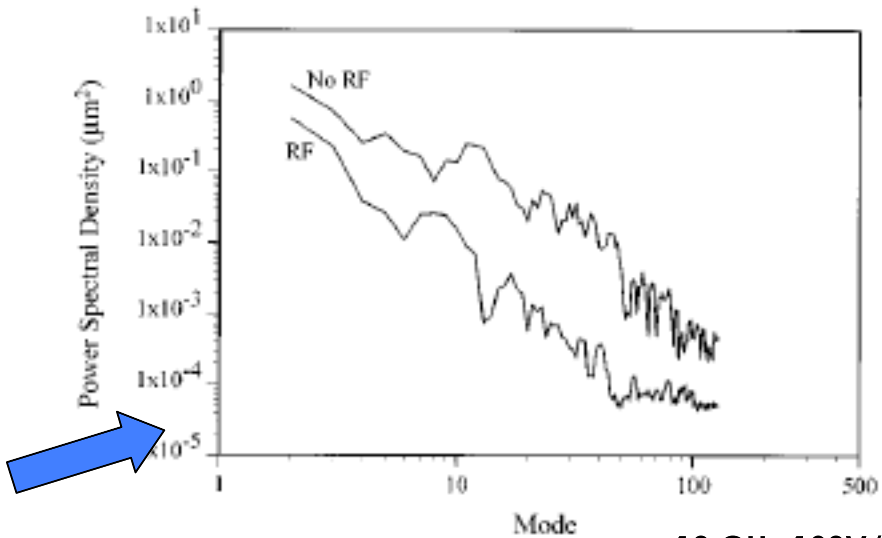

10 GHz 190V/cm

•G. W. Collins et al, Heat-flux induced changes to multicyrstalline D2 surfaces, Phys. Rev B. (63), 195416, 2001

† E. R. Mapoles et al, Soothing of deuterium -tritium ice by electrical heating of the saturated vapor, Phys. Rev E (55) 3, 3473, 1997

Plasma discharge layering has potential to quickly make smooth layers at low temperatures

- **Target random motion in Fluidized Bed should overcome non-uniformities in previous plasma layering experiments**
  - Target held in fixed position with its fill tube*
- **10K is field discharge minimum at 2.45 GHz for D2 IFE target**
- **Norimatsu had layering redistribution time of 1.3 min**
  - Native beta-layering this is 26 min
  - Implies layering plant could be even smaller

•We propose adding to fluidized bed to plasma discharge layering method of Norimatsu (ILE)*

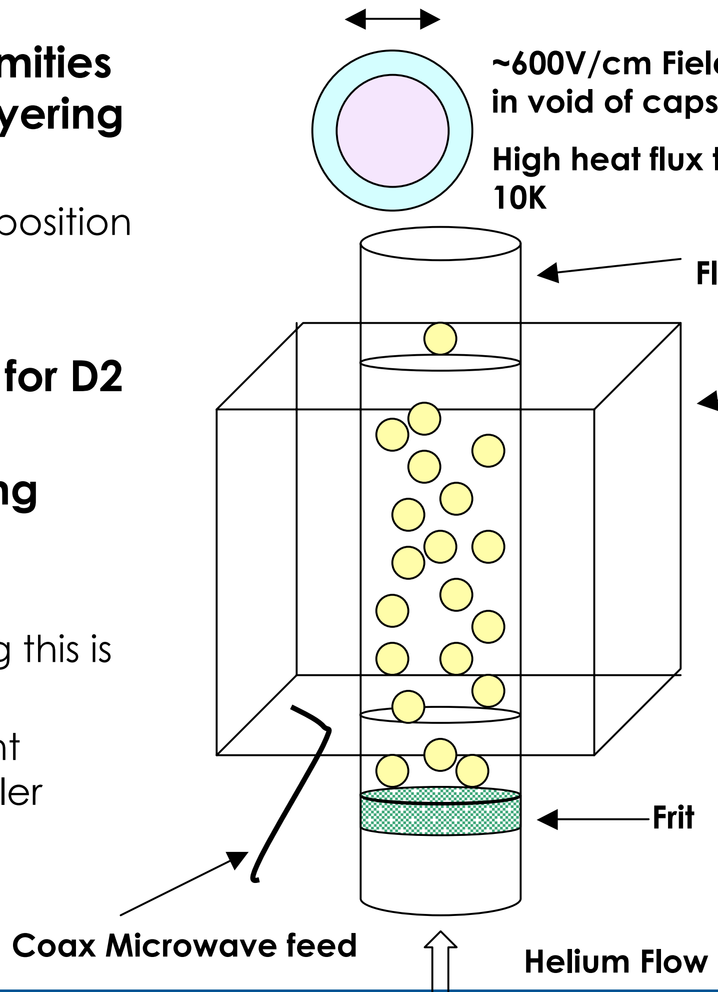

~600V/cm Field at 2.45GHz creates plasma discharge in void of capsule (D2 vapor pressure over solid)

High heat flux through layer smoothes layer even at 10K

***T. Norimatsu, M. Ishihara, Y. Izawa, and S. Nakai; Plasma Layering Technique to Make Uniform Solid Fuel Layer for Laser Fusion Target, 12th Laser Interaction and Related Plasma Phenomena, April 24-28, 1995, Osaka, Japan**

Gold layer on capsule causes some field loss

- **300 Å is very thin**
- **Skin depth of gold at 2.45GHz**
  - 1.6 micron at room temperature
  - 740 Å at 8K
    - There is some variability in low temperature resistivity data
- **Field loss is only 33% into capsule interior**
  - (1-exp(-300A/740A))
- **If needed use:**
  - Lower frequency
  - Add Palladium to raise lower temperature electrical conductivity

Plasma layering may impose tolerances on the capsule uniformity

- Polymers will absorb some heat from microwaves
- Heat in capsule will impose some of the non-uniformity of the capsule onto the DT
- Effect is to be analyzed

Progress on Surface Roughening of W/SIC Exposed to IFE

Michael Andersen and Nasr M. Ghoniem

University of California Los Angeles (UCLA)

Goal: Predict material life from crack nucleation formation by modeling surface roughening

Problem Statement

- Experimental data show that the surface of tungsten exposed to laser, ion, and X-ray irradiation undergoes substantial roughening with a variety of patterns and features. Control of surface conditions is essential to the design of these systems, since it can lead to crack formation, adverse effects on heat absorption because of emissivity changes, and eventual failure. For this reason, a quantification of the surface must be studied and utilized to determine surface integrity.

Grooving patterns can appear in long rows, but notice that a crosshatch formation ends the valleys from continuing indefinitely.

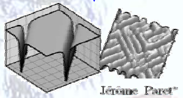

Jérôme Paret
Phys.Rev.L, in press

Review of Earlier Work

- First an energy spectrum is determined from a given target, which can then be used to find the atomistic characteristics of each pulse using a program called the Stopping and Range of Ions in Matter (SRIM). SRIM determines on average where an ion with a given energy ends up. Also with the energies from each ion we can find flight time and ultimately time of interaction on the material. With this information we can use a modeling program to determine temperature of the material over a given time.

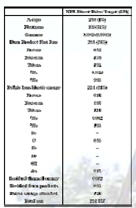

Spectrum provided by ARIES, UCSD

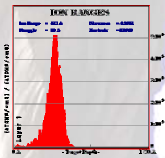

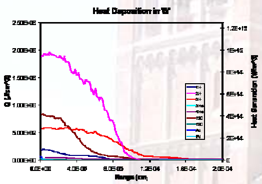

- In order to study the evolution of the surface profile, a description of the chemical potential and how it applies to material transport needs to be established. The chemical potential, μ, can be described as

$$\mu = \mu^* + \gamma\Omega\kappa + \Omega\omega$$

Where μ^* is the chemical potential of a flat surface bounding the solid with bulk stress σ^o, γ is the surface energy, Ω is the atomic volume, κ is the surface curvature, and ω is the strain energy. The strain energy is found from Hooke's law as:

$$\omega = \frac{1}{2}\varepsilon_{ij}\sigma_{ij}$$

$$\omega_b = \frac{(1-\nu^2)}{E}\sigma^{\infty}$$

$$\omega_s = \frac{1}{2E}\sigma_{tt}^2$$

Stress on the surface turns out to be one of the tricky parts of the problem. Here we will use BEM or

Where ω_b is the bulk strain energy and ω_s is the surface strain energy for plane strain. The surface material transport is determined by the Nernst-Einstein relation of the diffusion flux proportional to the surface gradient of the chemical potential given as

$$J = -\frac{D_s}{kT}\frac{\partial\mu}{\partial s}$$

Where D_s is the surface diffusivity, k is the Boltzmann's constant, T is the absolute temperature and the derivative with respect to the arc length, s, is evaluated along the surface. The normal velocity of the surface V_n, is then proportional to the divergence of J:

$$V_n = -\frac{D_s\Omega\nu_s}{kT}\frac{\partial^2\mu}{\partial s^2}$$

Where ν_s is the number of atoms per unit area of the material in the plane normal to the flux direction. This can be extended to the surface profile h(x,t) as

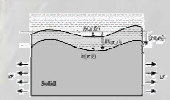

$$\frac{\partial h}{\partial t} = D\frac{\partial}{\partial x}\left[\left(1+h_x^2\right)^{-\frac{1}{2}}\frac{\partial}{\partial x}(\gamma\kappa+\omega)\right]$$

$$D = \frac{D_s\nu_s\Omega^2}{kT}$$

Here we can see a roughening zone created by the bi-axial stress state. With the normal velocity found we can determine the movement on the surface

Roughening Mechanisms

- There are several test facilities running experiments on the nature of surface reactions to laser, ion, and x-ray. These included the Dragonfire facility at UCSD, XAPPER at Lawrence Livermore, and the RHEPP at Sandia. The hope is to create a model that agrees with these experiments.

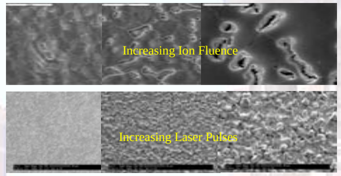

Effect of increasing ion fluence and increasing number of pulses. Ion work done by T. Renk, SNL presented for HAPL. Laser work done by F. Najmabadi and J. Pulsifier at UCSD and again presented for HAPL.

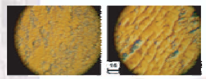

Roughening increases with pulses and deepens with temperature.

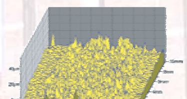

Roughness on the order of 10's of microns…measured as the distance from peak to valley. (Renk, SNL)

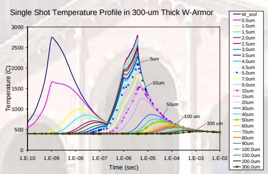

Modeled using ANSYS

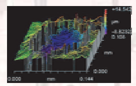

Roughness from the x-rays seems to be negligible mostly because of short incident time. (J.F. Latkowski, LLNL)

$$F(E)dE = F(x)dx$$

$$F(x) = F(E)*\frac{dE}{dx}$$

$$C(x) = \frac{F(x)dx}{dV} = F(x)$$

$$\tilde{C}(x) = C(x)*\Omega = F(x)*\Omega$$

$$G(x) = \tilde{C}(x)*Hz.$$

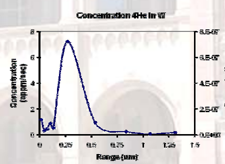

By knowing the spectrum of ions with respect to energy and finding the dispersion of ions with respect to distance into the material, the concentration can be found analytically. This allows quick calculations for new target spectrums—all that is needed is the percentage of ions released from a target and at what energies.

$$\sigma_{rr} = -2\mu\left[\frac{1}{r}\frac{\partial}{\partial r} + \frac{\partial^2}{\partial z^2}\right]\vartheta$$

$$\sigma_{\theta\theta} = -2\mu\left[\frac{\partial^2}{\partial r^2} + \frac{\partial^2}{\partial z^2}\right]\vartheta$$

$$\sigma_{zz} = -2\mu\left[\frac{1}{r}\frac{\partial}{\partial r} + \frac{\partial^2}{\partial r^2}\right]\vartheta$$

$$\sigma_{rz} = 2\mu\frac{\partial^2\vartheta}{\partial r\partial z}$$

$$\nabla^2\vartheta = mT, \quad m = \left(\frac{1+\nu}{1-\nu}\right)\kappa$$

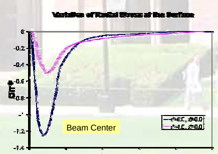

Surface Stresses can be relatively straight forward to calculate when the surface is flat, but as it begins to roughen the problem becomes out of the scope of simple equations and needs a modeling approach. Above, we can see a straight forward approach to finding surface stresses from a laser energy source. Hector and Hetnarski JAM '96

Boundary Element Method (BEM)

- A key component of this problem is determining the stress along the surface as the morphology changes. This was first approximated with general elasticity, but needed to be more clearly defined around the changes in the surface. As the valleys deepen toward a crack, the stress increases dramatically as does the need for more definition with increasing curvature. A boundary element method is used based upon discretizing only the surface instead of the whole volume. This makes it much easier to code and follow changing surfaces. The defining equation for this method is shown below.

$$\int_S \bar{T}_{ij}(x,\xi)u_j(\xi)dS(x)$$

T is the elastic Green's function that satisfies the periodic boundary conditions and u is the displacement field. The key to this method is that it is only over the surface and does not need information from inside the material. Stresses can be found inside the material nonetheless.

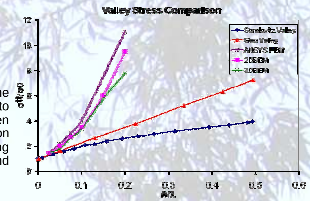

Stress at the valley of the roughened zone is shown to increase quite dramatically as the amplitude over wavelength increases. This is as expected as local stress around valley would eventually approach that of a crack tip.

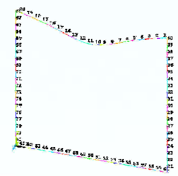

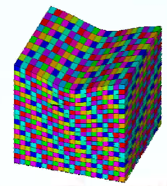

There are two BEM codes used for this work. The first is 2D with 3 nodes/element and the second is 3D with 8 nodes/element. Input for the codes is same: node coordinates, nodal connectivity to the elements, traction and surface displacements.

- It should be noted that BEM has one flaw. Stresses inside the boundary can be found, but they contain a 1/r parameter that leads to a singularity when you approach the surface. A more accurate way is used where the stresses on the surface are calculated by differentiating the surface displacements. This is how the graph below is so smooth without fluctuations.

As a validation to how well the BEM works, it is compared to a FEM analysis (ANSYS). As can be seen the results are very agreeable. The BEM has the advantage of being programmable with automatic surface changes without the recurring user interface needed with FEM.

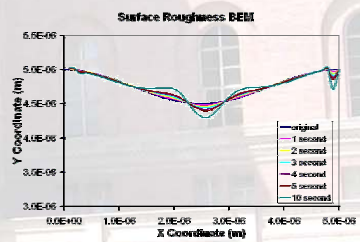

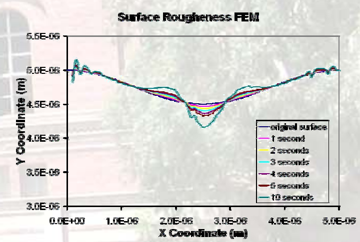

Status Report

- 2D needs to be finished off with a few advancements including transient inclusion, long-time runs, effects of plasticity, and the possible addition of defects around the crack tip. Previous research has stopped once the roughness begins to form. The curvature and stress approach extreme values and calculations become too excessive to continue the growth. By including plasticity and consequent dislocations and blunting, we can control these stresses and continue the nucleation.

- The work eventually needs to be extended to 3D where the derivatives over the surface becomes slightly more complicated as the Laplace-Beltrami operator must be used to find the derivatives of the chemical potential. Key to this work will be the BEM because as the surface changes, the stress calculation will become more and more difficult. Only needing to mesh the surface will make this possible.

Shown here are dislocations coming from the crack tip. This keeps the stress from approaching a discontinuity.

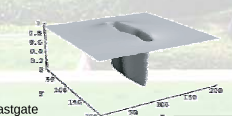

L.O. Eastgate
Phys.Rev.E,65

Simulated phase field solution in a fracturing sample.

UCLA

The behavior of liner surfaces used for compression to MG fields in magneto-inertial fusion

B.S. Bauer, R.E. Siemon, T.J. Awe, M.A. Angelova, S. Fuelling, T.S. Goodrich, I.R. Lindemuth, V. Makhin, R. Presura
University of Nevada, Reno

W.L. Atchison, R.J. Faehl, R.E. Reinovsky, P.J. Turchi
Los Alamos National Laboratory

IFE Science and Technology Strategic Planning Workshop
San Ramon, California
April 26, 2007

BSB 4/21/07

Abstract

At the energy density required for Magnetized Target Fusion (MTF), the liner, or in general any pusher material that compresses the target, is subjected to high pressures and intense Ohmic heating, as well as radiation and possibly particle bombardment from the target plasma. A series of experiments are underway to study the response of aluminum to the megabar pressures and MG fields anticipated in MTF experiments. To allow good diagnostic access, a simple geometry has been adopted. The MG fields are generated at the surface of cylindrical metal conductors that carry current. The configuration is therefore a classic z pinch in which the metal to be studied is the object being pinched. At MG fields the pressure is so high that material strength can mostly be ignored, and the configuration is unstable to the classic MHD modes. Generally parameters are chosen so that the growth time for instability is longer than the time to reach peak field, and in addition the skin depth of the field is chosen to be small compared to the conductor radius. This skin depth regime is distinct from that of exploding wires in which the skin depth is made larger than the conductor radius.

*Work supported by DOE-OFES grants DE-FG02-04ER54752 and DE-FG02-06ER54892.

Test modeling with experiment: 1 MA in 100 ns through 1-mm-diameter Al wire

1. What is Magnetized Target Fusion (MTF)?

2. When can a z-pinch be used to study liner physics?
   - When current skin depth < cylinder radius i.e., when $\delta/a < 1$, so *not* a wire explosion
   - When m=0 & m=1 instability growth is limited
   - When plasma formation by electric field is limited

3. Zebra experiment: 1 MA in 100 ns through 1-mm-diameter Al wire: $\delta/a \sim 0.05$

4. Modeling with MHRDR is being compared with experimental data

Magnetized Target Fusion (MTF) seeks minimum-cost trade-off between input energy & power

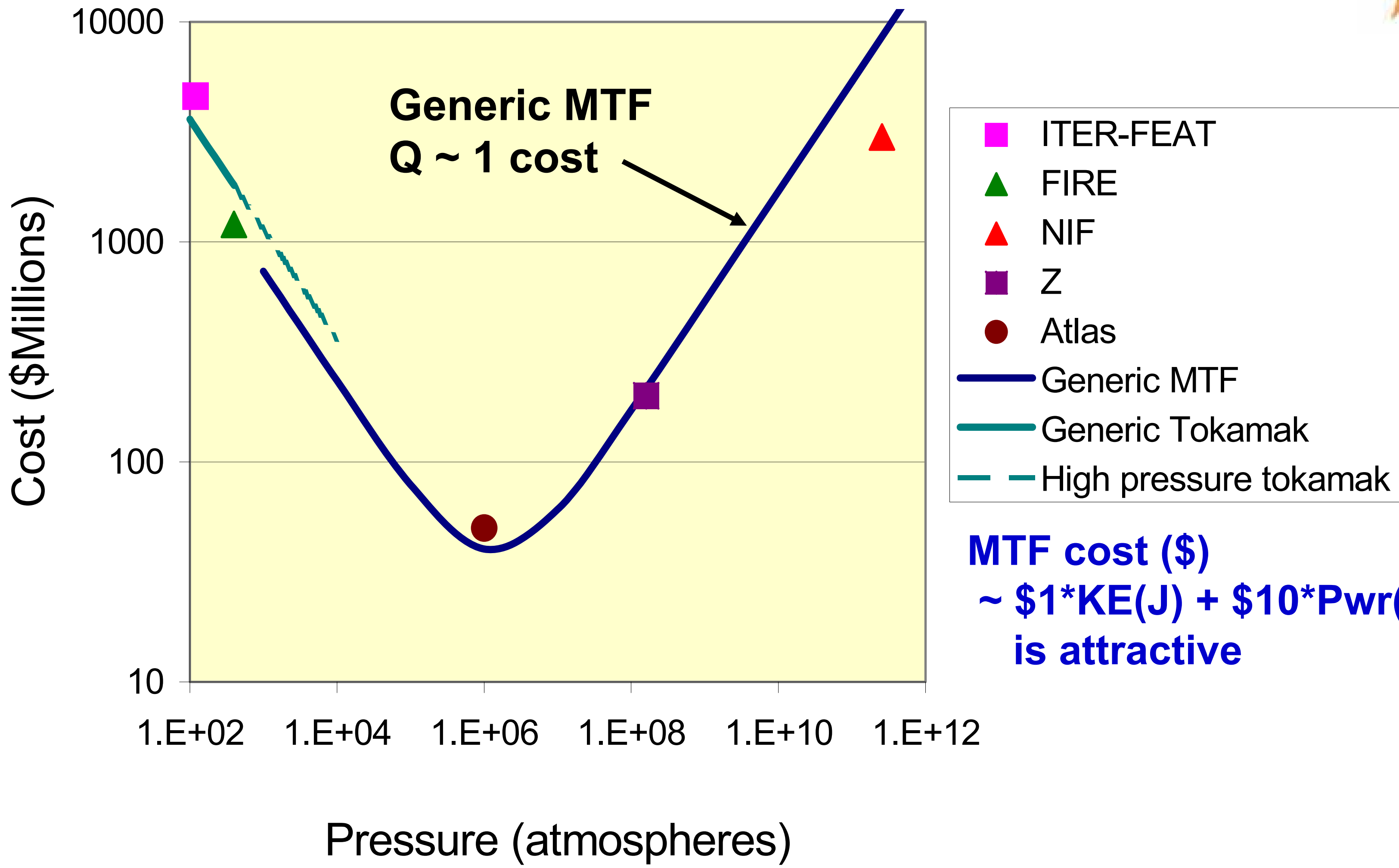

MTF cost ($)
~ $1*KE(J) + $10*Pwr(MW)
is attractive

RES, BSB 10/20/03

Imploding a magnetized plasma could yield Magnetized Target Fusion

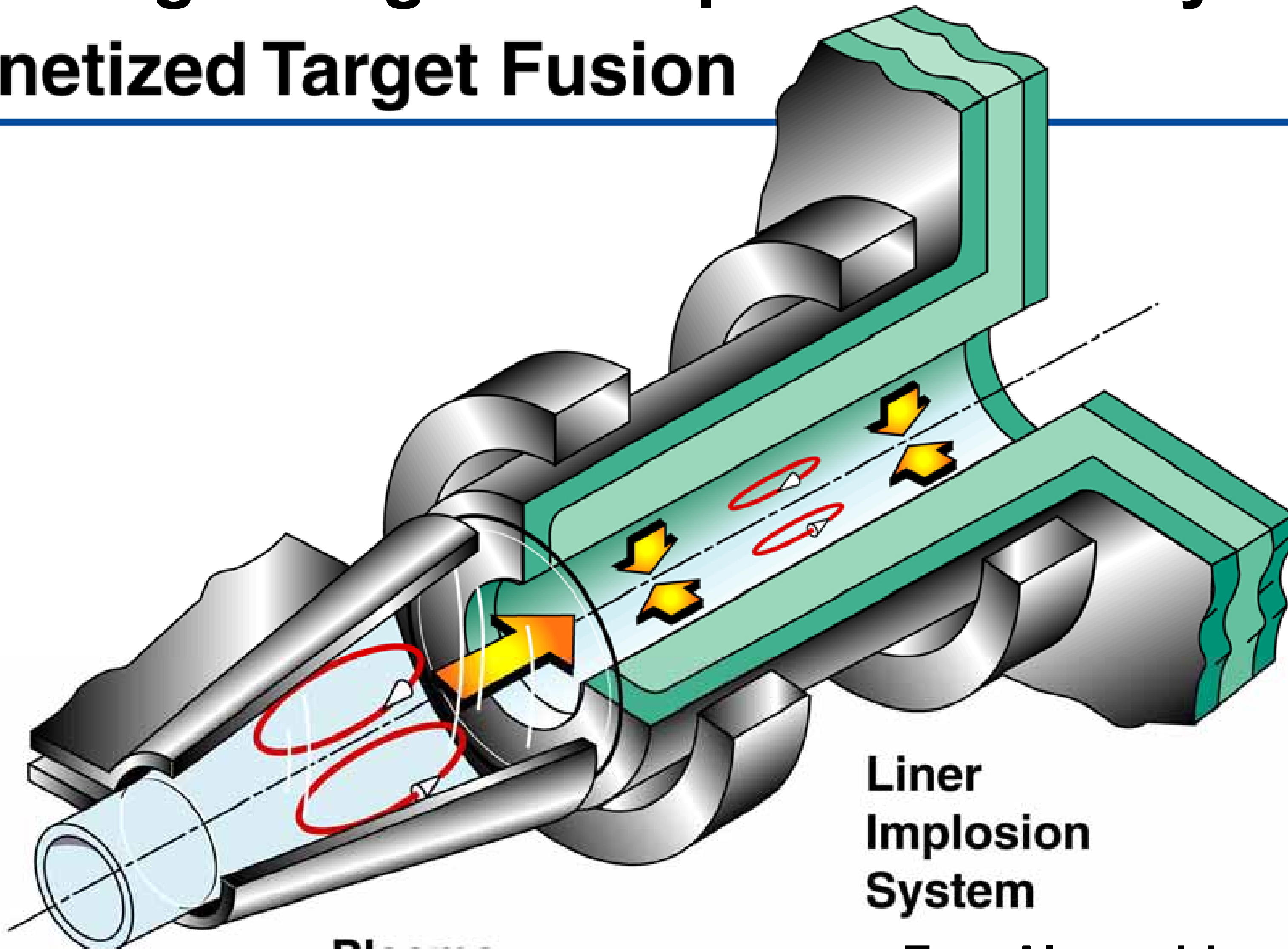

- E.g., Al can driven by $I > 1$ MA, $B_\theta \sim 100$ T

Magnetic and inertial fusion are separated by 10^{11} in fuel density & confinement time

Gain=1 (Lawson): $n\tau_E \geq$ 12 kT/ $<\sigma v>$ E_f
$\sim$ 10^{14} $cm^{-3}s$ ~ 10^{-9} s g/cm^3

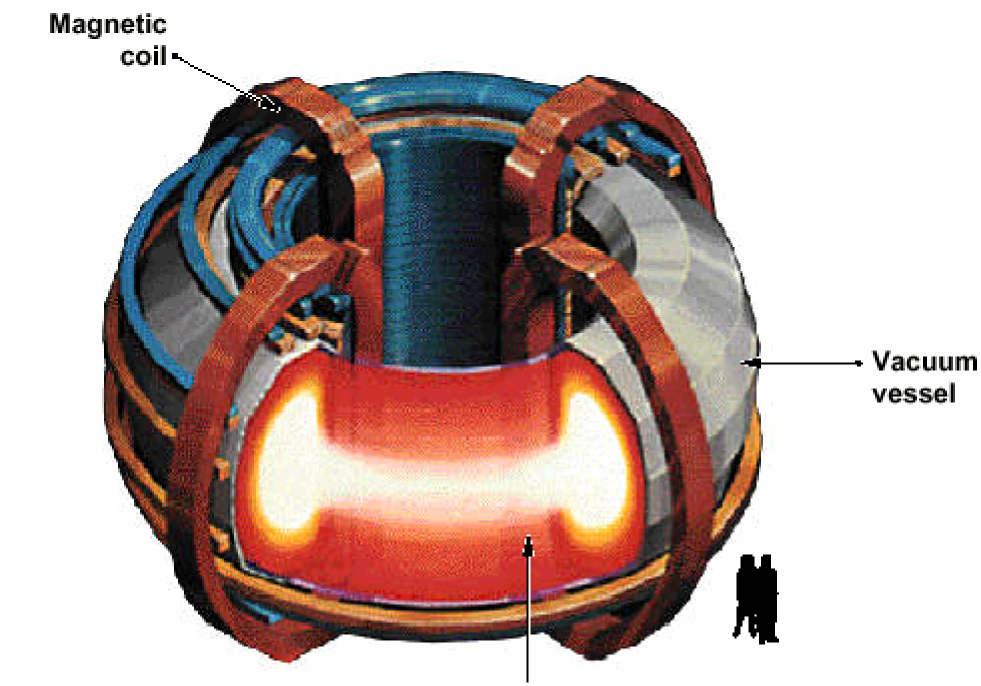

DT fuel: 10^{-9} gm/cm^3
$j \times B = \nabla p$: $\tau_E \sim 1$ s

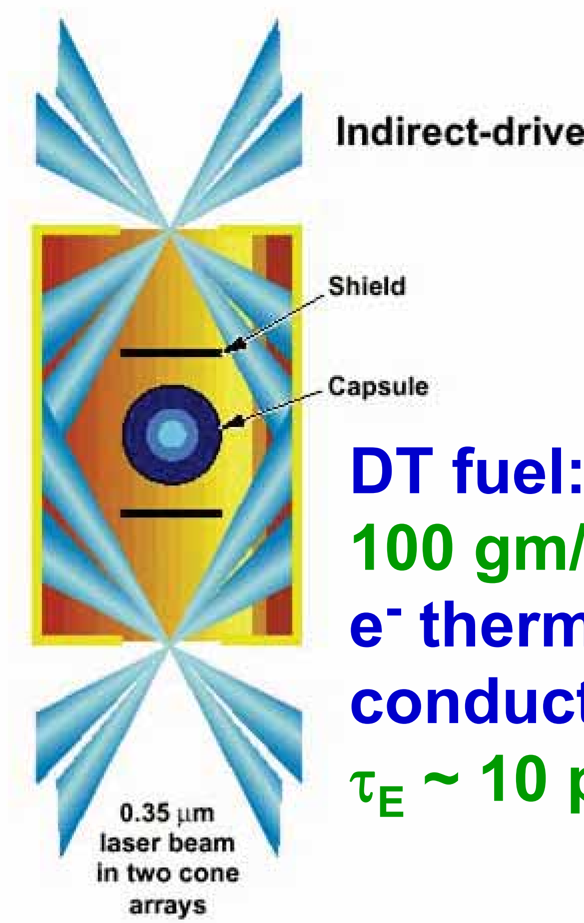

DT fuel:
100 gm/cm^3
e^- thermal conduction:
$\tau_E \sim 10$ ps

RES, BSB 9/20/03

Low-cost electric pulsed power can apply plenty of pressure, energy, & power

- **Superconducting magnets (constant)**
  B < 15 Tesla
  p < $\beta B^2/2\mu_0$ ~ 100 atmospheres

- **Liner technology (pulsed 10^7J / 10^{-5}s ~ 10^{12} W)**
  B < 500 Tesla
  p < $\beta B^2/2\mu_0$ ~ 10^6 atmospheres

- **Laser compression (pulsed)**
  p ~ 10^{11} atmospheres

The input energy & power required for fusion are set by the fuel pressure & β

T = 10 keV; p, β ➔ $n = p/(2kT)$
$\tau_E = [n\tau_E] / n$
$B = (2nkT/\beta)^{1/2}$

➔ Thermal diffusivity $\chi = f(n,T,B)$
e.g., $\chi_{Bohm} = kT/(16eB) \sim 1\ m^2/s$

➔ $R = (\chi\tau_E)^{1/2}$, Volume = const*$R^3 \propto \tau_E^{1\frac{1}{2}} \propto p^{-1\frac{1}{2}}$

➔ Energy = 3nkT*Volume $\propto p^{-1/2}$
Power = Energy/$\tau_E \propto p^{1/2}$

MTF regime is intermediate between MFE and ICF

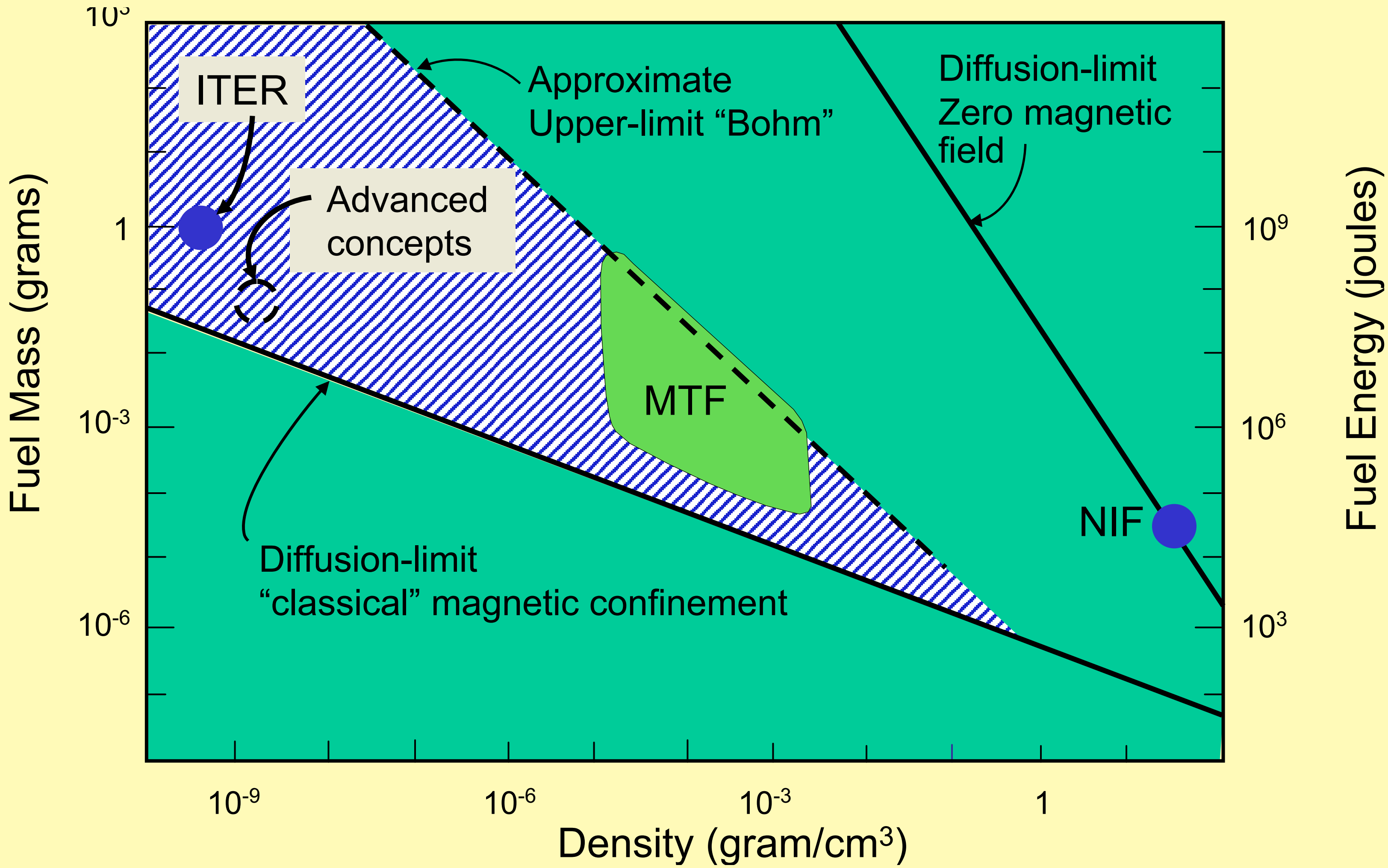

DT Fuel Mass heated to 10 keV

RES, BSB 6/14/05

Principal MTF issues

- Plasma target issues
  - -- formation method ?
  - -- stability ?
  - -- energy confinement ?
- Liner physics issues
  - -- what determines maximum B ?
  - -- what about RT during liner deceleration ?
  - -- how much high-Z mixing with DT fuel ?
- Can economical and practical MTF be developed?

Radiographs of liner implosion demonstrate good liner performance

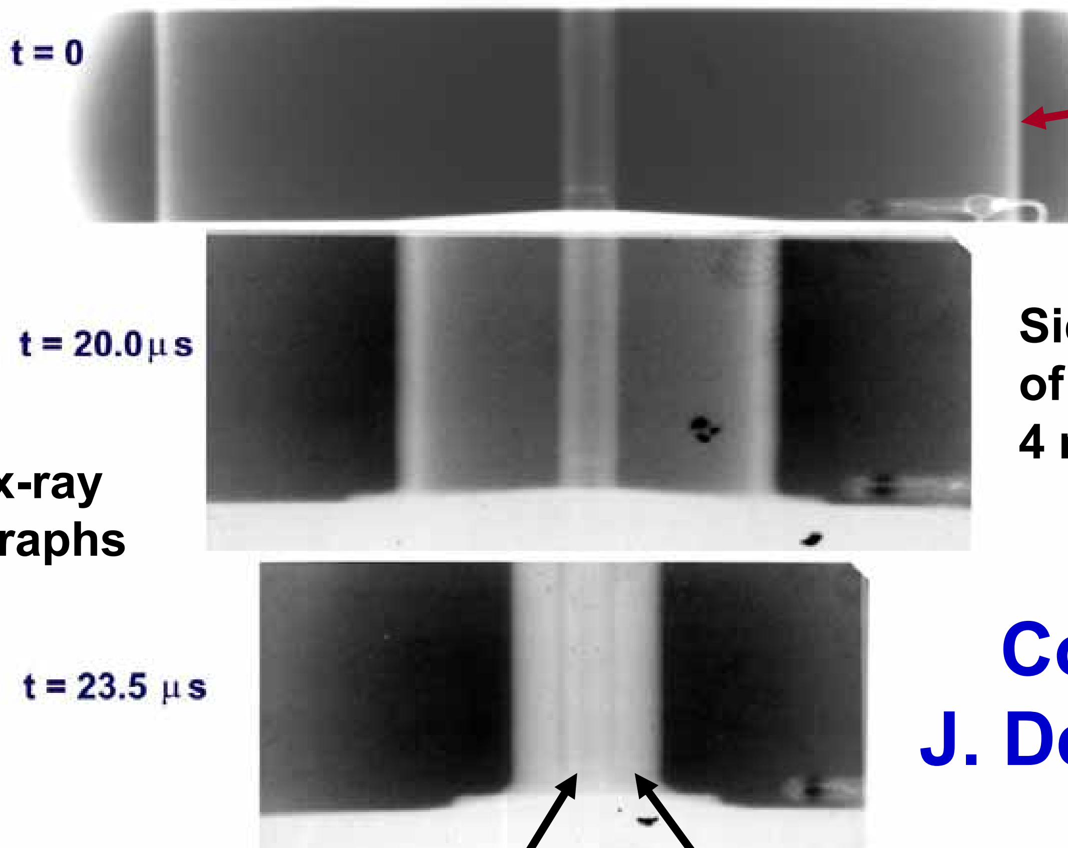

Initial 1-mm thick Aluminum liner

Side-on view of liner moving 4 mm/μs

Flash x-ray radiographs

Courtesy of J. Degnan, AFRL

Stationary 6-mm probe jacket

Elastic-plastic deformed 7-mm thick liner at 12:1 radial compression

Study liner physics with a z-pinch when surface conditions are similar

End view of cylindrical liner for axial flux compression before implosion

Metal conductor in Z pinch at peak current

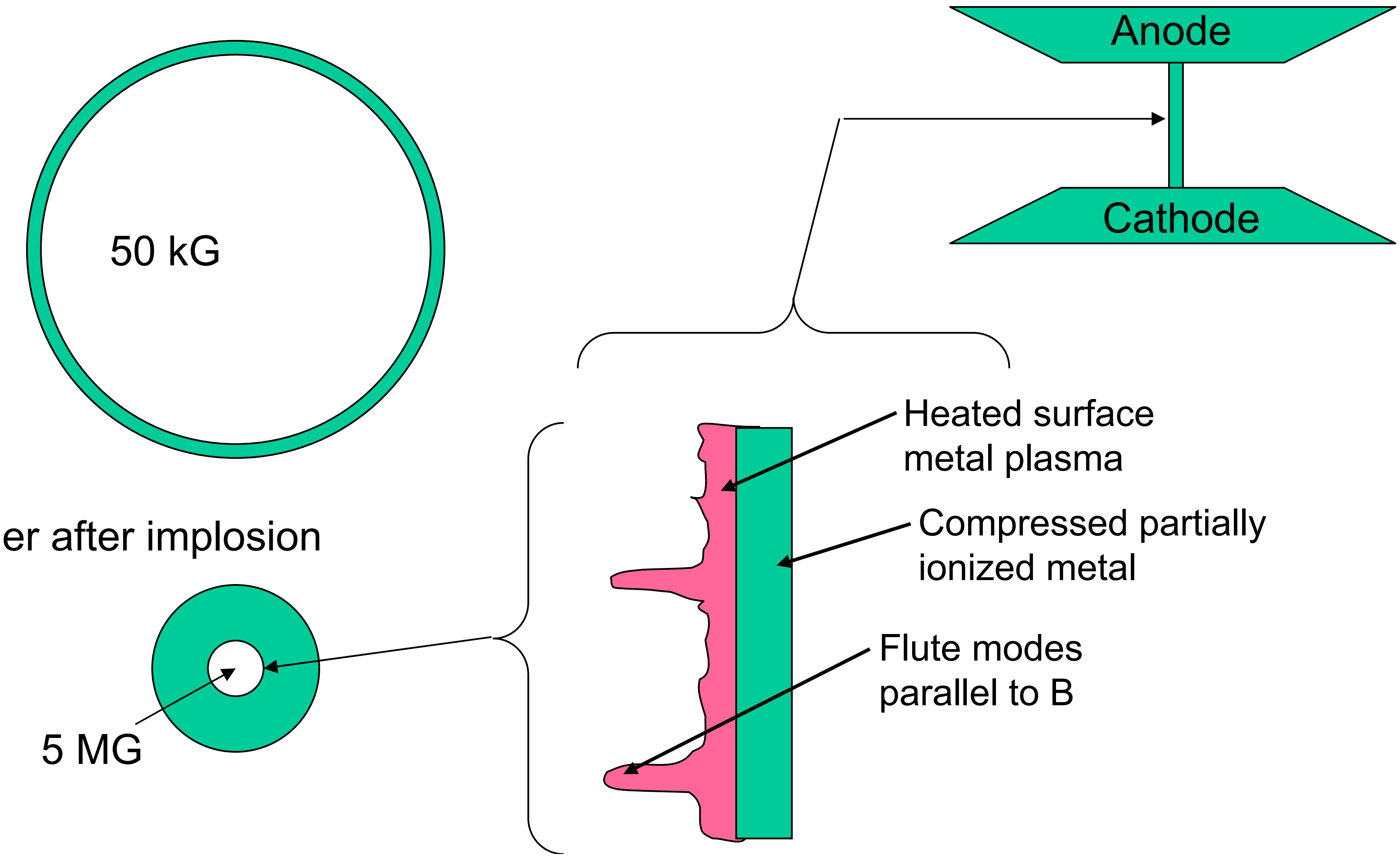

Regimes depend upon ratio δ/a = skin depth / radius

This is discussed in many places, eg., Knoepfel's book

Magnetic field diffusivity $\chi_B = \eta/\mu_0$ $\delta = \mathrm{sqrt}\,(\tau\,\chi_B)$

Define V_A with surface B field and internal metal density

Consider Ohmic heating of ionized metal with some <Z>

$\delta/a >> 1$

$kT \sim M_i\, V_A^2\, (\delta/a)^2$

Plasma pressure >> magnetic pressure

Regime of exploding wires

$\delta/a << 1$

$kT \sim M_i\, V_A^2$

Plasma pressure ~ magnetic pressure

Regime of liner surfaces

B is limited by stability

Assuming rod with density ρ will disrupt after time τ

$$\tau \sim \frac{R}{V_A} = f_s \frac{R}{B}(\mu_0 \rho)^{1/2}$$

where f_s is a semi-empirical number

then rod radius should be chosen based on current I and rise-time τ

$$R = \left(\frac{\mu_o I \tau}{2\pi f_s}\right)^{1/2} \frac{1}{(\mu_o \rho)^{1/4}}$$

thus $$B = \left(\frac{\mu_o f_s I}{2\pi\tau}\right)^{1/2} (\mu_o \rho)^{1/4}$$

2D simulation suggests stability $f_s \sim 6$

Metal density contours

Initial rod surface

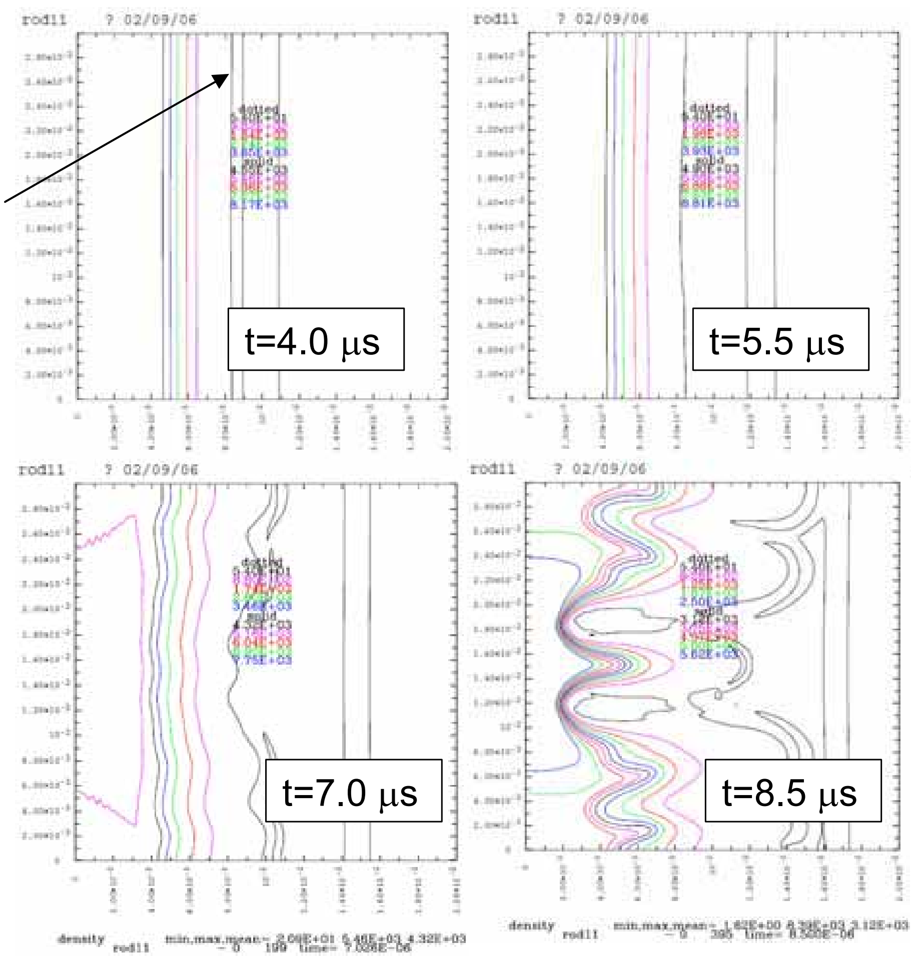

Current: Sine wave to 20 MA in 6 μs

z

r

Minimum rod radius & maximum B are constrained by stability for given current & rise time

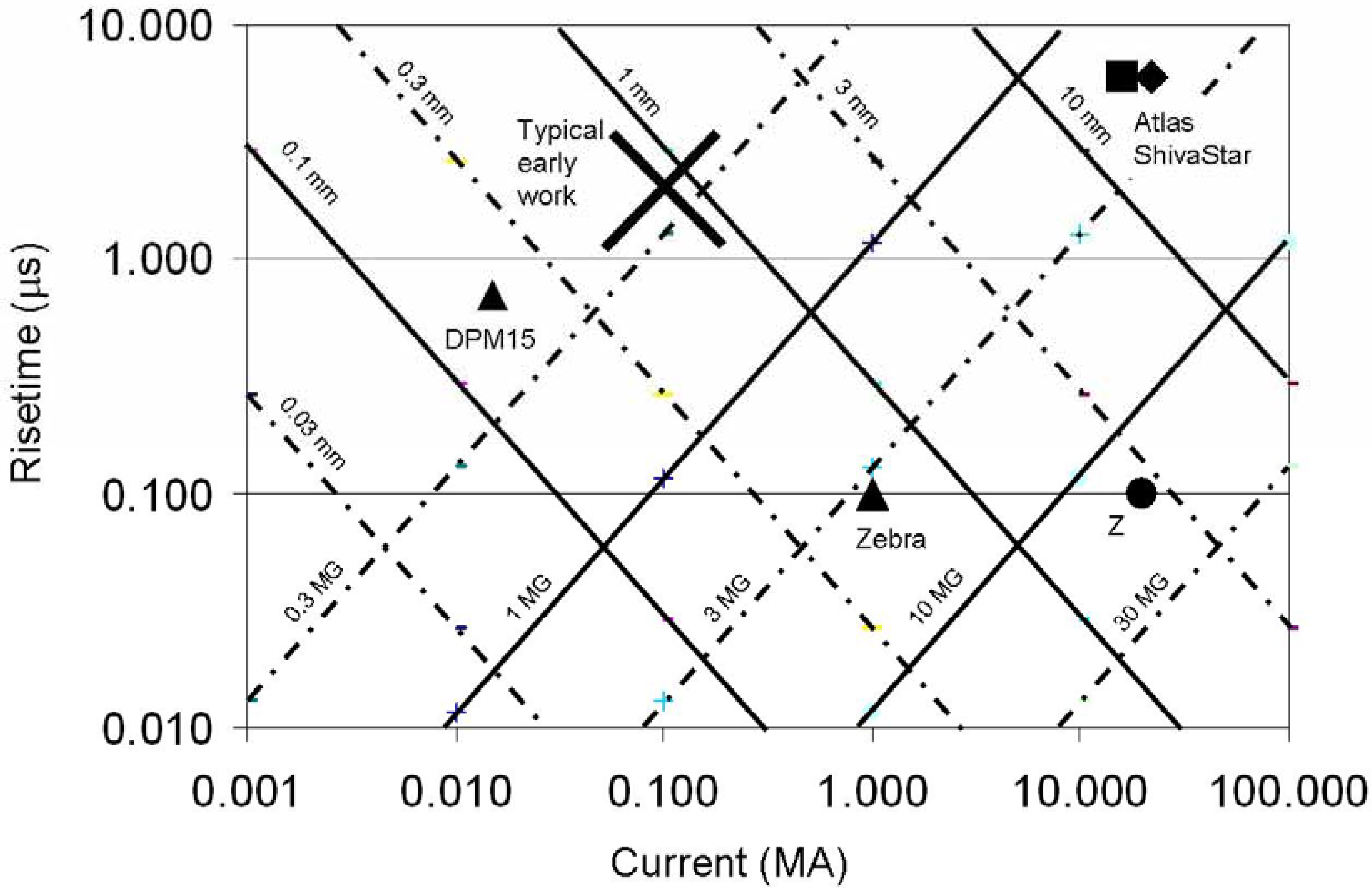

Pulsed Power Facilities

Atlas at
Nevada Test Site

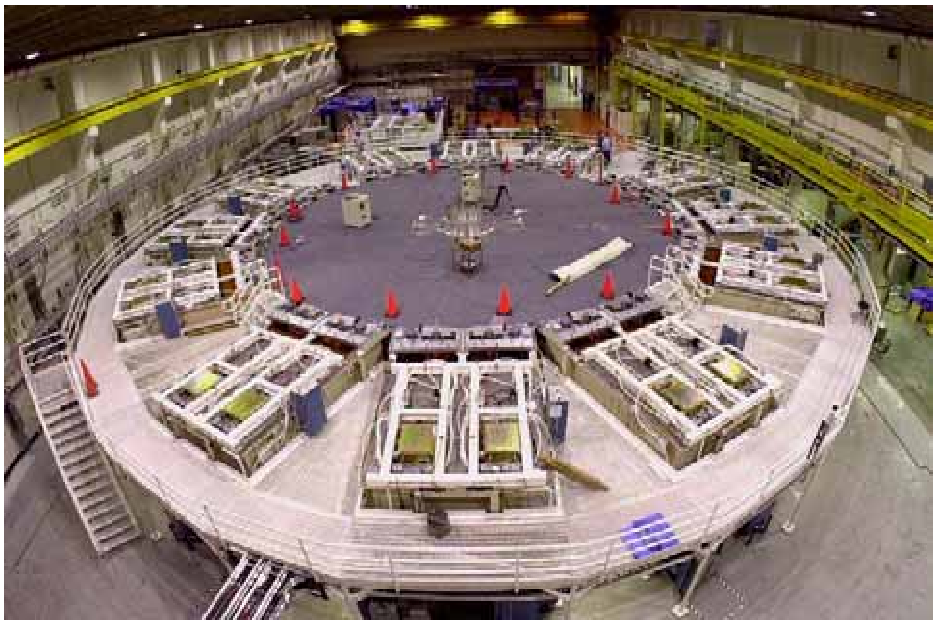

24 MJ
30 MA
6 μs

Shiva Star at
Air Force Research Laboratory

10 MJ
12 MA
10 μs

Zebra delivers two trillion watts

Typical operation:

Marx charged to	85 kV	Load current	0.9 – 1 MA
Stored energy	150 kJ	Rise-time	70 ns (10%-90%)
PFL voltage	2.2 MV	Current rise	10^{13} A/s (10 kA/ns)

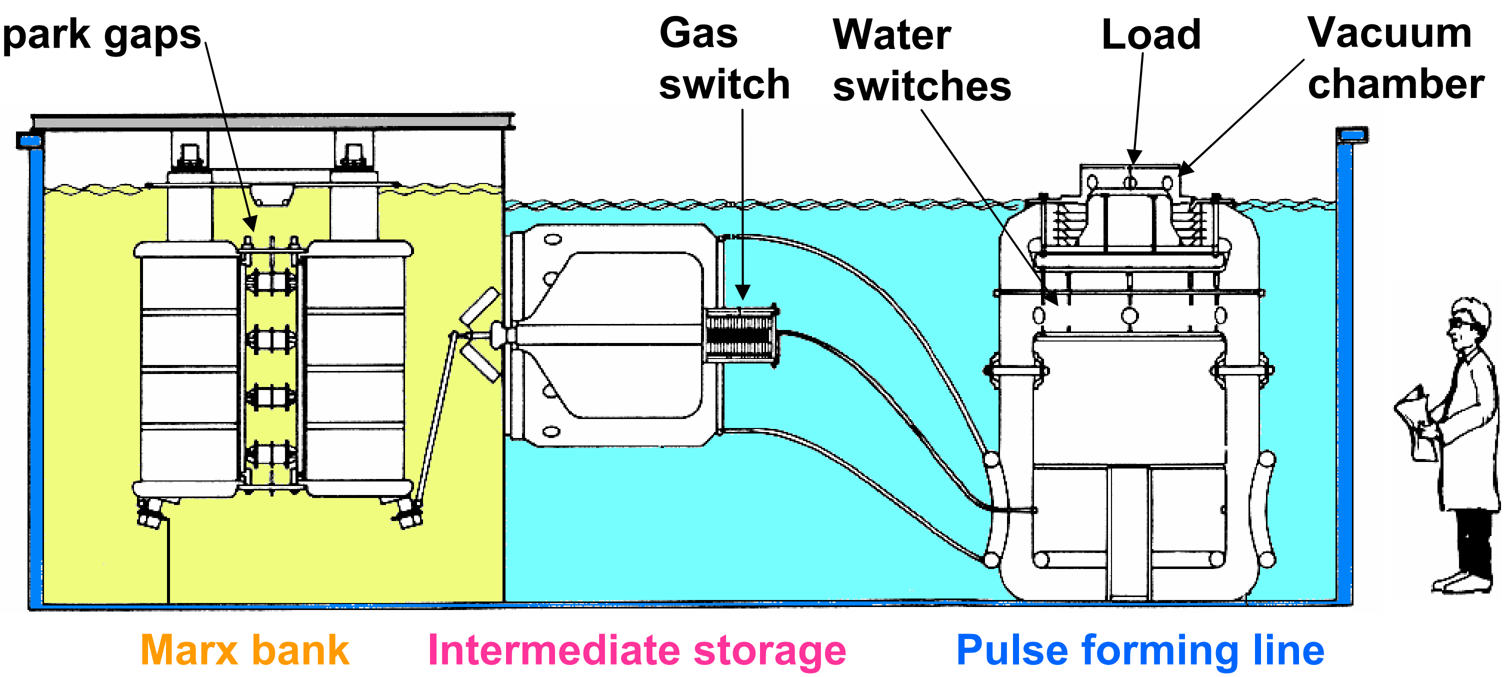

Aluminum mm-wire experiments

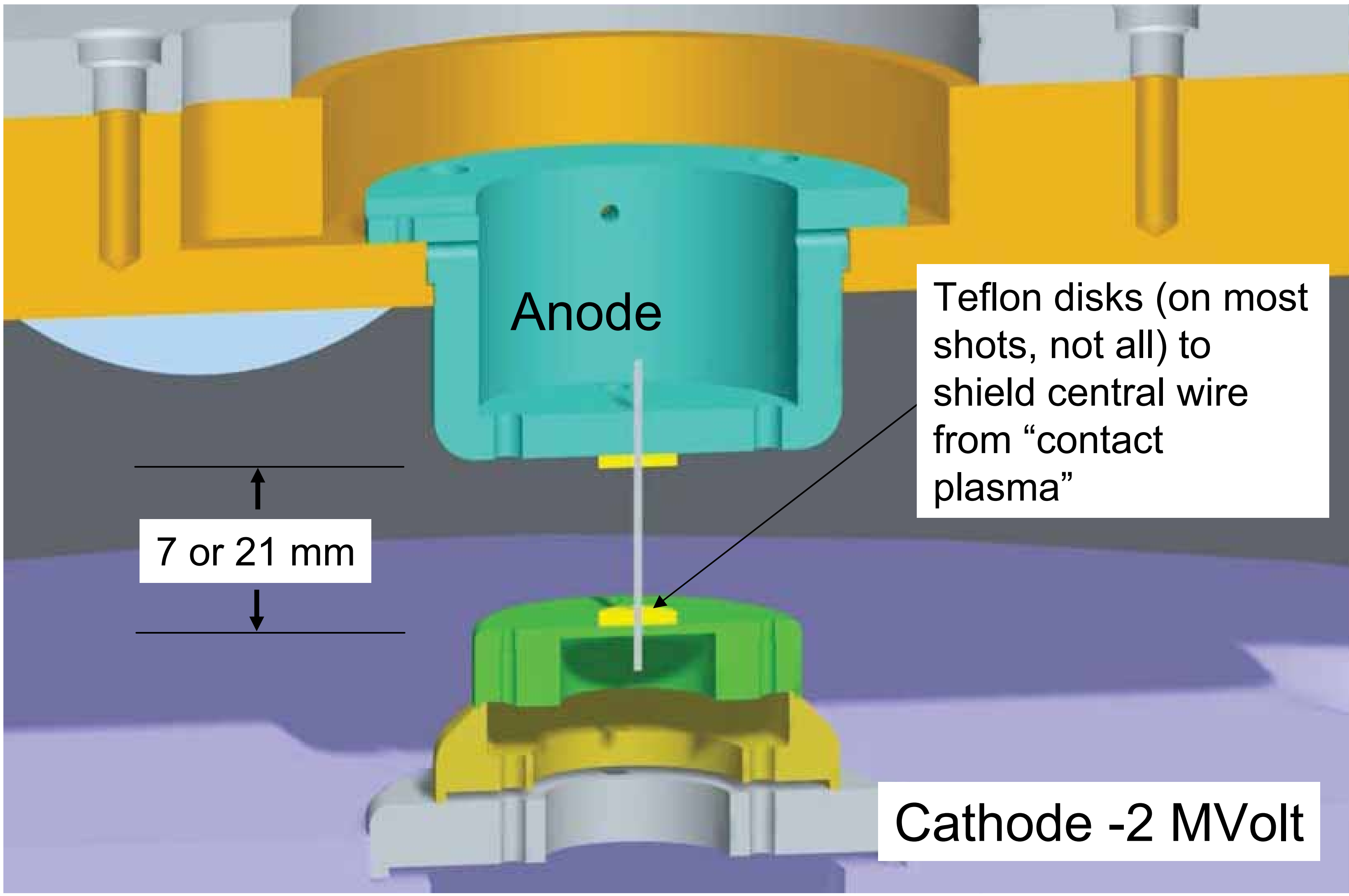

5-ns light emission images (ICCD)

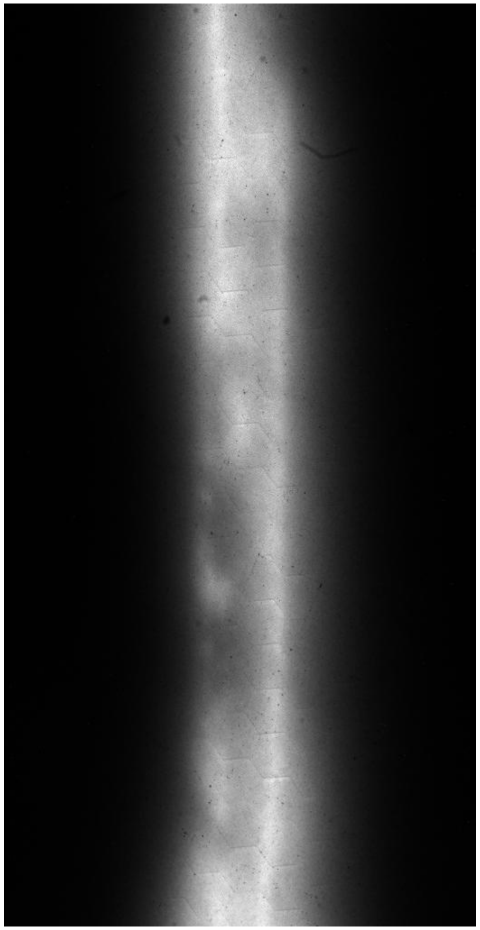

Non-uniform light

21-mm-long aluminum 1100 **wire**
no Teflon (shot 878 at 306 ns)

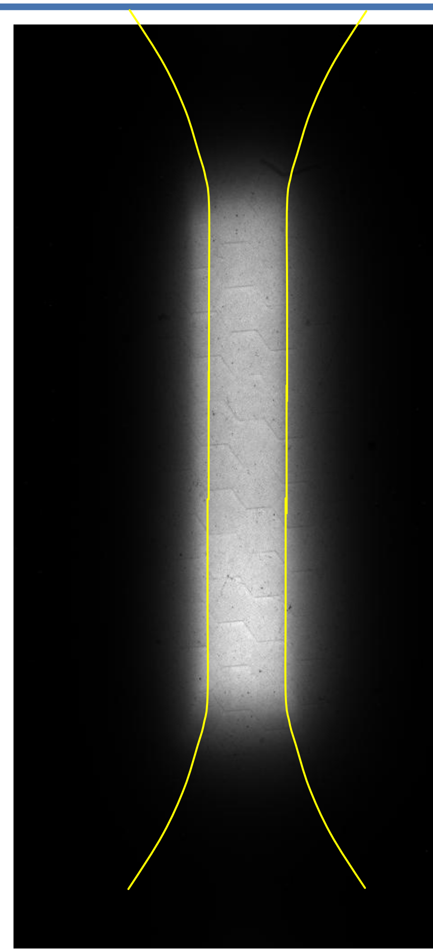

Uniform light

Hourglass 7-mm-long
machined aluminum 6061
(shot 891 at 330 ns)

Hourglass interferograms (V. Ivanov)

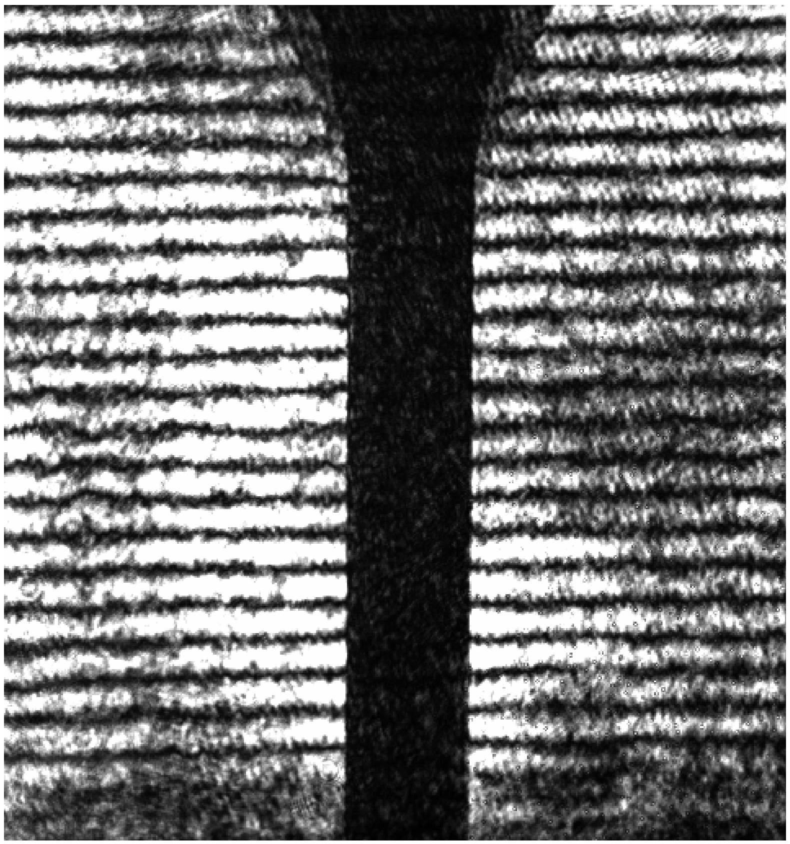

Reference for 1mm hourglass

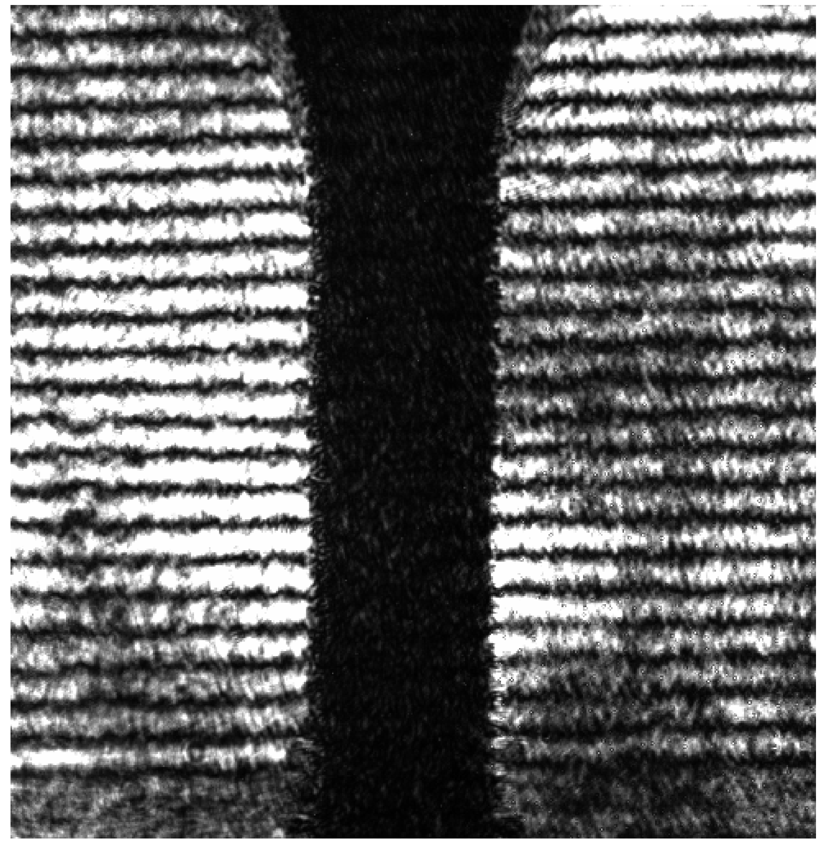

Time = 336 ns; shot 890

1-mm Al wire on streak camera

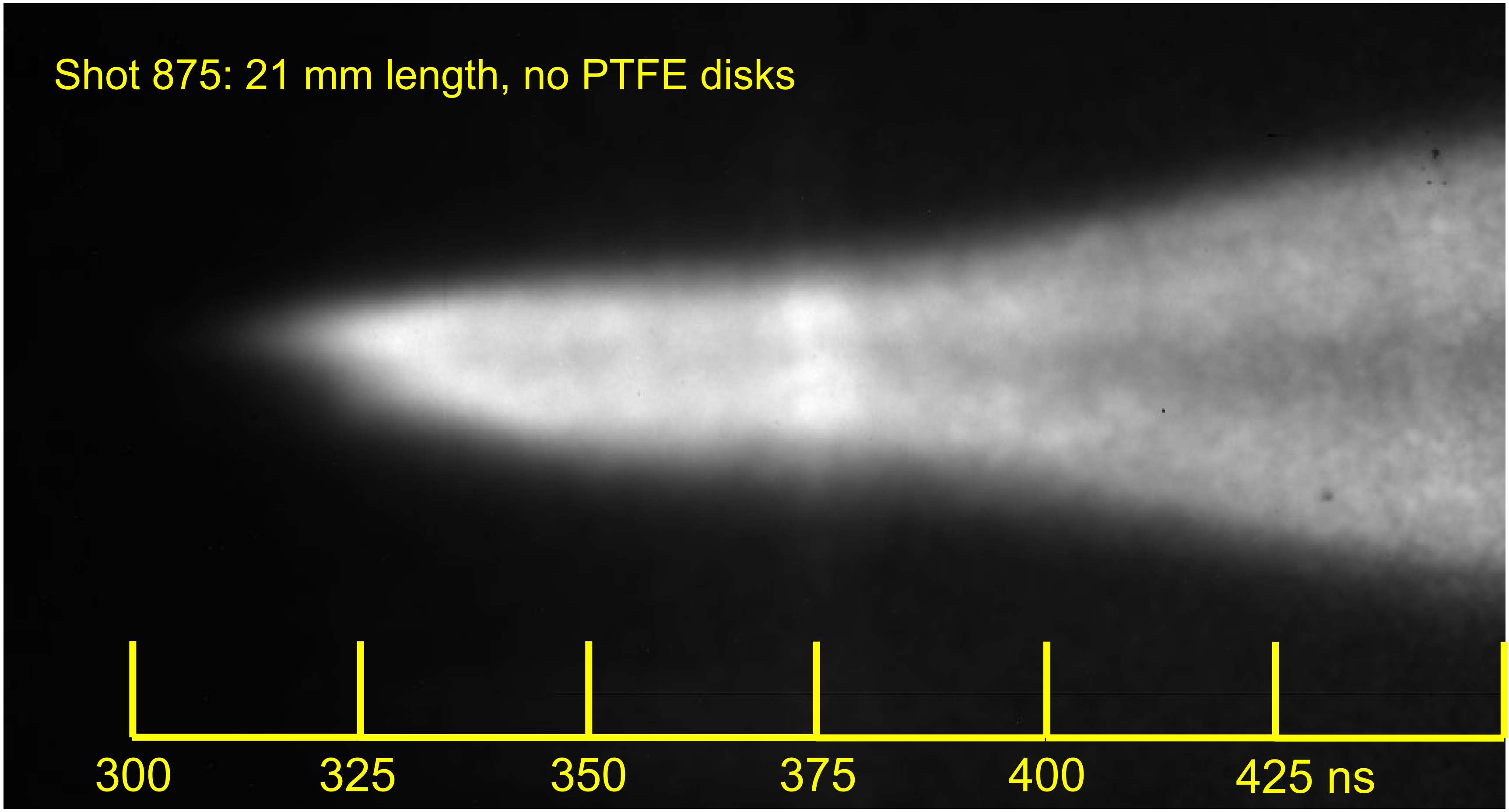

The new ‘hourglass’ load design

Extra care was taken to shield the 1mm thin central wire feature from arcs where the load makes contact with the current carrying hardware.

Streaked self-emission & laser shadowgrams show consistent plasma expansion

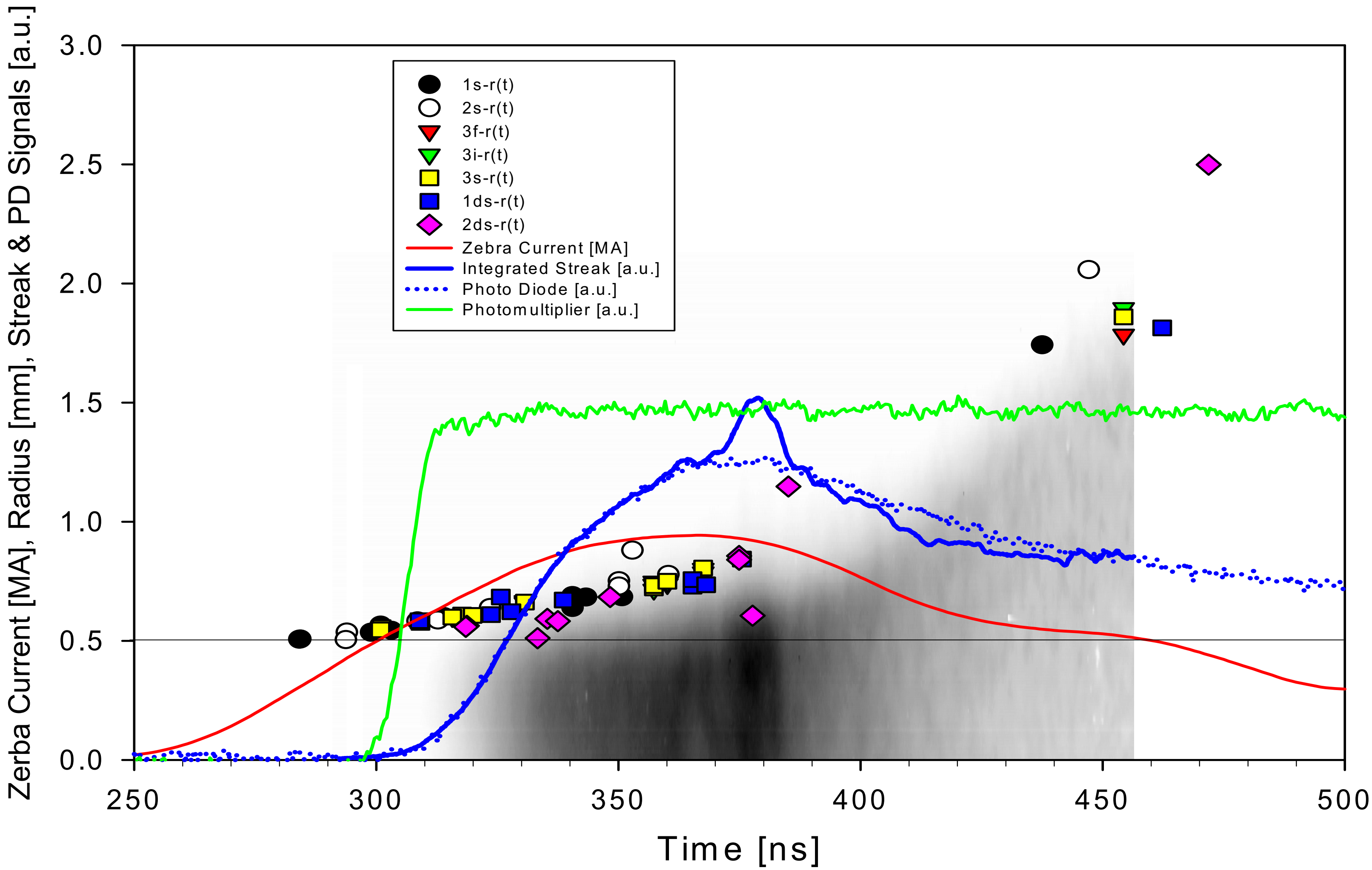

SF, BSB 2/09/07

Hourglass interferograms (V. Ivanov)

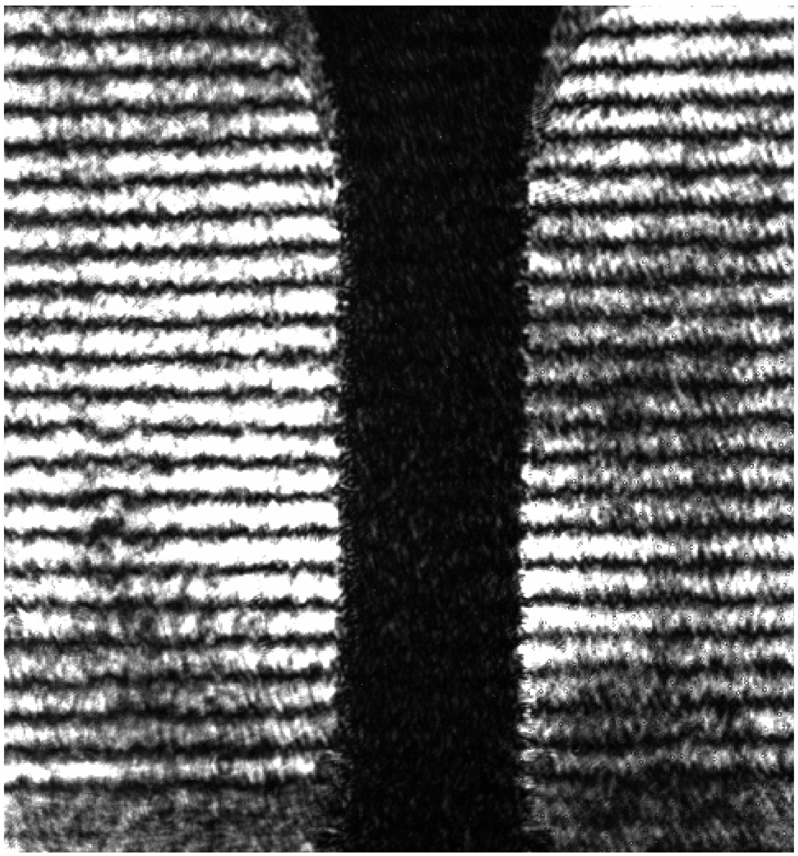

Time = 336 ns; shot 890

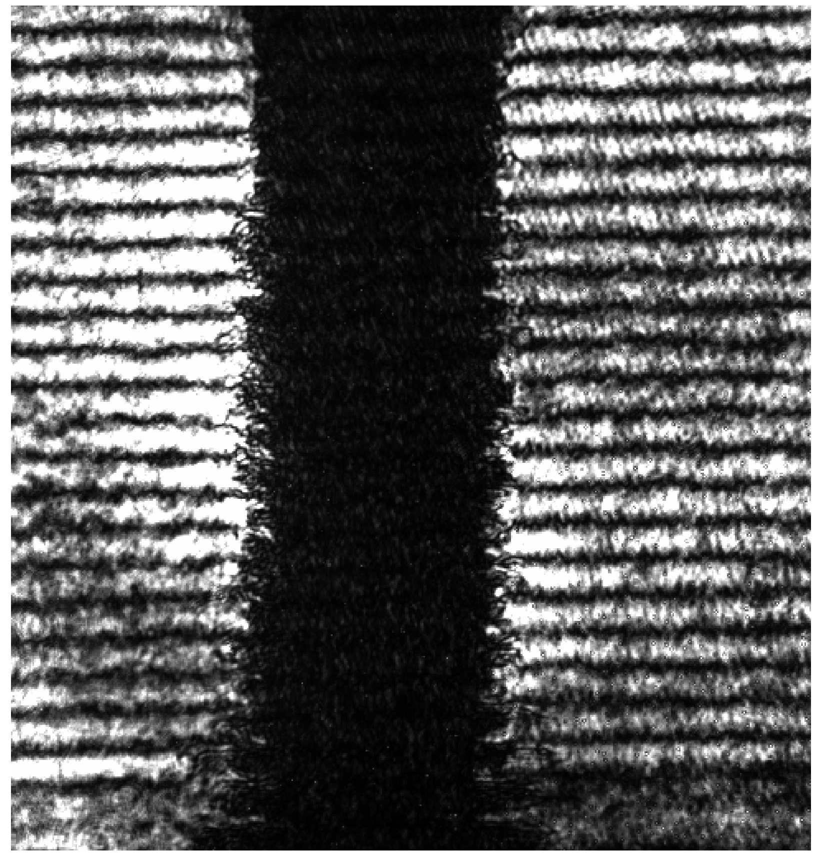

Time = 360 ns; shot 891

Streak of hourglass emission

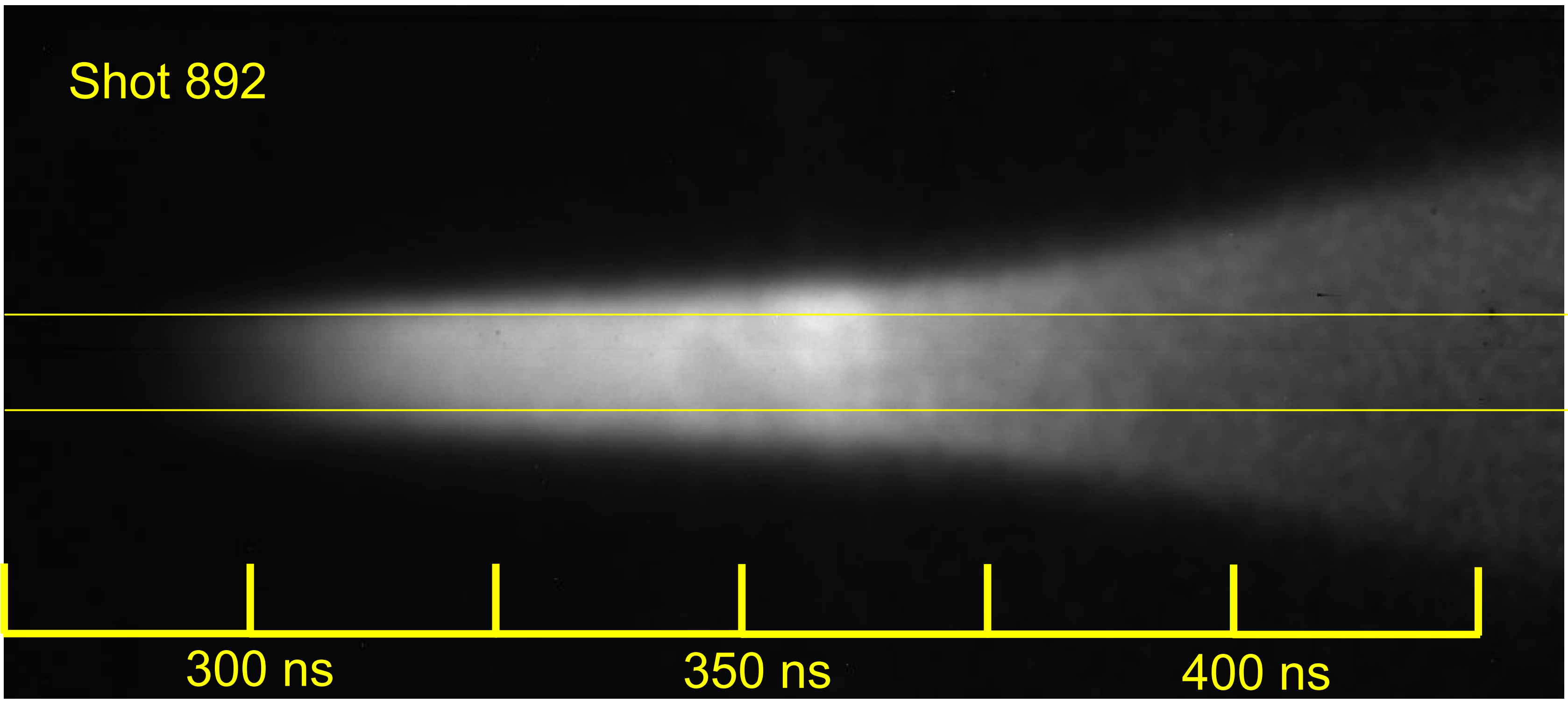

Simulation of B diffusion

- Surface plasma results from Ohmic heating
- Correct numerical modeling depends upon:
  -- careful zoning,
  -- material properties (significant uncertainty)
  -- radiation transport plus electron thermal conduction
- Plasma forms at surface when B ≅ 3 MG
- For B < 10 MG, small fraction of current flows in the surface plasma

δB due to surface plasma

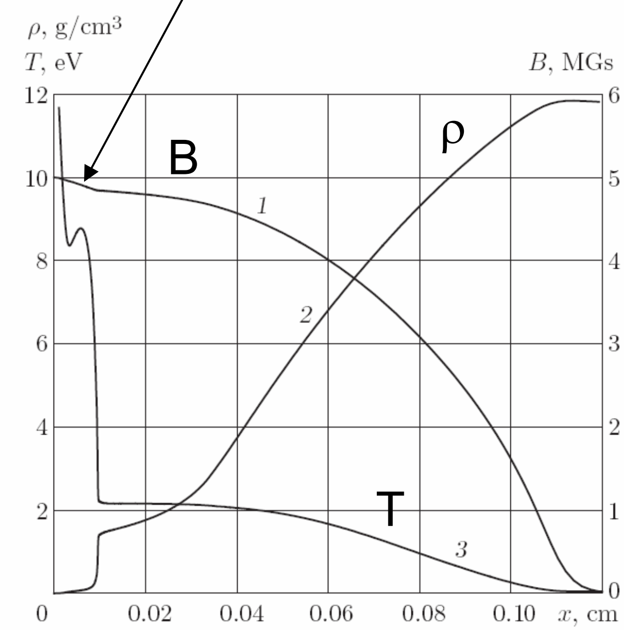

Fig. 3. Spatial curves of the magnetic field $B(x)$ (1), material density $\rho(x)$ (2), and material temperature $T(x)$ (3) calculated for an open system with a linearly increasing magnetic field at the boundary for $dB_0/dt = 5$ MGs/μsec at $t = 1$ μsec.

S.F. Garanin, G.G. Ivanova, D.V. Karmishin, and V.N. Sofronov, *Diffusion of a megagauss field into a metal*, J. of Applied Mechanics and Tech. Physics **46**, 153 (2005).

Electrical conductivity varies by table

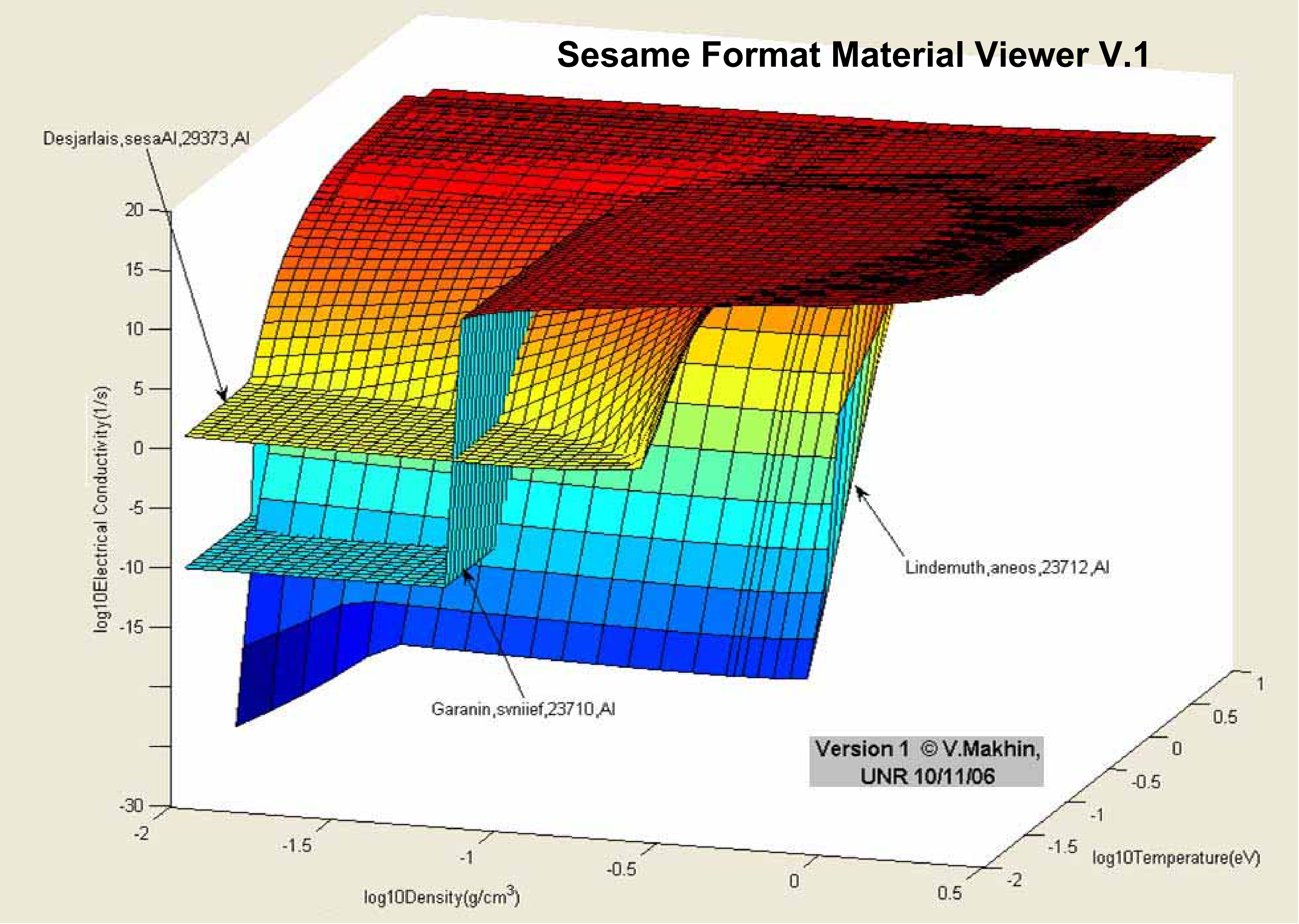

MHRDR rad-MHD modeling finds plasma formation on surface

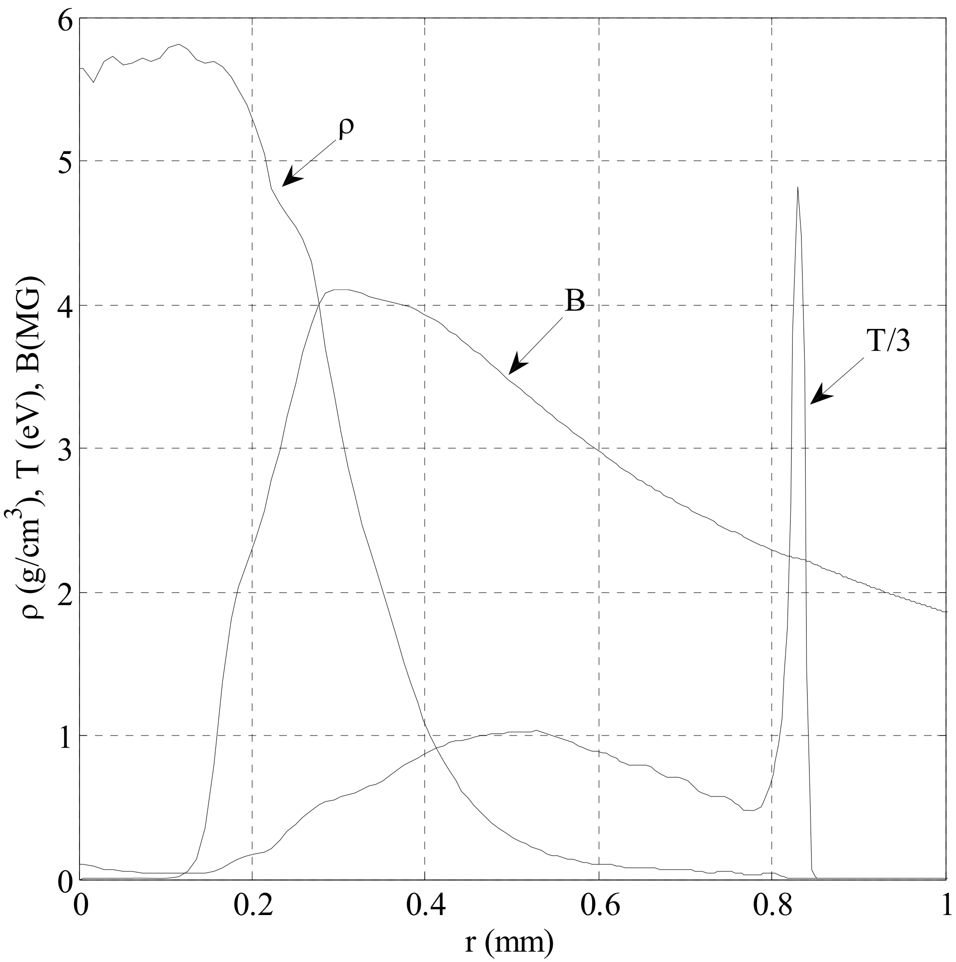

Density, B, and temperature vs. radius, at 170 ns (I = 935 kA)

Conclusion

- ✓ **MTF is an exciting possibility for economical fusion**
- ✓ **MTF liner physics is being cost-effectively studied by using a z-pinch configuration**
- ✓ **The effect of multi-MG field with $\delta/a < 1$ is being studied with experiments on the 1-MA Zebra z-pinch**
- ✓ **Hourglass-shaped loads emit most uniform light => may compare best with 1-D modeling**
- ✓ **Comparisons with rad-MHD models show promise**

Diagnostics for ion beam driven targets and warm dense matter experiments

Frank Bieniosek, Pavel Ni
for the HIFS-VNL

IFE Science and Technology Strategic Planning Workshop

April 24-27, 2007

Ion beams provide an excellent tool to generate homogeneous, volumetric warm density matter.

- Warm dense matter (WDM)
  - T ~ 0.1 to 10 eV
  - ρ ~ 0.01 -1 * solid density
- Techniques for generating WDM
  - High power lasers
  - Shock waves
  - Pulsed power (e.g. exploding wire)
  - Intense ion beams
- Some advantages of intense ion beams
  - Volumetric heating: uniform physical conditions
  - Any target material
  - High rep. rate
  - Benign environment

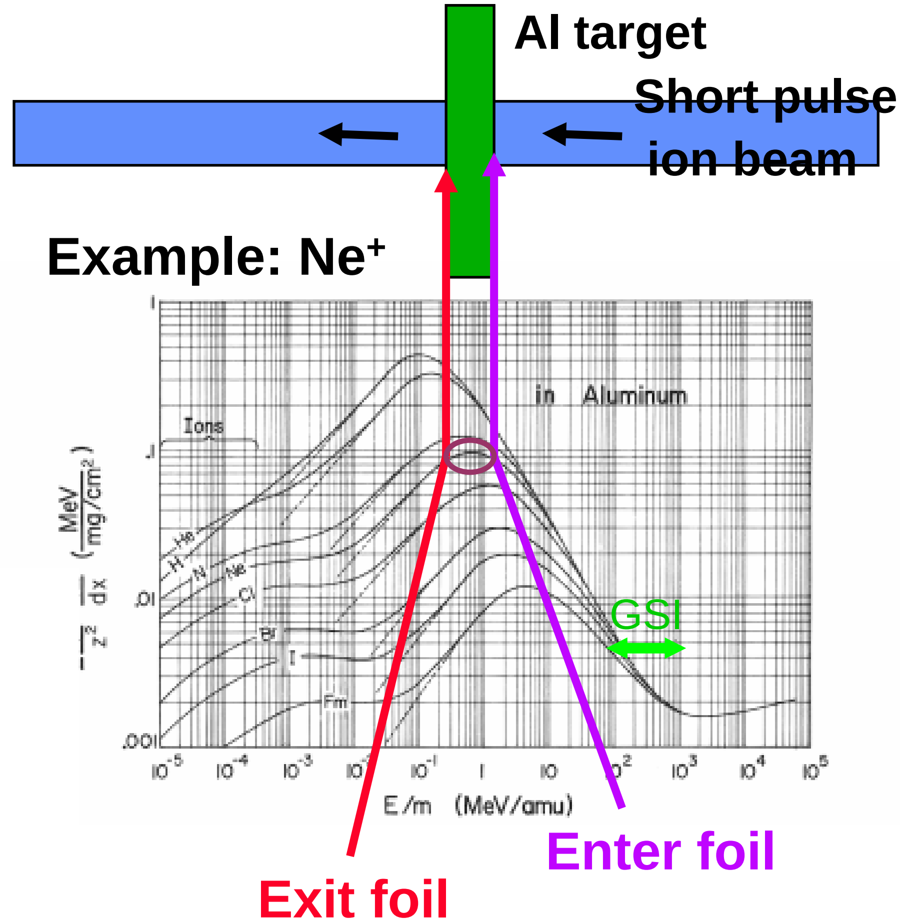

L. Grisham, Phys. Plasmas 11 (2004) 5727.

First experiment: Check WDM atomic models using transient darkening of quartz at low temperature.

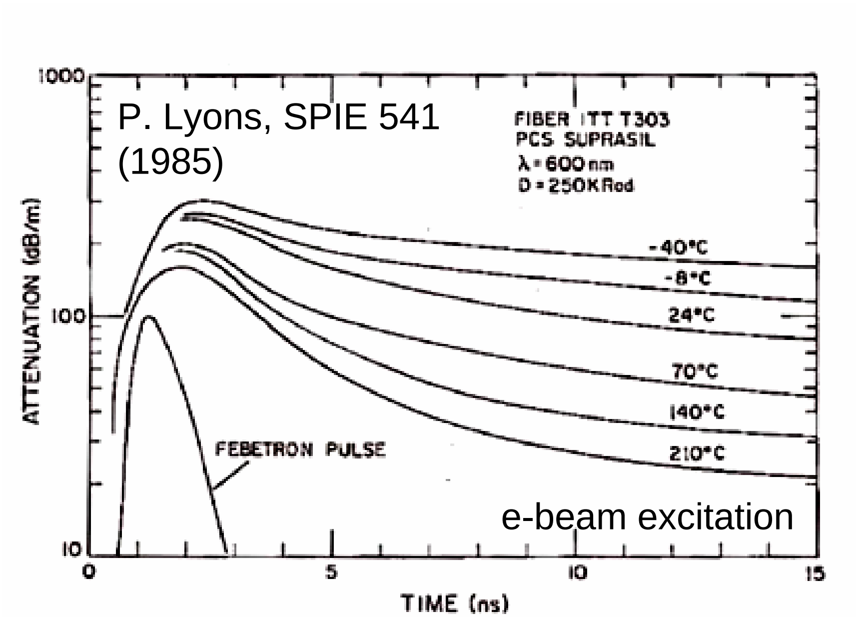

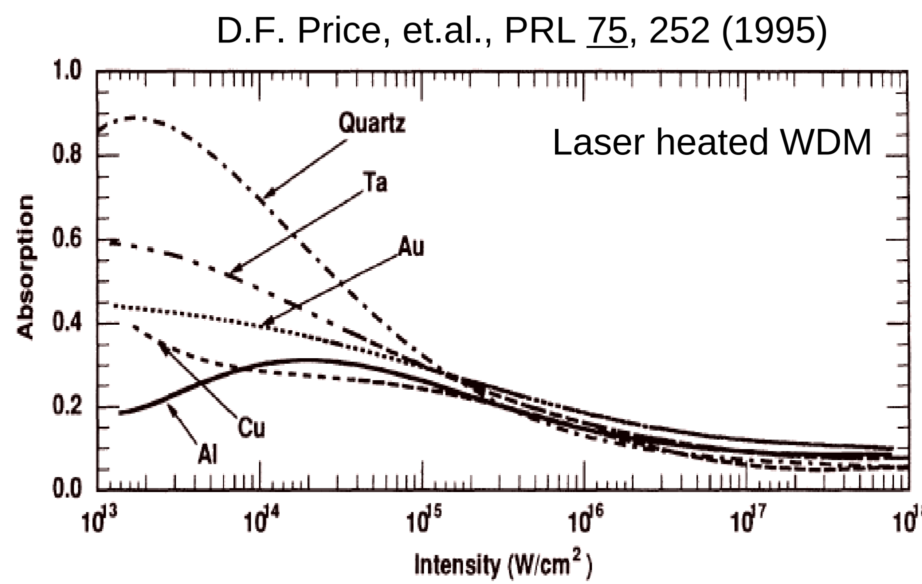

In quartz, electrons excited from 2s, 2p (ground state) to 3s leave holes in ground state to absorb photons in both cases. Measure decay rate of excited electrons by studying decay of absorption and emission rates.

Significance: interpret WDM data, possible temperature measurement, fast switching of optical properties

Initial transient darkening experiments in quartz fiber (with H. Yoneda, U. of Electro-communications, Tokyo).

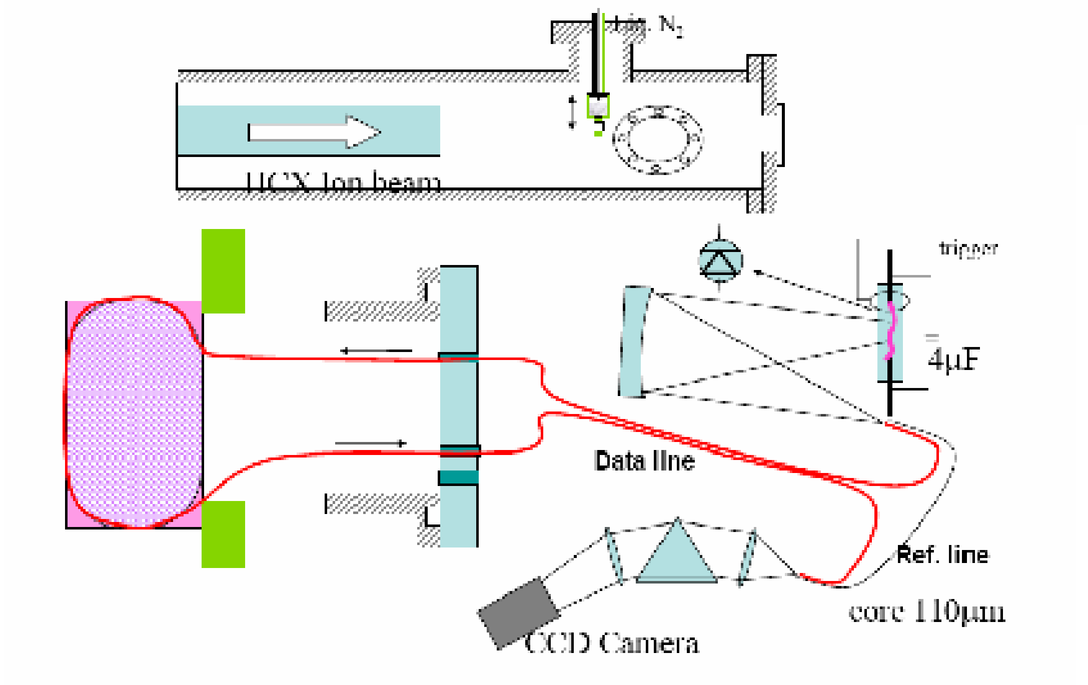

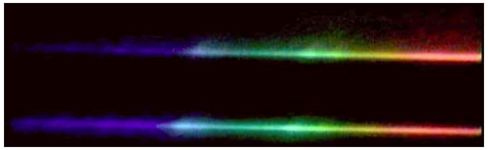

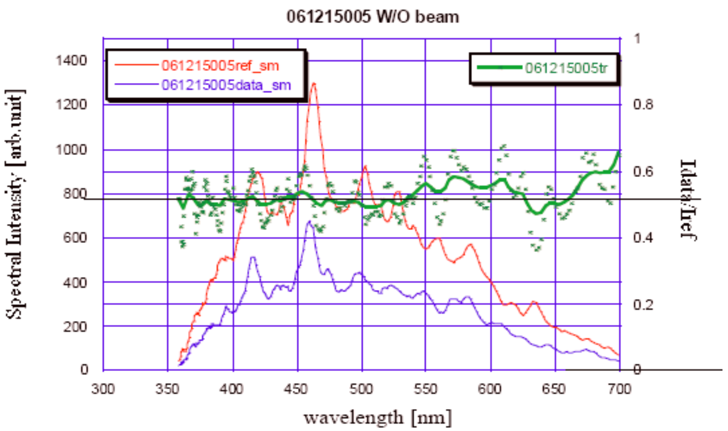

No beam

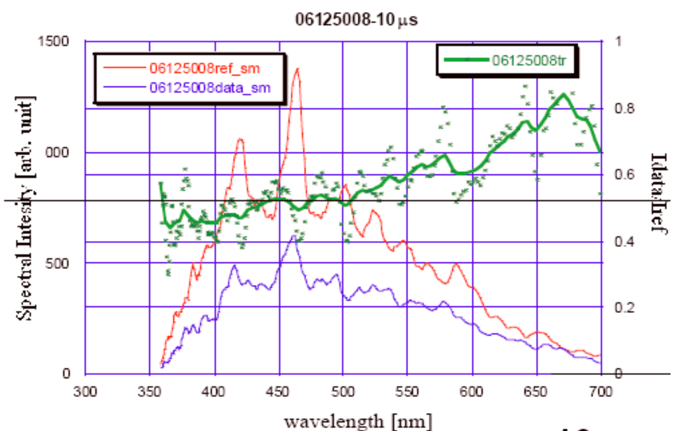

10μs

Optical transmission experiment: look for difference in fiber transmission with and without beam.

Modeling of effect of ion beam on optical fiber transmission is going on.

Porous target experiment Dec. 2006 at GSI HHT target station (with GSI Plasma Physics group; IPCP Chernogolovka; ITEP Moscow).

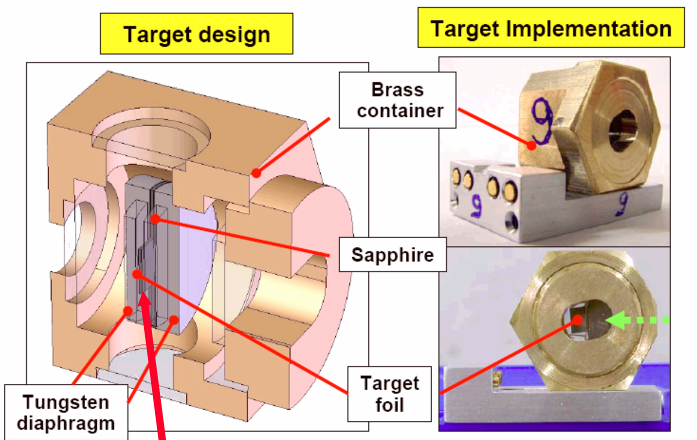

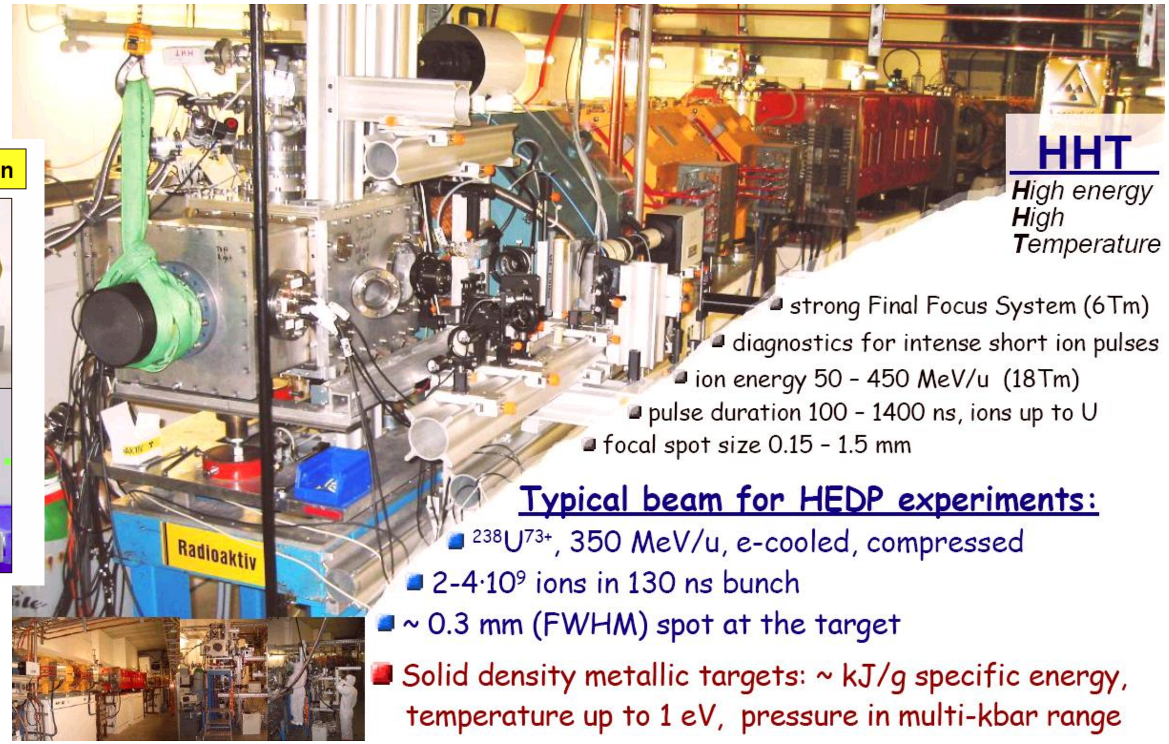

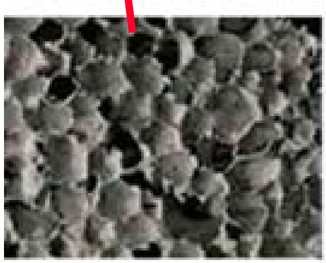

- Replace target foil with porous material.
- Study effect of pore size on target behavior using existing diagnostics.
- Sample targets: LLNL (Au, 50 nm), Mitsubishi (Cu, 50 micron).

Data analysis from GSI experiments is underway.

- **Gold targets heated to about 6000 K (T-boil = 2435 K). Solid and porous gold targets show similar behavior (temp, 1.4 km/s expansion).**

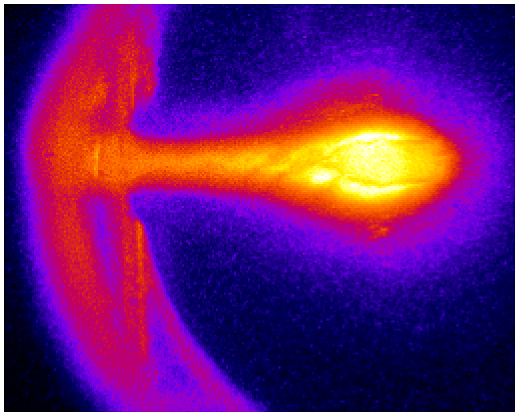

solid gold (note Bragg peak)

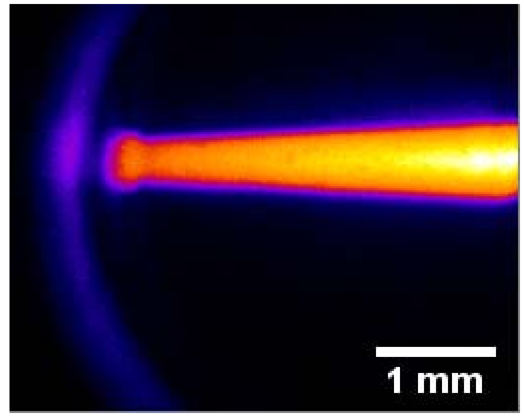

Porous gold

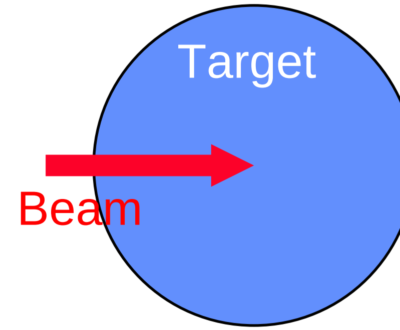

- **Copper targets heated to about 3000 K (T-boil = 3200 K). Porous copper broke up into droplets.**

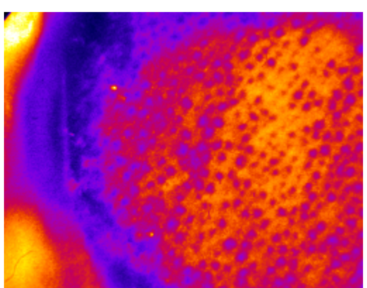

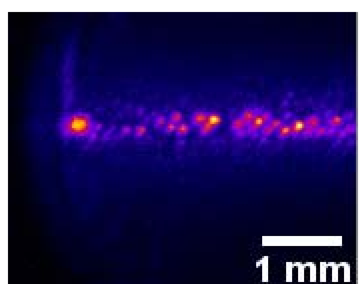

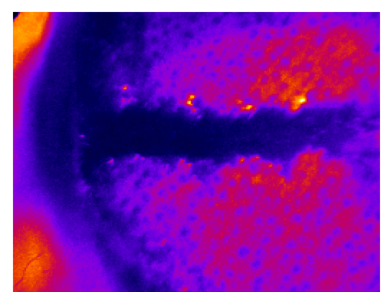

Porous copper – before, during, after beam pulse

WARM DENSE MATTER EXPERIMENTS
PROTOTYPE TARGET CHAMBER

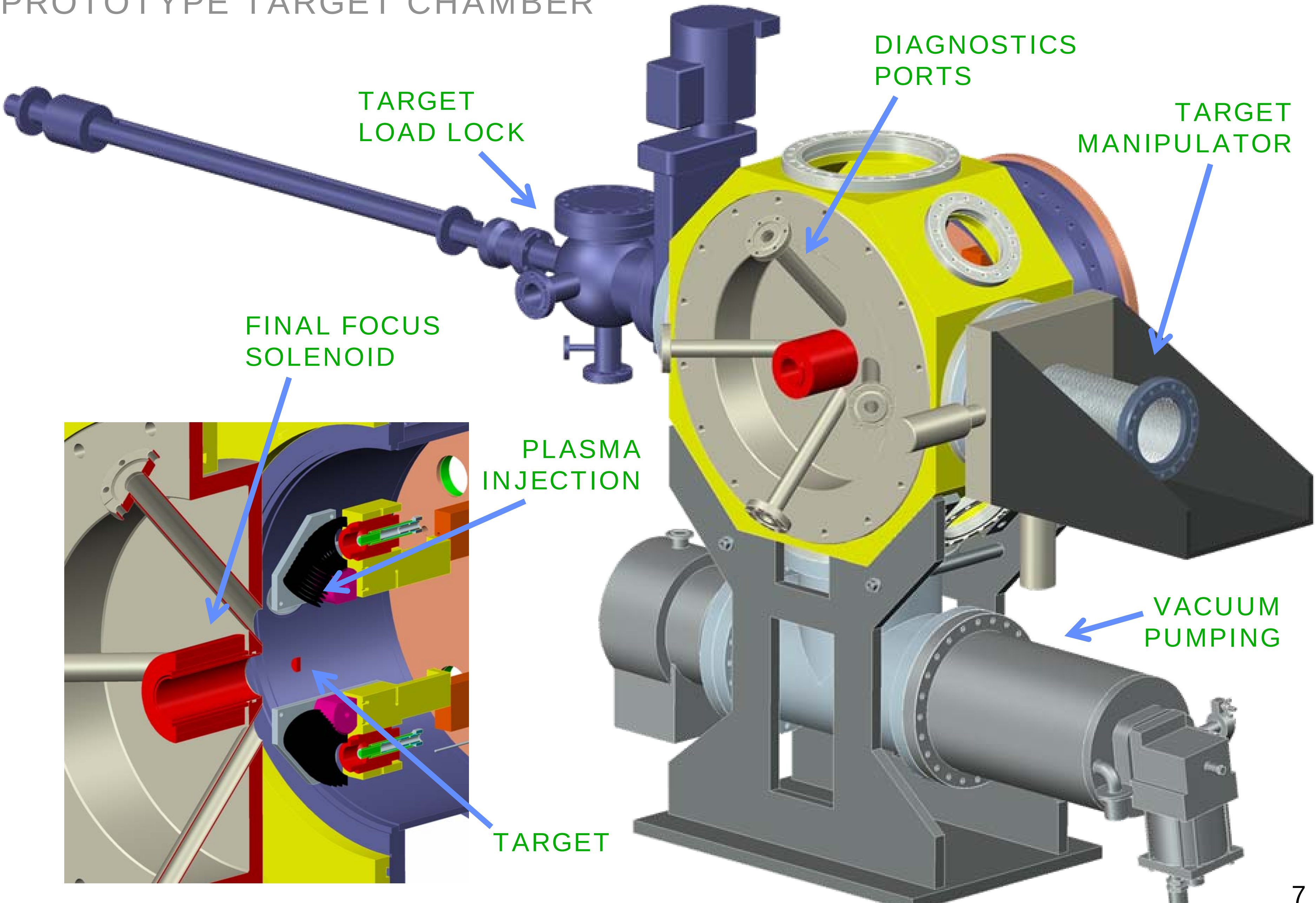

PROTOTYPE TARGET MODULE

(Size: 5.66 cm wide, 2.29 cm high)

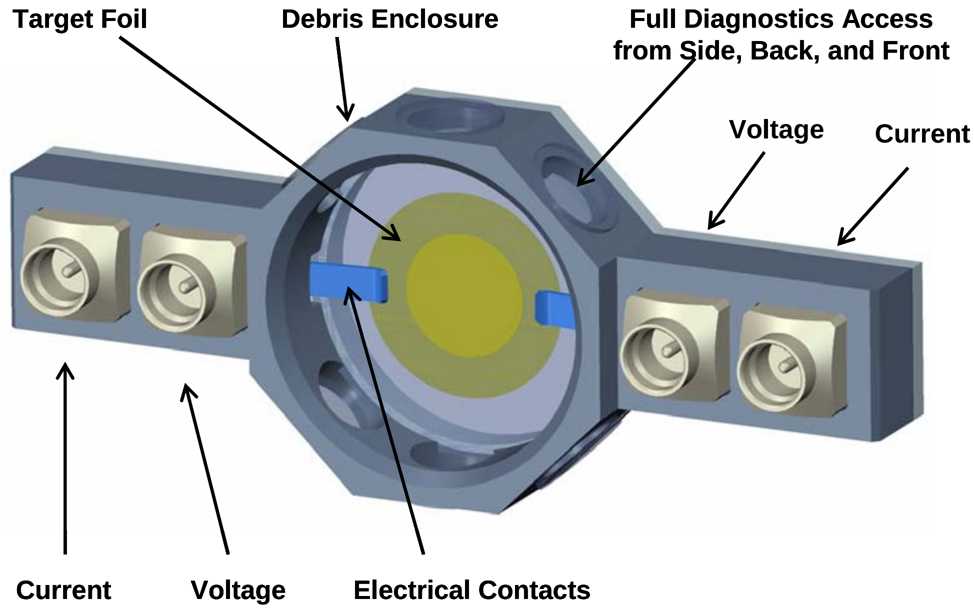

TARGET CHAMBER UNDER CONSTRUCTION

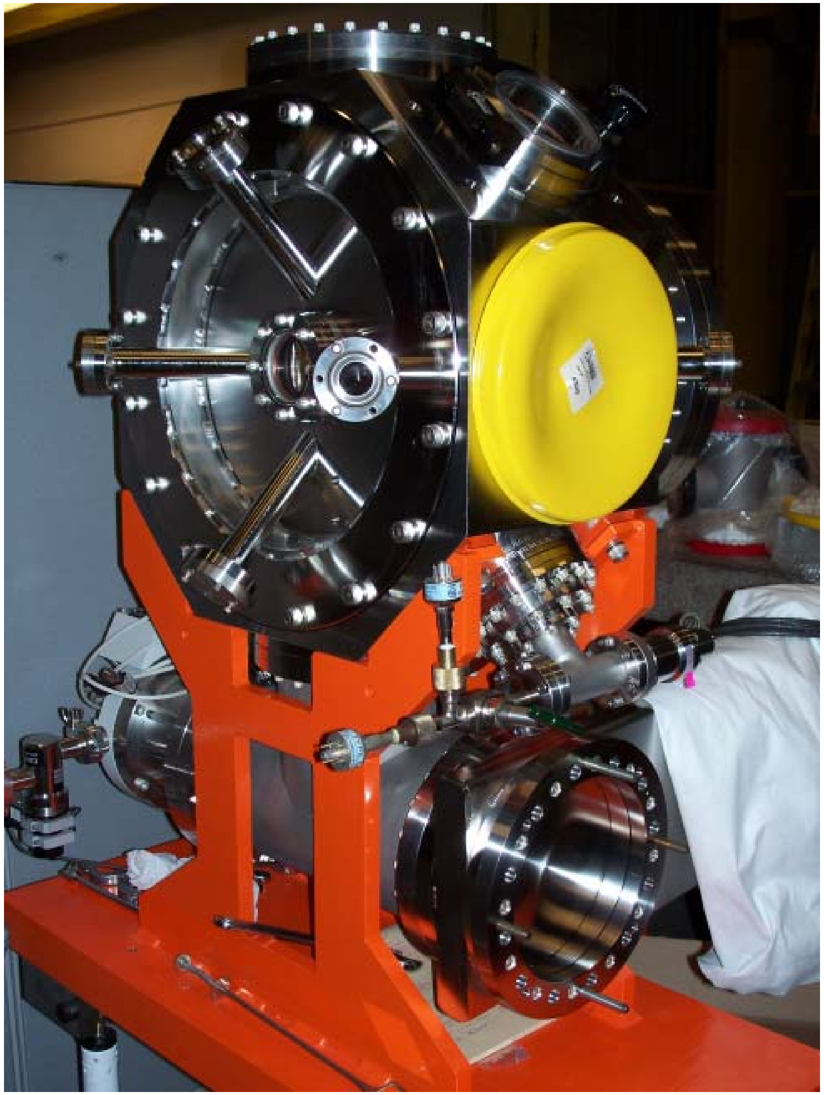

Target diagnostics - 1

- **Fast optical pyrometer**
  - **fast response (<1 ns) and improved sensitivity at lower threshold temperature**
  - **Temperature accuracy 5% for T>1000 K**
  - **Position resolution about 400 micron**
  - ***Parts are being ordered – to be assembled in FY07***

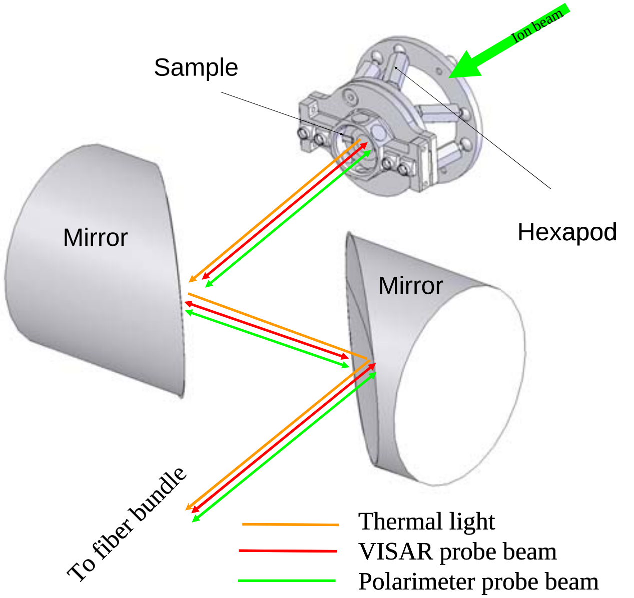

- **Fiber-coupled VISAR system – *completed bench test***
  - **Martin Froescher & Associates**
  - **ps resolution**
  - **1% accuracy**

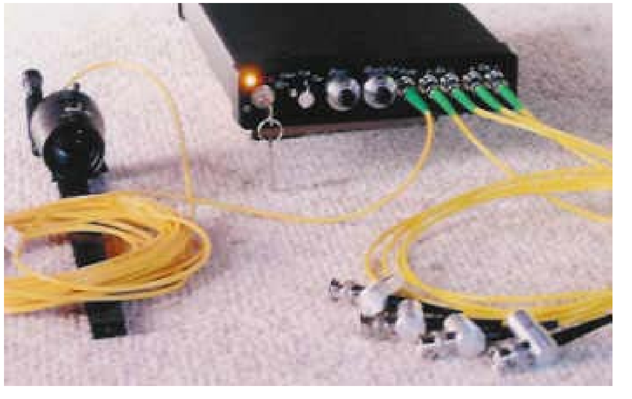

- **Hamamatsu visible streak camera with image intensifier**
  - **ps resolution**
  - ***arrived Feb. 2007***

Target diagnostics - 2

- **Princeton Instruments PI-MAX cameras (*2 on hand*) for single frame images of target – 16 bits, 512 x 512, 1 ns and 10 ns resolution.**

- **Electrical conductivity**
  - **initial test to be based on electrical transmission line circuit**
  - **conductivity may switch between insulator ←→ conductor**

- **Diagnostics to be developed include**
  - **Laser optical transmission/reflection/polarimetry**
  - **X-ray diagnostics**

Two-wavelength pyrometer (classical)

- -750 nm and 1400 nm channels
- -Fixed, high gain, broad band photo-receivers (conversion   gain up to 2.5 x 103 V/W)
- -180 ps temporal resolution
- -High sensitivity, can measure down to 1000 K
- -Ideal for initial experiments
- -Can be used for target “preheat” measurements

Working scheme:

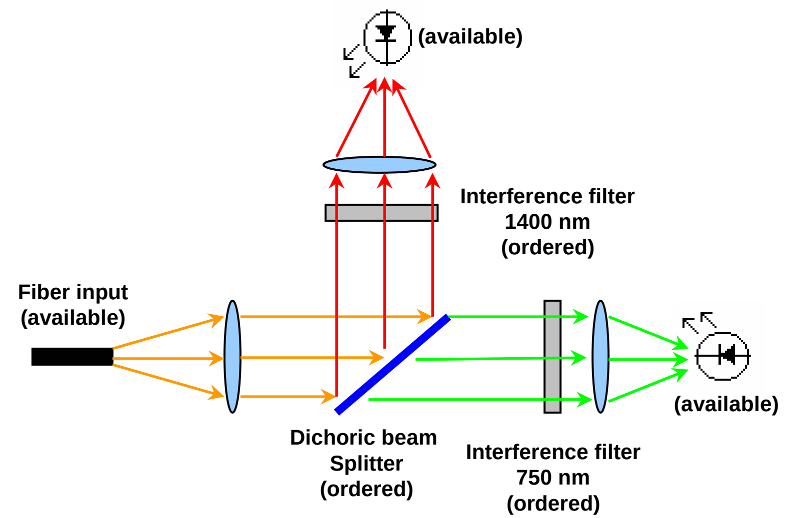

CAD model:

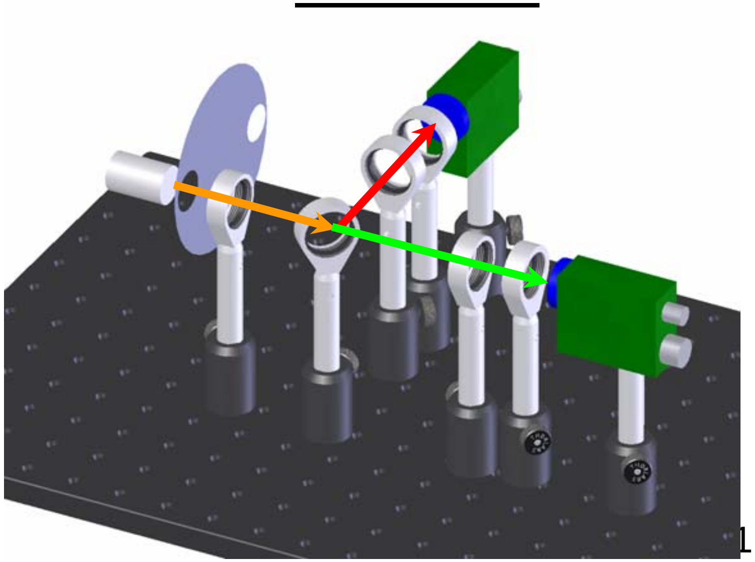

Radiance calibration with tungsten strip lamp (ordering)

Calibration lamp: Osram W 17/G

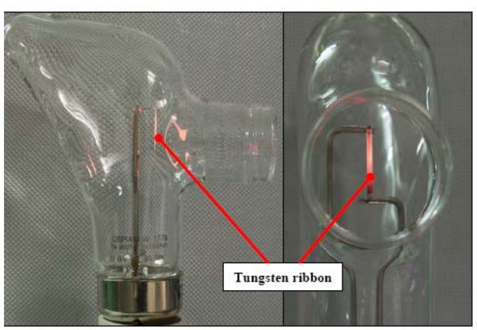

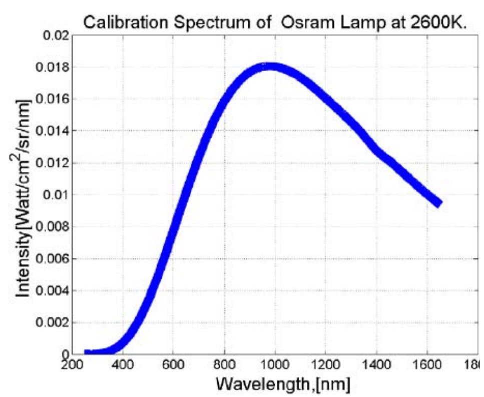

Streak pyrometer (new)

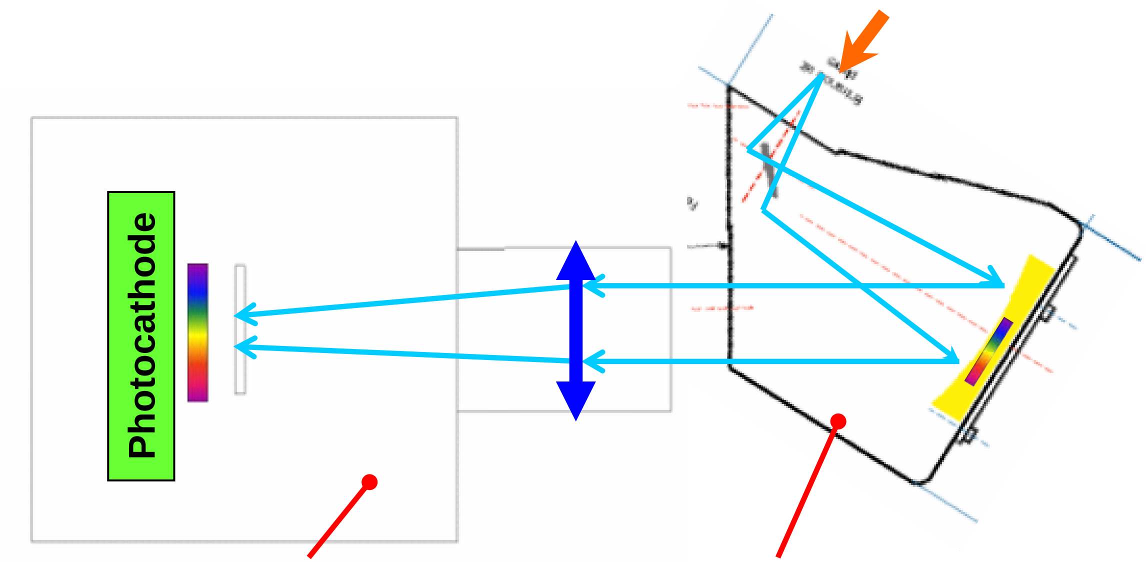

Streak Camera Unit Imaging Spectrograph

Imaging spectrograph
HORIBA, CP-140
400 nm -900 nm
(on order)

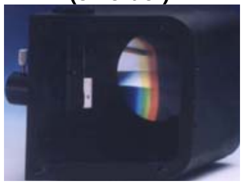

Hamamatsu streak, C7700
(available)

Radiance calibration with tungsten strip lamp (ordering)

Calibration lamp: Osram W 17/G

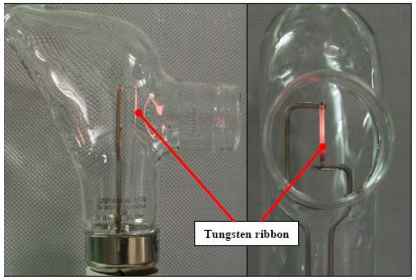

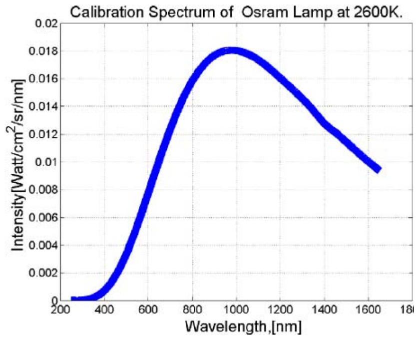

Wavelength calibration with
Mercury-Argon Calibration lamp (available)

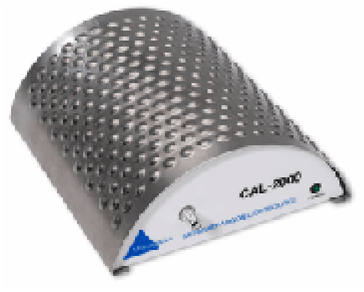

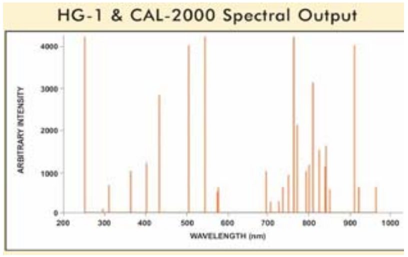

Cameras

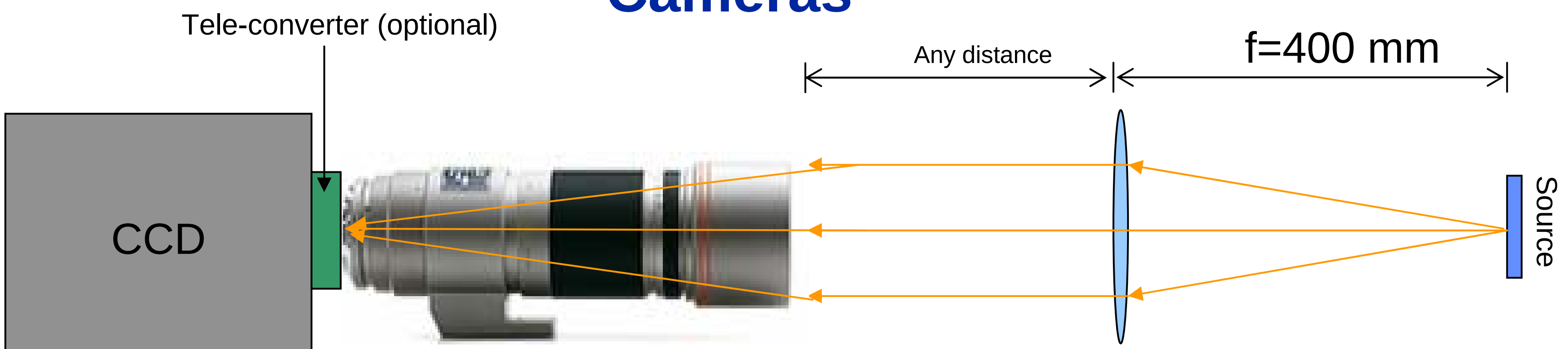

Tele-zoom objective, **Elicar**, f=1600 mm (ordering)

Precise coated doublet achromat for visible light
Free of aspherical and coma aberrations.
D=100 mm (ordering)

Positioning of cameras:

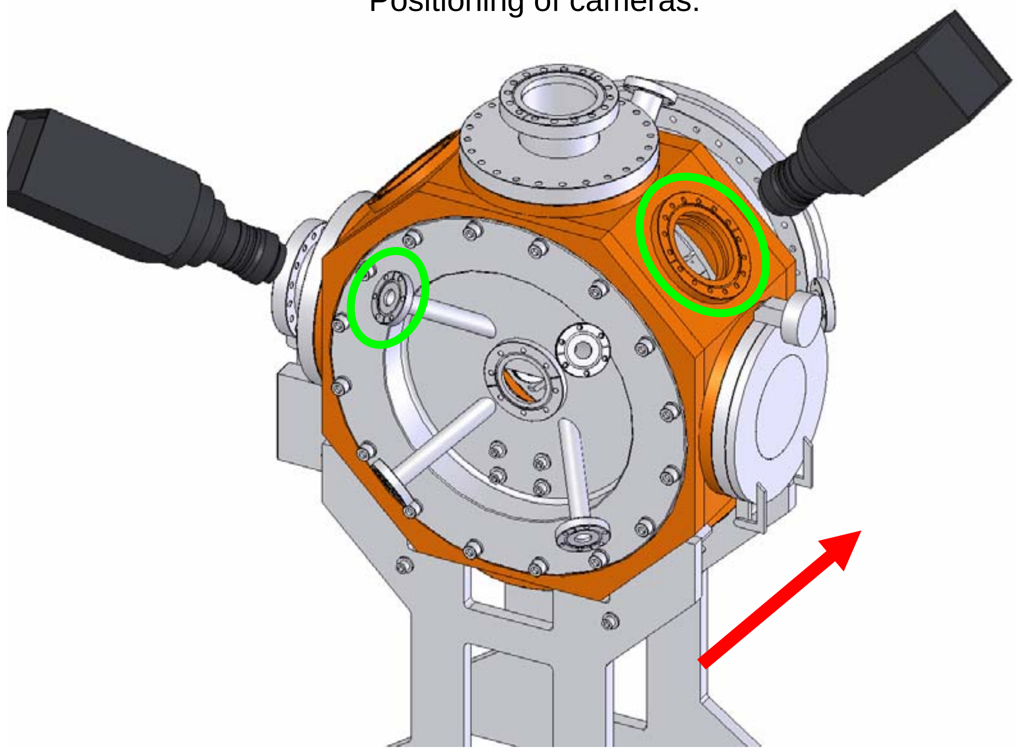

-Two cameras used for beam diagnostics, target positioning and experimental snapshots
-4 times magnification
-Spatially calibrated
-Camera resolution ~10 μm

Tungsten target before shot (GSI)

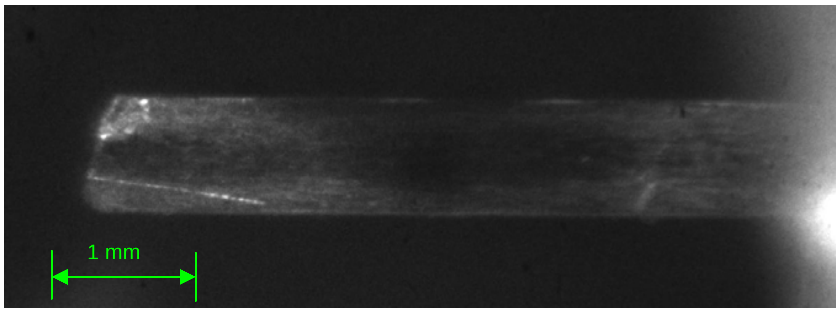

Testing VISAR

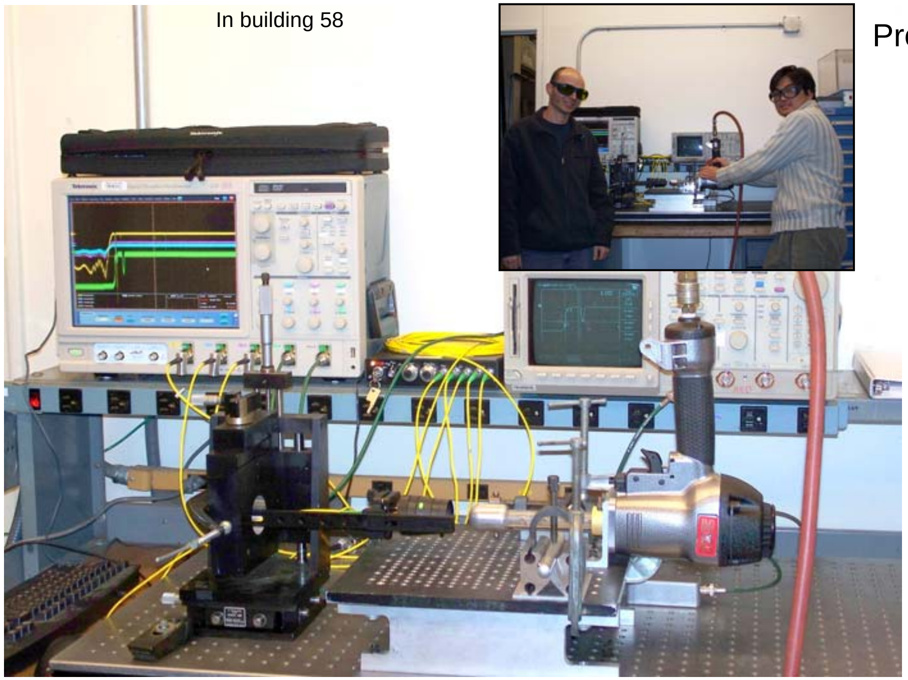

Protection enclosure

Photo-diode for triggering

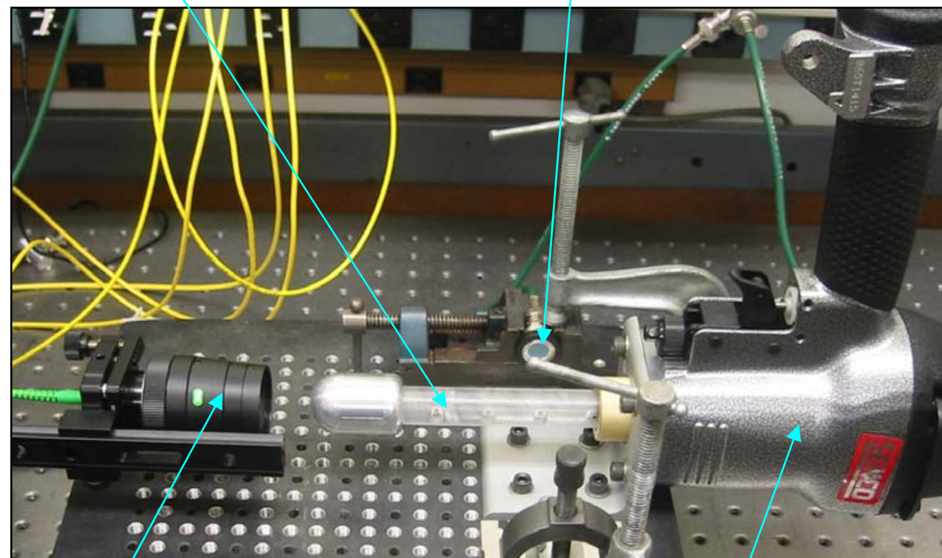

Focusing/collection optics

Nail Gun
(purchased in “Bad, Bath & Beyond”)

**Martin, Froeschner & Associates All Fiber
Push-Pull Doppler Velocity Interferometer (VISAR) Systems**

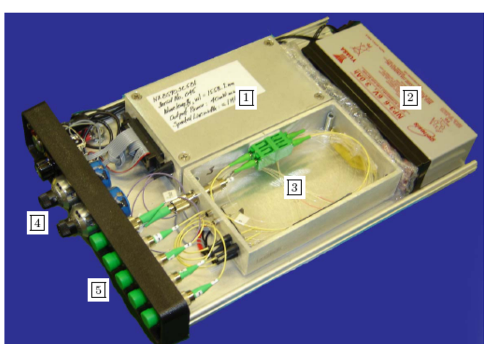

Mirror-polished aluminum foil

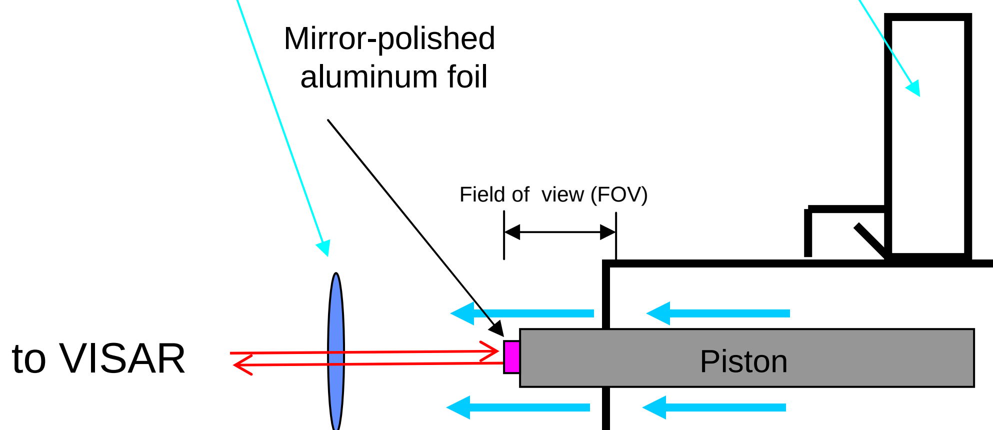

Experiment layout

Experimental layout:

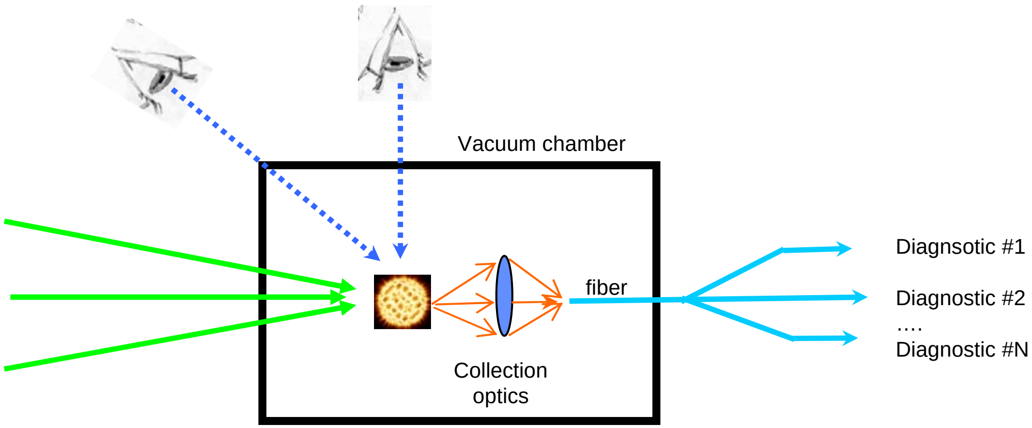

Target chamber:

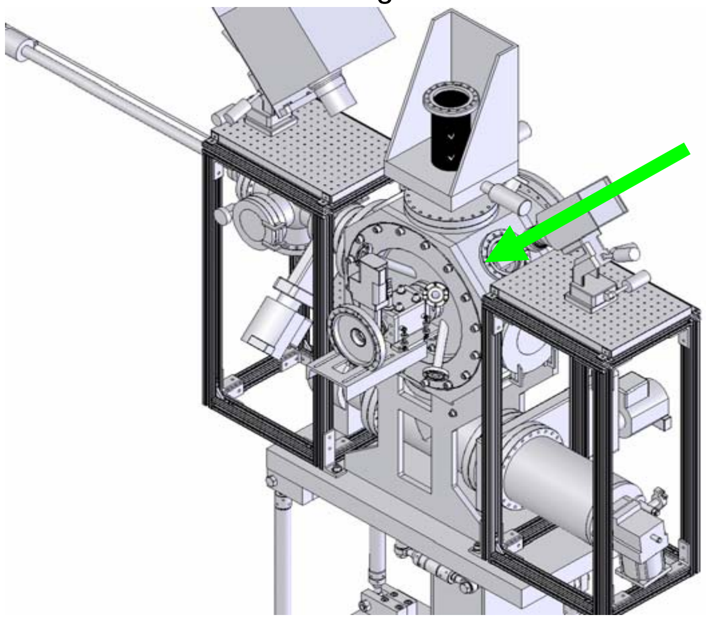

- In first experiments target positioning with manual hexapod and collection optics with manual linear stages
- Motorized in future (hexapods)
- Positioning accuracy <10 μm

6-axis hexapod from PI

Pig tail

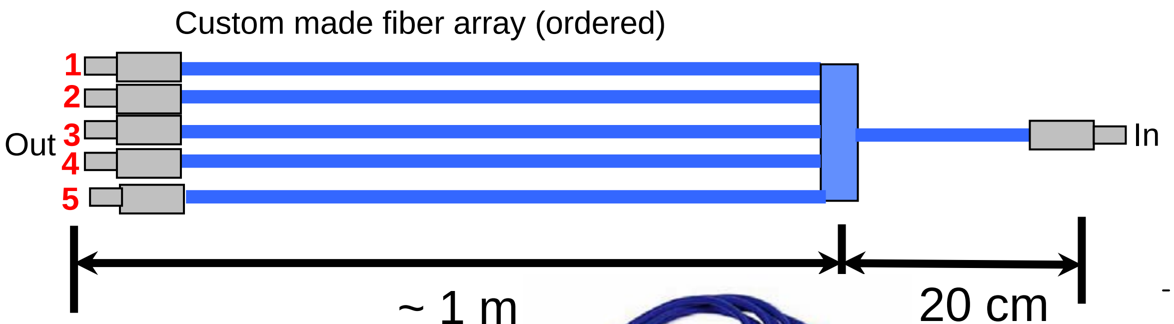

1-125 μm-VISAR
2-400 μm-Pyrometers
3-200 μm-Pyrometers
4-125 μm-VISAR
5-125 μm-VISAR

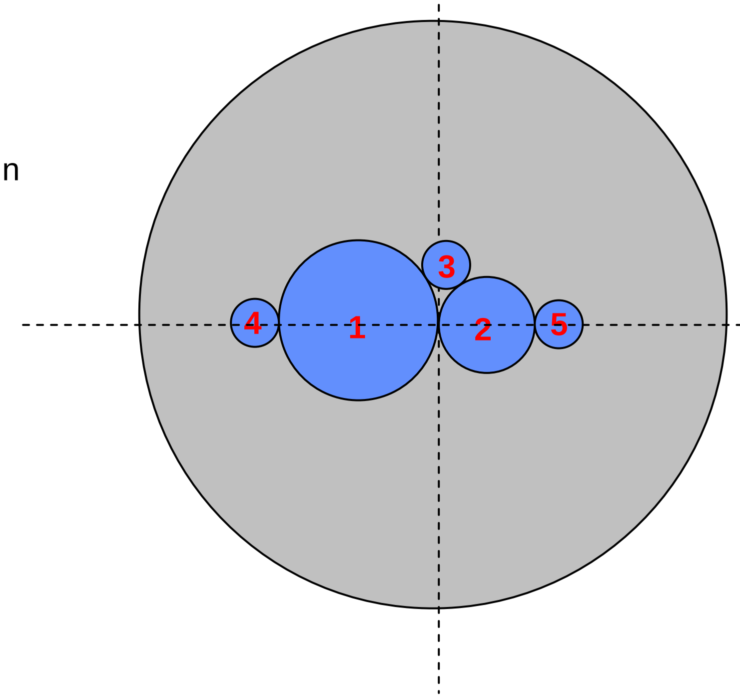

-Signal levels (i.e. temperatures) are unknown!
-Must be prepared for various scenarios.
-Spatial resolution of probing optics is determined by the size of the fiber (from 50 μm to 1000 μm)

Worst case: low temperatures (<1000 K), fibers **1** (VISAR) and **4** (2-channel pyrometer)

Ideal case: high temperatures, fibers **5** (VISAR) and **2** (Streak pyrometer)

Benchmark of both pyrometers: fibers **1**(2-channel pyrometer), **2** (Streak pyrometer) and 3 (VISAR).

IFE Reactor Core Magnetic Intervention (MI)

IFE Strategy Workshop, April 24 – 27, 2007. San Ramon, CA

F. Dahlgren[1], T. Kozub[1], T. Dodson[1], C. Priniski[1], C. Gentile[1], I. Zatz[1], J. Sethian[2], G. Gettelfinger[1], A. E. Robson[2], A. R. Raffray[3], M. Sawan[4]

[1]Princeton Plasma Physics Laboratory, [2]Naval Research Laboratory, [3]University of California-San Diego, [4]University of Wisconsin

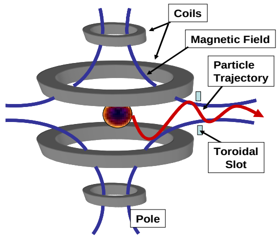

Solid Wall Magnetic Deflection

- **Cusp magnetic field stops the radially expanding ion shell**
- **Ion flux to wall is minimized**
- **Field is resistively dissipated in blanket/wall**
- **Ions, at reduced energy and power, are directed through cusp poles and into mid-plane toroidal dumps**

In Direct Drive (IFE) implosions, approximately 28% of energy released is carried by charged particles. The ion species include the usual DT and DD fusion reaction products and these charged particles represent the biggest "threat" to the survival of the first wall. To ease this threat, the concept of "Magnetic Intervention" has been proposed using a cusp shaped magnetic field to deflect the ions away from the first wall and into external dumps.

In a cusp geometry the field is zero at the target origin and presents a positive (convex) curvature to the expanding ion flux during the pulse. The interaction of the radially directed ions and electrons with this field will result in an induced rotational current in the expanding plasma. This induced current would be opposite that in the coils (clockwise in the upper hemisphere of the plasma, counterclockwise in the lower half) and thus would exclude the magnetic field from the interior of the expanding plasma. Because flux is excluded, the magnetic field is pushed outward and is compressed since it cannot move past the external cusp coils. The expansion will continue until the increased magnetic pressure is balanced by the expanding plasma pressure, i.e. the system produces a beta of ~1.0. If the chamber wall is made of a resistive material, such as SiC, some of the energy of expanding magnetic field can be dissipated in the wall material as heat, thus effectively converting into a volumetric deposition of that heat.

A cusp geometry has an open toroidal belt at the mid-plane and openings at the poles. The ions, with reduced energy eventually leak out these openings where their energy can be absorbed external to the chamber. Additional energy would be dissipated via Bremstralung and other photon radiation.

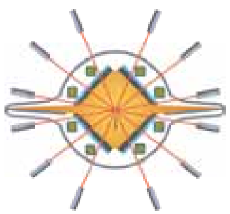

General Conceptual Arrangement for a Magnetic Intervention Chamber

Cusp Field Coil Analysis

COIL	A M IN	Z M IN	NI AT AT	FZ N LB	FR/L N/M LB/IN	FZ/L N/M LB/IN	S-HOOP N/M SQ PSI	COMBINED STRESS PSI	DFL-R
1	3.400	5.000	4.000E+06	-8.105E+06	2.660E+06	-3.794E+05	1.159E+07		
	133.858	196.850	4.000E+06	-1.823E+06	1.520E+04	-2.168E+03	1.682E+03	1.912E+03	1.407E-02
2	3.400	-5.000	-4.000E+06	8.106E+06	2.660E+06	3.794E+05	1.159E+07		
	133.858	-196.850	-4.000E+06	1.823E+06	1.520E+04	2.168E+03	1.682E+03	1.912E+03	1.407E-02
3	6.100	2.250	4.800E+06	4.511E+07	9.559E+05	1.177E+06	7.472E+06		
	240.157	88.583	4.800E+06	1.015E+07	5.461E+03	6.723E+03	1.084E+03	3.537E+03	1.627E-02
4	6.100	-2.250	-4.800E+06	-4.511E+07	9.559E+05	-1.177E+06	7.472E+06		
	240.157	-88.583	-4.800E+06	-1.015E+07	5.461E+03	-6.723E+03	1.084E+03	3.537E+03	1.627E-02

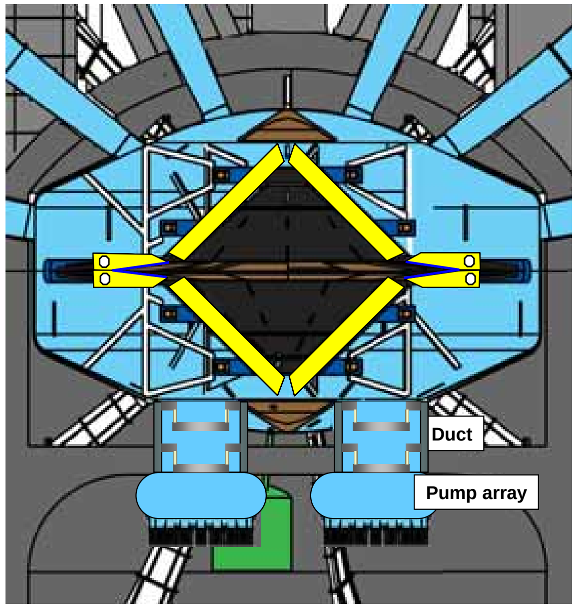

Baseline Design of Cusp Coils

The current baseline design of the cusp coils uses a Cable in Conduit Conductor (CICC) comprised of Nb-Ti superconductor with a forced flow super-critical LHe coolant. Two typical cross-sections of the coil are presented in the figures below. A high current density option can be considered because AC fields are not present in the coil windings. The coil and case will be force-cooled with 4.5-5 K LHe. An additional LN2 shroud will be positioned around the coil structure and support columns to be a thermal shield. Radiation and neutronics studies* suggest that a minimum 50 cm thick water/316L-SS shield will be required between the SiC blanket and coil.

Other coil conductor options, including the use of Rutherford cable and HTS YBCO are also under consideration.

*per M. Sawan, U.W., HAPL Meeting, GA, August 8-9, 2006

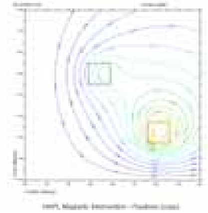

High Current Density Option

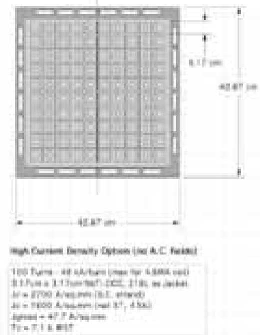

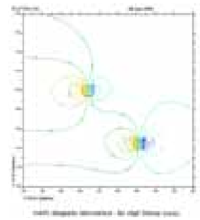

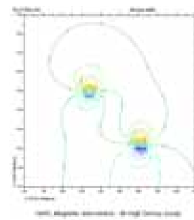

Low Current Density Option

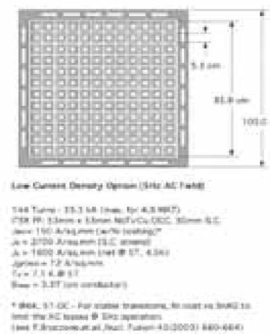

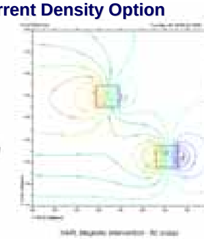

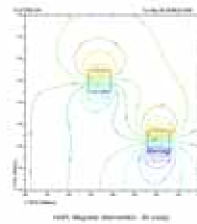

Progress on compression of FRC's

For Presentation at DOE IFE 2007 Workshop
San Ramon, CA
24-27 April 2007

presented by

Dr J. H. Degnan

Air Force Research Laboratory
Directed Energy Directorate

Progress on compression of FRC's

J.H.Degnan, A. Brown (2), T.Cavazos (1), S.K.Coffey (2), M. Domonkos, M.Frese (2), S. Frese (2), D.Gale (1), C.Gilman (1), C. Grabowski (1), T.P.Intrator (3), R.Kirkpatrick (3), G.F.Kiuttu, F.M.Lehr, J. V. Parker (1), R.E.Peterkin, Jr (1), N.F.Roderick (4), E.L.Ruden, R.E.Siemon (5), W.Sommars (1), W. Tucker, P.J.Turchi (3), G.AWurden (3)

Directed Energy Directorate, Air Force Research Laboratory, Kirtland AFB, NM, USA
(1) SAIC, Albuquerque, NM, USA
(2) NumerEx, Albuquerque, NM, USA
(3) Los Alamos National Laboratory, Los Alamos, NM, USA
(4) Permanent address: Department of Chemical and Nuclear Engineering, University of New Mexico, Albuquerque, NM, USA
(5) University of Nevada Reno, Reno, NV, USA

This research was sponsored by DOE-OFES

Abstract

Magnetized Target Fusion (MTF) is a means to compress plasmas to fusion conditions that uses magnetic fields to greatly reduce electron thermal conduction, thereby greatly reducing compression power density requirements (1, 2). The compression is achieved by imploding the boundary, a metal shell. This effort pursues formation of the Field Reversed Configuration (FRC) type of magnetized plasma, and implosion of the metal shell by means of magnetic pressure from a high current flowing through the shell.

We reported at Megagauss 9 that we had shown experimentally (3) that we can use magnetic pressure from high current capacitor discharges to implode long cylindrical metal shells (liners) with size, symmetry, implosion velocity, and overall performance that is suitable for compression of Field Reversed Configurations (FRC's). We also presented considerations of using deformable liner – electrode contacts of Z-pinch geometry liners or theta pinch driven liners, in order to have axial access to inject FRC's and to have axial diagnostic access. Since then, we have experimentally implemented the Z-pinch discharge driven deformable liner – electrode contact, obtained full axial coverage radiography of such a liner implosion, and obtained 2D-MHD simulations for a variety of profiled thickness long cylindrical liners. The radiographic results indicate that at least 16 times radial compression of the inner surface of a 0.11 cm thick Al liner was achieved, with a symmetric implosion free of instability growth. We have also made progress in combining 2D-MHD simulations of FRC formation with imploding liner compression of FRC's. These indicate that capture of the injected FRC by the imploding liner can be achieved with suitable relative timing of the FRC formation and liner implosion discharges.

Since the compressed plasma and stagnating liner energy densities can exceed a megabar in MTF, this constitutes a potentially very useful High Energy Density Physics (HEDP) application.

(1) K.F.Schoenberg, R.E. Siemon et al, LA-UR-98-2413, 1998

(2) J. M. Taccetti, T. P. Intrator, G. A. Wurden et al, Rev. Sci. Instr. 74, 4314 (2003).

(3) J.H.Degnan et al, IEEE Transactions on Plasma Science 29, p.93-98 (2001).

Magnetized Plasma Compression (MPC) Also Known as Magnetized Target Fusion (MTF)

LANL

- Magnetized target fusion (MTF) identified in US and Russia as an alternate approach intermediate between magnetic and inertial fusion parameter regimes
- Closed magnetic field configurations reduce electron thermal conduction losses
- Enables (slower) adiabatic compression with modest driver requirements
- ~10X radial compression required
- Typical precompression plasma parameters: 200 eV, 10^{17} cm^{-3}, 2 T

Since the compressed plasma energy densities exceed a megabar in MTF, this constitutes a potentially very useful High Energy Density Physics (HEDP) application.

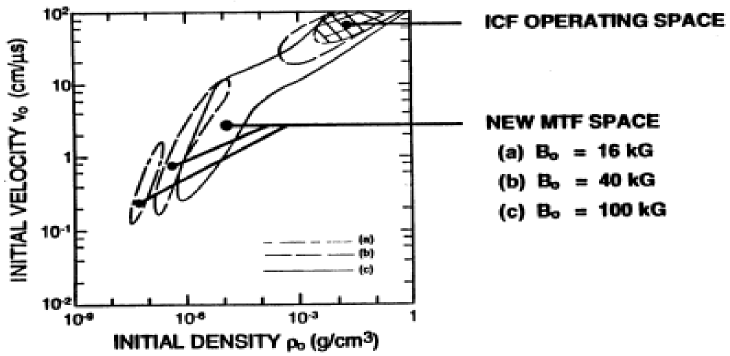

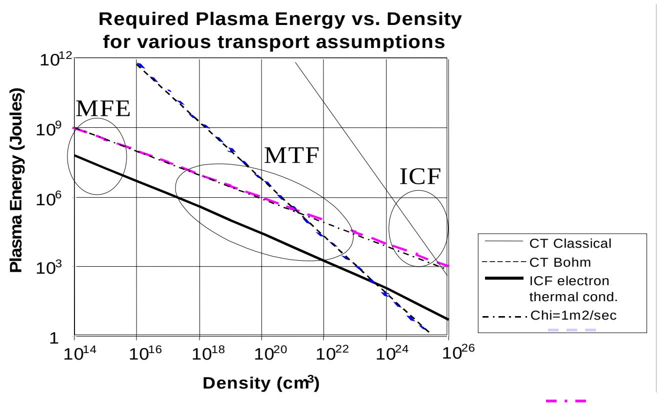

Magnetized Plasma Compression (MPC) can be achieved by imploding a metal liner with compact torus (CT) or a diffuse pinch plasma inside

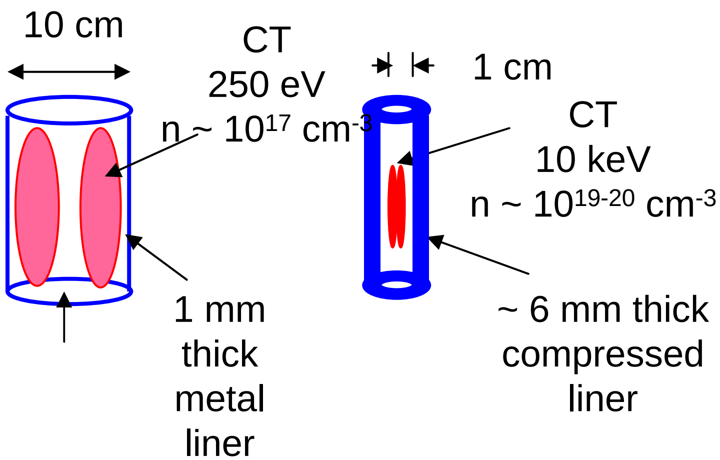

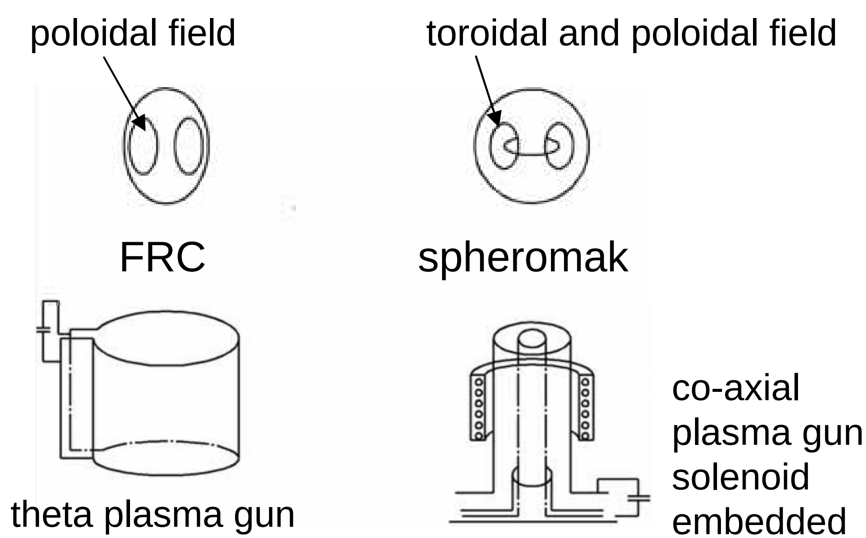

- **Two types of CT's are Field Reversed Configurations (FRCs) and spheromaks**
- **Both types of CT's can be formed by plasma guns and injected into liners**
- **Coaxial plasma gun without solenoid can form and inject diffuse Z-pinch into liner, which is also a magnetized plasma (with toroidal field only)**
- **Liner is imploded by JxB force from high current (> 10 megamp) discharge**

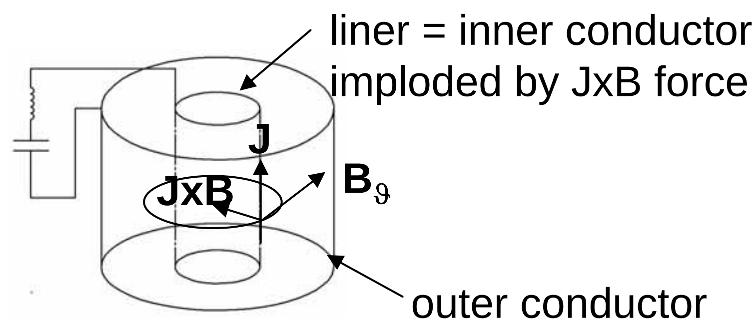

Since the compressed plasma and stagnating liner energy densities can exceed a megabar, this constitutes a potentially very useful High Energy Density Physics (HEDP) application.

Elements Of Magnetized Plasma Compression, aka Magnetized Target Fusion (MTF)

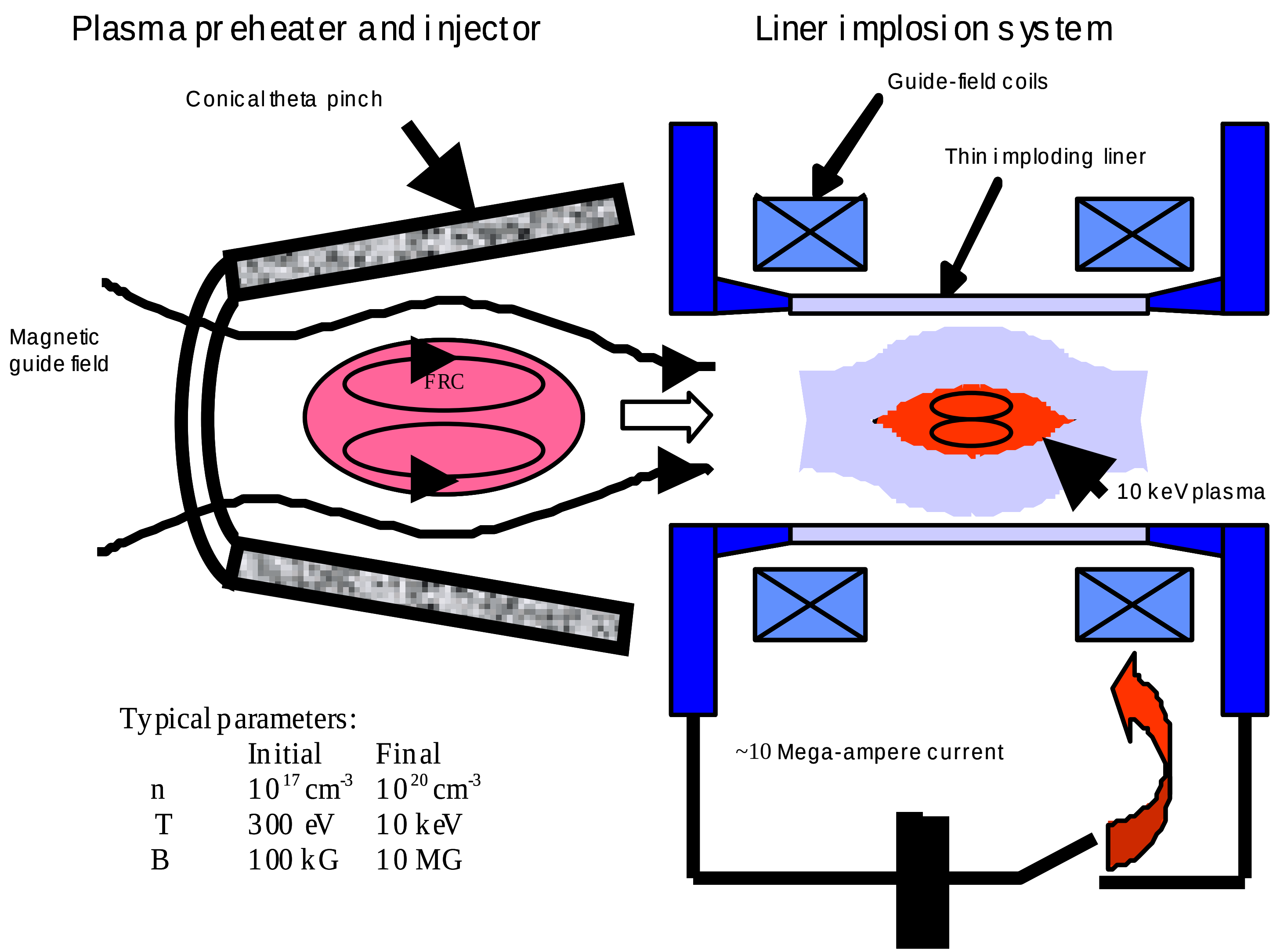

Typical parameters:

	Initial	Final
n	10^{17} cm^{-3}	10^{20} cm^{-3}
T	300 eV	10 keV
B	100 kG	10 MG

Recent progress in DOE_OFES sponsored effort: Lower upstream inductance crowbar switch reduced modulation of main theta discharge current

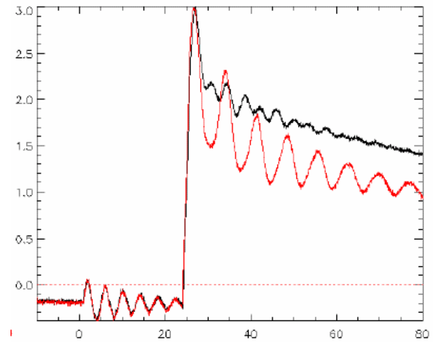

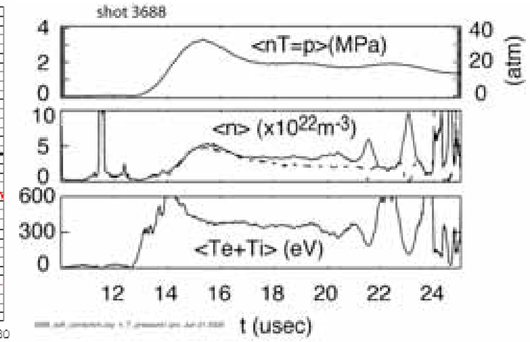

- **This enabled formation of higher average density, better quality FRC's**
- **Multi-chord HeNe laser interferometry (By DEHP's Dr Ruden) obtained density distribution of FRC**
- **Tomography of such data (by Dr Ruden) enabled measurement of FRC rotation, assuming n=2 rotation**
- **magnetic field exclusion probes (by LANL) enabled measurement of plasma pressure**
- **density and pressure info enabled estimate of FRC temperature**

These FRC formation experiments were done at LANL TA-35 using AFRL support for Pulsed Power and interferometry. See, for example, S. Zhang, T. P. Intrator, G. A. Wurden, W. J. Waganaar, J. M. Taccetti, R. Renneke, C. Grabowski, and E. L. Ruden, Phys. Plasmas 12, 052513 (2005). Such FRC experiments are to begin at AFRL adjacent to Shiva Star this year.

FRC formation hardware now exists in Shiva Star facility.

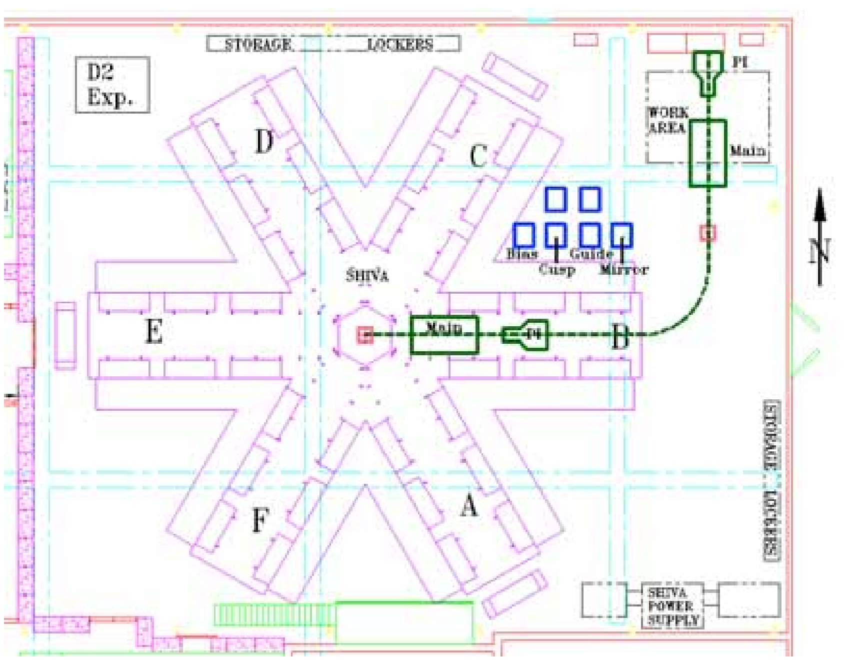

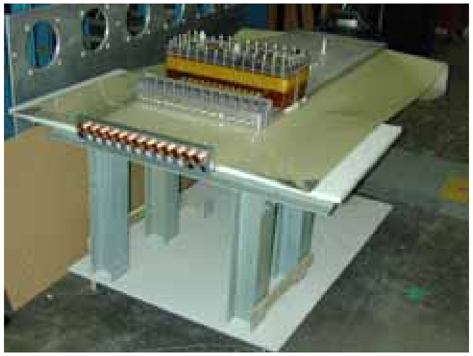

- Left: Planned layout of FRC formation banks and hardware in Shiva Star bay, in inserted and retracted positions.
- Right, top to bottom: Main FRC formation bank (a single Shiva star module), pre-ionization bank, initial magnetic field bias bank.

FRC Compatible Imploding Liner Hardware Design

- The 30 cm long liner implosion experiments extend our experience to longer liners

- The diagnostics on these initial shots include flash radiography, interior magnetic field compression, discharge current and voltage, and an interior instrumented impact package

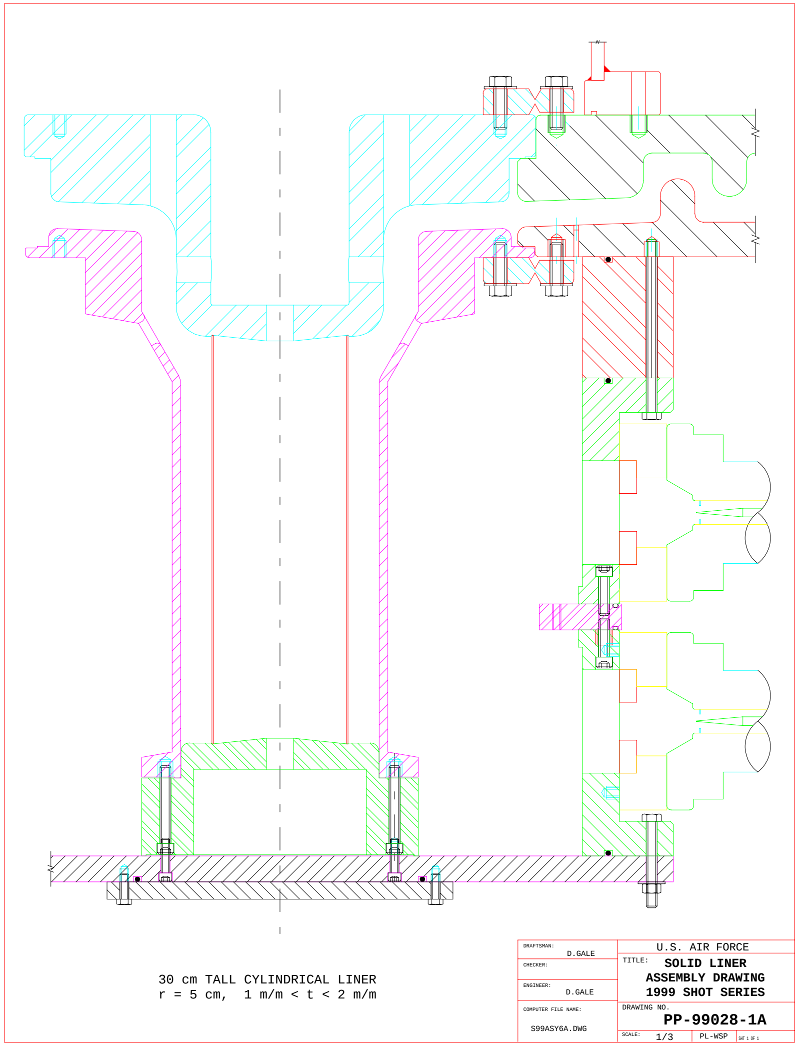

Shiva Star Facility at AFRL

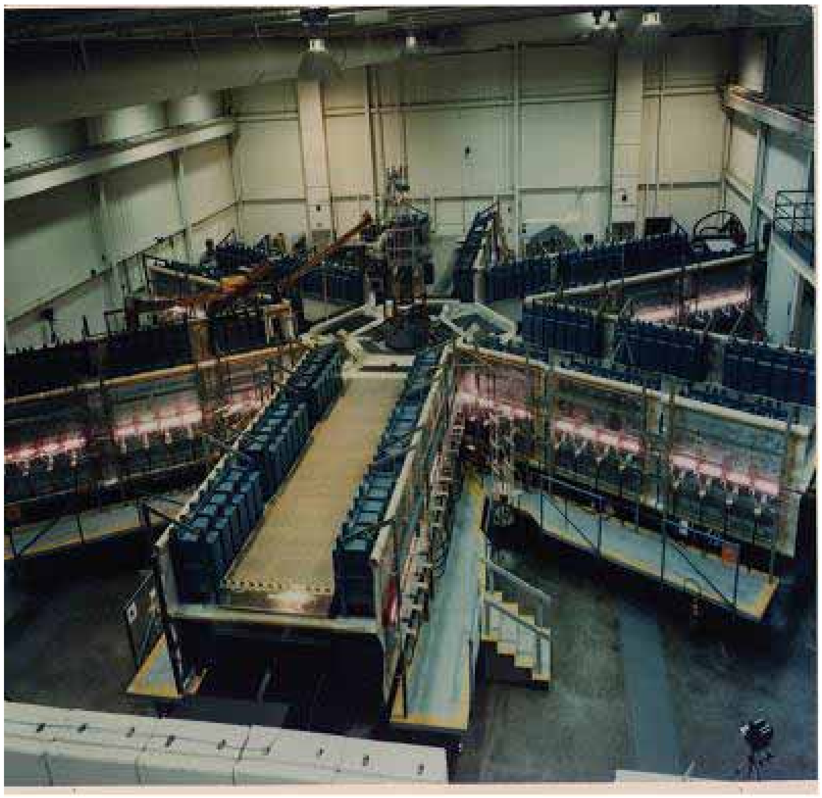

- 82 kV, 1300 uF, 44 nH for first Z-pinch driven long liner experiments

- ~12 Megamp, ~10 μsec risetime discharge implodes 30 cm long, 10 cm diameter, 1.1 mm thick Al liner in 24 μsec

- 4.4 MJ energy storage gives 1.5 MJ in liner KE

Shiva Star Capacitor Bank (up to 9 Megajoules, 3 μsec) available now for implosion - compression experiments

Radiographs from FRC compatible Liner Implosion on Shiva Star

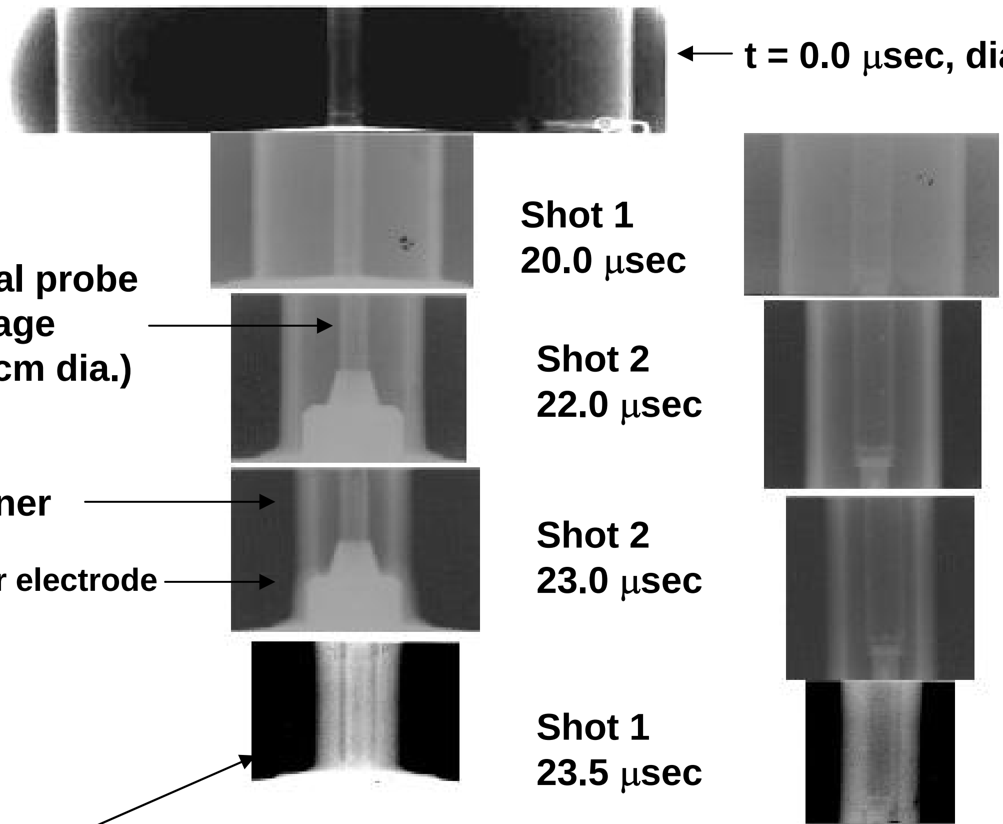

Achieved velocity, radial convergence, symmetry, stability needed for compression of FRC’s to MPC conditions

Connecting current to the liner

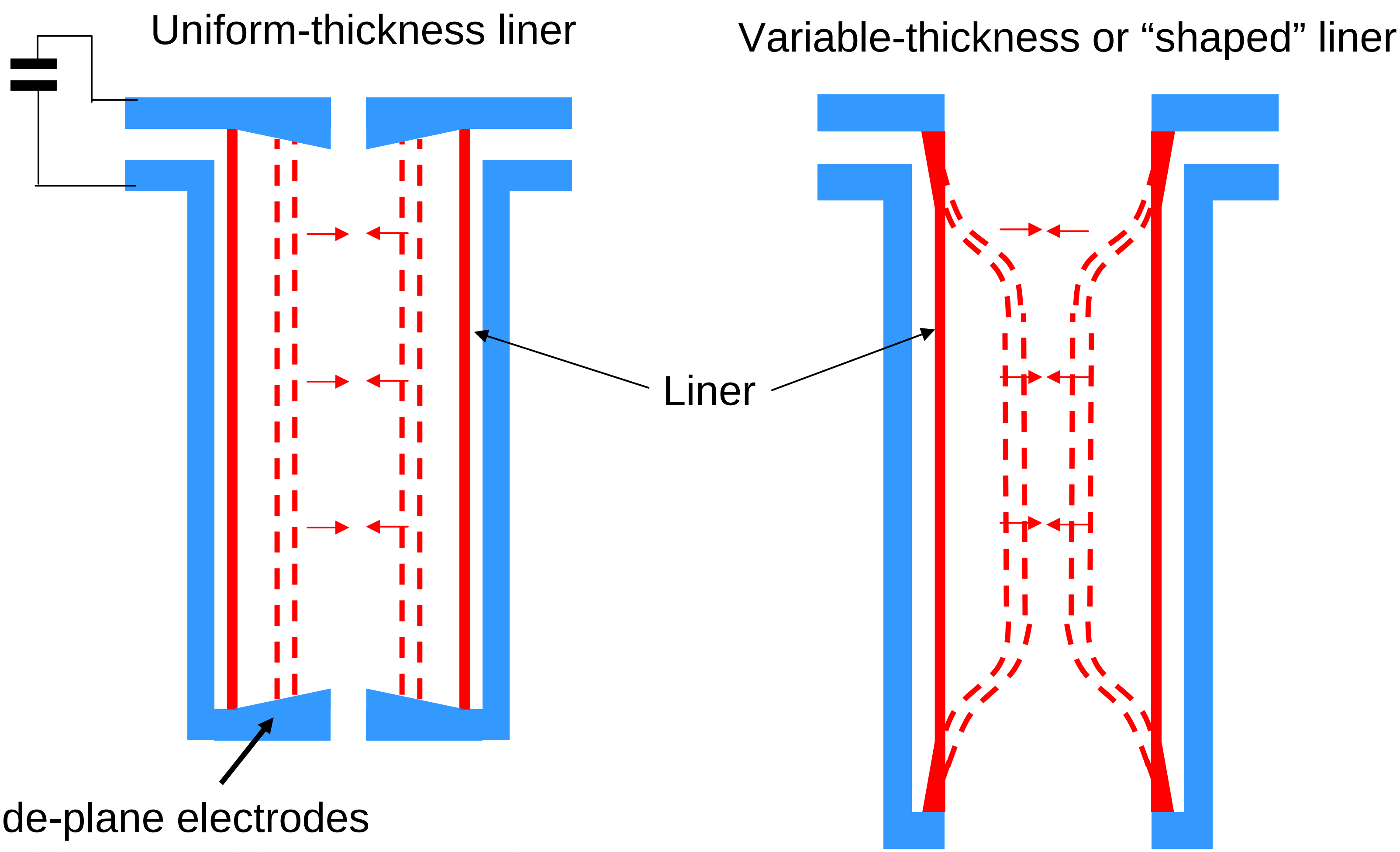

Glide-plane electrodes
used in 1999 Shiva-Star experiments
would interfere with FRC injection

Shaped liner recently tested

2D-MHD simulations indicate feasibilty of deformable liner-electrode concept

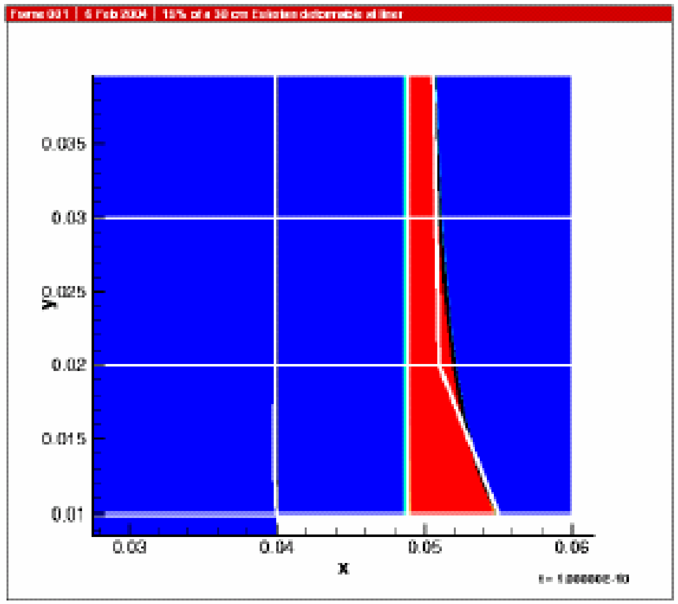

Double frustrum and smooth liner initial thickness profiles

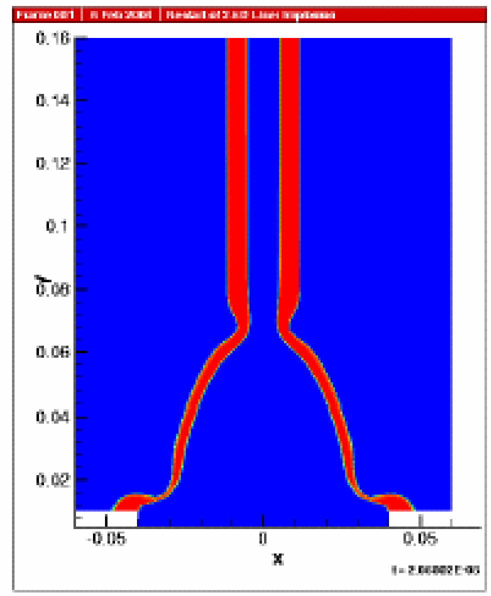

Double frustrum profiled liner density contours at ~ 1 μs before peak compression

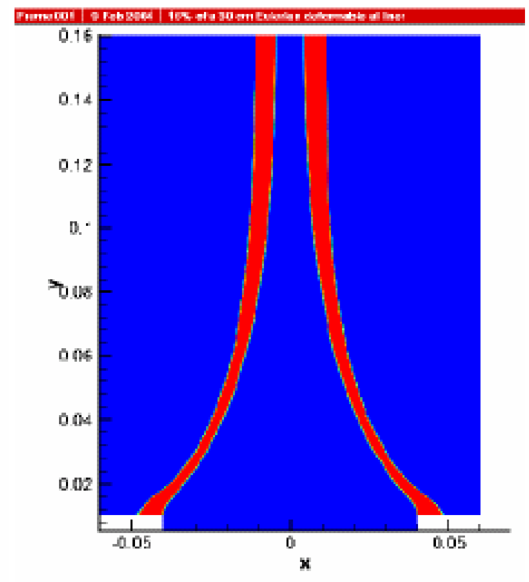

Smooth profiled liner density contours at ~ 1 μs before peak compression

Deformable Liner-Electrode Contacts Offer Advantages in Purity of the Compressed Plasma and Diagnostics Access for Z-pinch Driven Liner; these examples are for 8 cm diameter electrode apertures

Deformable contact liner implosion performed with 8 cm diameter electrode apertures; results indicate that Z-pinch imploded liner approach is feasible

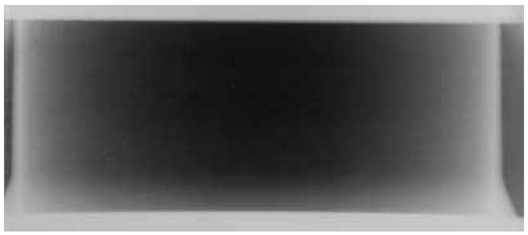

Static radiograph of portion of liner adjacent to electrode, prior to experiment. Inner diameter = 9.78 cm.

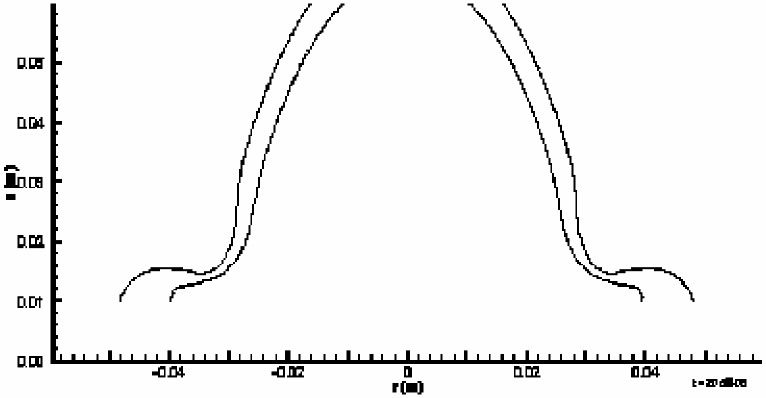

2D-MHD simulated density contours for similar parameter liner implosion, at 0.5 µs before stagnation.

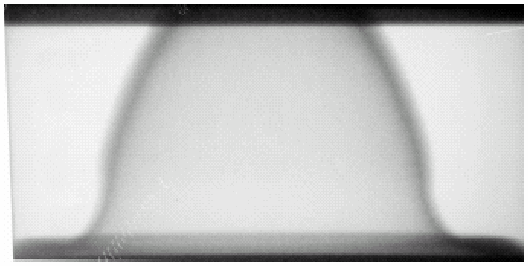

Experimental radiograph for portion of liner adjacent to electrode, at 22 µs after start of current, approximately 0.5 µs prior to peak compression. Bottom of liner to top of field of view is approximately 4.5 cm.

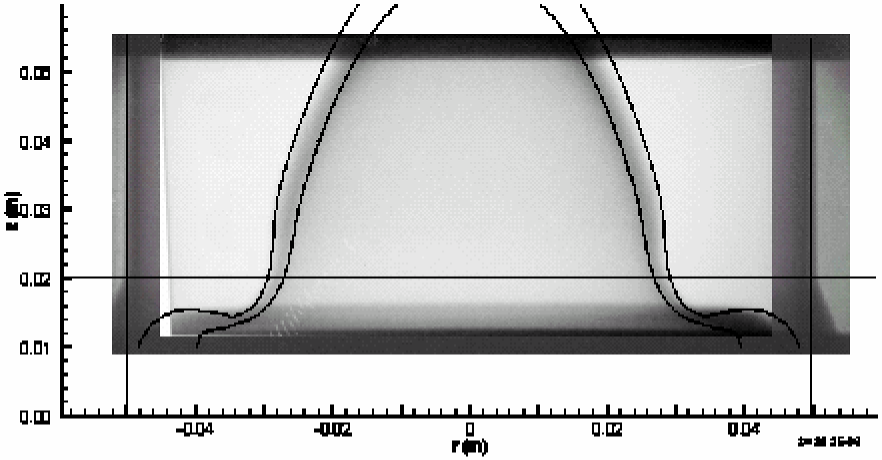

Overlay of 2D-MHD simulation density contours and radiographs at approximately same size scales.

Mid-gap radiograph indicates ~ 17 x radial compression of inner surface

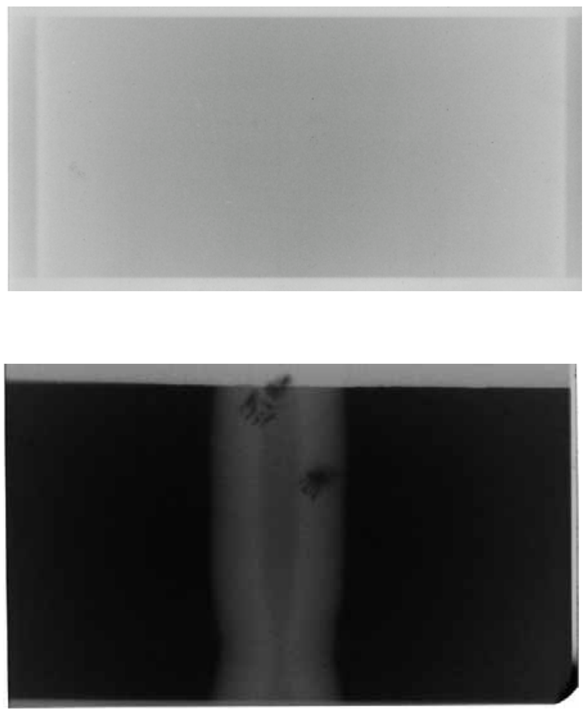

Top: radiograph of liner at t=0, near mid-gap, ID = 9.78 cm, OD = 10.0 cm.

Bottom: radiograph of liner at t = 22 μsec, near mid-gap. ID of non-m=0 portion ≅ 0.58 cm, corresponding to radial compression of inner surface ~ 17. We believe that the m=0 portion is right at mid-gap. If there had been an FRC inside, it would be compressed > 10x radially prior to significant growth of this instability.

We suspect this late m = 0 feature is due to release of initial axial compression, combined with thickness derivative discontinuity (from double frustrum thickness profile) at 9 cm from mid-gap. Both the initial axial compression and the thickness derivative can be removed by design change.

Axial view fast optical photos indicate symmetric implosion of inner surface of liner with inner diameter consistent with simulation

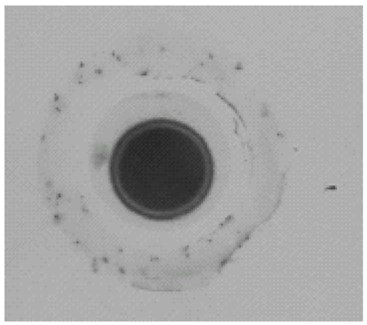

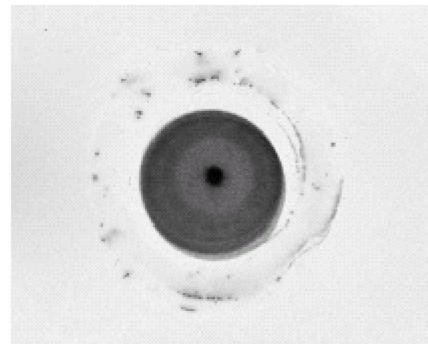

Left: 200 nanosec optical framing photo, axial view, of load. Inner diameter of opening is 8.0 cm. Photo used Xenon flash backlighting.

Right: 200 nanosec optical framing photo, axial view, of load at 21μsec into implosion discharge. Inner diameter of smallest part of liner (most imploded part) is 1.5 cm.

Deformable contact liner experiment geometry for near full axial coverage radiography

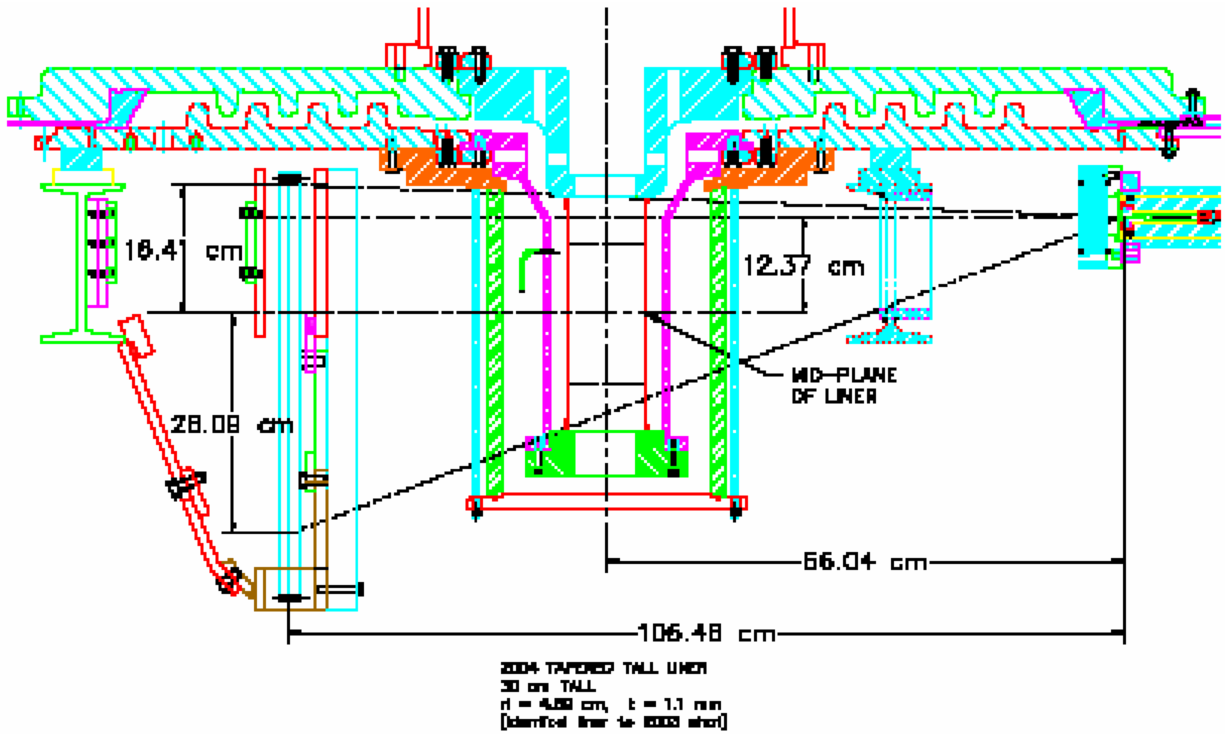

This experiment used the same liner thickness vs axial position, and same capacitor discharge parameters, as for the partial axial coverage radiography experiment.

Implosion of deformable liner suitable for compressing FRC's to MTF conditions demonstrated

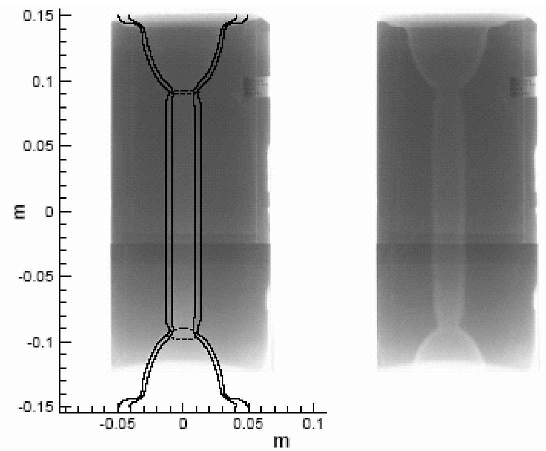

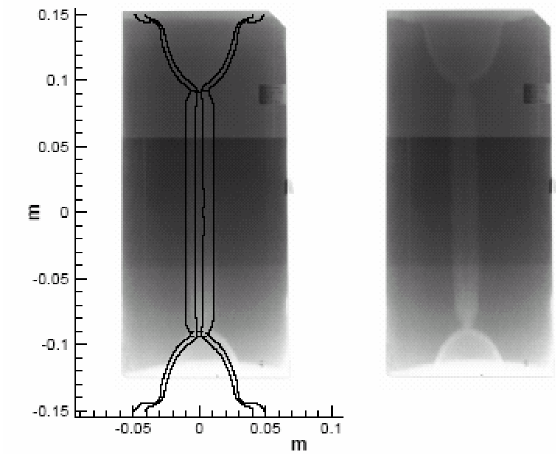

- **Radiographs and 2D-MHD simulations of implosion of 30 cm long, ~ 1mm thick, 5 cm radius Al liner indicate feasibility of deformable liner – electrode contact.**
- **This enables 8 cm diameter electrode apertures, sufficient for FRC injection into liner interior.**
- **Left: 21 μs after start of current. Right: 22 μs after start of current.**
- **Driven by 12 megamp Shiva Star axial discharge thru liner.**

Sponsored by DOE-OFES

Normal current delivery to liner and symmetry were obtained for experimental Bi-frustrum profile)case

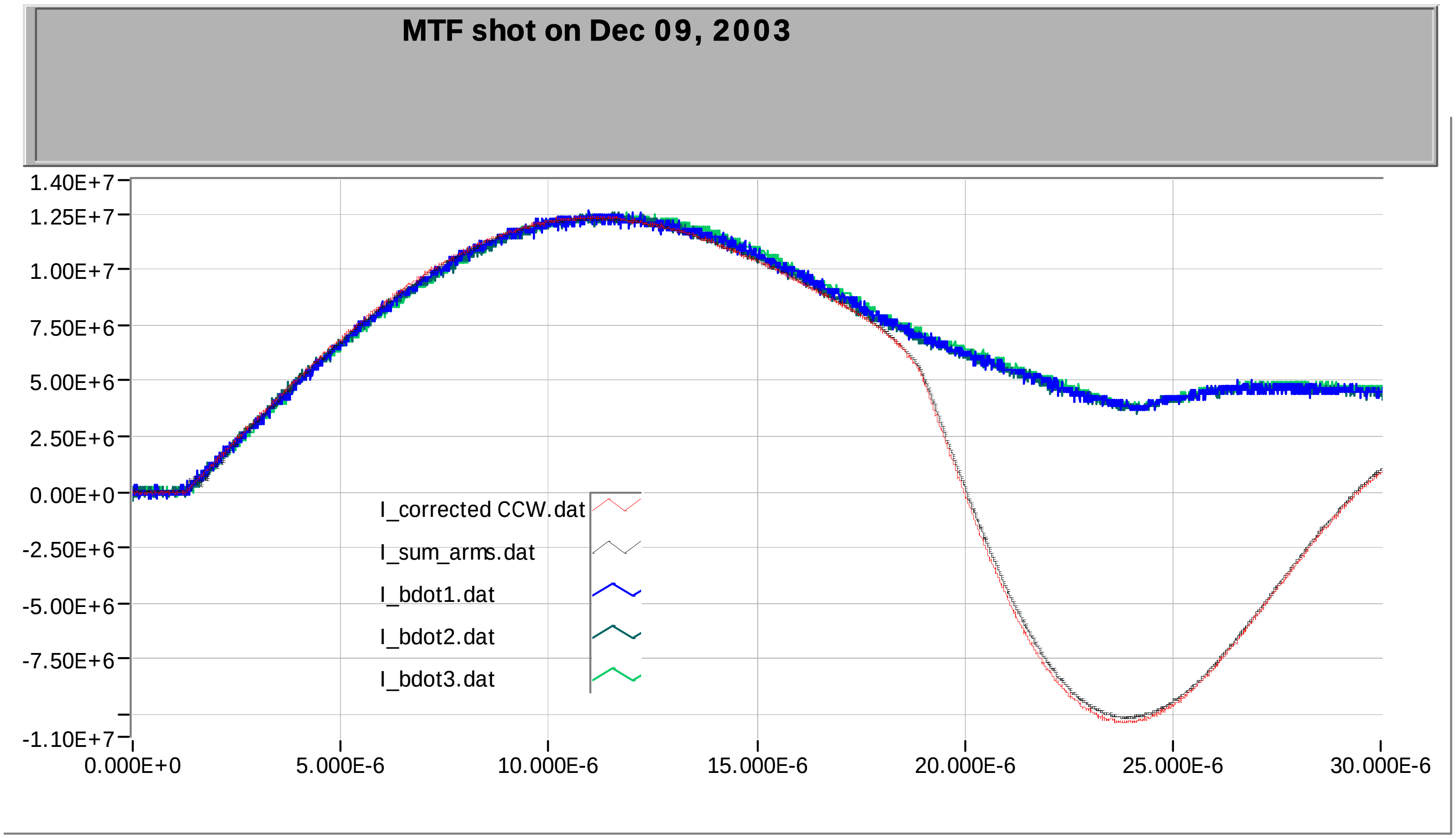

Current peaked at ~ 12 megamps, at ~ 10 μs after start of current rise. Insulator crowbar occurred at ~ 17 μs, as expected.

Alternative liner thickness vs profiles are being examined via Mach2 simulations

A family of such simulations uses an analytic profile which includes Gaussian thinning region a few cm from electrodes

$$r(z) = \left[R_3 + \left(\frac{A}{B-z} \right)^{1/n} + \left(\frac{A}{B+z} \right)^{1/n} \right] \left[1 - \alpha \exp\left[-\left(\frac{z - z_{00}}{\Delta} \right)^2 \right] \right]$$

Z_0 = distance from liner midplane. Z_o = 11.5 corresponds to 3.5 cm up from electrode. Z_{00} = 3.5

Δ is the half width at half max and α is a measure of the amplitude.

Other parameters are defined in following table (next slide)

Deformable liner thickness profile parameters

Case	A	n	R_0	R_1	z_1	z_0	α	Δ	
Base line	1.3	0.5	5.0	5.5	15	11.5	0.0	1.0	
01	1.3	0.5	5.0	5.5	15	11.5	0.001	0.50	
03	1.3	0.5	5.0	5.5	15	11.5	0.005	0.5	
05	1.3	0.5	5.0	5.5	15	9.5	0.003	0.5	
06	1.3	0.5	5.0	5.5	15	9.5	0.005	0.5	
07	1.3	0.5	5.0	5.5	15	8.5	0.003	0.5	
07_1	1.3	0.5	5.0	5.5	15	8.5	0.004	0.5	
07_2	1.3	0.5	5.0	5.5	15	8.5	0.005	0.5	
08	1.3	0.5	5.0	5.5	15	9.5	0.003	1.0	
08_01	1.3	0.5	5.0	5.5	15	9.5	0.004	1.0	
08_2	1.3	0.5	5.0	5.5	15	9.5	0.005	1.0	
09_01	1.3	0.5	5.0	5.5	15	10.5	0.004	1.0	
09_02	1.3	0.5	5.0	5.5	15	10.5	0.005	1.0	

2D-MHD simulations indicate that use of Gaussian thinning regions a few cm from electrodes controls divergence of liner ends; variants of this are being investigated computationally

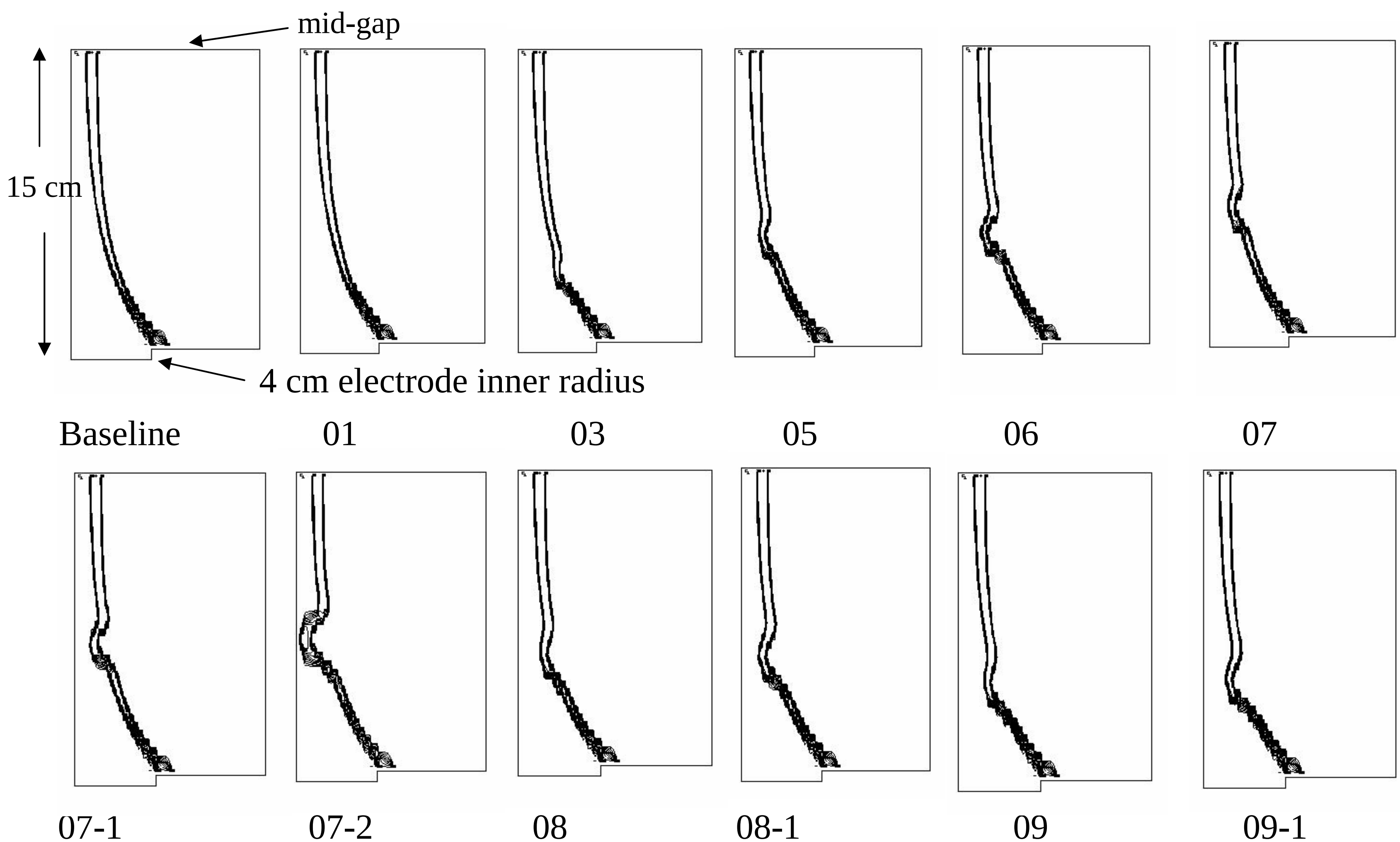

Contour plots show half (15 cm) of 30 cm tall, 5 cm initial outer radius, Al liner position and shape at 21 microseconds after start of 1300 microfarad, 80 KV, 44 nanoHenry initial inductance Shiva Star discharge, with standard safety fuse. Initial liner thickness is 1.1 mm at mid-gap (15 cm above lower electrode).

Temperature contours from Mach2 2D-MHD simulations of FRC formation, translation, and liner compression

2 μs

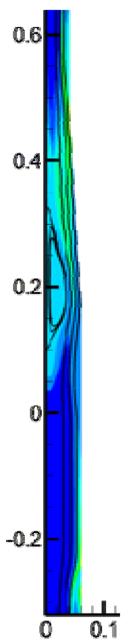

5 μs

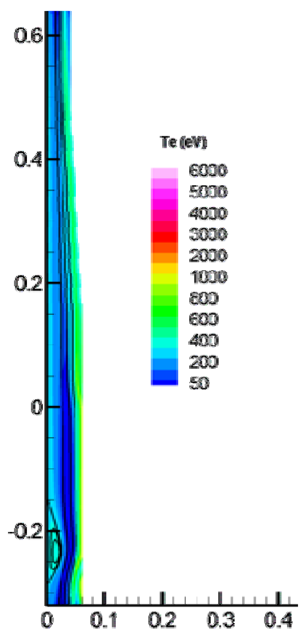

4 to 5 μs

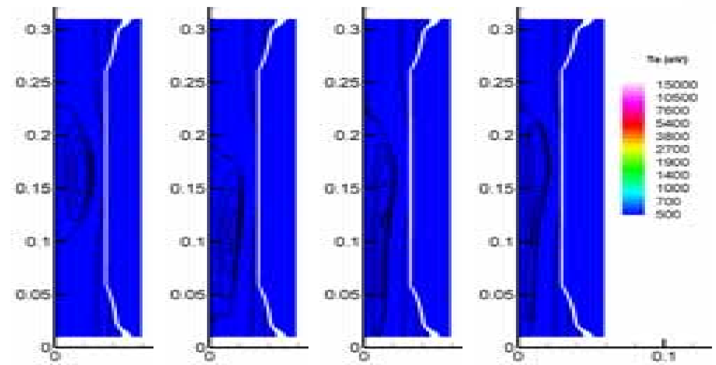

15 to 19μs

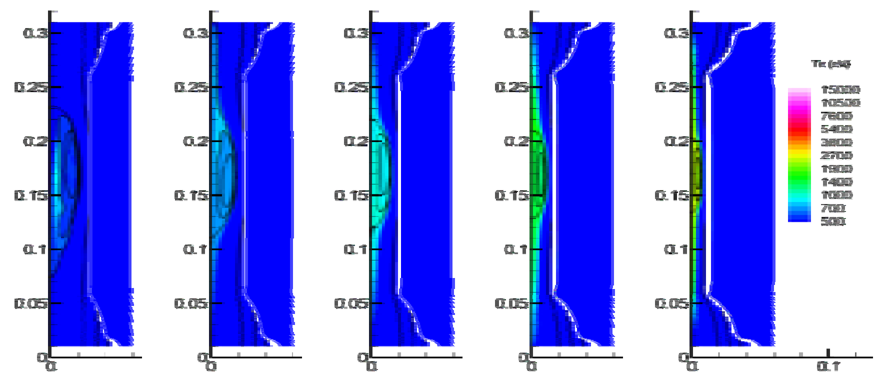

19, 20μs

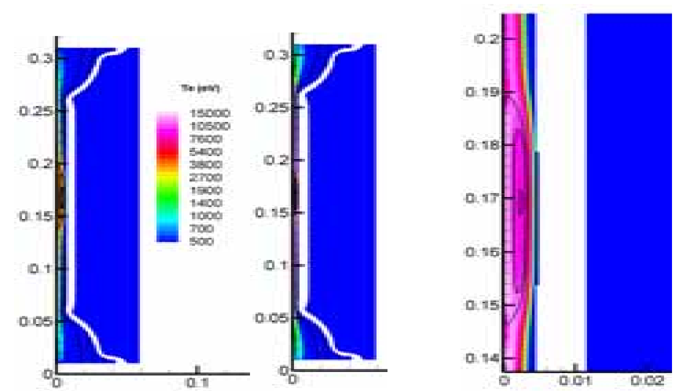

FRC initially moving down. Eulerian after 17.5 μs. FRC captured with liner implosion discharge started 9 μs prior to FRC main theta discharge. Delay window for capture ~ 1 μs Calculated FRC T > 8 KeV.

Sponsored by DOE-OFES

Technical Issues - MPC

- Principal technical issue is propagation of liner material into plasma *(though 2-D MHD simulations look promising, they may not be at sufficient resolution and 3-D effects need study)*
  - Capacitor driven experiments can answer this issue

- Other technical issues and options:
  - Field topology (diffuse Z pinch vs compact torus with poloidal and toroidal field vs compact torus with only poloidal field)
  - Injected vs *in-situ* formation of pre-compression plasma
  - Spherical vs cylindrical liner
  - Fusion yield vs driver energy, size

Concluding remarks

- By use of liner thickness vs axial position profiling, it appears possible to use a Z-pinch type discharge to compress ~ mm thick Al shells with sufficient radial convergence (>10 x inner radius), symmetry, and velocity (~ 0.5 cm/μs), and with sufficiently large electrode apertures, for injection of FRC's and for their subsequent compression to Magnetized Target Fusion (MTF) conditions.
- Preparation of FRC formation apparatus adjacent to Shiva Star capacitor bank and integration with imploding liner apparatus is progressing.
- Combined 2D-MHD simulation of FRC formation and compression by imploding liner indicates that compression and heating of FRC from ~ 10^17 ions/cc , ~ 200 eV to ~ 10^19 ions/cc, several KeV is feasible with existing capacitor banks.

Can Imploding Liner Magnetized Plasma Compression Be Made Repetitive?

- **Implosion-compression of several-cm-radius shells on the 1 to 10 microsecond time scale can be used for magnetized target fusion (MTF)**
- **This can be done in a manner with standoff of the driver, *e.g*., using arrays of laser or particle beams, which enables repetitive operation (for power plants or propulsion)**
  - **Similar to inertial confinement fusion (ICF) drivers, but with 10^3 to 10^4 times slower pulses, hence easier**
- **There are also schemes for repetitive operation of magnetic pressure driven liner implosions (R.W. Moses et al, LA-7683-MS, 1979, and G.E.Rochau et al, presented at IEEE-Pulsed Power Plasma Sciences Conference, Las Vegas, Nevada, June 2001, O5D7, p.592, IEEE-PPPS-2001 Conference Record-Abstracts, IEEE Catalog 01CH37255), and for pneumatic pressure driven implosions of rotationally stabilized, re-usable liquid Li liners (P.J. Turchi *et al*, Phys. Rev. Lett. 36, 1613 (1976))**
- **A plasma jet spherical array compression scheme has also been proposed (Y.C.F.Thio et al, Proceedings of Second Symposium of Current Trends in International Fusion Research, 1999)**
- **Single shot versions of such implosion-compression can be done now via magnetic pressure implosions, using our existing large capacitor bank**
- **Such single shot implosion-compression experiments can be used to investigate critical technical issues before developing and building more expensive, repetitive drivers**

Failure Strength Measurements of VPS Tungsten Coatings for HAPL First Wall Armor

Jaafar El-Awady, Hyoungil Kim, Jennifer Quan, Shahram Sharafat, Vijay Gupta, and Nasr Ghoniem

Mechanical and Aerospace Engineering Department, University of California Los Angeles (UCLA)

Introduction

- The **High Average Power Laser (HAPL)** project is pursuing development of an IFE power reactor using a solid First Wall Chamber. Tungsten is the primary candidate for armor material protecting the low activation ferritic steel first wall (FW) chamber.
- The tungsten armor is less than 1-mm thick and is applied by vacuum plasma spraying (VPS).
- Adhesion of the tungsten-armor to the ferritic steel is critical, thus the interfacial strength between the W-armor and the substrate is measured using a state-of-the-art technology developed at UCLA.
- VPS W-coated steel samples were tested using the laser spallation technique and the failure strength of the W-coatings was quantitatively determined. It is shown that the interfacial strength between ferritic steel and the W-coating is much greater than the failure strength of the W-coating.

The Laser Spallation Interferometer Experiment

- A 6-ns long Nd:YAG laser pulse is made to impinge over a ϕ3mm area on the back surface of the ferritic steel substrate through a deposited layer of SiO_2.
- The melting-induced expansion ferritic steel under confinement of SiO_2 generates a compressive stress pulse that propagates towards the bonding interface.
- This compressive stress wave reflects as a tensile stress wave from the free surface of the coating and leads to its spallation at a sufficiently high amplitude.
- This critical tensile stress, causing failure of the coating, is obtained by measuring the transient displacement history of the coating's free surface (induced during pulse reflection) by using an optical interferometer (Pronin and Gupta, 1993).

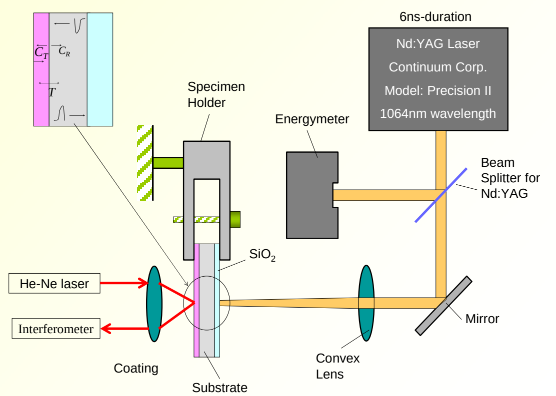

Experimental Results

- The tungsten/F82H sample was impinged with the laser beam at different locations and different laser intensities to determine the critical energy that would result in failure of the coating.
- The sample was cross-sectioned at the locations of impingement to detect any interlayer failure in coating layer.
- The following table shows the effect of increasing laser intensity on the failure of the coating:

Laser Intensity	22.9 kJ/m²	25.6 kJ/m²	28.5 kJ/m²	75.0 kJ/m²	110.4 kJ/m²
Type of Failure	No Failure	No Failure	Some Crack nucleated in the coating	Crack opening and popping of the coating	Complete delamination of the coating

- The impinged sample:

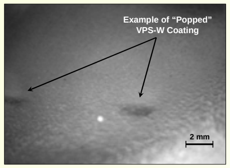

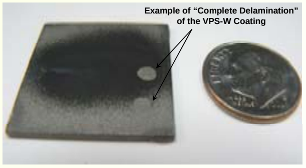

- The following figures are SEM micrographs showing the failure in the W-armor coating for different laser intensities.

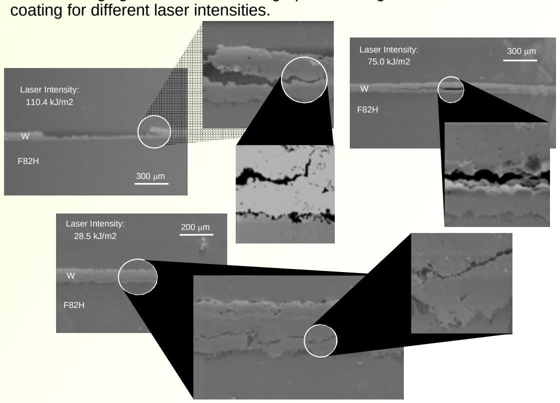

- Cracks nucleate in the area located one third of the distance between the W-F82H interface and the coating free surface.

Conclusions

- The laser spallation technique was used to quantify the failure strength of the VPS W on F82H.
- It is observed that the failure of the sample occurs within the W-coating and not at the interface. This is due to that the morphology of the VPS coating (splat formations).
- The failure strength estimates depends on the mechanical properties of the coating (VPS – coating properties), such as density, Young's modulus, Poisson's ratio need to be experimentally measured for more accurate failure strength estimates.
- Further analysis taking into account the morphology of the VPS coating failure strength may differ.

Specimen and Materials Properties

- The Vacuum Plasma Sprayed (VPS) samples were supplied by **PPI** (S. O'Dell).
- W-Coatings were polished to ~65 mm thickness at **ORNL** (G. Romanoski)
- Elastic properties of the coating depend on the coating process. Plasma Spraying results in a lower density, ρ, and a lower Young's Modulus, E.
- The material properties for the W-coating and the F82H substrate are shown in the following table:

Properties	F82H	W (Bulk)	80% Dense W (VPS)
Young's Modulus (GPa)	217	410	54*
Poisson's ratio	0.29	0.29	0.1
Density (kg/m³)	7870	19246	15397
Wave speed (km/s)	6.011	5.284	1.894

*Matejicek, 2005

Failure Strength Measurements

- The critical laser intensity, 28.5 kJ/m², at which the first evidences of crack nucleation appears in the coating is used to calculate the failure strength.
- The generated compression pulse at this critical laser intensity is determined experimentally by monitoring the transient displacement history of the substrates free surface by using an optical interferometer. The corresponding stress wave profile is then derived using standard interferometery procedures.

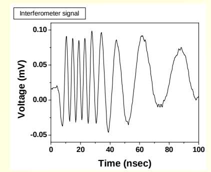

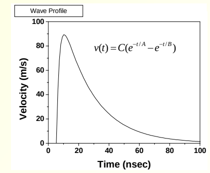

- Finally, the failure strength is determined, at the location of crack nucleation, by reading the velocity history into a finite element code (ANSYS).

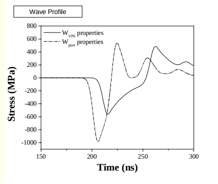

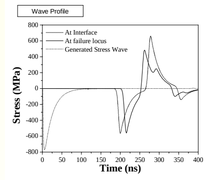

- Based on the idealistic assumptions, the failure strength of the VPS W-coating, was calculated to be in the following range:

$$450MPa \le \sigma_c \le 550MPa$$

Acknowledgement

This work was supported by the US Department of Energy, NNSA/DP

IFE Target Chamber Plasma Exhaust Fuel Recovery System (FRS)

IFE Strategy Workshop, April 24 – 27, 2007. San Ramon, CA

C. A. Gentile[1], S. W. Langish[1], T. Kozub[1], C. Priniski[1], T. Dodson[1], G. Gettelfinger[1], L. Ciebiera[1], J. Wermer[2], K. Sessions[3], J. Sethian[4], A. E. Robson[4]

[1] Princeton Plasma Physics Laboratory
[2] Los Alamos National Laboratory
[3] Savannah River National Laboratory
[4] Naval Research Laboratory

- The Receiving and Analysis System (RAS) designed to receive the target chamber effluent gas stream, and hold the gas temporarily for analysis.
- The Bed Regeneration System (BRS) designed to provide a method for regenerating the Molecular Sieve Dryer, Nickel (Ni), and ZrFe beds in both the RCS and the GCS, and the Molecular Sieve Dryer and the Nickel beds in the HPS.
- The Hydrogen Purification System (HPS) configured to receive the target chamber effluent gas stream and separate the hydrogen isotopes from that gas stream with a DF of greater than (>)10^4.
- The Residual Cleanup System (RCS) configured to remove tritium from the residual gas in the Gas Holding Tanks.

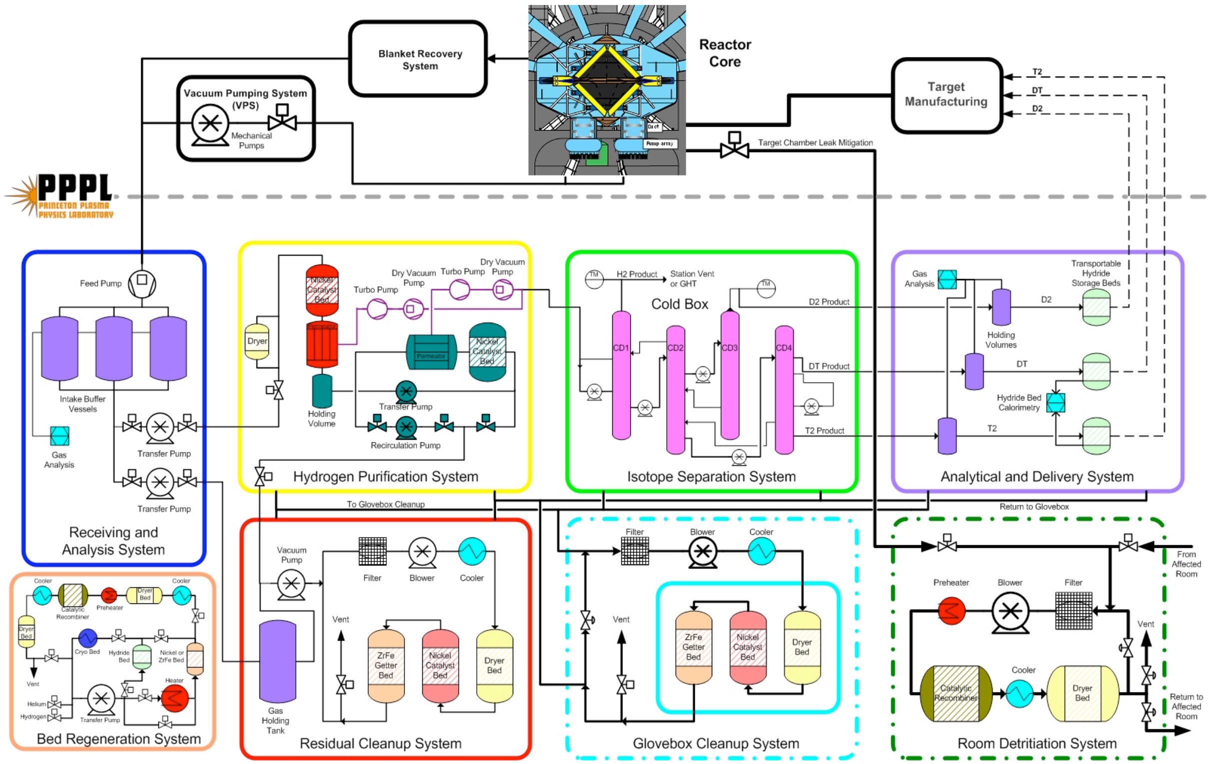

- The Isotopic Separation System (ISS) for the IFE target chamber exhaust is configured to receive hydrogen isotopes from the HPS and separate them using cryogenic distillation into hydrogen, deuterium, and tritium (or a deuterium-tritium mix).
- The Glovebox Cleanup System (GCS) designed to remove tritium and maintain a dry argon atmosphere in each of the facility glove boxes.
- The Analytic and Delivery System (ADS) designed to receive deuterium, tritium, and/or a deuterium-tritium mix from the ISS.
- The Room Detritiation System (RDS) designed to detritiate a room in the event that the tritium level in that room exceeds a predetermined value. Additionally the RDS can be used for target chamber leak mitigation.

Path Forward: The next step in the development of the FRS design is to analyze the interactions between this subsystem and other systems within the reactor complex, including target design and target manufacture. Currently different breeding blanket concepts are being evaluated to best fit the requirements of fueling. Of paramount importance is the safe operations and efficiency of this system as it integrates into the larger reactor complex. To the highest extent possible, proven commercial off-the-shelf (COTS) technologies are incorporated into the design for the purpose of providing a highly reliable and cost effective system. As a result of implementing these strategies the FRS is not a pacing item in the development of a closed fuel loop IFE power reactor.

PPPL PRINCETON PLASMA PHYSICS LABORATORY

Los Alamos NATIONAL LABORATORY EST.1943

SRNL We Put Science To Work

Target Fabrication Status for the HAPL Program

QWER

J.F. HUND, R.R. PAGUIO, D.T. GOODIN, D. SCHROEN, W. LUO, D. STEINMAN, J. STREIT[1], N. PETTA[1]
W. HOLLOWAY[2], N. ROBERTSON[2], M. WEBER[2]

[1]Schafer Corporation
[2]University of California San Diego

Introduction

The current high-gain HAPL target design is a 4.6 mm diameter foam capsule

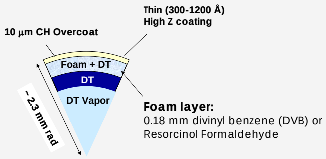

Important Specifications

Foam shell:
- Out of round - <1%
- Wall uniformity - <1-3%

Plastic Overcoating:
- Gas tight
- Smooth (50 nm RMS)

Foam Layer Material

Resorcinol Formaldehyde (RF)
- CHO polymer
- Very small pore size (~10-100 nm)
- Aqueous precursor

Divinyl Benzene
- CH polymer
- Large pore size (~1000 nm)
- Organic precursor

Foam Shell Fabrication Process

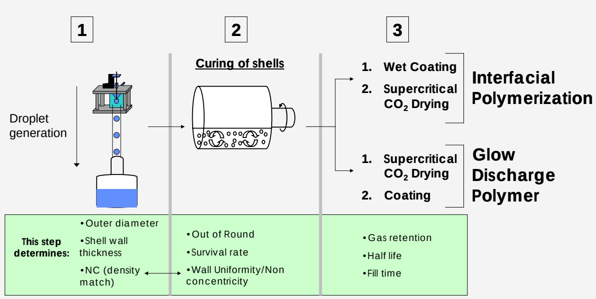

1. **A triple orifice droplet generator is used to form an emulsion of spherical shells out of the liquid precursor of the shell wall**
2. **While the shells are gelling, they are agitated in order to center the inner droplet - creating a uniform shell wall**
3. **The shells can be coated before or after drying**
   Glow discharge polymer allows the coating of shells after they have been dried.

References
1) C.P. Lee and T.G. Wang, J. Fluid Mech. 188, 441 (1988).
2) T. Norimatsu, *Fusion Technol.* **35**, 147 (1999).
3) B. McQuillan et al., 15th HAPL Workshop August 2006.
4) Roark and Young, *Formulas for Stress and Strain* (1982)

IFT/P2007-020

Wall Uniformity

The current foam wall uniformity specification is described in terms of shell Non-Concentricity (NC)

The Current specification for NC is: $\frac{offset}{Wall} \leq 1-3\%$

Which corresponds to an offset of ~5 μm

Theories of centering
- Modes of Oscillations [1,2]
- Rotational Shear: Journal Bearing Model [3]

These models indicate several important parameters for centering of the inner droplet during curing:
- **Surface tension –** changes oscillation of shell, increased surface tension also improves sphericity of shell
- **Density mismatch –** inner fluid and shell wall densities should be very similar,
- **Deformation -** Rate of collisions (size of container, # of shells, etc.)
- **Viscosity –** dampens out movement of inner droplet in shell; increases centering force in rotational shear model
- **Gelation time –** related to viscosity; inner droplet must be given time to center, but must be short enough to avoid compromising shell integrity

Idealized viscosity profile of shell wall during centering process

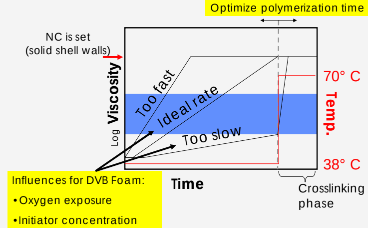

An optimization of parameters, has been done for large DVB shells and is beginning for large RF shells

Percentile of plot of shells indicating yield at a given %NC

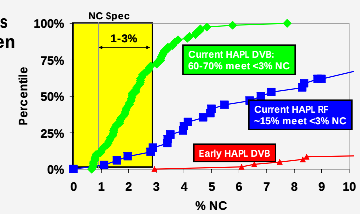

Conclusion

- **DVB Shell Uniformity – The shells have acceptable yield after optimizing conditions**
- **RF Shell Uniformity- Continuing work on improving the wall uniformity**
  - Increasing interfacial tension between shell wall and outer fluid
    - Has been demonstrated to improve the NC in 1mm diameter RF shells
  - Optimizing the inner & outer oil densities & run conditions
- **A Glow Discharge Polymer on RF Foam is a promising pathway for a smooth, gastight coating**

Overcoating

- **Must be gas tight and smooth (<50nm RMS)**
- **Pressure differentials in the coating process can cause leaks**

One challenge of fabricating a HAPL overcoat is the high aspect ratio required of the polymer coating

- The high aspect ratio causes the shells to have a low buckle strength

Buckle strength Formula for a Thin Shell

$$\Delta P_{buckle} = \frac{2 \cdot E}{\sqrt{3 \cdot \left(1-\nu^2\right)}} \left(\frac{w}{r}\right)^2$$

$\frac{r}{w} =$ Aspect ratio of shell radius to coating thickness
$E =$ Elastic modulus
$\nu =$ Poisson's ratio

Alternate form from Roark[4] suggests buckle may be even less

$$\Delta P_{buckle} = 0.365\, E \left(\frac{w}{r}\right)^2$$

Calculated Buckle Strength of Parylene

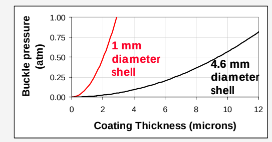

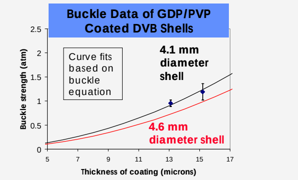

The Burst Strength is higher

$$\Delta P_{burst} = S \cdot \frac{2w}{r} \quad \text{~5-10 atm}$$

The burst strength depends linearly on the aspect ratio, allowing the shell to be less sensitive to overpressure

Elastic (tensile) modulus (*E*) of various polymers are similar

Polymer	*E* (kpsi)
Polystyrene	**260-551**
Polyimide	**189 - 580**
Parylene	**348**

Low buckle strength will be a problem with any high aspect ratio shell with a polymer coating

Primary Coating Technique:
Glow Discharge Polymer (GDP)
- Compatible with small pore size of R/F
- Improved surface roughness
- Successful on smaller R/F shells for OMEGA
- "Dry" coating
  - Coating deposited after supercritical CO2 drying
  - Avoids burst and buckle pressures on the shell from drying process

Initial GDP on RF gas testing results

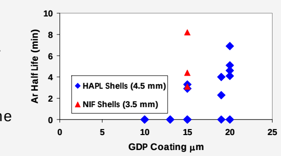

Alternate Techniques Possible for DVB and RF:
Interfacial Polymerization (PVP)
- Wet coating chemistry
- Requires solvent exchanges and drying for foam shell application

2 layer coatings – (PVP/GDP)
- Interfacial layer covers the larger pores, GDP seals shells

Surface Smoothness
Coated R/F foam shells are smoother than over-coated DVB shells to date

Roughness* of ~4mm Shells with Different Coating Types

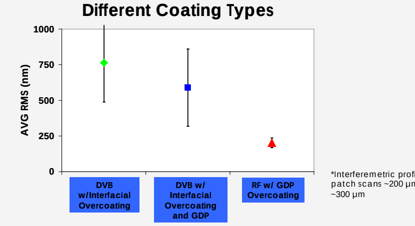

*Interferemetric profiler patch scans ~200 μm x ~300 μm

Measurement of Electron Clouds in Heavy-Ion Beam Drivers for HEDP and IFE*

M. KIREEFF COVO, LLNL and UCB, A.W. MOLVIK, R. COHEN, A. FRIEDMAN, LLNL,
P. A. SEIDL, J-L. VAY, F. BIENIOSEK, B. G. LOGAN, LBNL, J. VUJIC, UCB

In order to focus ion beams to high-power density for high-energy-density physics studies and ultimately inertial-fusion power production, we must be able to transport high-current, high-energy beams while preserving their brightness (minimizing their emittance). With this aim, the US Heavy Ion Fusion Sciences program developed the High Current Experiment (HCX), consisting of a single beam injector, an electrostatic matching section, and electrostatic and magnetic quadrupole transport sections, that provides a K+ ion beam current of 183 mA for 5 μs. It constitutes a unique facility to study the physics of high brightness transport under conditions of a large "fill factor" (ratio of beam radius to tube radius), as necessary for cost minimization. A deleterious effect that can arise when ions strike the pipe wall is the development of a stray "Electron Cloud," a recognized problem that limits the current and brightness on many large accelerators. Our goal here is to understand this effect using new diagnostics coupled with state-of-the-art simulations, and to develop techniques for minimizing such clouds.

* This work performed under the auspices of the U.S Department of Energy by University of California, Lawrence Livermore and Lawrence Berkeley National Laboratories under contracts No. W-7405-Eng-48 and DE-AC02-05CH11231.

Fusion power plant cost reduced by high fill factor beams

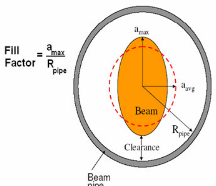

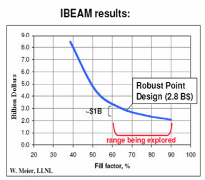

(fixed number of beams, initial pulse length, and quadrupole field strength)

▪ **Cost of a Fusion Power Plant is function of fill factor**

At the range of interest (beyond 60%), the beam runs closer to the walls and starts to produce secondary electrons and desorbed gas, which could move to the beam path and be ionized. The electrons produced are trapped by the space charge beam potential. We start to lose control of the beam transport and produce more secondary electrons and desorbed gas. It is the beginning of the "Electron Cloud Effect".

Physical mechanism of electron production

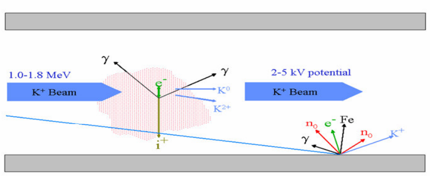

▪**Beam hitting gas or walls creates electrons and gas**

At grazing incidence, each ion of K+ ion with energy of 1MeV desorbs 10,000 molecules of gas and produces 100 electrons, which can multiply.

HCX instrumented to perform Electron Cloud density accumulation experiments

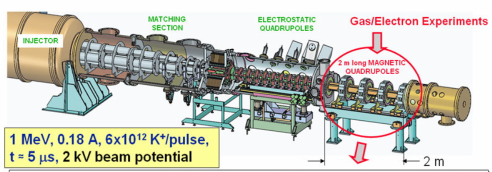

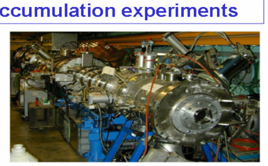

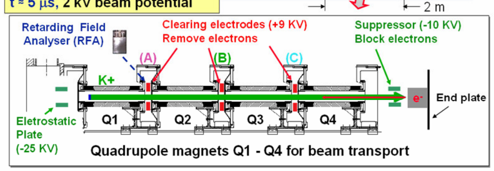

▪ **Electron Clouds were observed inside the Magnetic transport Section**

The magnetic transport section can work as an electron trap device. Electrons can be confined axially between the suppressor at one end and the last electrostatic quadrupole plate at the other end, and radially by the beam space-charge potential of 2 KeV. Clearing electrodes and suppressor can work as switches to allow electron accumulation experiments.

Absolute measurement of Electron Cloud density*

*M. Kireeff Covo et al., Phys. Rev. Lett. 97, 054801 (2006)

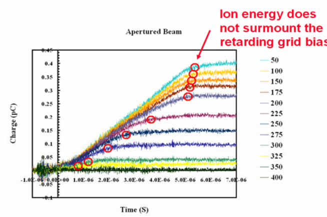

▪ **Retarding Field Analyzer (RFA) measures depressed beam potential by electron accumulation**

The produced cold ions are expelled by the beam space charge, so the maximum energy of the ion is given by the beam potential. As the RFA is a high-pass energy filter, when the RFA does not collect more ions is the moment that the beam potential decayed to the retarding grid bias.

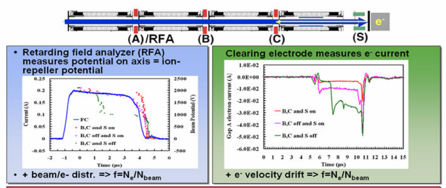

Absolute electron fraction can be inferred from RFA and clearing electrodes

Beam neutralization	B, C, S on	B, C off S on	B, C, S off
Clear. Electrode A	~ 7%	~ 25%	~ 89%
RFA	(~ 7%)	~ 27%	~ 79%

▪ **Measurements of Electron Cloud accumulation**

We used clearing electrodes B and C, and suppressor S to control electron accumulation. If we turn on all the electrodes (B, C and S on), we minimize electrons from all sources and the beam potential has the same slope of the Faraday cup current, showing that the beam neutralization remains constant. When we turn off the clearing electrodes (B, C off, S on), we see a higher slope, showing the beam potential depressed by the Electron Cloud accumulation. Finally, if we also turn off the suppressor (B, C, S off) we allow electrons from end plate to drift upstream and fill the quadrupole magnets.

WARP simulations show phase space similar to the experiments

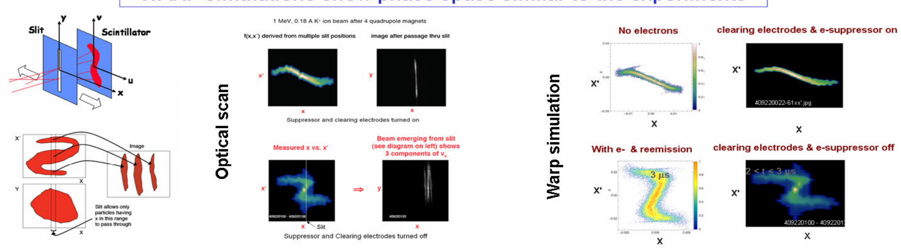

Conclusions

• The High-Current Experiment (HCX) is an unique platform to explore sources of electron generation and accumulation in positively charged beams.
• We developed a new technique to measure electron accumulation by probing the depressed beam potential with expelled ions produced from the interaction of the beam with the background gas. The simulations show not only the qualitative aspects of the experiments, but also some unanticipated physical effects from the beam degradation by the Electron Cloud accumulation. Such degradation must be minimized, by techniques such as we are developing, in order to focus beams to high power density.

Inaugural IFE Science and Technology Strategic Planning Workshop: Updates on Progress, Visions, and Near-Term Opportunities

UCRL-POST-230299

Beam Focusing Concept for a Modular Heavy Ion Driver

by

Edward Lee

Lawrence Berkeley National Laboratory

for

The IFE Science and Technology Strategic Planning Workshop

April 24 - 27, 2007

A modular heavy ion driver uses many synchronized linacs $(N \approx 20-100)$ at relatively low kinetic energy $(E \approx 100-1000\, MeV)$

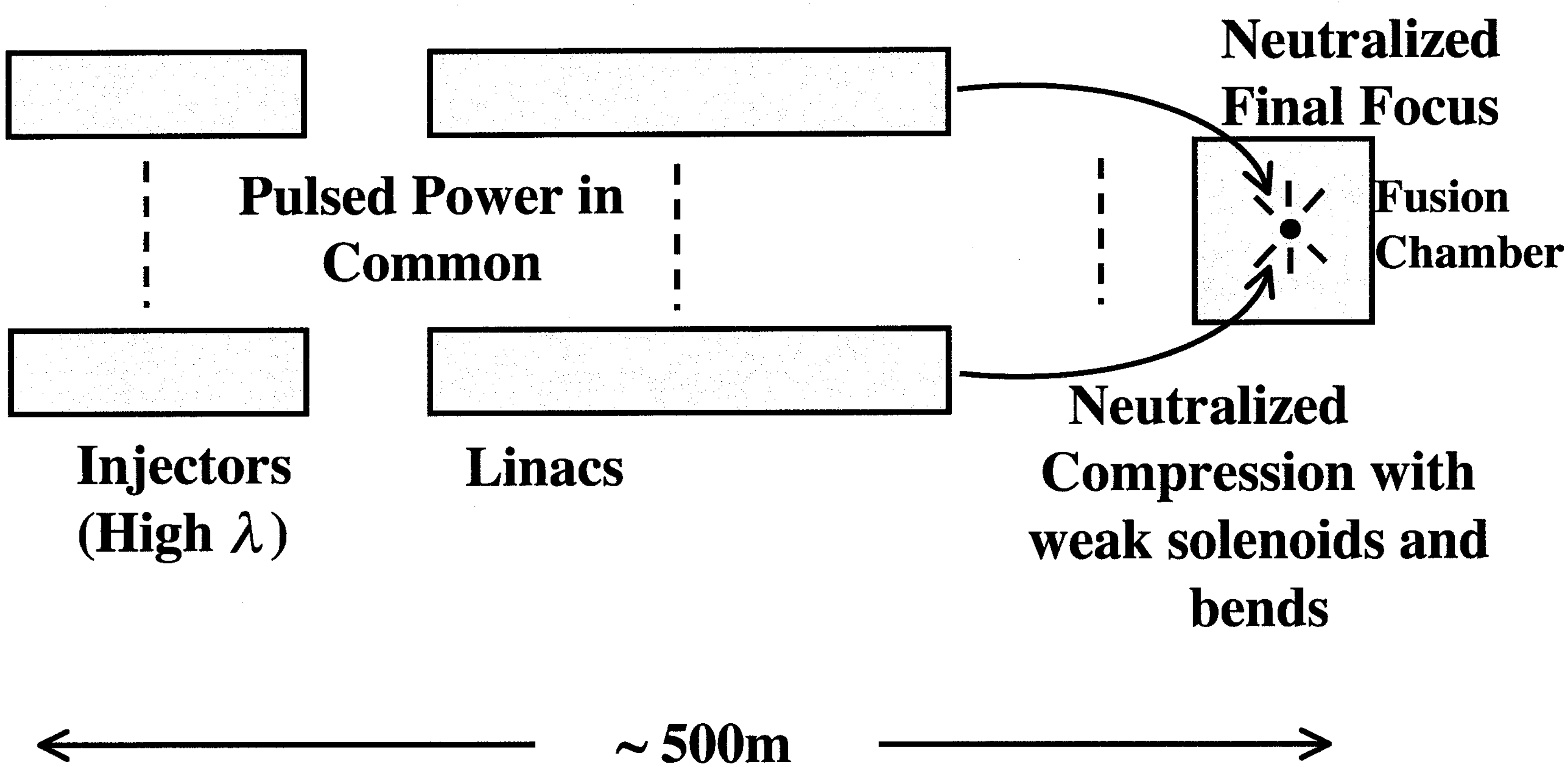

Why Consider Solenoids for HIF Now?

- Solenoids transport higher line charge density beams at low kinetic energy than quadrupoles:

$$T \lesssim 16\,MeV \qquad C_s^+$$

$$T \lesssim 40\,MeV \qquad N_e^+$$

- Solenoids are essential for several high current source concepts
- Solenoids may aid neutralized drift compression
- Final Focus for neutralized, highly stripped beams is simplified
- Transverse dynamics in vacuum transport is more stable and has less "flutter" than with quadrupoles and electron production from pipe walls may be suppressed

These Solenoid Features Suggest A Modular Driver Architecture

- $N \approx$ 20-100 parallel separate accelerators in two opposed clusters
- Moderate mass ions are accelerated to relatively low energies (e.g. 200-300 MeV N_e^{+}) or 500 MeV K_r^{+8}
- High line charge density is transported by solenoids during acceleration $(\lambda \approx 5 - 20 \;\mu C/m)$
- Final Compression, Final Focus and Chamber Transport are neutralized to accommodate very high final line change densities

Modularity allows an attractive development path

A solenoid-based final focus system for a modular driver has attractive features

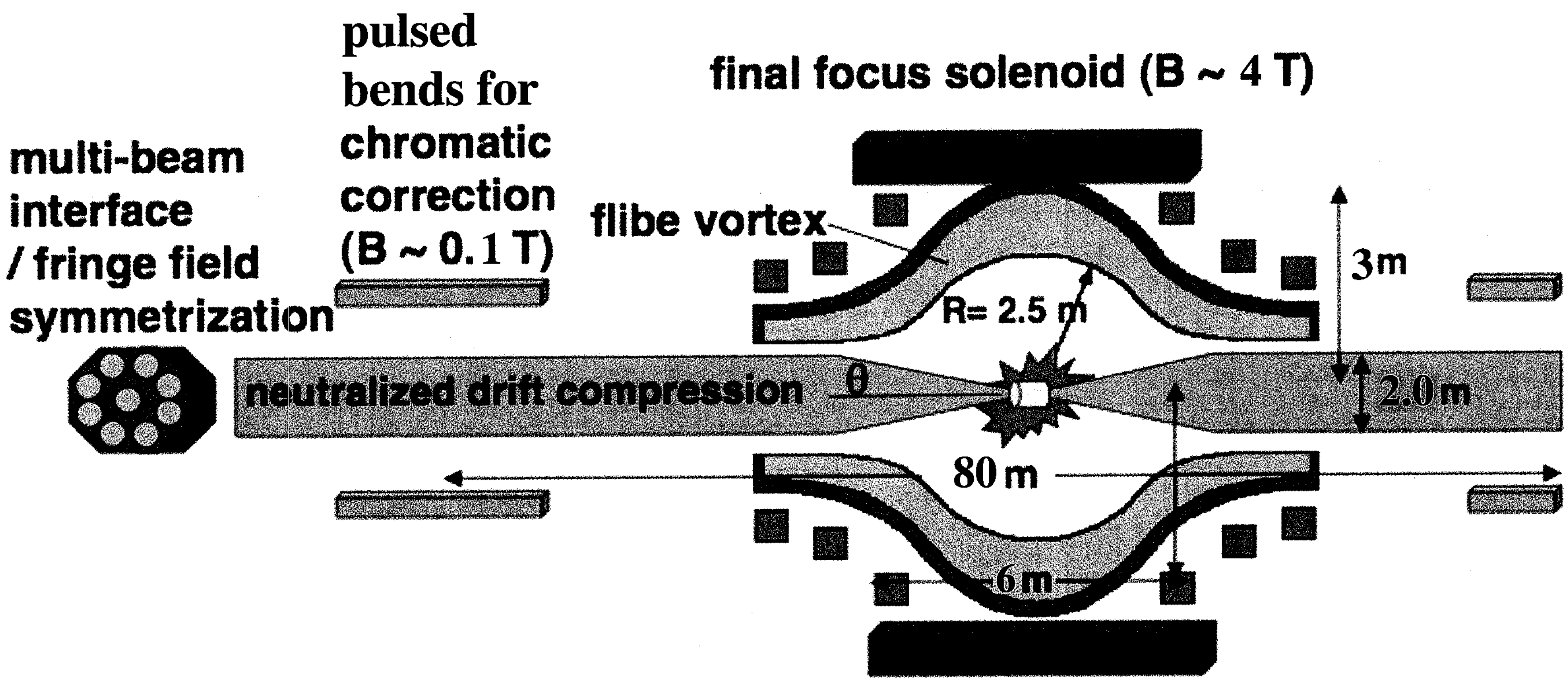

- Large cone angle θ ~ 200 mr produces a small spot (~ 1 mm) on target for ε ~ 4×10^{-6} m-rad
- Moderate fields allow normal magnets
- Highly stripped ions (eg q=+8)
- Fringe field aberrations minor

A modular driver may simultaneously accelerate several ion species

- Useful for "pulse foot" or target interaction at different latitudes
- All ions must have about the same magnetic rigidity

$$\text{rigidity} = \frac{\text{momentum}}{\text{charge}} = B\rho \;=\; 3.107\beta\gamma\, A/q$$

Example $(B\rho = 3.7\mathrm{T-m})$: range in cold carbon

320MeV Xe^{+8}	.003gm/cm^2
500MeV Kr^{+8}	.006gm/cm^2
1040MeV Ar^{+8}	.1gm/cm^2

Features of a final focus system

- Low magnetic rigidity $\longrightarrow$ solenoids may be used
- Require very high degree of charge and current neutrality
- Beams injected off-axis (~1.0m) are all focused to an on-axis target $\longrightarrow$ $\frac{\varepsilon}{\theta} \approx$ rspot
- Small solid angle for neutron escape
- Time-dependent kicker compensates for momentum variation within a pulse
- Beam spot radius $r_s \leq 1.0mm$ (direct drive) for plausible emittance and thermal momentum spread
- Capability for rapidly rotating spot position on fusion target

Focal Design Features (cont.)

- Parallel-to-Point Focus on axis includes effects on aberrations
- Weak solenoids produce an intermediate focus - good for neutron confinement and corrections for momentum variation
- Strong central solenoid produces a small beam spot radius
- Large final angles (100 - 300mr)

Issues

- Does a beam's emittance and charge state remain constant while traversing the gas density profile required for neutralization?
- Are beam instabilities (hose, two-stream, …) benign in their effect on focusing?
- Can a fast kicker be designed with the required low jitter $\left(\Delta B/B \le 10^{-3}\right)$?
- Can a high field solenoid operate close to a fusion chamber?
- Can high charge state ion sources produce beams with the desired current and quality?

An Ion is Focused by the Interaction of Its Azimuthal Velocity with Bz

$$F_r = qe(E_r + v_\theta \mathrm{B}_z)$$

$$F_\theta = -qev_z \mathrm{B}_r$$

- **Azimuthal velocity v_θ is impressed on an ion when it passes through the fringe field.**
- **A beam <u>spins</u> in a cold equilibrium with space charge field $\mathrm{E_r}$ balanced by Bz (Brillouin flow).**
- **This is not like a magnetized plasma or most non-neutral plasma experiments.**
- **Dynamics are simplified in the Larmor frame (rotates at $\theta = -\omega_c/2$)**

Computation of ion orbits must include geometric and fringe field aberations

Assuming charge and current neutrality:

$$\frac{d^2x}{dz^2} = \frac{\left(1 + x'^2 + y'^2\right)^{1/2}}{B\rho}\left[y'B_z - \left(1 + x'^2\right)B_y + x'y'B_x\right]$$

$$\frac{d^2y}{dz^2} = -\frac{\left(1 + x'^2 + y'^2\right)^{1/2}}{B\rho}\left[x'B_z - \left(1 + y'^2\right)B_x + x'y'B_y\right]$$

$$B_z = B_o(z) - \frac{B_o''r^2}{4} + \frac{B_o''''r^4}{64} - \ldots$$

$$B_r = -\frac{B_o'r}{2} + \frac{B_o'''r^3}{16} - \frac{B'''''_o r^5}{384} + \ldots$$

$$B_x = \frac{xB_r}{r} - \frac{B_\theta y}{r}$$

Pulsed kicker

$$B_y = \frac{yB_r}{r} + \frac{B_\theta x}{r}$$

An on-axis solenoidal field profile suitable for 500 MeV K_r^{+8}

Ion rigidity $B\rho = 3.7T - M$

Solenoid #	center	length	current radius	current length K	scale field (μ_0K)
1	14m	26m	2m	370,000A/m	.465T
2	32	10	2	-92,000	-0.116
3	40	6	3	-4,900,000	6.166
4	48	10	2	-92,000	-0.116
5	66	26	2	370,000	0.465

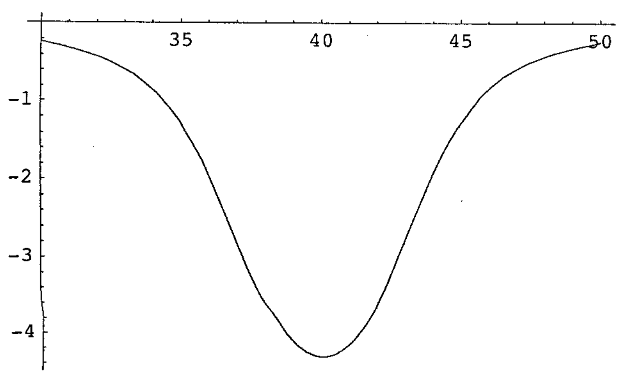

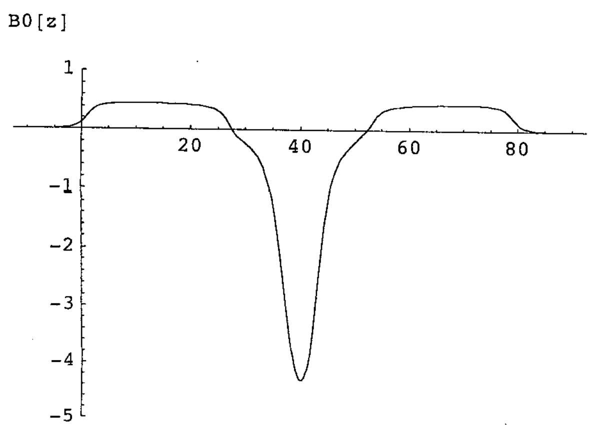

Particle Trajectories $(B \quad = 3.7Tm)$

Initial values

at $z = \quad 1.0$

$$\left\{ \begin{array}{ll} x = 1.0 & x \; = 0.0 \\ y = 0.0 & y \; = \#.00822 \end{array} \right\}$$

$$\left(\begin{array}{l} \text{Initial } y \text{ is adjusted to make } P \; = 0 \\ \text{Field profile adjusted for focus at } z = 40\text{m} \end{array} \right)$$

$x(z)$ and $y(z)$

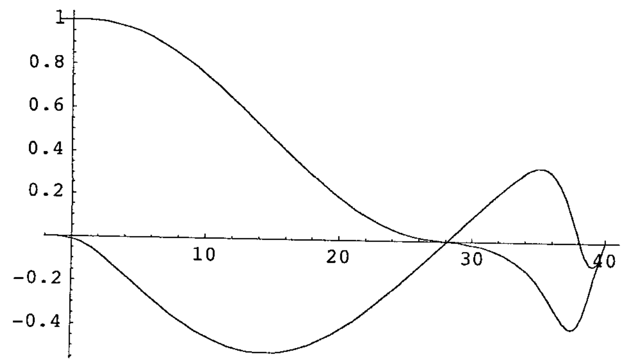

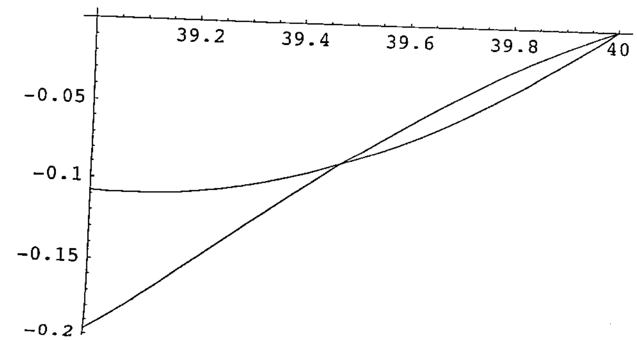

$r(z)$

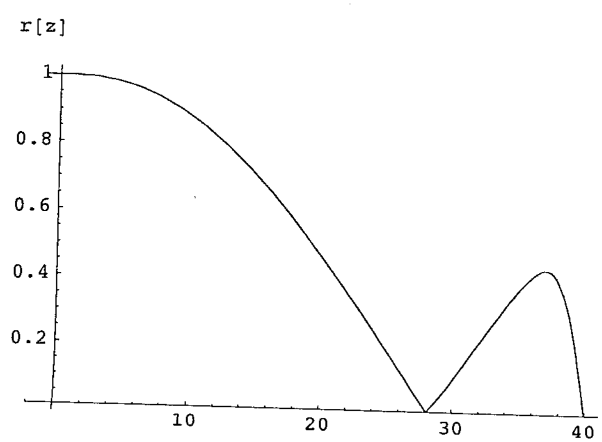

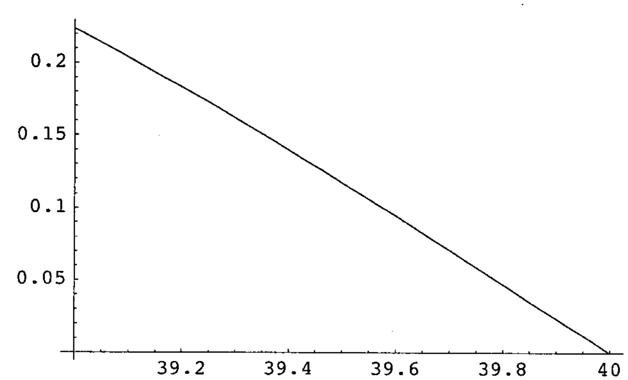

Ion Trajectories (cont.)

x and y as seen from target

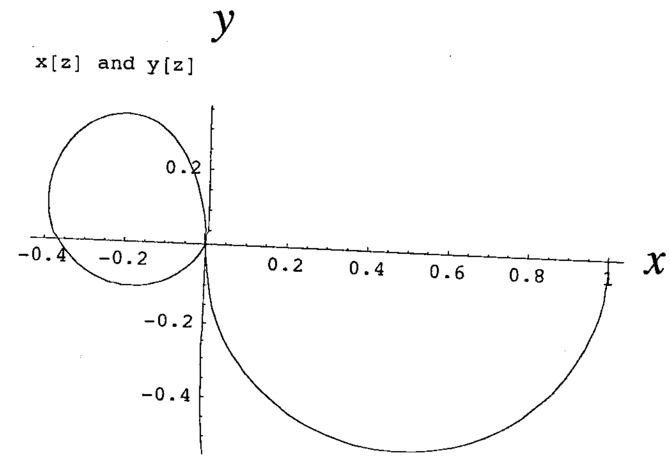

Beam envelope with linear dynamics:

$$a(o) = .02m,\quad \varepsilon = 10^{-5}\, m - r \quad z x 10^{-6}\, m - r$$

$a(z)$

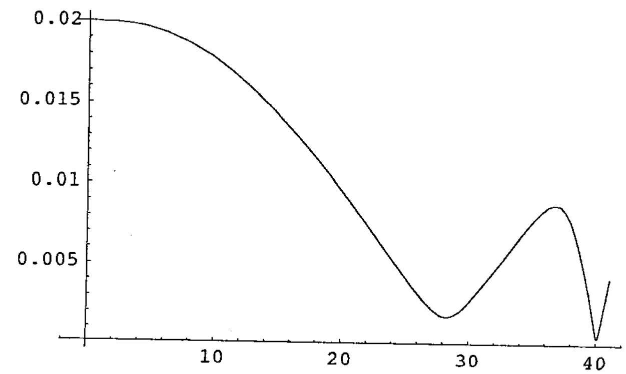

Corrected off momentum Trajectories

Energy	Kicker Field
400 MeV	−.1004T
450 MeV	−.0484T
500 MeV	.0000T
550 MeV	.0504T
600 MeV	.1043T

$r(z)$

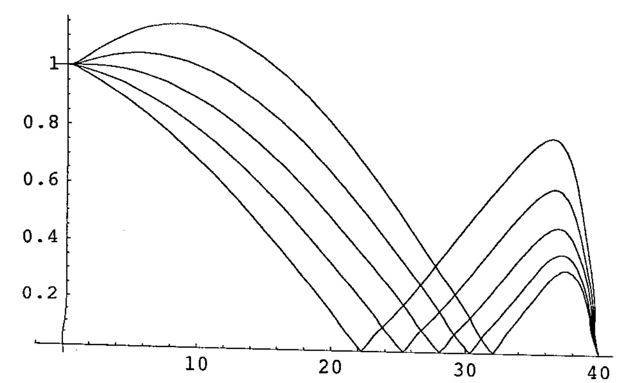

Simple Field Calculations

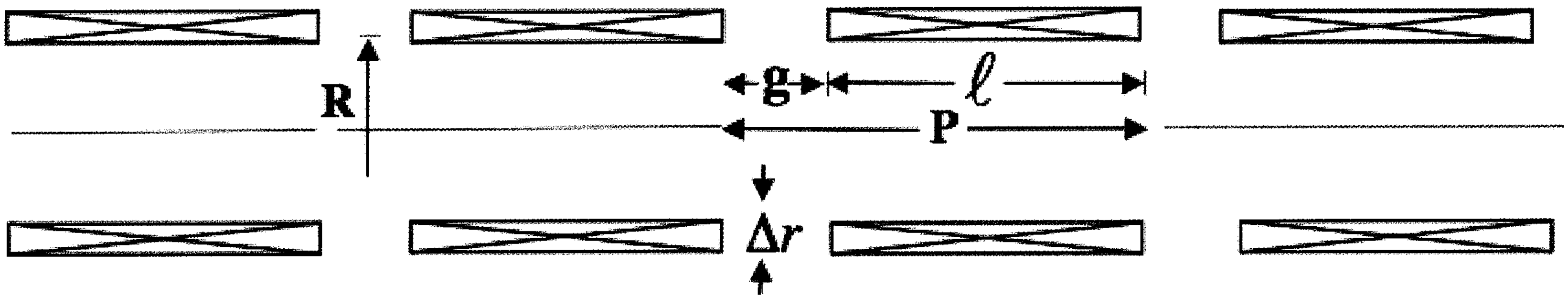

Thin current layer centered at r=R:

$$K(z) = J_\theta \Delta r$$

On axis field:

$$\mathrm{B}_0(z) = \frac{\mu_0 R^2}{2} \int_{-\infty}^{+\infty} \frac{dz' \;\; K(z')}{\left[(z'-z)^2 + R^2\right]^{3/2}}$$

off axis (r<R)

$$\mathrm{B}_z = \mathrm{B}_0 - \frac{\mathrm{B}_0'' r^2}{4} + \frac{\mathrm{B}_0'''' \; r^4}{64} - \ldots$$

$$\mathrm{B}_r = \underbrace{-\frac{\mathrm{B}_0' r}{2}}_{\text{Linear Part}} + \underbrace{\frac{\mathrm{B}_0''' r^3}{16} - \frac{\mathrm{B}_0''''' \; r^5}{384}}_{\text{Aberrations}} + \ldots$$

Simple Fields

Semi-infinite layer:

$$B_0(z) = \frac{\mu_0 K}{2}\left(1 - \frac{z}{\sqrt{z^2 + R^2}}\right)$$

Build useful design fields from this case.

Lens of length ℓ :

$$B_0^{Lens} = \frac{\mu_0 K}{2}\left[\frac{\left(z + \ell/2\right)}{\sqrt{\left(z + \ell/2\right)^2 + R^2}} - \frac{\left(z - \ell/2\right)}{\sqrt{\left(z - \ell/2\right) + R^2}}\right]$$

Lattice:

$$B_0 = \sum_i B_0^{Lens}(z - Pi)$$

A New, "First Principles" Look at the Parameter Space for Controlled Thermonuclear Fusion

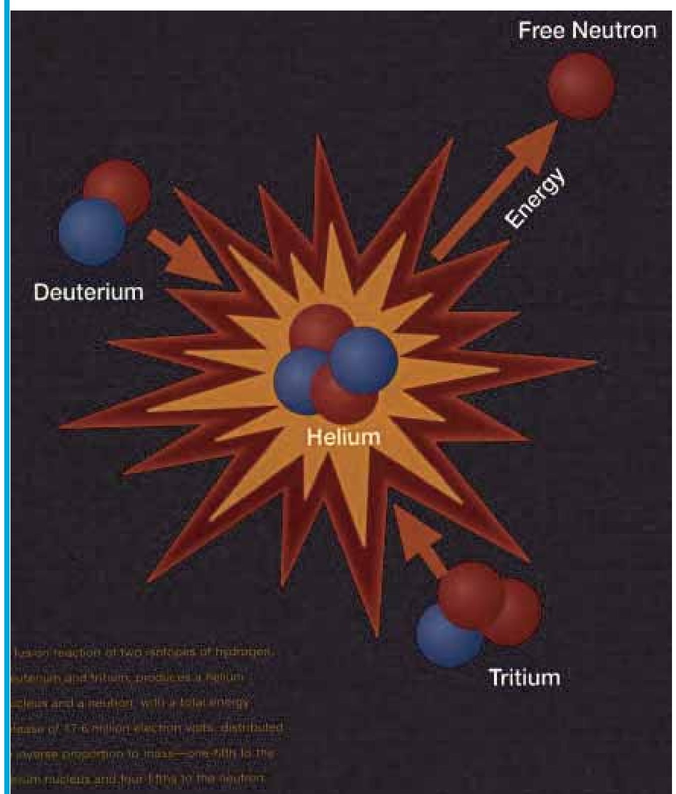

Irvin R. (Irv) Lindemuth
Richard E. (Dick) Siemon

Department of Physics
University of Nevada
Reno NV

Poster paper presented at the IFE Science and Technology Strategic Planning Workshop
April 24-27, 2007
San Ramon CA

Abstract

The conventional pathways to fusion—MCF and ICF—have proven to be very long and very expensive. These two approaches are now embodied in two multi-billion-dollar facilities, ITER for MCF and NIF for ICF. These two approaches differ by many orders of magnitude in fundamental physical quantities (density, burn time, fuel pressure, and fuel volume). Given such large differences, it is reasonable to ask an obvious question:

is there anything in between the extremes of MCF and ICF?

In this paper, we take a new "first principles" look at the conditions under which fusion can occur. We review the fuel conditions (e.g., confinement time, density, temperature) that must be met to achieve significant fusion energy release. By comparing loss rates with fusion rates, we can identify the density-temperature space where fusion gain can be achieved. This simple analysis offers a general understanding of the extreme differences between the conventional approaches to controlled fusion, MCF and ICF. The analysis shows that the constraint of steady-state operation forces MCF to operate at the low end of the density spectrum and that the constraint of unmagnetized fuel forces ICF to operate at the high end. Most importantly, the analysis shows that using a magnetic field in the fusion fuel allows operation at an intermediate density (10e18-10e22/cm3), a density range that has many attractive features and potentially overcomes some of the obstacles, particularly cost, faced by the more conventional approaches.

FUSION 101--what they should have taught us in freshman physics > 40 years ago.

- **What fusion fuel density, temperature, magnetic field, etc. are required to achieve fusion?**
- **Why is the National Ignition Facility (NIF) forced to operate at very high density?**
- **Why is the International Toroidal Experimental Reactor (ITER) forced to operate at low density?**
- **Why are there so many orders of magnitude in density, volume, etc., between NIF and ITER?**
- **Why is fusion so costly?**
- **Has all the fusion parameter space been explored, or are there promising, but unexplored, regions in parameter space?**

Thermonuclear fusion occurs at high temperature.

- **For thermonuclear fusion, the reaction rate is given by a Maxwellian averaged cross section:**

$$\frac{dn_1}{dt} = \frac{dn_2}{dt} = -\overline{\sigma v} n_1 n_2, \qquad n_1, n_2 = \# \ \text{particles/cm}^3$$

- **D-T is the preferred fuel because of its higher cross-section**

$$n_D = n_T = \frac{n_i}{2}, \qquad \frac{dn_i}{dt} = -\frac{\overline{\sigma v} n_i^2}{2}, \qquad n_i = \# \ \text{ions/cm}^3$$

- **To reach a value of even 1% of peak, a temperature of 4 keV (50,000,000 deg. K) must be reached and sustained.**

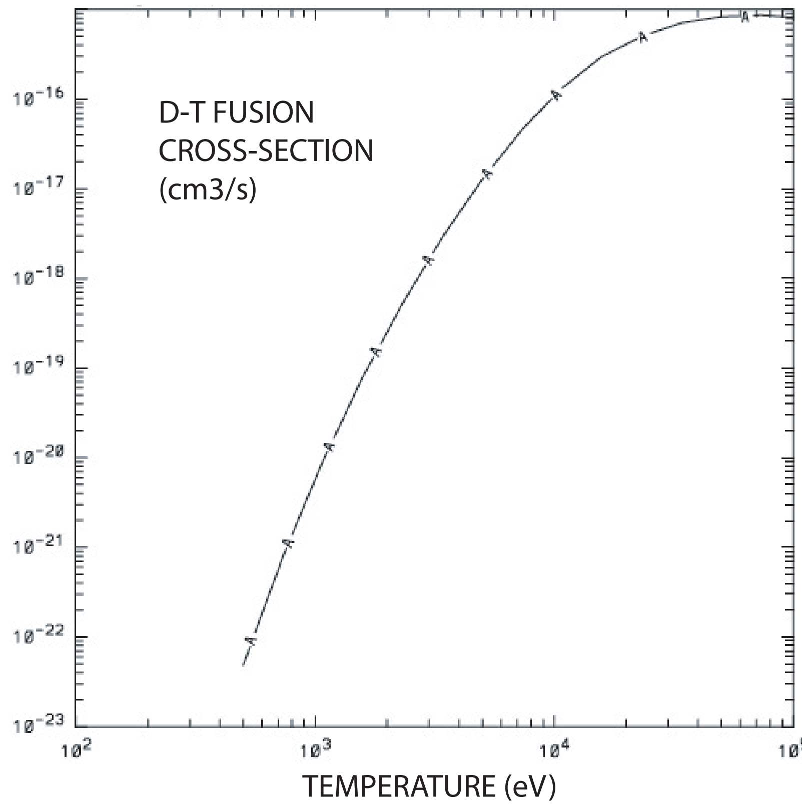

The rate equation can be integrated to give expressions for the number density and fusion energy produced as functions of time.

- **Number density:** $\frac{dn_i}{n_i^2} = -\frac{\overline{\sigma v}}{2} dt, \qquad \frac{\overline{\sigma v}}{2} t = \frac{1}{n_i} - \frac{1}{n_o}, \qquad n_i = \frac{n_o}{1 + \frac{\overline{\sigma v}}{2} n_o t}$

- **Energy produced:** $E_{FUS} = \varepsilon_{FUS} \frac{n_o - n_i}{2} = \varepsilon_{FUS} n_o^2 t \frac{\overline{\sigma v}}{4} \frac{1}{1 + \frac{\overline{\sigma v}}{2} n_o t}, \qquad \varepsilon_{FUS}$ =17.6 Mev

$$\dot{Q}_{FUS} = \frac{dE_{FUS}}{dt} = -\frac{\varepsilon_{FUS}}{2} \frac{dn_i}{dt} = \varepsilon_{FUS} n_i^2 \frac{\overline{\sigma v}}{4}$$

- **Initial plasma energy:** $3n_o T_o$

- **Gain:**

$$G = \frac{E_{FUS}}{3n_o T_o} = G_{\max} n_o t \frac{\overline{\sigma v}}{2} \frac{1}{1 + \frac{\overline{\sigma v}}{2} n_o t}, \qquad G_{\max} = \frac{\varepsilon_{FUS}}{6T_o}$$

- **G depends only on $n_o t$, tells how long plasma must be "confined"**

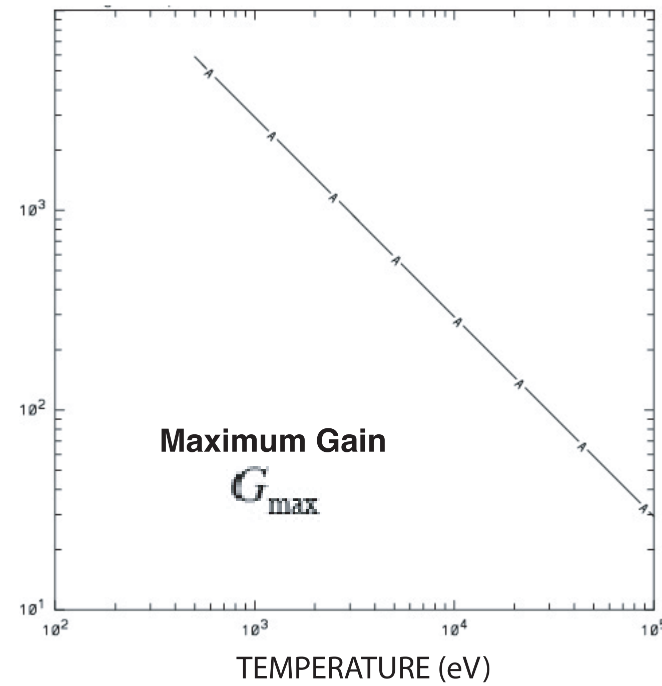

"Scientific breakeven" (G=1) is a continuing goal of fusion research

- **G=1 when** $n_o t = \dfrac{2}{\overline{\sigma v}} \dfrac{1}{G_{max} - 1} = L,$ $\quad L = \text{Lawson product}$

- **Plasma must be confined for the "Lawson time" to achieve scientific breakeven:**

$$\tau_L = \frac{1}{n_o} \frac{2}{\overline{\sigma v}} \frac{1}{G_{max} - 1} \approx \frac{2}{n_o \overline{\sigma v} G_{max}}$$

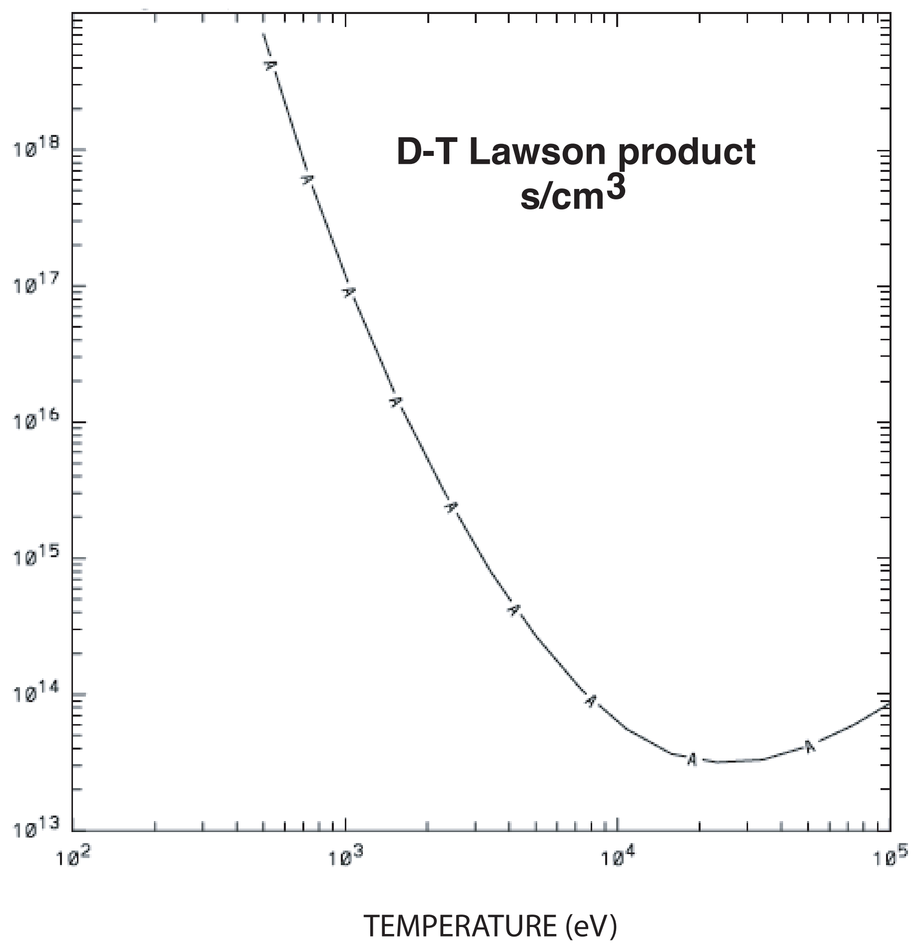

Unfortunately, plasma energy loss to cold surroundings by thermal conduction and radiation is a major obstacle to fusion

- **Losses reduce the effective gain:**

If $\dot{Q}_{loss} = \phi \dot{Q}_{FUS}$, $\quad G_l = \dfrac{E_{FUS} - E_{loss}}{3n_o T_o} = (1-\phi)\dfrac{E_{FUS}}{3n_o T_o} = (1-\phi)G, \qquad (G_l)_{\max} = (1-\phi)G_{\max}$

- **Losses also increase the time to achieve breakeven:**

$$G_l = 1 \text{ when } t = \frac{1}{n_o}\frac{2}{\overline{\sigma v}}\frac{1}{(G_l)_{\max} - 1} = \tau_L \frac{G_{\max} - 1}{(G_l)_{\max} - 1} \approx \tau_L \frac{1}{1-\phi} = N\tau_L$$

$\dot{Q}_{FUS} / \dot{Q}_{loss}$	1	1.1	1.25	2	5	10
ϕ	1	0.9	0.8	0.5	0.2	0.1
N	infinity	10	5	2	1.25	1.11

- **Losses also mean heating equal to $\dot{Q}_{loss}$ is required to sustain plasma.**

- **Useful energy production requires G > 1, i.e, confinement for many "Lawson times"-- t = XNτ_L for G = X, e.g., G = 10 requires t = 20 τ_L if ϕ = 0.5.**

Comparing loss rates with fusion rates identifies the density-temperature space where fusion gain can be achieved

- $\dot{Q}_{loss} = \dot{Q}_{TC} + \dot{Q}_{RAD}$ $\qquad$ $\dot{Q}_{RAD} = C_{RAD} n_i^2 T^{1/2}$ (Bremsstrahlung)

  $\dot{Q}_{TC} = -\nabla \bullet (K \nabla T) \quad (K = \text{thermal conductivity})$

- **Radiation losses determine a minimum temperature:**

$$\frac{\dot{Q}_{FUS}}{\dot{Q}_{RAD}} = \frac{\varepsilon_{FUS} n_i^2 \frac{\overline{\sigma v}}{4}}{C_{RAD} n_i^2 T^{1/2}} = \frac{\varepsilon_{FUS} \frac{\overline{\sigma v}}{4}}{C_{RAD} T^{1/2}}, \quad \text{independent of } n_i \qquad \frac{\dot{Q}_{FUS}}{\dot{Q}_{RAD}} \geq 1 \quad \text{when } T > 3\ keV$$

- $\dot{Q}_{TC}, \nabla T$ **must be approximated:**

$$\dot{Q}_{TC} \approx -\frac{1}{V} \int \nabla \bullet (K \nabla T) dV = -\frac{1}{V} \oint_S K \nabla T \bullet d\vec{S} \approx -\frac{S}{V} K \nabla T \approx \frac{KT}{\gamma \alpha a^2}$$

$$a = \text{characteristic dimension}, \quad V = \varepsilon a^3, \quad \frac{V}{S} = \gamma a, \quad \nabla T \approx -\frac{T}{\alpha a}$$

- ε, γ **are geometric quantities, i.e., for spheres $\varepsilon = 4\pi/3$, $\gamma = 1/3$; simulations show $0.1 < \alpha < 0.5$; this paper uses $\alpha = 0.25$.**

- **Loss rates depend upon *n_i, T, a*, model for *$K = K_i + K_e$*, geometry (ε, γ), profile details (α), and, possibly, magnetic field *B* (through *K*).**

IL-5_07-2

The conduction rate can be used to determine the minimum system size and other relevant parameters for a desired loss ratio ϕ.

- $$a_{\min}^2 = \frac{KT}{\gamma\alpha} \frac{1}{\phi E_{FUS} - E_{RAD}},$$
  $$a_{\min} = a_{\min}(n_i, T, B)$$
- $$M = n_i (m_i + m_e) \varepsilon a_{\min}^3$$
- $$E_{PLAS} = 3 n_i T \varepsilon a_{\min}^3$$
- $$P_{HEAT} = (\dot{Q}_{TC} + \dot{Q}_{RAD}) \varepsilon a_{\min}^3$$
- $$I_{HEAT} = \frac{P_{HEAT}}{S}$$
- **If heating by compression, req'd velocity:** $$v_{IMP} = \frac{I_{HEAT}}{p}$$

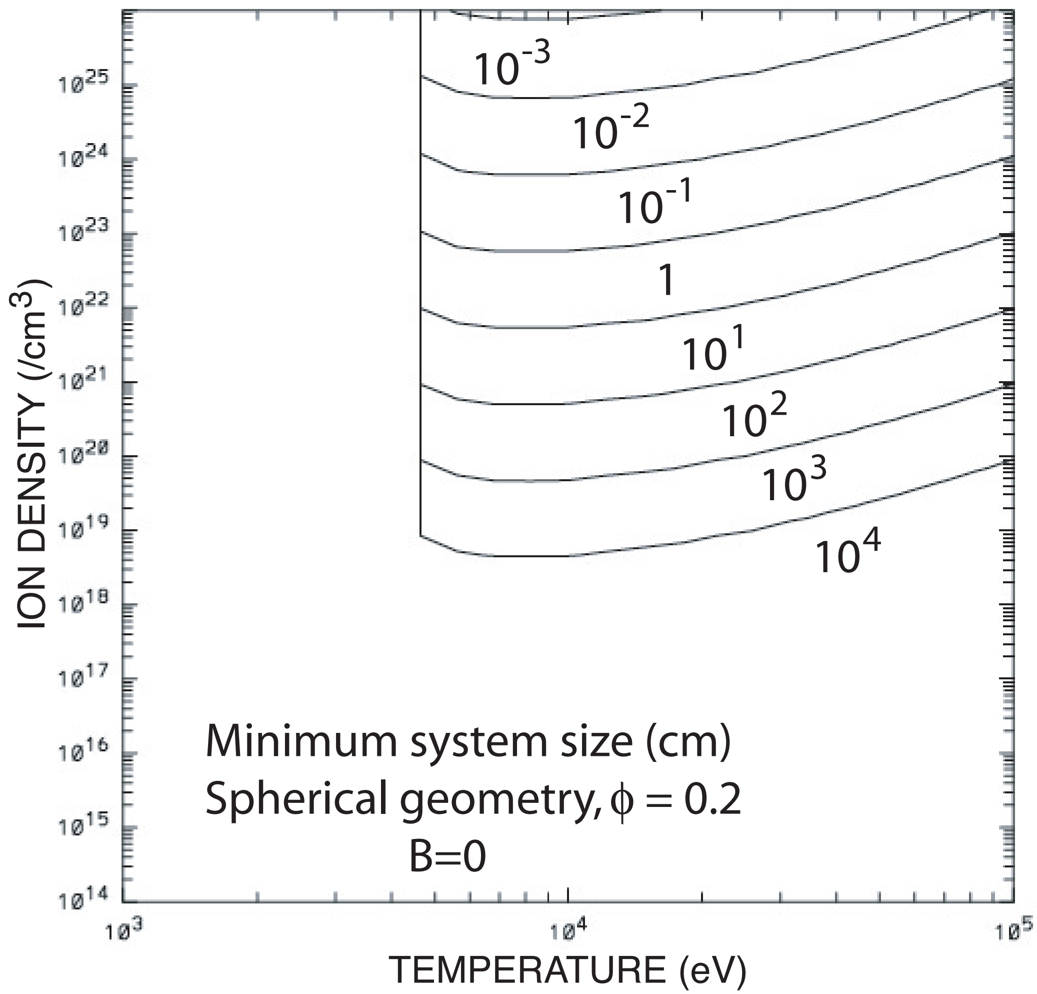

IL-5_07-3

The mass, energy, and power requirements for unmagnetized (B=0) fuel are prohibitive except at very high density, pressure (>1e10 atm).

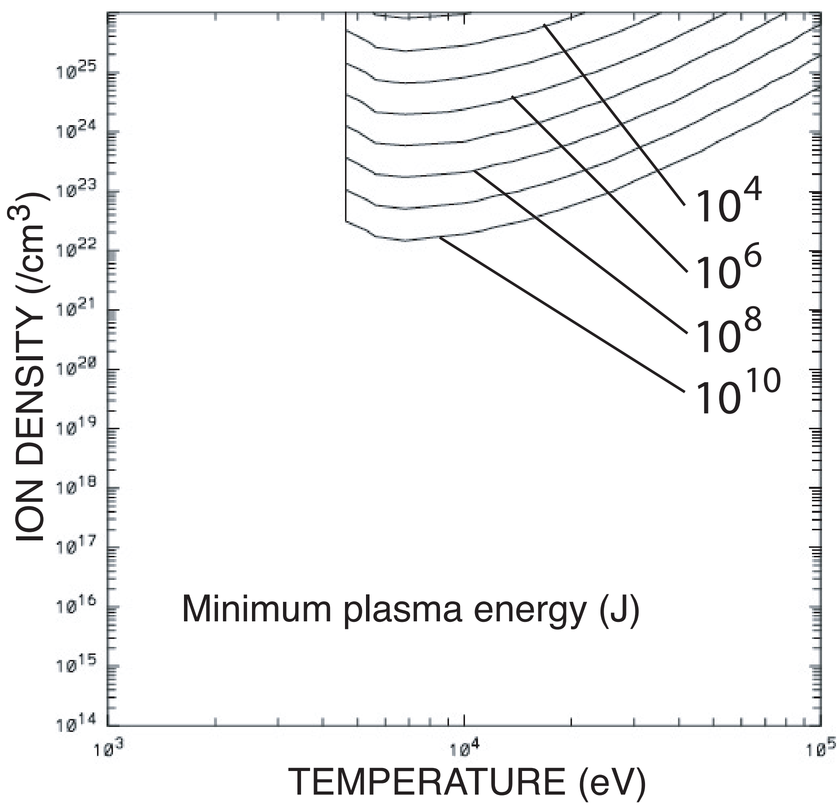

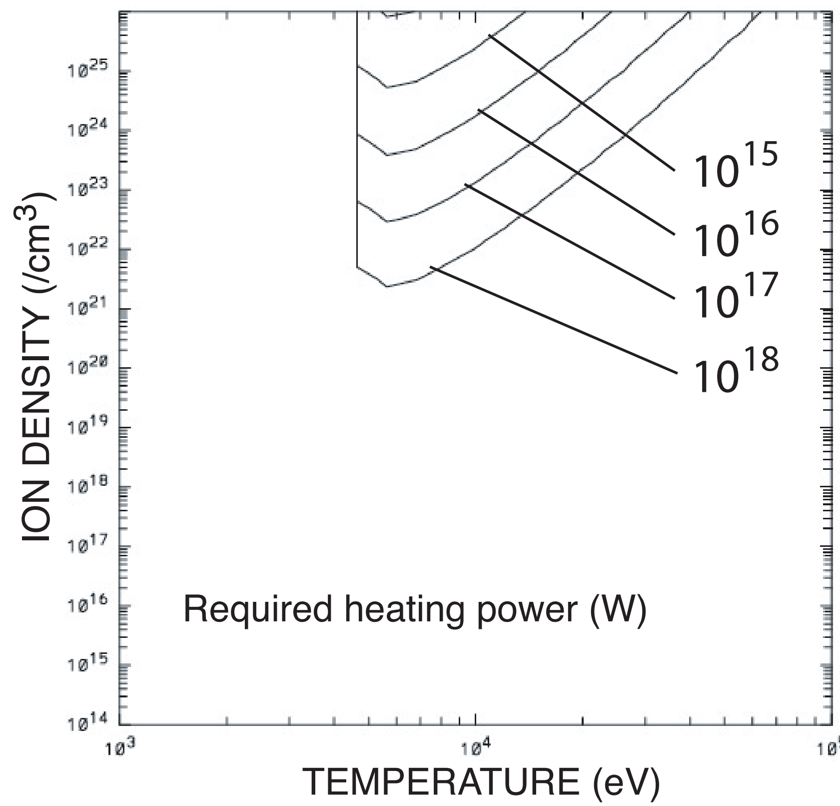

Electron thermal conductivity establishes the density lower limit; the dominant role of thermal conductivity was recognized early.

- **Reference: Enrico Fermi, "Super Lecture No. 5--Thermal Conduction as Affected by a Magnetic Field," Los Alamos Report 344, Sept. 17, 1945.**

  "A posible method of cutting down the conduction to the walls would be the application of a strong magnetic field, H. This tends to make the electrons go in circles between collisions, so impedes their mobility. Actually, it makes them go in spirals, and does not reduce the conductivity parallel to H but only to the other two dimensions, so one would probably want to design the container elongated in the direction of H, or even toroidal...with the lines of force never leaving the deuterium...rather large fields will be required...thus a field in excess of 20,000 gausses would help reduce conduction loss. While it would not be possible to produce such fields in a large volume in a steady state, the technical problem of making the field is much aided by the fact that the time during which the field is needed is much shorter than the usual relaxation time of magnetic fields, so it need be applied only instantaneously."

A magnetic field can significantly reduce the size of the burning plasma.

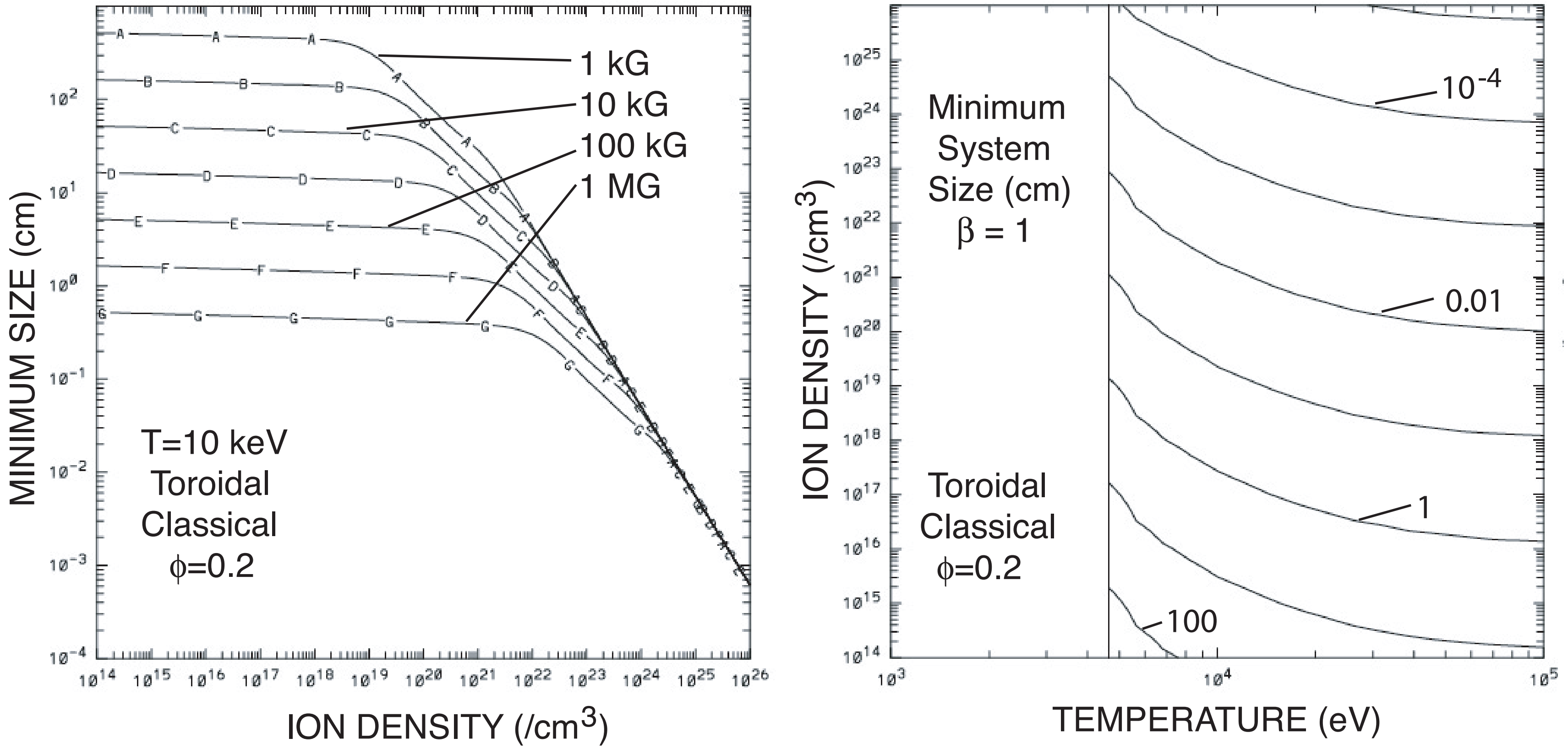

Note: β=plasma pressure/magnetic pressure

At every temperature/density point, magnetization of the fuel reduces the energy and power requirements, often by orders of magnitude.

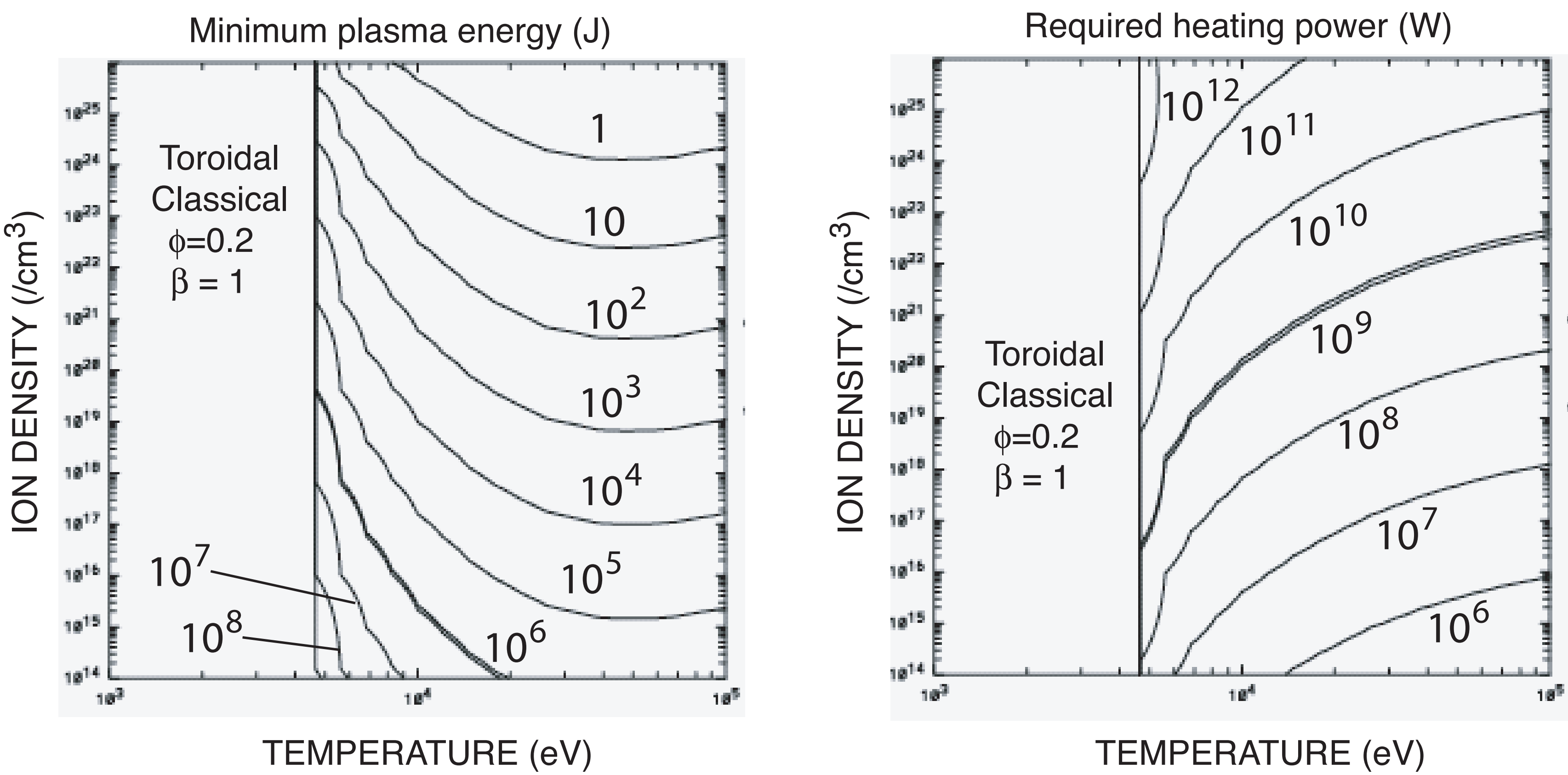

- **In contrast to unmagnetized fuel, the required heating power decreases with decreasing density. A priori, this might be expected to have a significant impact on cost.**

FUSION 501--what they should have taught us in first-year graduate school.

- What regions in parameter space do NIF and ITER access?
- Is it possible/feasible to consider other regions in parameter space?
- Can existing facilities be used to access other regions?
- Is there anything in between the extremes of Magnetic Confinement Fusion (MCF) and Inertial Confinment Fusion (ICF)?
- What would be the cost of a facility to access an intermediate region?
- Is it possible that fusion could be obtained at low cost?

Using published parameters (ni, T, B) and size (a or M), the loss rate expressions show extreme differences between NIF and ITER.

- To apply the simple expressions to NIF and ITER, we note the following:
  - the "hot spot" conditions (ni, T, mass) prior to ignition (self-heating by alpha particles) is somewhat ambiguous (ice evaporation).
  - the large toroidal field in tokamaks (50 kG in ITER) provides stability only, does not reduce thermal conduction.
  - thermal losses based upon the tokamak poloidal field (10 kG in ITER) are 30 X classical.
  - if losses had been classical, breakeven could have been achieved in a TFTR-class machine

	n	T	a	M	Eplas	Pheat	Iheat	ϕ
	cm3	keV	cm	g	J	W	W/cm2	loss ratio
NIF	5e25	10	2.8e-3	20e-6	23e3	1.3e15	1.3e19	0.07
ITER	1e14	8.4	230	0.3	300e6	157e6	25	0.45
min. tok.								
classical	1e14	8.4	66	7e-3	6.8e6	1.6e6	3.2	0.2

For unmagnetized fuel (e.g., ICF), fusion energy production rate exceeds loss rate (i.e., $\dot{Q}_{FUS} \geq \dot{Q}_{loss}$) only at very high density

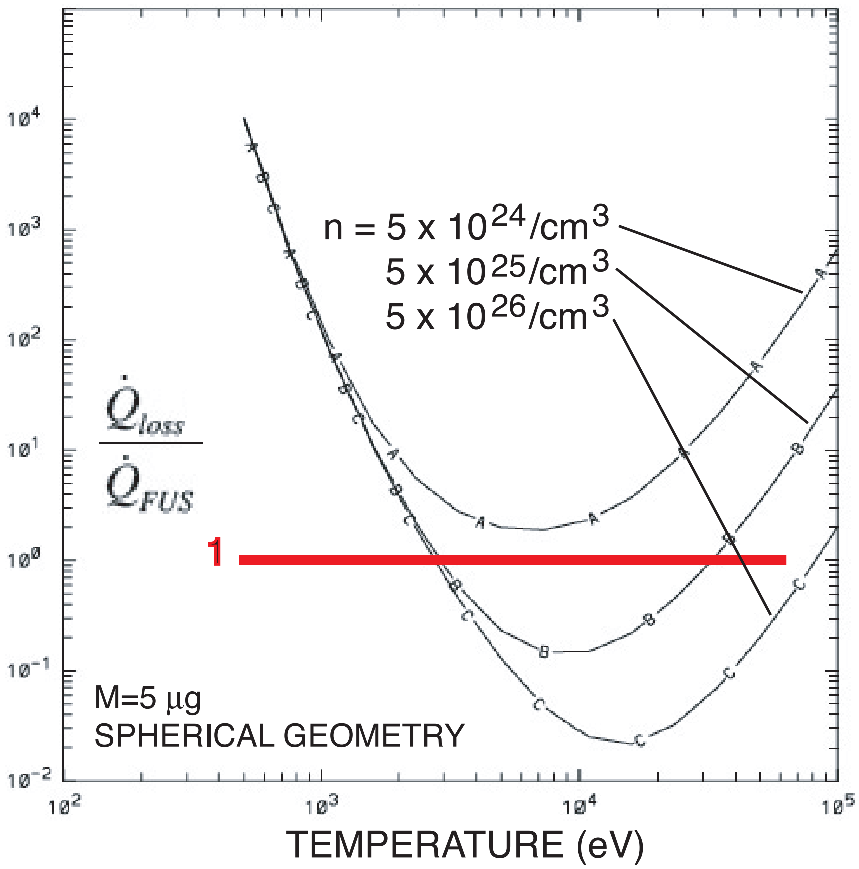

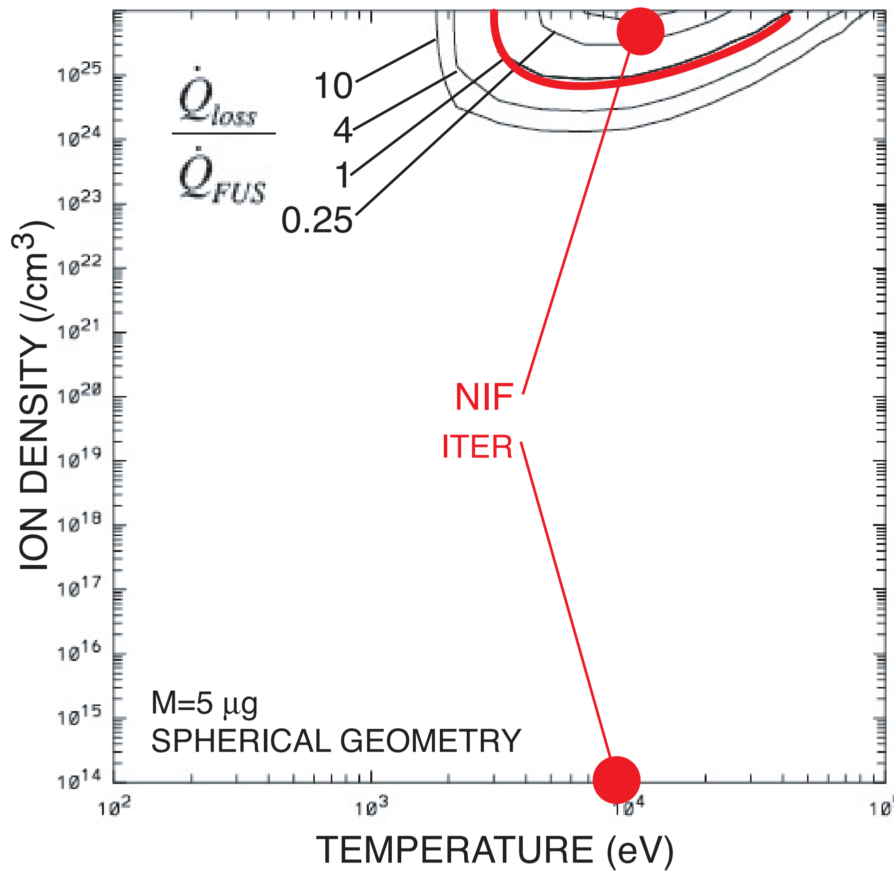

- **The NIF "hot spot" (M ~ 5 µg, n ~ 5 x 10^{25}/cm^3, t ~ 10 keV) reaches a point where $\dot{Q}_{loss}/\dot{Q}_{FUS}$ ~ 0.1 when the ignition rapid rise in temperature occurs due to alpha particle deposition.**

IL-9_06-10a

The limited operating space for unmagnetized fuel is not strongly sensitive to the fuel mass.

- Increased mass reduces the effect of thermal conduction.

$$\dot{Q}_{TC} \approx \frac{KT}{\gamma\alpha}\left(\frac{\varepsilon n_i(m_i + m_e)}{M}\right)^{2/3}$$

- Even for the fuel mass of ITER (~ 0.3 g), unmagnetized fuel must operate at high density

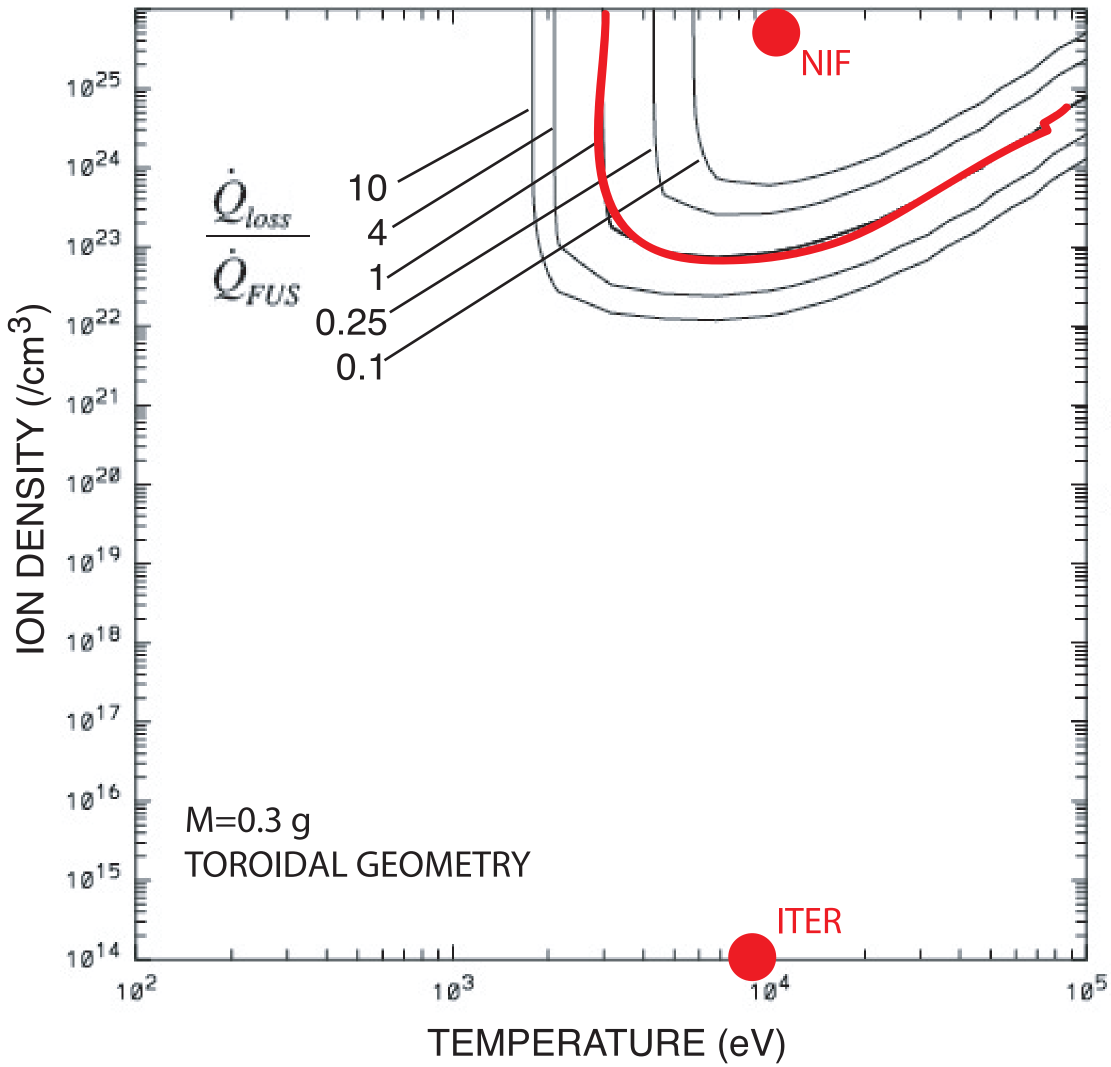

A magnetic field reduces the thermal conductivity across the magnetic field by ~ $1+(\omega\tau)^2$.

- Even for the NIF hot spot mass (~ 5 μg), a field of 10 kG opens up a low-density "island" where $\dot{Q}_{FUS} \geq \dot{Q}_{loss}$.

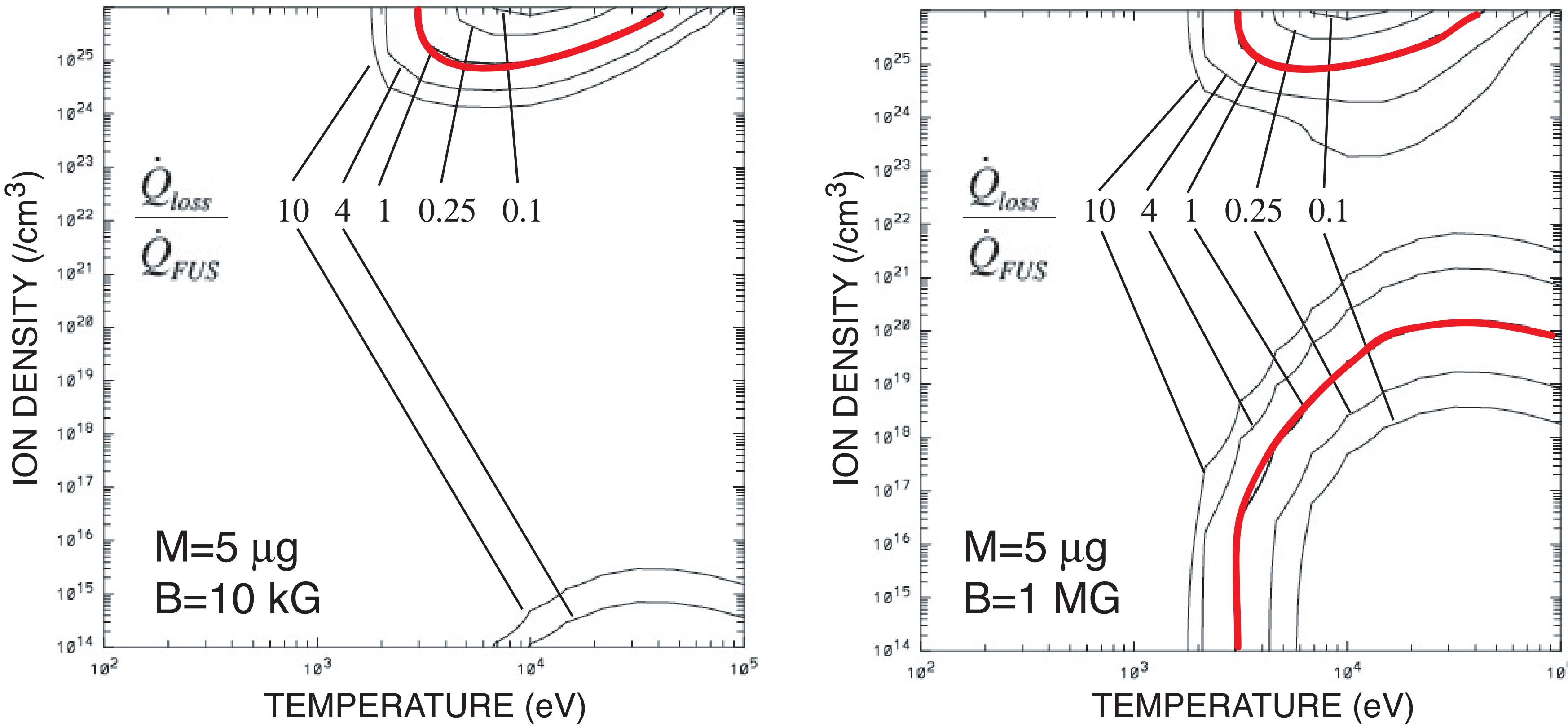

- For 1 MG, there is almost a continuum between the usual MCF and ICF space.

ITER uses a poloidal field of ~ 10 KG to limit conduction losses; tokamak data suggests that transport is 30 x classical

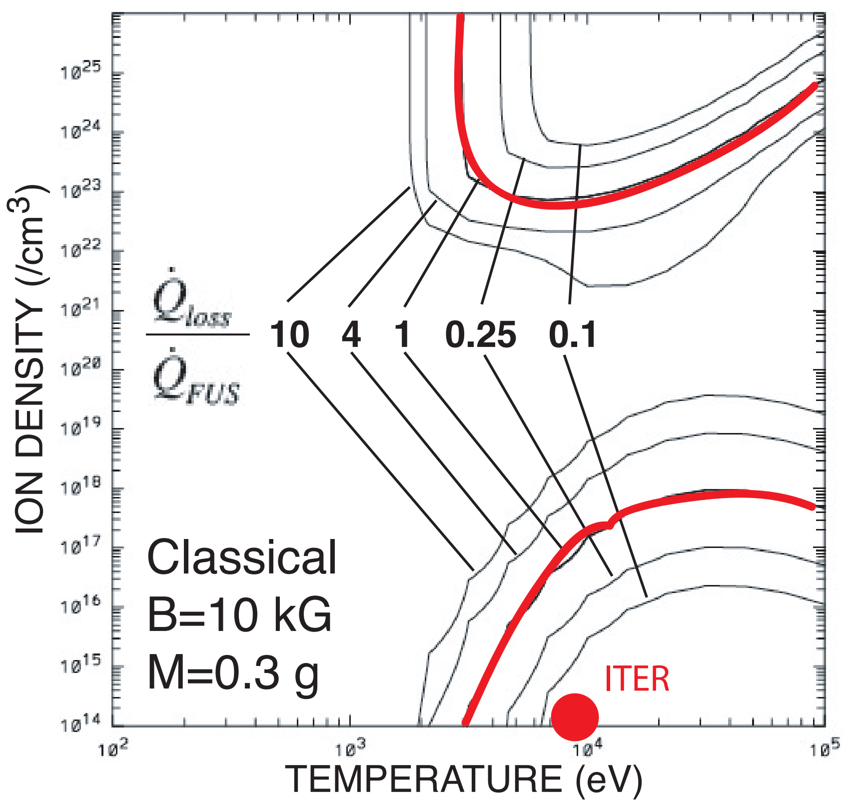

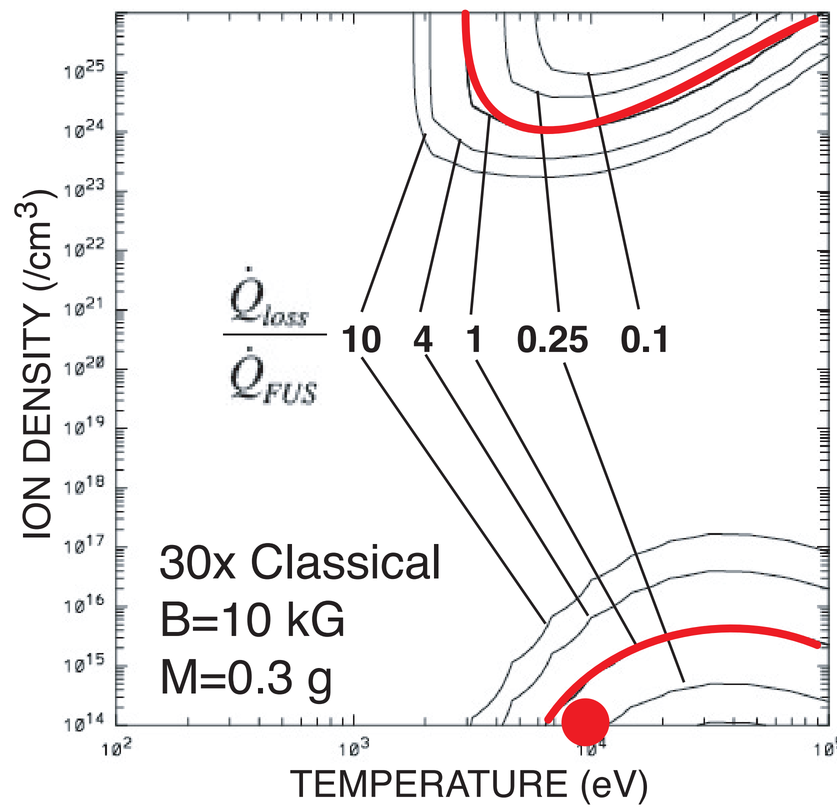

- **The 30x increase means that ITER operates in a range where losses are 0.35 x fusion, instead of only 0.03, i.e., ϕ=0.35.**

Knowing the cost of ITER and NIF, the cost of fusion facilities in any region of parameter space can be estimated.

$$Cost = c_1 E_{PLAS} + c_2 P_{HEAT} \approx \frac{\$10B}{E_{ITER}} E_{PLAS} + \frac{\$3B}{P_{NIF}} P_{HEAT}$$

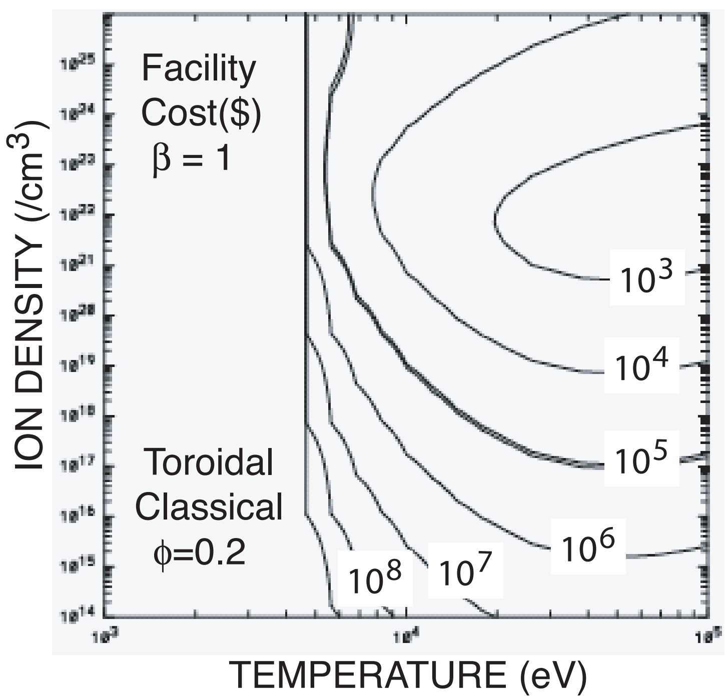

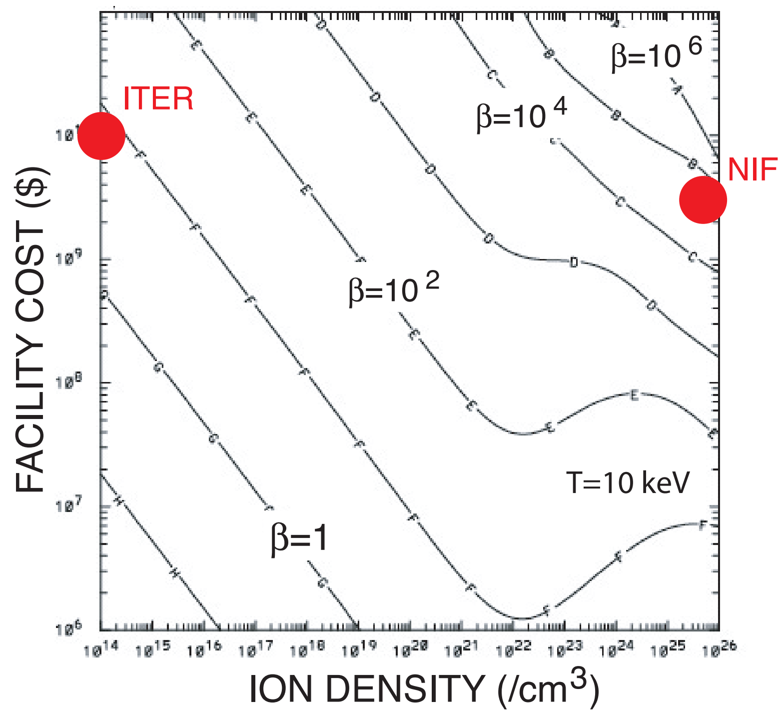

- **The reduced size/energy (when compared to ITER) and reduced power (when compared to NIF) lead to a very much lower cost at an intermediate density using magnetized fuel.**

For magnetized fuel, the reduced size/energy and reduced power in the intermediate density region lead to lower cost, even if 30x classical or Bohm transport is encountered.

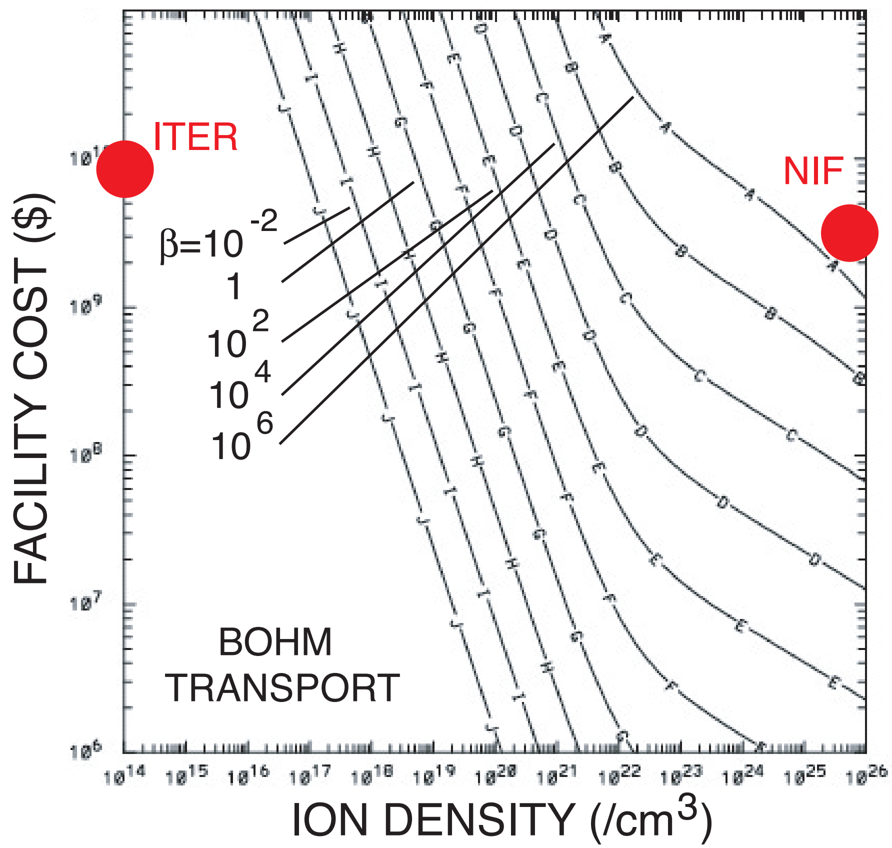

- **Bohm transport would make the cost prohibitive at ITER density.**

If very efficient compressional heating, as in ICF, is used to access the intermediate region, the required energy and implosion velocity is in the range already demonstrated by liners driven by modern high-current pulsed power machines (Atlas, Shiva-Star) and modern flux compression generators (DEMG).

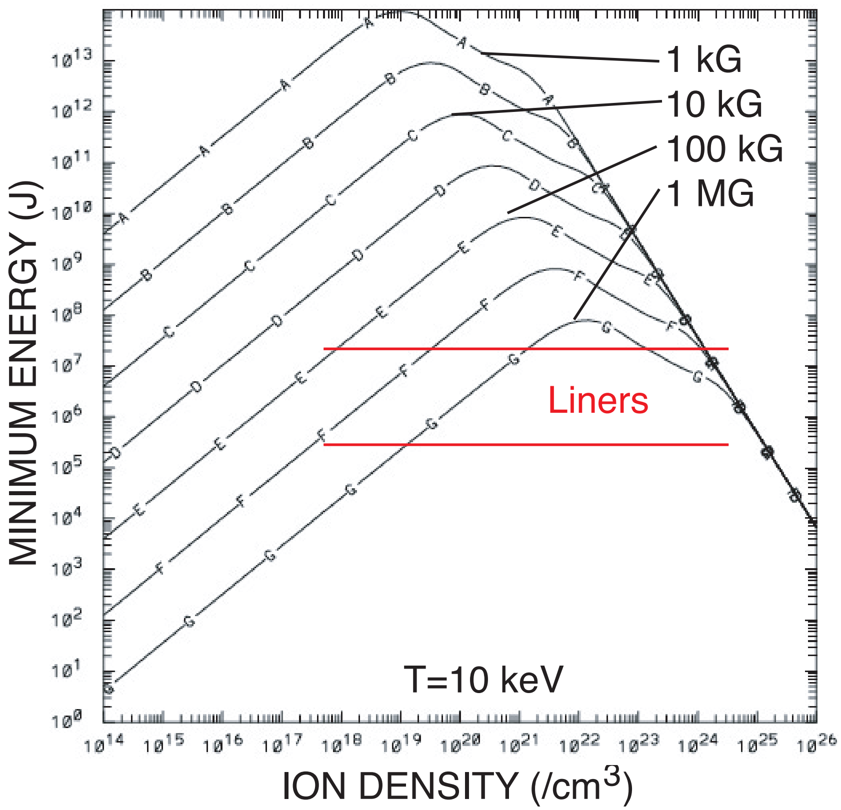

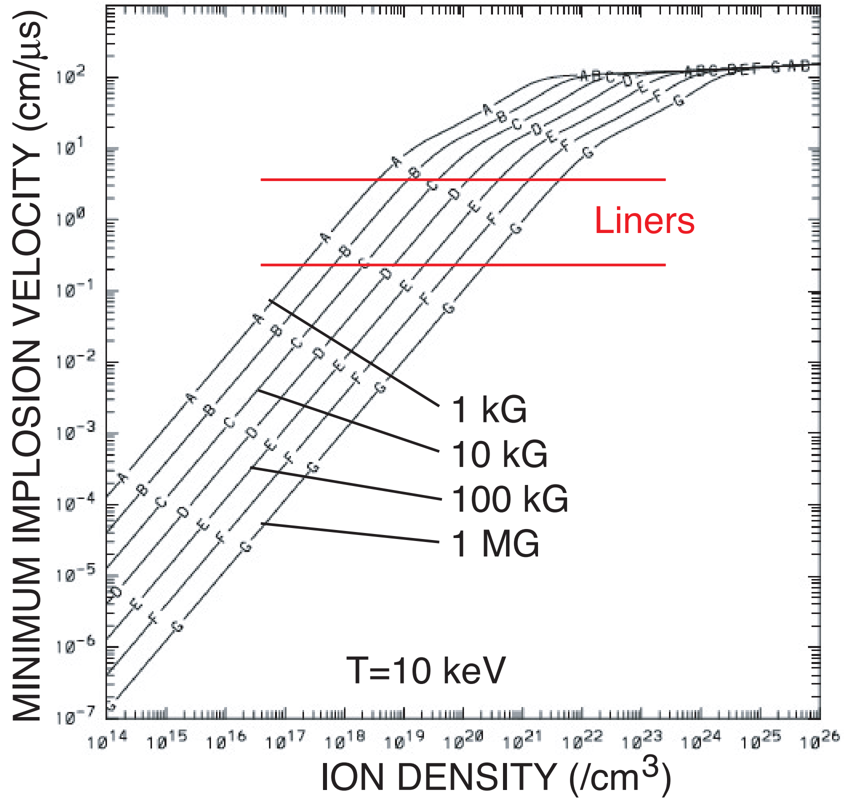

The Atlas capacitor bank (23 MJ, 30 MA, 6 μs) at NTS was designed to drive imploding liners in the range of 1-10 MJ, 0.1-1 cm/μs to create high energy density environments.

- **Atlas is, serendipitously, an ideal machine for accessing the intermediate density regime by compressing magnetized fuel with a magnetically driven liner.**

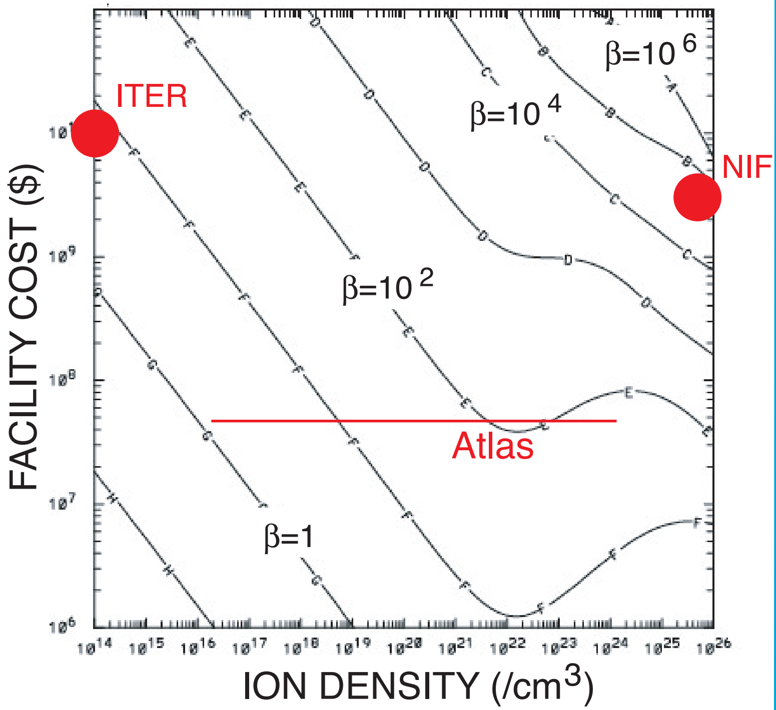

- **Atlas' cost of $50M confirms the simple cost estimates for fusion facilities.**

Modern imploding liner technology opens a new pathway to fusion: Magnetized Target Fusion (MTF)

- **MTF operates in the unexplored density space between MCF and ICF.**
- **The space is accessed by liner compression of magnetized plasma.**
- **Assume adiabatic compression, flux conservation:**

Quasi-spherical $\frac{n}{n_o} = \left(\frac{r_o}{r}\right)^3 \quad \frac{T}{T_o} = \left(\frac{r_o}{r}\right)^2 \quad \frac{B}{B_o} = \left(\frac{r_o}{r}\right)^2 \quad \frac{\beta}{\beta_o} = \frac{r_o}{r} \quad \frac{\omega\tau}{(\omega\tau)_o} = \left(\frac{r_o}{r}\right)^2$

Cylindrical $\frac{n}{n_o} = \left(\frac{r_o}{r}\right)^2 \quad \frac{T}{T_o} = \left(\frac{r_o}{r}\right)^{4/3} \quad \frac{B}{B_o} = \frac{r_o}{r} \quad \frac{\beta}{\beta_o} = \left(\frac{r_o}{r}\right)^{4/3} \quad \frac{\omega\tau}{(\omega\tau)_o} = \frac{r_o}{r}$

- **To limit r_o/r=10, but reach n=1e20/cm3, T=10 keV, B=1 MG:**

Quasi-spherical--initial n, T, B = 1e17/cm3, 100 eV, 10 kG

Cylindrical--initial n, T, B =1e18/cm3, 464 eV, 100 kG

- **In MTF, there is a trade-off between convergence r_o/r and initial n, T, B.**
- **MTF does not need the high convergence (r_o/r ~ 30) that makes ICF difficult.**

To fully determine the initial parameters (or final conditions), detailed implosion computations are needed.

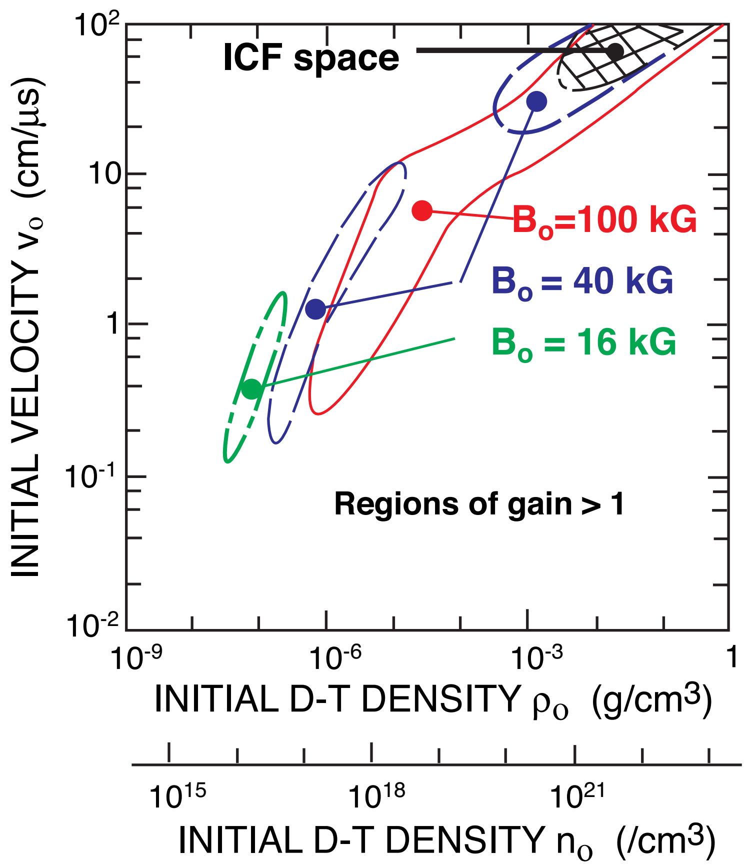

- **Lindemuth and Kirkpatrick (Nuc. Fus. 23, p. 263, 1983) formulated a simple implosion model and found a surprisingly broad parameter space.**
- **The results were confirmed by LASNEX and other computations.**
- **The simple model continues to serve as a guide for more detailed, multi-dimensional MHD computations.**
- **At the time the model was formulated, lasers were considered the most likely drivers, and plasma creation was considered a challenge (so use implosion E=10 kJ, T_o=50 eV).**

Since the L-K model, advances in drivers and plasma formation allow consideration of more energetic implosions (e.g., 20 MJ) and higher plasma density and temperature (e.g., 1e18/cm3, 300 eV)

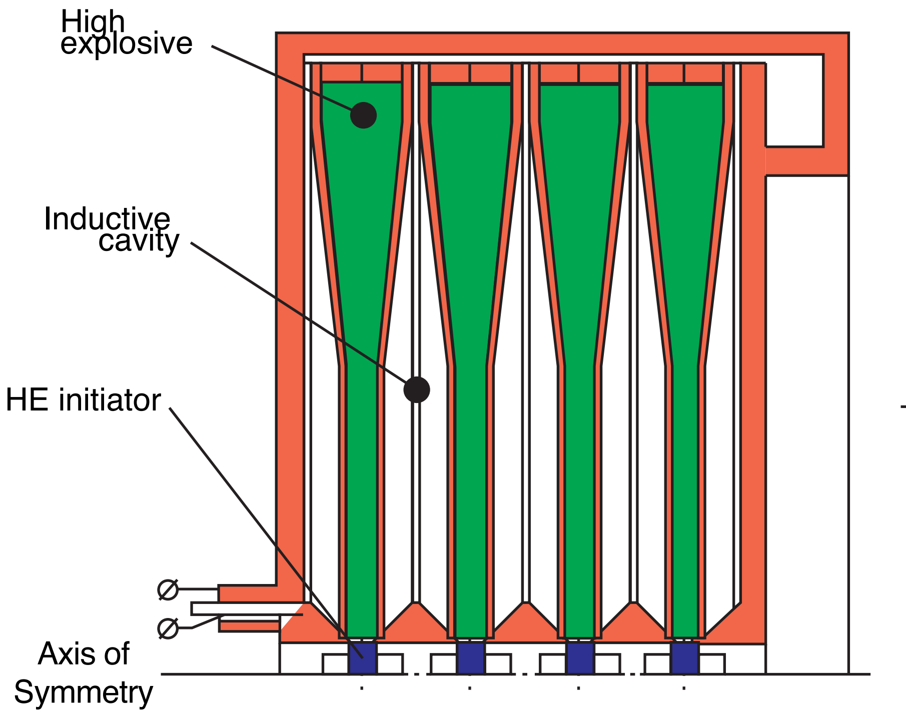

Disk Explosive Magnetic Generator (DEMG)

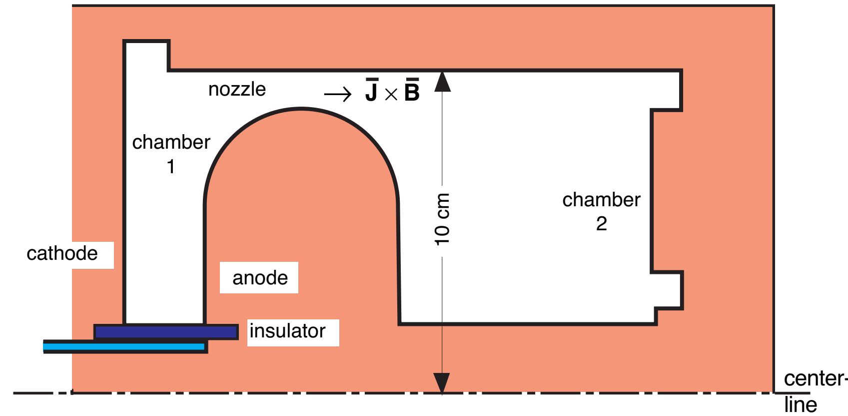

MAGO (Magnitnoye Obzhatiye)

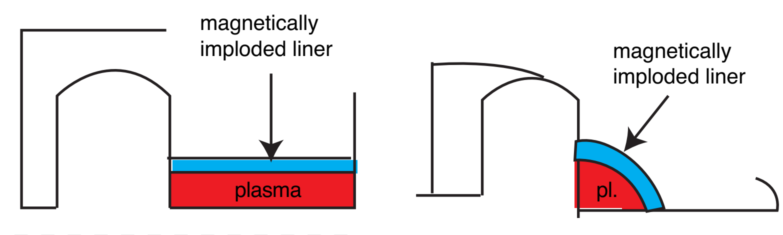

Implosion scenarios

- **DEMG and MAGO systems developed by the All-Russian Institute of Experimental Physics (VNIIEF) have catalyzed a growing international interest in MTF, e.g., Los Alamos National Lab. (LANL), Air Force Research Lab. (AFRL), India Institute for Plasma Research (IPR), and the University of Nevada-Reno (UNR).**

MTF is <u>not</u> magnetic confinement (e.g., MFE); MTF is <u>not</u> polarized fuel

- Simple field topologies $\rightarrow$ easier plasma creation
- Shorter lifetime required
- Wall contact tolerable, maybe desirable
- $\omega\tau \gg 1 \rightarrow$ magnetic thermal insulation
- if $\beta \gg 1 \rightarrow$ reduced instabilities
- if $\beta \gg 1 \rightarrow$ little work compressing B
- Polarized fuel: $\sigma v \rightarrow 1.5\ \sigma v$, relatively little effect

MTF is <u>not</u> merely the addition of a magnetic field to a "conventional" ICF Target--it is the complete rethinking of the compressional heating approach.

- B_o $\rightarrow$ approximately adiabatic compression (no shocks)
- Low ρ $\rightarrow$ bigger targets, reduced radiation rates
- T_o $\rightarrow$ reduced radial convergence (e.g., < 10)
- Low v $\rightarrow$ less power, intensity
- Less power, intensity $\rightarrow$ more, and less expensive, energy possible
- Big targets, low v $\rightarrow$ more massive pushers
- Massive pushers $\rightarrow$ long dwell, burn times
- Low v $\rightarrow$ adiabatic $\rightarrow$ no pulse shaping
- $\bar{B}$ $\rightarrow$ $r\bar{B}$, not ρr, for alpha deposition
- T_o, $\bar{B}_o$ $\rightarrow$ fuel prep. prior to implosion
- Low ρ with $\bar{B}$ $\rightarrow$ new physics regimes

IL-9_06-23

CONCLUDING REMARKS--an unexplored fusion parameter space may mean fusion could yet be possible at low cost.

- MTF is a research topic, has not yet been demonstrated to provide substantial fusion yield. Although some physics uncertainties exist, no insurmountable obstacles have been identified.

- MTF is an "orthogonal," complementary alternate to MFE and ICF. Required technology (Atlas and/or DEMGs) exists for demonstration--no major capital investment in new facilities.

- Because MTF is qualitatively different from inertial or magnetic confinement fusion--different time, length, and density scales--MTF reactors will have different characteristics and trade-offs, increasing the chances that a practical fusion power scheme can be found.

- "The fusion fire--which men have contemplated in awe since they first raised their eyes to the stars--but first brought to Earth in our age, will clearly propel man beyond his Solar nursery, and forever foster and energize his terrestrial and cosmic endeavors. We may speak today of fusion fire as Aeschylus, the ancient Athenian poet, said of Prometheus' gift to mortals of the chemical fire: it will prove the means to inconceivably mighty ends."
  --L. Wood and J. Nuckolls, 1971.

Modeling of Shock Attenuation in the Electra Circulator Loop

B. Lu, C. Lascar, J. Dion, and S. Abdel-Khalik - IFE Strategic Planning Workshop - April 24-27, 2007

Problem Definition

- A shock wave is created following e-beam energy deposition in the laser gas.
- Shock is gradually attenuated as it propagates around the circulator loop prior to the next pulse.
- Density gradients in the laser cell caused by the shock "remnants" may impact beam quality.

Objectives

- Numerically simulate shock propagation and attenuation in the Electra main amplifier circulator loop following e-beam energy deposition in the laser gas.
- Quantify the extent of non-uniformity in the gas density prior to the next pulse for 5 Hz operation at prototypical gas conditions.
- Explore means by which the pressure wave can be further attenuated to achieve the desired uniformity in gas density for long-term (5 Hz) operation without significant increase in circulator power requirements.

Approach

- Use FLUENT 6.2.16 to model gas heat-up by e-beam energy deposition (100 ns) and subsequent shock propagation and attenuation prior to the next shot (200 ms); multiple shots can be modeled.
- Initial studies used a simplified 2D loop to assess the code's suitability and examine effect of modeling options, geometry, and boundary conditions on shock attenuation.
- Current studies use actual Electra main amplifier circulator loop geometry and operating conditions.
- Results obtained for 2D simplified analyses.
- Calculations using actual 3D geometry are in progress.

Electra Circulator 2D Loop Nodalization

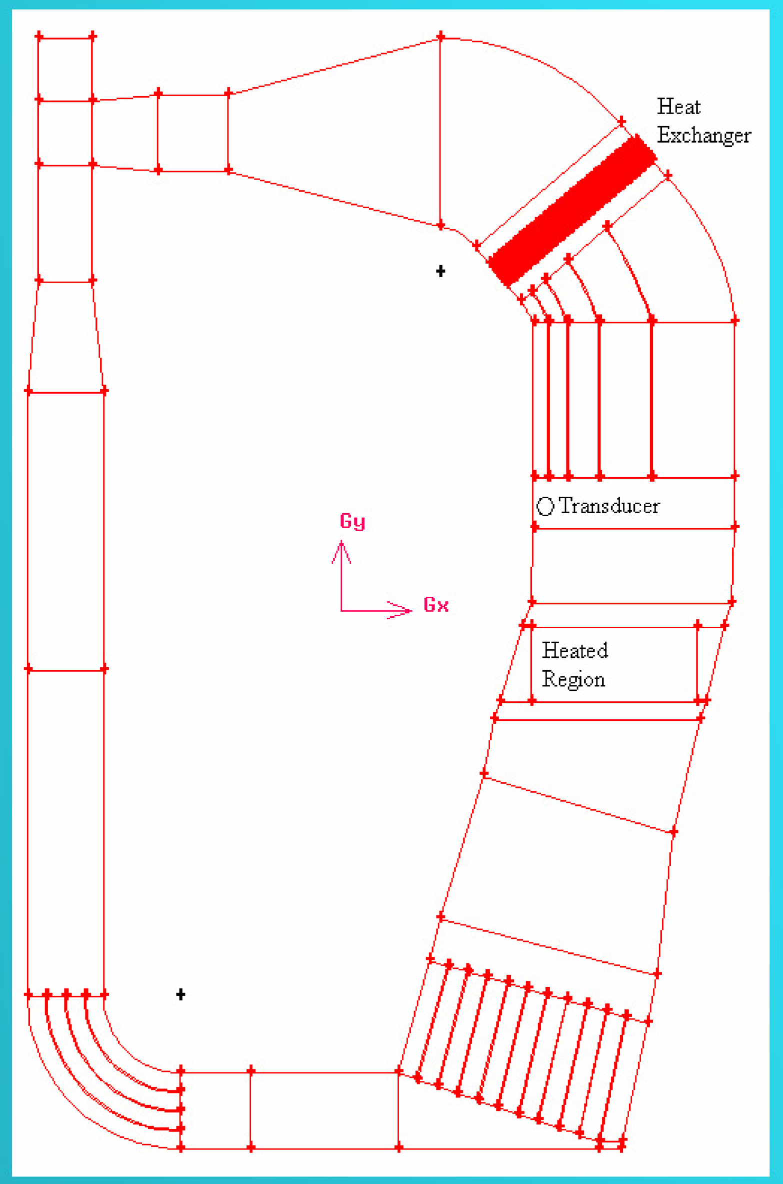

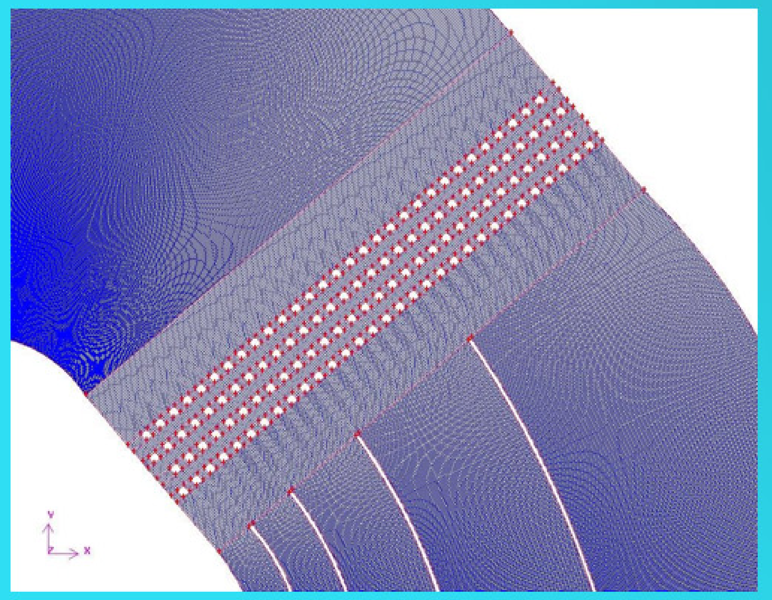

No. of mesh points (2D model): 847,648

Initial Conditions:

- Loop contains stagnant argon.
- Initial pressure = 1.5 atm (152 kPa).
- Initial temperature = 300 K.

Boundary Conditions:

- Adiabatic loop walls.
- No slip boundary walls and straightener surfaces.
- "Smooth" surface.

Assumptions

- Argon is assumed to be a compressible ideal gas with constant Cp, k, and μ.
- Source term/energy generation rate during the 100 ns heating period selected to produce the same temperature rise as that produced by the electron beams' deposition (~ 50 K).

Pressure Contours in the 2D Loop after 100ns of Heating

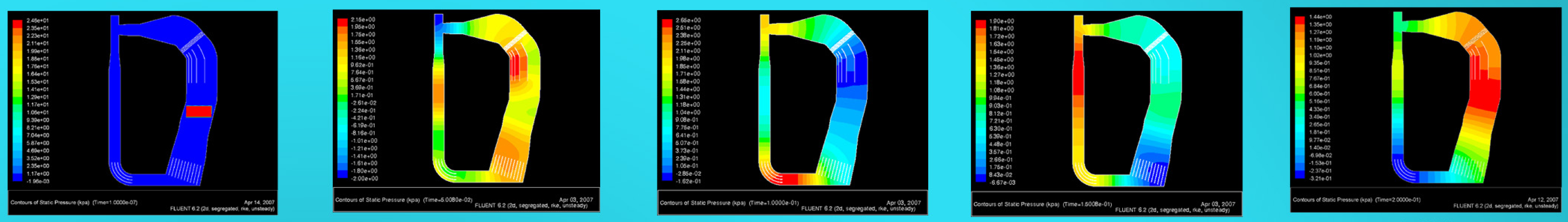

t=0s t=50ms t=100ms t=150ms t=200ms

Pressure History & Dominant Frequencies at Transducer Location

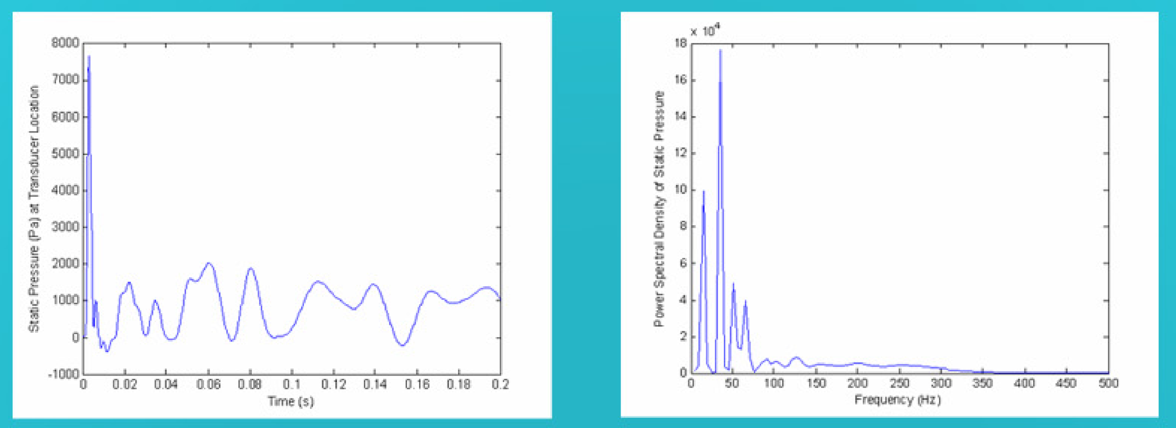

Field Distribution in the Laser Cell after 200 ms

Pressure Density Temperature

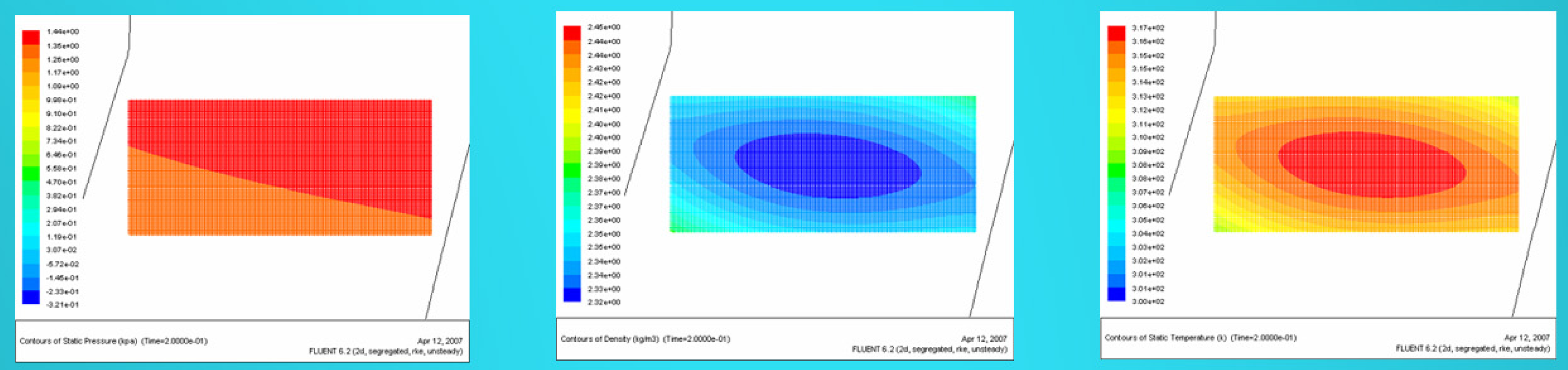

Simplified Loop Geometry and Results for Parametric Studies after 400 ms (2 pulses)

Pressure Density Temperature

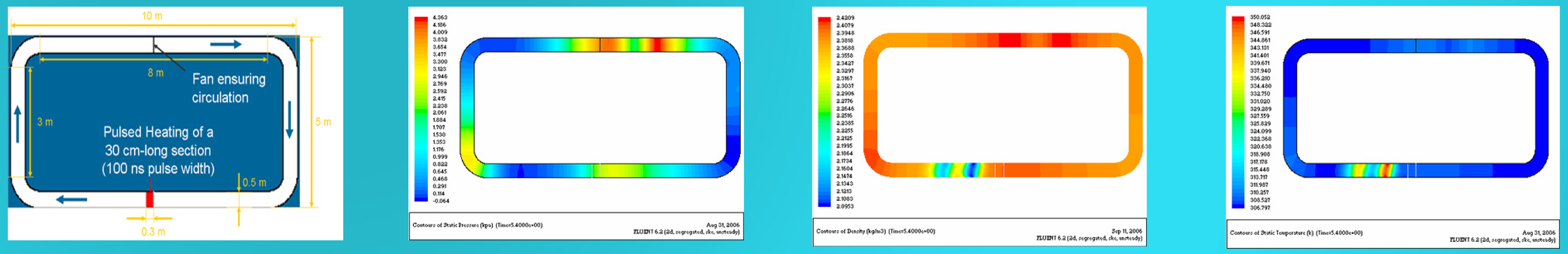

Effects of Surface Roughness

- Previous simulations assumed a smooth surface corresponding to roughness height = 0 mm.
- Slight effect (1%) on shock attenuation when roughness height is increased up to 4 mm.

Effects of Convection Heat Loss

- Previous simulations performed assuming adiabatic boundaries.
- New simulation, heat transfer coefficient = 20 W/m².K.
- Slight effect (<1%) on shock attenuation.

Porous Absorber Cones

- Can significantly attenuate shock with modest increase in loop pressure drop.
- Parametric studies indicate that optimum porosity ≈ 60%.

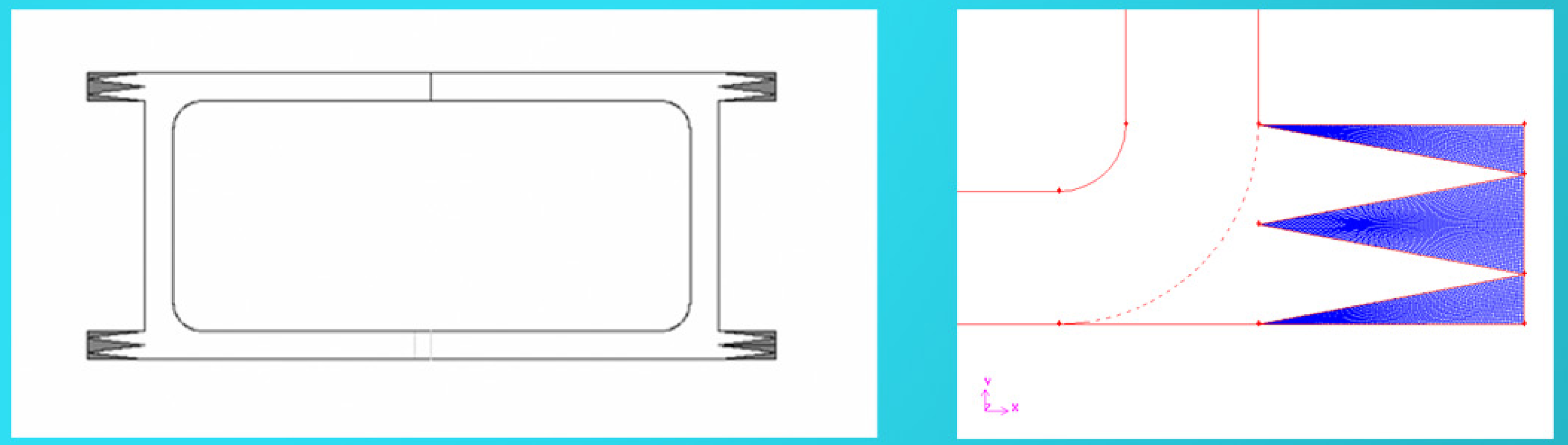

Conclusions

- Shock propagation and attenuation can be modeled using FLUENT.
- Model needs to be extended to simulate actual 3D geometry with flow "obstructions" at prototypical flow conditions.
- Code results for pressure/frequency at instrumented locations should be experimentally validated prior to hardware modification.

G. W. Woodruff School of Mechanical Engineering, Atlanta, GA 30332–0405 USA

Georgia Institute of Technology

Accelerated Plasma Blocks Driven by Petawatt-Picosecond Laser Pulses for Igniting Near Solid Density DT

George H Miley[1] and Heinrich Hora[2]

[1]U of Illinois, Urbana, IL 61801,USA

[2]U of New South Wales, Sydney, 2052, Australia

Outline

- Review of prior volume ignition studies.
- Badziak effect and non-linear ion acceleration.
- Plasma block acceleration as an alternative to fast igniter electron beam ignition.
- Fusion regime involving 10-kJ input to produce 100 MJs or more output.

Introduction

- 30 years ago it was impossible to
  - ignite solid deuterium-tritium by pulsed laser irradiation
  - irradiation by ion beams had current densities of low magnitude
- This changed as improved drivers and targets were designed and the fast ignitor concept was introduced. However, very high compressions are still envisioned.
- Recently a method that avoids high compression was proposed based on an anomalous effect observed using PW-ps laser pulses

Basis

- Both experiments and theory concludes that suppression of prepulses by a factor 10^8 would
  - avoid relativistic self-focusing allowing broad area compression
  - gives directed 80-keV DT ion current densities in space- charge neutral plasma blocks of modest temperature. These blocks can reach parameters that allow them to produce fusion flame in the nearly uncompressed or solid DT target. The parameter that it can exceed are:
    - 10^{11} Amps/cm^2,
    - energy flux densities of 10^8 J/cm^2,
    - block thickness.
- Conditions for the energy flux are further relaxed by
  - considering interpenetration effects
  - the quantum modification of collisions
  - collective reduction of stopping power and double layer mechanisms

Review Of Prior Volume Ignition Studies

- Prior measurements at Rochester, Osaka, LLNL and Arzamas-16 agree with isotropic burn model.
- When radiation trapping and alpha reheat are included high gains occur with volume ignition above the threshold energy input.
- Optimized volume ignition requires high density and mass targets than does spark ignition,but is much simpler to implement.

Experiments Agree Well with Isentropic Burn Model

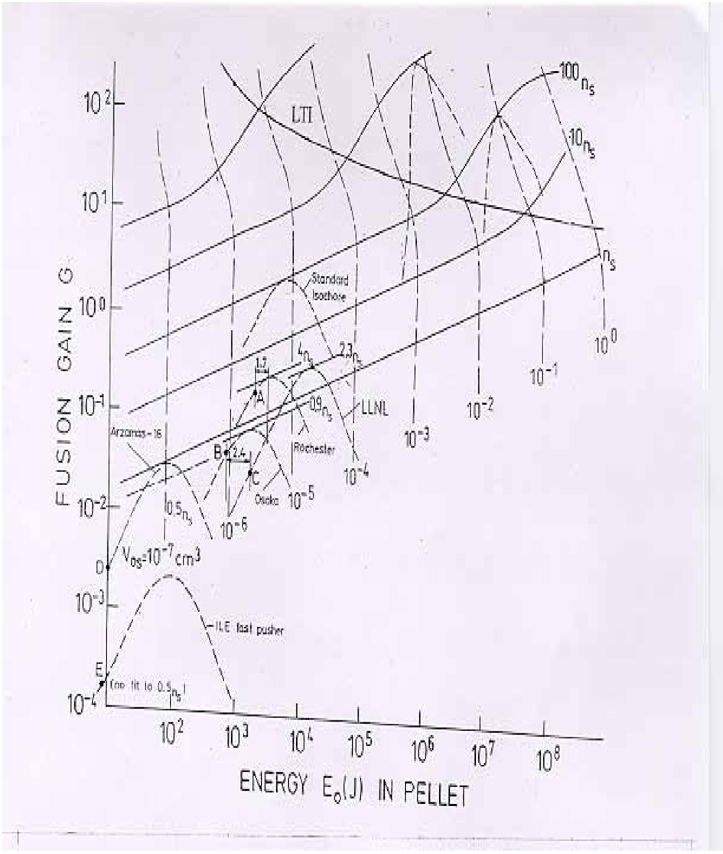

- Optimized core G (*full lines*) for 3-D self-similar volume comp. and simple burn (G<8) (~ quenching:1995) and volume ignition for G>8 with low T ignition above LTE line. Measurement at Rochester (*A*), Osaka (*B*), LLNL (*C*) and Arzamas-16 (*D*) agree with isentropic volume burn model, while the earlier fast pusher (*E*) with strong shocks does not.

Badziak Effect & Non-Linear Ion Acceleration

- 5 energy groups of Ions observed for irradiation of a copper target during 1.2 ps Nd glass laser.
- Fast ions attributed to relativistic self focusing of laser beam.
- Slow ions characteristic of nonlinear force acceleration.
- Analysis suggests plasma block acceleration possible.

Badziak Effect Results In Large Number Of Fast & Thermal Ions

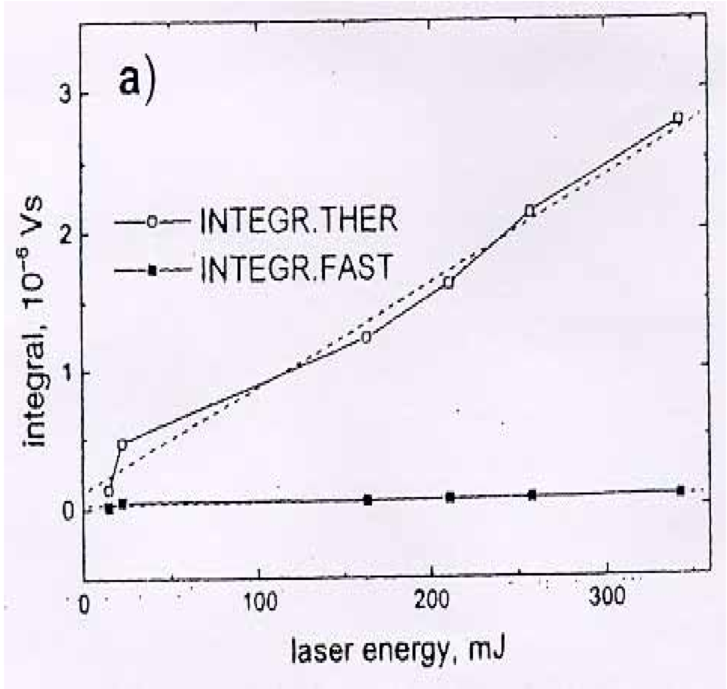

- Badziak et al type anomalous ion emission: No. of fast and thermal ions emitted from a copper target at Nd glass laser irradiation of (1.2 ps) focused to 30 wave length dia. with pre-pulse suppression of 10^8 for <0.1 ns before the main pulse.

Ion Energy Groups Observed During Irradiation

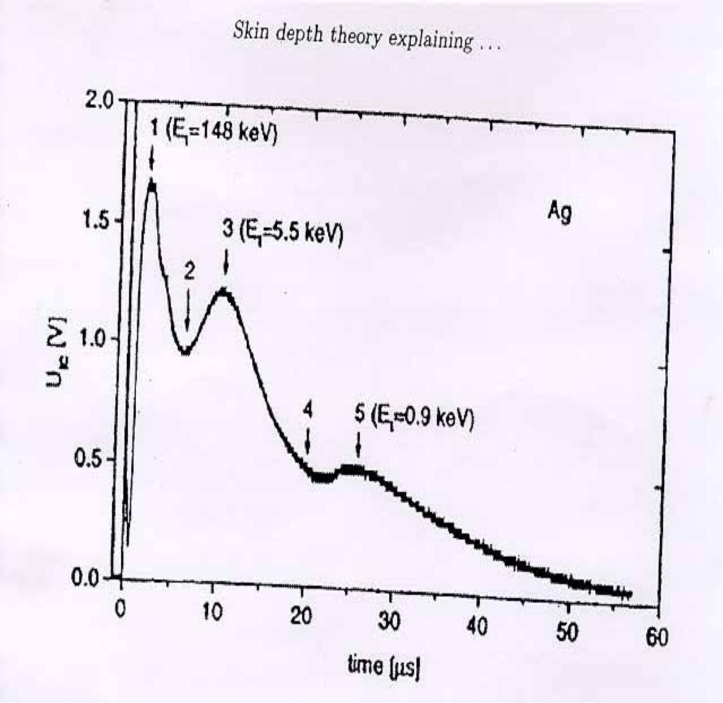

- TOF signal from a flat ion collector with a silver target irradiated by an iodine second harmonic laser pulse of 14 J and 0.35 ns. Three groups of ions appear! The fastest ions (*1*), the second fastest ions (*3*) and the slow thermal ions (*5*).

Fast Ion Velocity Scales As $I^{0.52}$

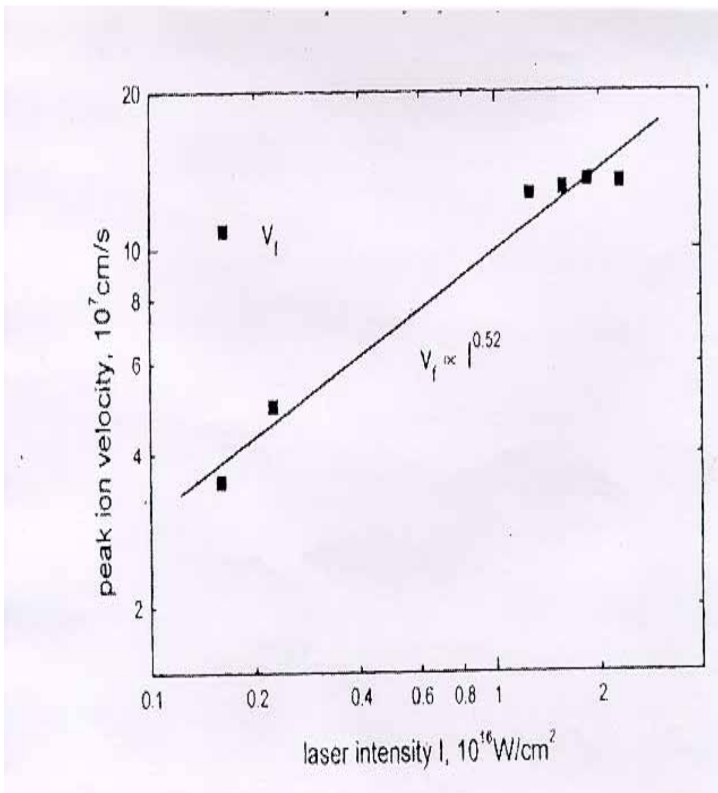

- Velocity of the fast ions measured by TOF.

Shorter Laser Pulses Lead to a Lowering Of the Average Charge

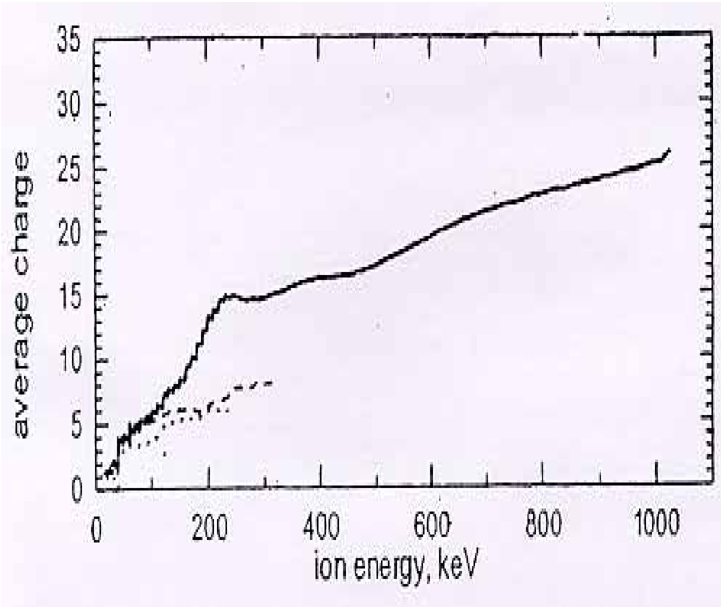

- Same as prior Slide but 1.2 ps –0.7 J laser pulses.

Plasma Block Acceleration As an Alternative to Fast Igniter Electron Beam Ignition

- Block acceleration requires pre-pulse suppression to prevent plasma self focusing.
- Using studies from light ion beam fusion volume ignition with a ion current of 10^{10} Amp/cm^2 from 10-kJ pulses, calculations predict high gain volume ignition is possible.

Pre-generated Plasma Causes Self-focusing

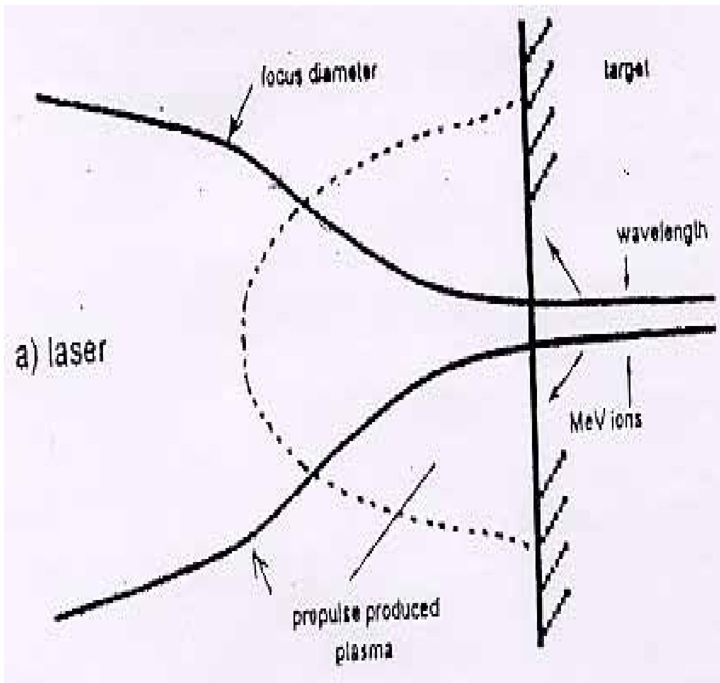

- Geometry for subsequent volume-forced nonlinear electron acceleration with separation by the ion charge Z. The pre-generated plasma before the target causes relativistic self focusing of the laser beam to less than a wave length dia. and very high acceleration due to the strong gradient of laser field density.

Elimination of Plasma Prevents Self-focusing

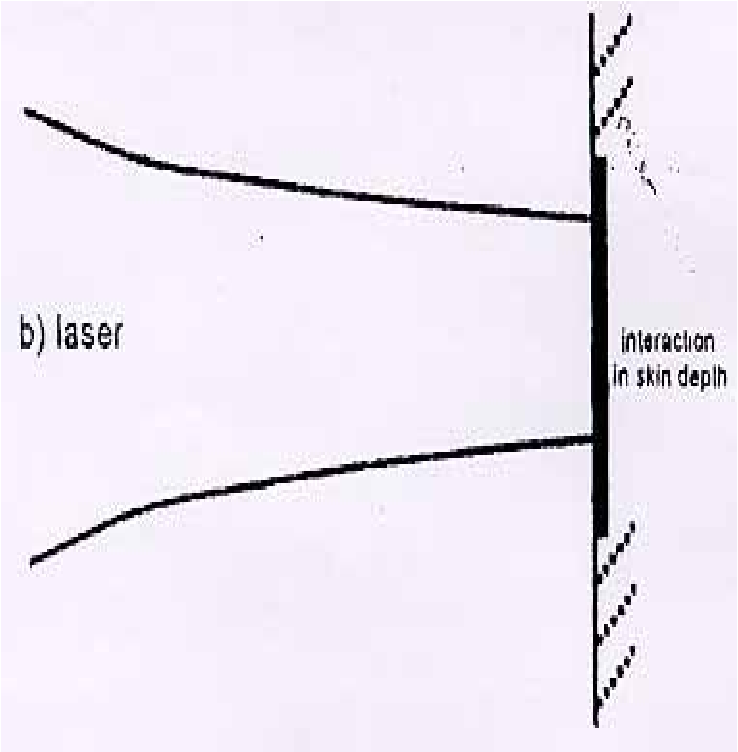

- The very thin plasma does not produce self-focusing, hence lower ion energies. This ideal geometry has frequently been assumed in prior studies.

Nonlinear Force Effects Create High Electric Field Amplitudes

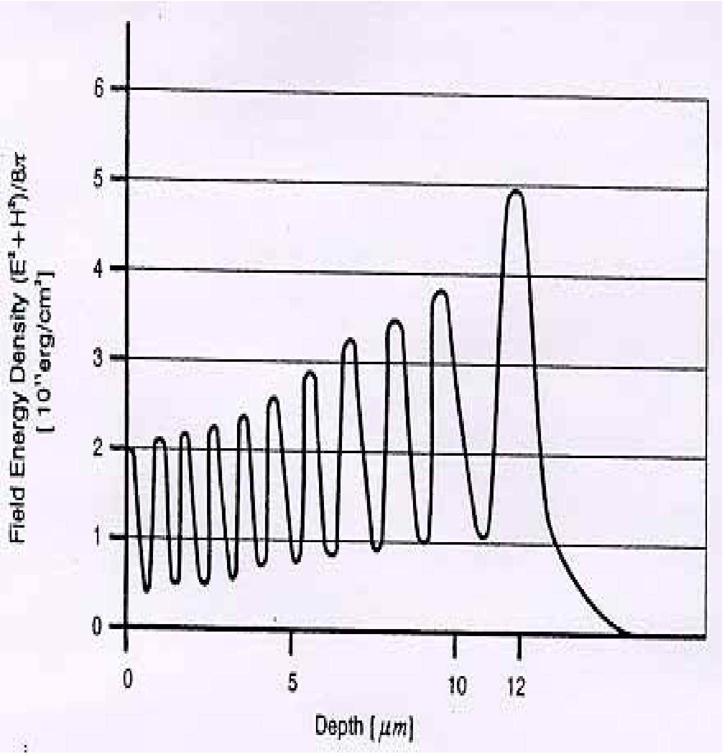

- Two fluid calculation of the electromagnetic energy density Nd glass laser 10^{16} W/cm^2 after n_e~ 5×10^{20} cm^{-3} is reached at 12um from the surface. The maximum corresponds E~3.1 times higher than vacuum due to dielectric swelling.

Plasma Block Acceleration By Non-Linear Force

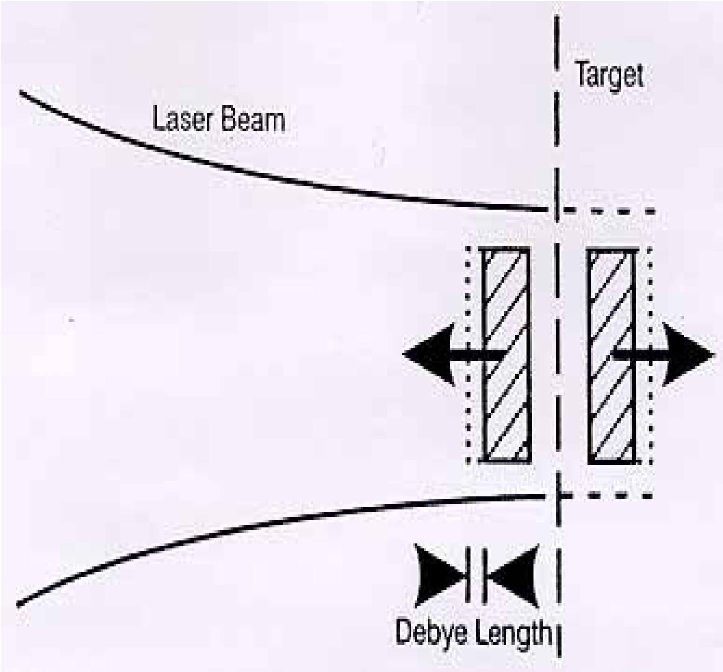

- Skin depth laser interaction: nonlinear force accelerates a plasma block against the laser light and another block towards the target interior. Election clouds form with a thickness of the effective Debye length.

Block Ignition Targets

- Design point-generation of reaction front with interpenetrating ion energies ~ 100 keV.
- Use high aspect ratio ps pulse defocused to large cross section.
- PW pulses with final intensity of few 10^{17} W/cm^2 – gives swelling of 2-3x.
- Resulting ion current density of 10^{10} Amp/cm^{2,} giving 10^6 J/cm^2.

Ignition Criteria

- Collective interaction of ions determines stopping power.
- Ignition condition for fusion reaction wave reduces to minimum energy density E_{min} for DT of $E_{min} = 10^6 J/cm^2$.
- Reaction wave of high intensity ion beam of minimum current density $j_{min} = 10^{10}\ A/cm^2$.

Conclusions

- This new approach overcomes the DT compression issues and electron beam issues of the fast ignitor
- Plasma block ignition,10-kJ laser pulses produce 100-MJs of fusion energy
- Potential for simplified and lower cost energy production

Thank you

If you have any questions, please contact

George H. Miley
Tel: (217) 333-3772
E-mail: ghmiley@uiuc.edu

Mitigation of helium-induced tungsten morphology change using the tamped target design*

G.A. Moses and T.A. Heltemes

HAPL Chamber Problem

The reference HAPL chamber design consists of a 10.5 m radius chamber with an ambient temperature of 600 °C and a nominal background gas pressure of 0.5 mtorr. 365 MJ deuterium-tritium targets are imploded in the chamber at a rate of 5 Hz. Until recently, it was thought that the first wall and breeding blanket lifetime was limited by neutron damage. Recent experiments with low-energy helium ion bombardment performed by the University of Wisconsin – Madison Inertial Electrostatic Confinement (IEC) experimental group indicate significant erosion of the plasma-facing surface due to alpha particle implantation. The limiting factors of the armor and/or first wall lifetime now appear to be:

1. Neutron damage due to atomic displacements in the crystal structure (DPA lifetime).
2. Thermal stress due to rapid cyclical temperature rise.
3. Morphology change and armor erosion due to low-energy alpha implantation.
4. Armor erosion due to high-energy alpha accumulation in subsurface grain boundaries.

MCNP neutronics simulations show that the DPA lifetime of the first wall and blanket structures is approximately 3¼ full-power years (FPY). The chamber radius was specified to be 10.5 m, based on thermal analysis that limits the temperature rise on any given target shot to 2400 °C with tungsten armor.

IEC experiments show that low-energy alpha implantation erodes the tungsten armor at rate of 1.1 μm per 10^{19} ions/cm². The current HAPL chamber design is based on a 250 μm layer of tungsten over a ferritic steel substrate. Based on the erosion rate from the IEC experiments and the alpha ion spectrum produced by simulations performed at Lawrence Livermore National Laboratory (LLNL), the tungsten armor will erode at a rate of 126 μm/FPY. Thus, the tungsten armor will be completely eroded in just under 2 FPY, neglecting the damage done by the high-energy (above 600 keV) alpha particles.

IEC Helium Ion Implantation Experimental Results

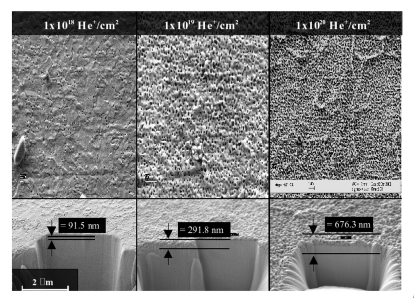

To prevent the low-energy alpha implantation from becoming the lifetime limiting damage mechanism, steps must be taken to prevent the low-energy alphas from reaching the armor. One can stop the ions by introducing a buffer gas. First we explored the possibility of stopping all alpha particles from reaching the armor by simply increasing the pressure of a xenon buffer gas. Our simulations indicated it would take an excessive amount of gas — on the order of 20 torr — to stop all alphas from impacting the armor. The amount of buffer gas required was determined to be unacceptable due to frictional target heating during injection into the chamber.

Xenon buffer gas causes alphas to lose energy before impacting the armor

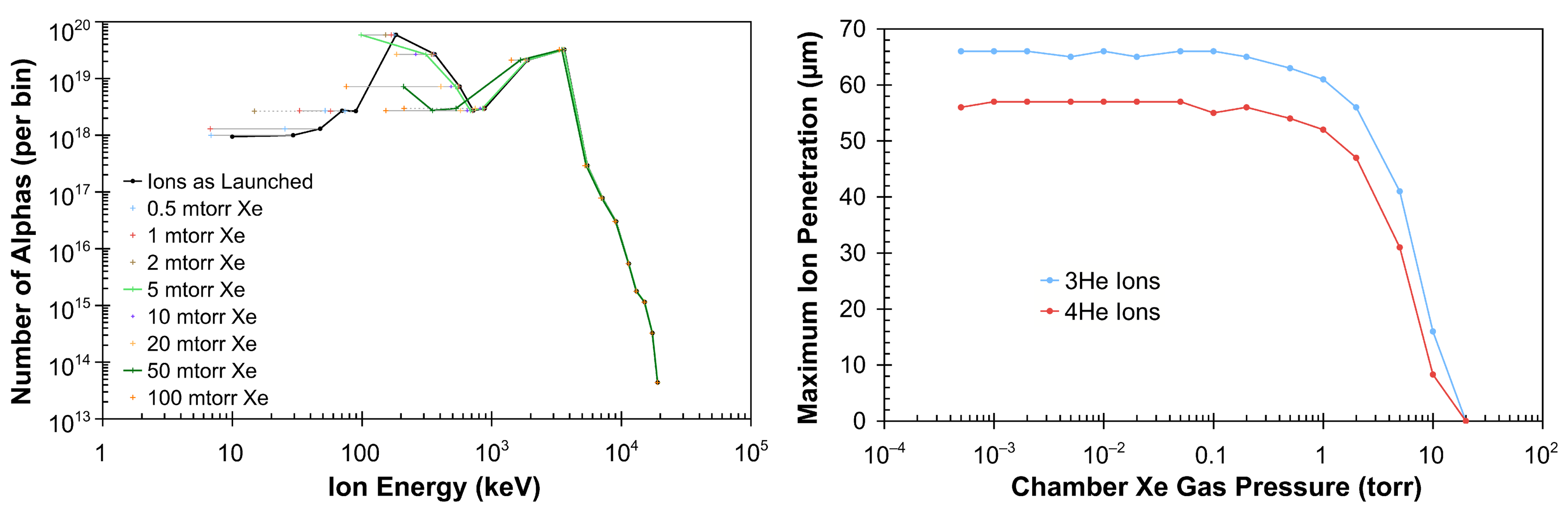

Tamped Target Solution

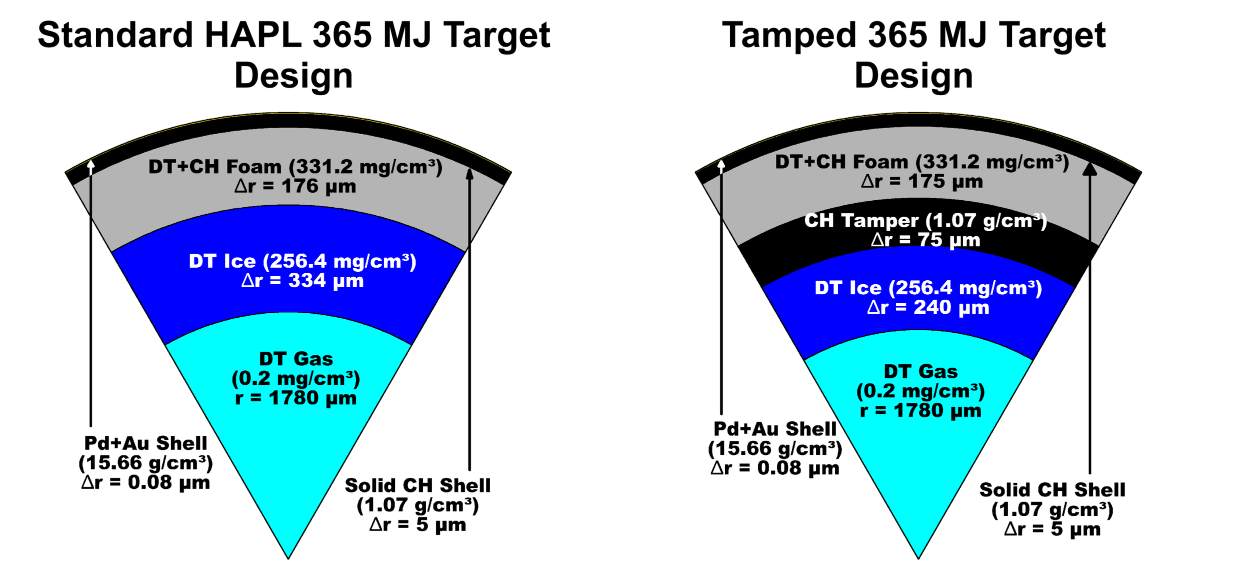

To prevent the alphas from reaching the tungsten armor, 0.35 g/cm² of areal density must lie between the burning DT plasma and the tungsten armor. This can be achieved via a high-pressure buffer gas (see previous panel) or the introduction of a tamper into the target design. The tamper is a material that lies in the compressed core of the target and reaches the appropriate ρR value of (0.35 g/cm²) during the fusion burn process.

For the purposes of this analysis, a 75 μm plastic tamper was added to the HAPL target between the DT ice and ice-wicked plastic foam layers. 1-D BUCKY simulations were performed that achieved a 364 MJ fusion yield using the same driver energy (2.4 MJ) and power profile as the original HAPL target design.

Plotted below are the x-ray and alpha spectra from both the HAPL target (produced by LLNL) and the BUCKY simulation of the tamped target design. Note that the energy from the high-energy alphas has been converted to x-rays by virtue of being stopped in the tamper region (0.5% of the fusion alphas escape the tamper).

1-D BUCKY Simulations show good target compression and burn

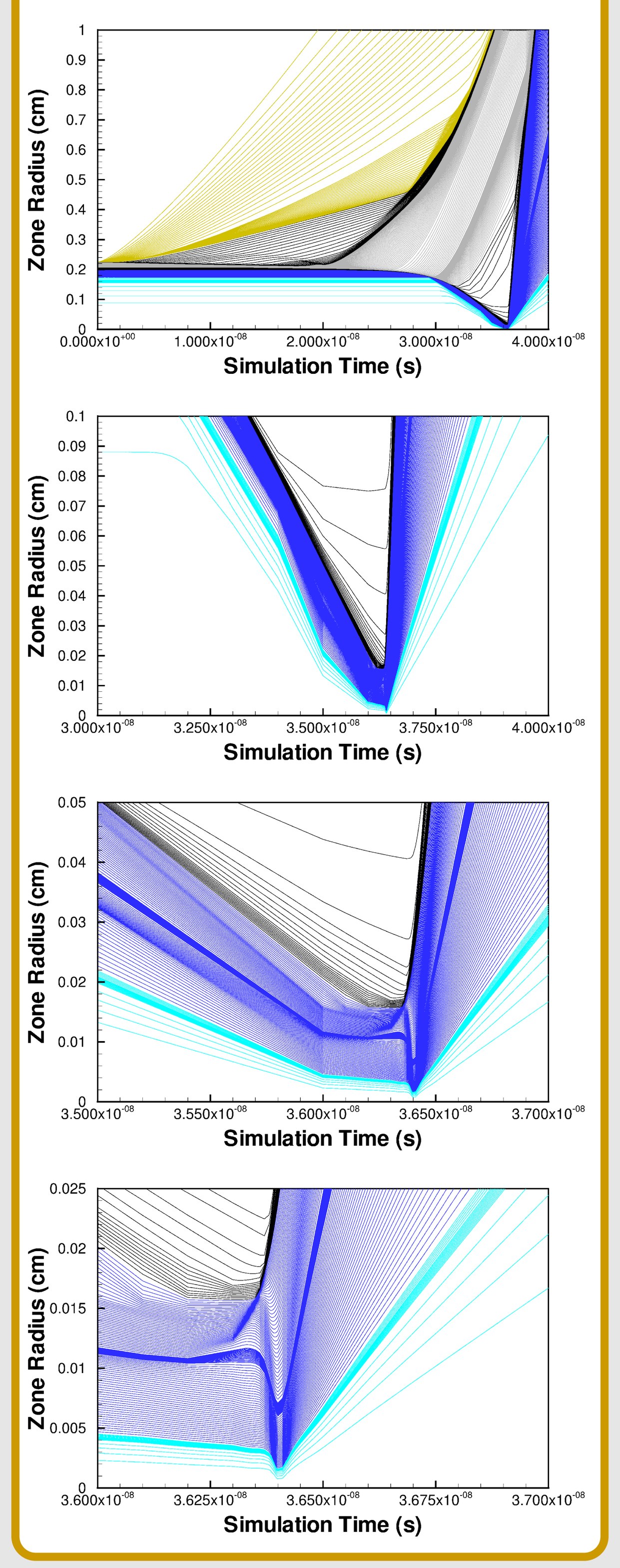

*This work supported in part by a grant from the Naval Research Laboratory, award no. N00173-03-1-G901.

Comparison of x-ray and alpha spectra from the LLNL and Tamped Targets shows significant improvement in the threat spectra

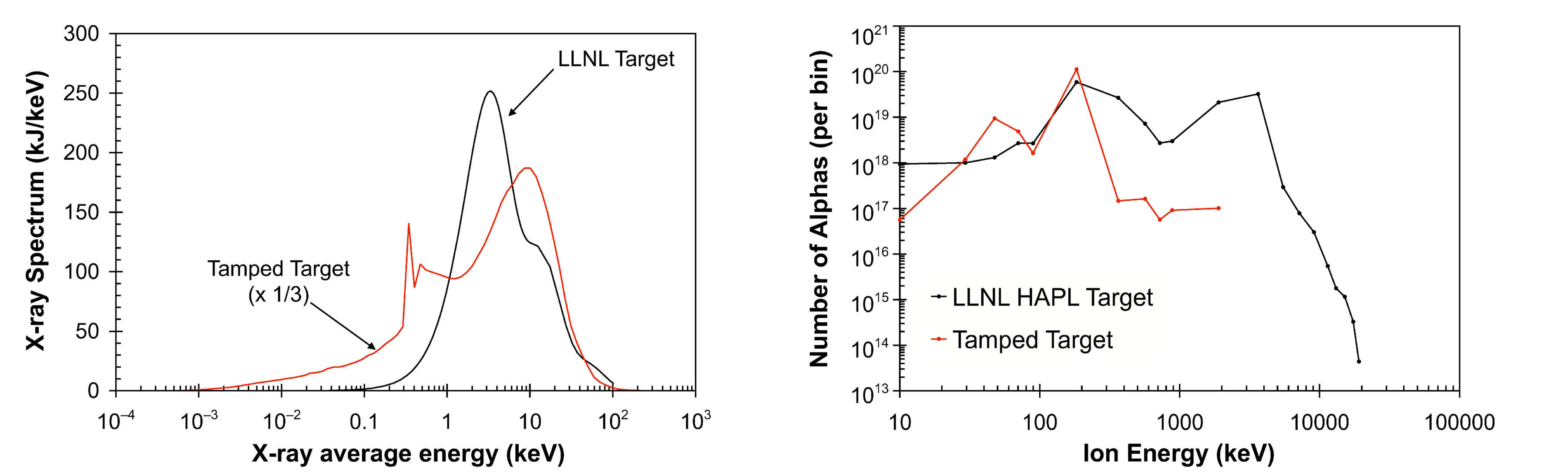

Chamber Buffer Gas is Essential

Xenon buffer gas stops the low-energy alphas, causing a significant increase in armor lifetime at a pressure of 35 mtorr

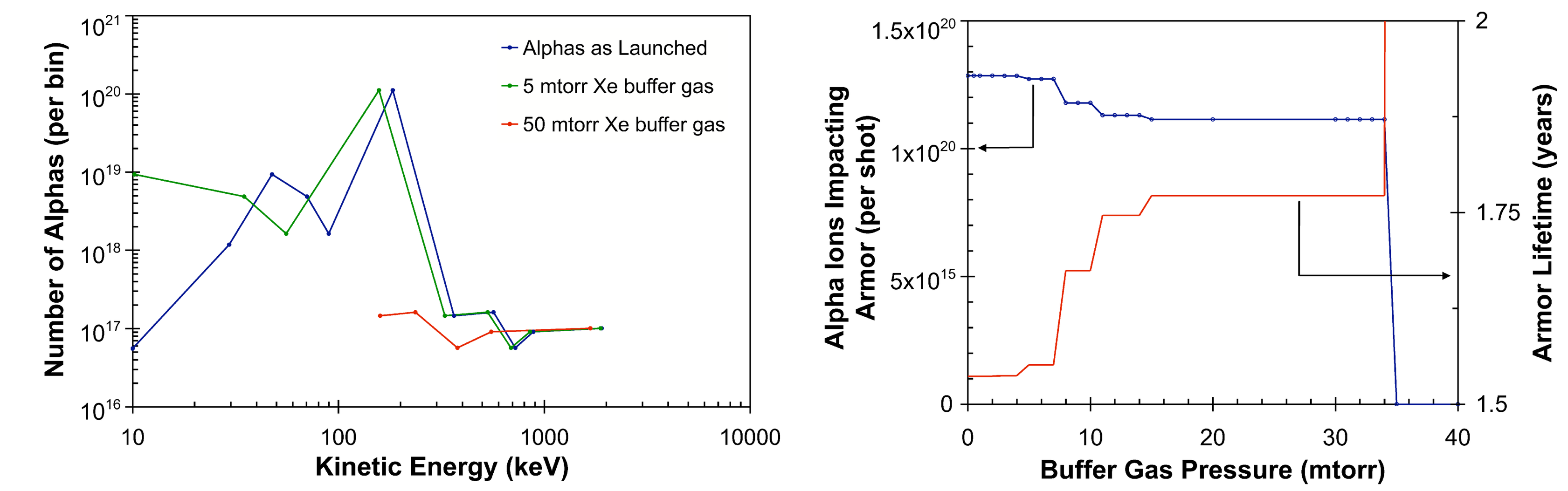

By itself, the tamped target design reduces the armor lifetime (from 2 FPY to 1½ FPY) by the production of more low-energy alpha particles. The tamped target design is only viable if used in conjunction with a low-pressure xenon buffer gas. Adding 35 mtorr of xenon buffer gas at 600 °C to the chamber is sufficient to stop nearly all alphas (see above), increasing the tungsten armor lifetime to 357 FPY (neglecting high-energy alpha and neutron damage).

As shown below, the tamped target design in conjunction with 35 mtorr of xenon buffer gas also satisfies the thermal stress limiting criterion of a surface temperature maximum of no greater than 2400 °C.

Additional 2-D simulations need to be performed to ensure that the target has enough hydrodynamic stability to ignite and burn without drastic modifications to the laser power profile or total driver energy delivered to the target.

1-D BUCKY Simulations show good target compression and burn

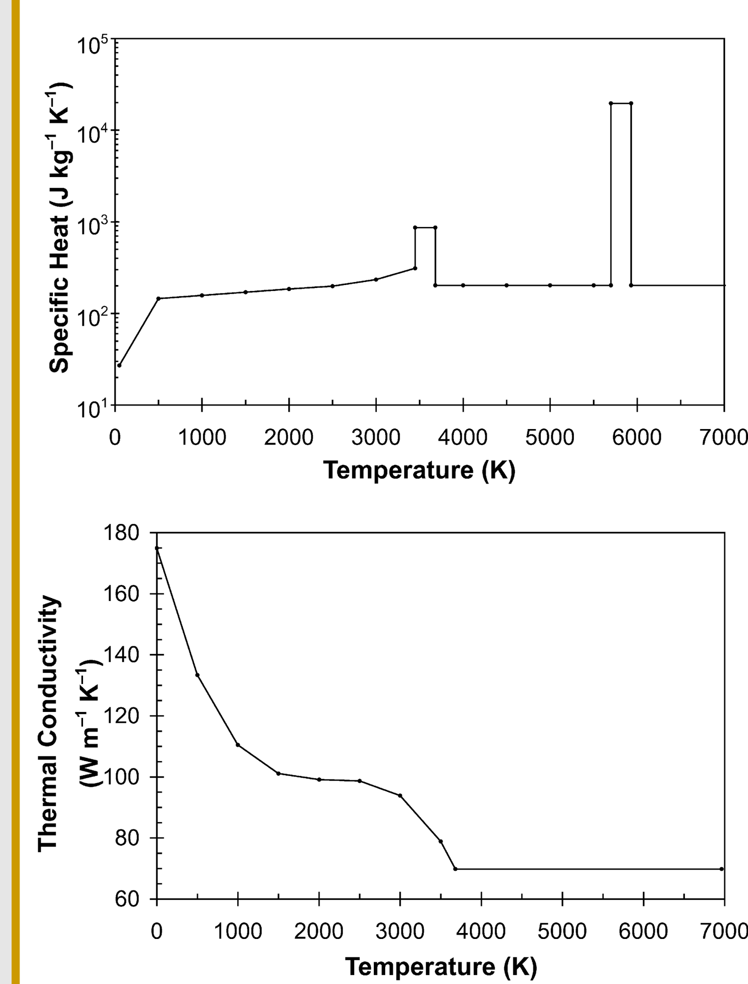

Tungsten Armor Surface Temperature — 10.5 m radius Chamber

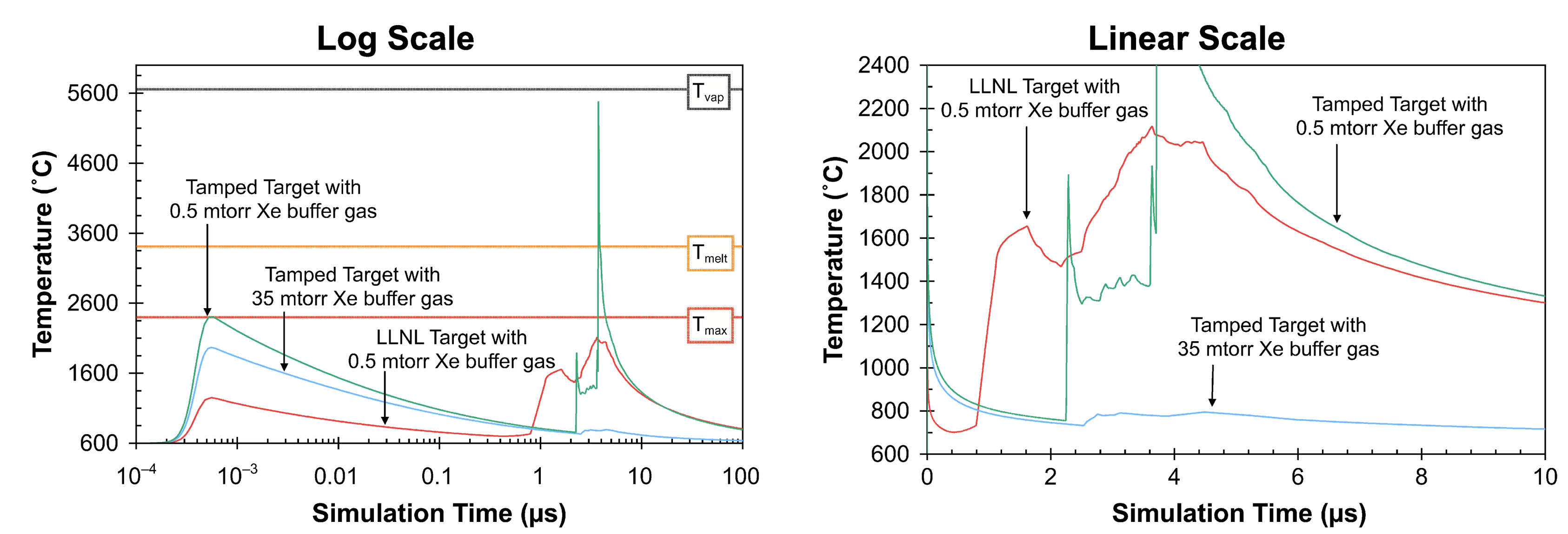

LA-UR-07-2572

Using HED Experiments and Computer Codes in the Study of Target Chamber Dynamics and Astrophysical Phenomena

Robert R. Peterson

Darrell Peterson, Tom Tierney, Bob Watt, Heidi Tierney

Los Alamos National Laboratory

IFE Science and Technology Strategic Planning Workshop

April 24-27, 2007

San Ramon, CA

ABSTRACT

In this talk, I describe how HED (High Energy Density) experiments are used to study the physics of IFE target chamber dynamics, including the transition of radiation-driven blasts in low density media from supersonic to subsonic and the rapid melting and re-solidification by intense burst of x-rays and ions. I also discuss how these experiments are useful in validating computer codes that model such phenomena. I discuss the connection of these phenomena to astrophysical applications,

HED Experiments, Physical Models, and Computer Codes are Required to Study IFE and Astrophysics

IFE Targets and Target Chamber Dynamics

- •Blast waves
- •Target x-ray and ion emissions
- •Vessel wall melting and re-solidification and thermal/ mechanical response
- •Target performance

Computer Codes

- •Lagrangian Hydro
- •Eulerian hydro
- •gravity
- •Radiation transport
- •Material Strength
- •Phase changes
- •Ion transport and deposition

Astrophysics

- Supernovae
- Solar flares
- Solar wind
- Coronal mass ejection
- Binary star mass accretion
- Molecular clouds
- Stellar Models
- Variable Stars
- Meteor impacts
- Jets
- Dynamics around black-holes
- ISM: star formation

Scaling

Scaling

Physics Models

- •Opacity theory
- •Equation-of-state
- •Multi-dimensional Hydro
- •Radiation transport
- •Phase changes

HED Experiments

- •Opacity expts on Z/ZR
- •Jets on Z/NIF (-> Hubble time)
- •Blast wave on Z/ZR/Omega
- •Radiation transport on Omega
- •Rapid ion heating on RHEPP
- •Rapid x-ray heating on Z/ZR
- •Cratering experiments

Z Produces Roughly 2 MJ of X-rays in a Several ns Pulse from 11.5 MJ of Prime Energy Storage

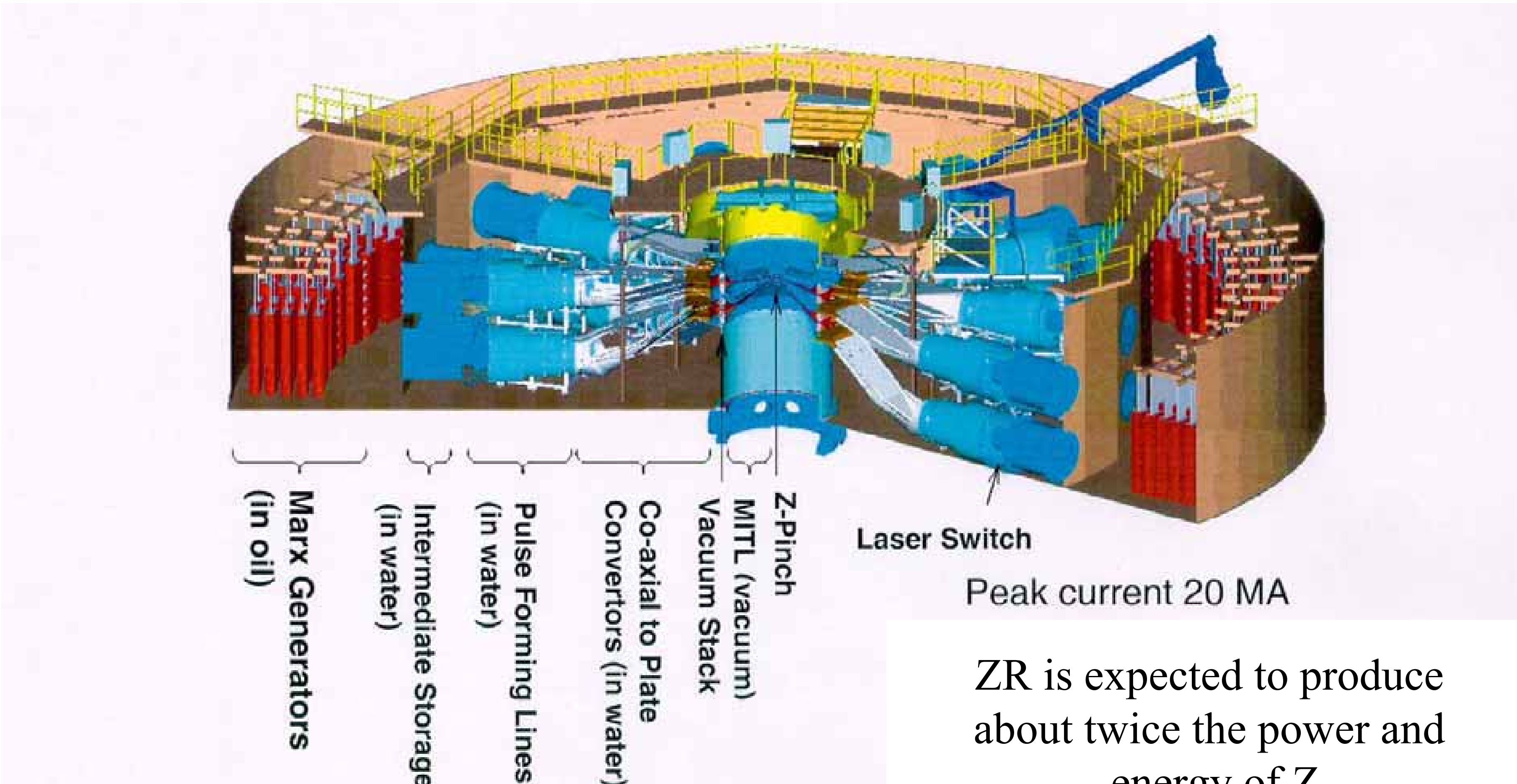

ZR is expected to produce about twice the power and energy of Z

The Z Dynamic Hohlraum (DH) Radiation Source: 20 MA of Pulsed Power Pinches Tungsten Wires onto a CH Foam

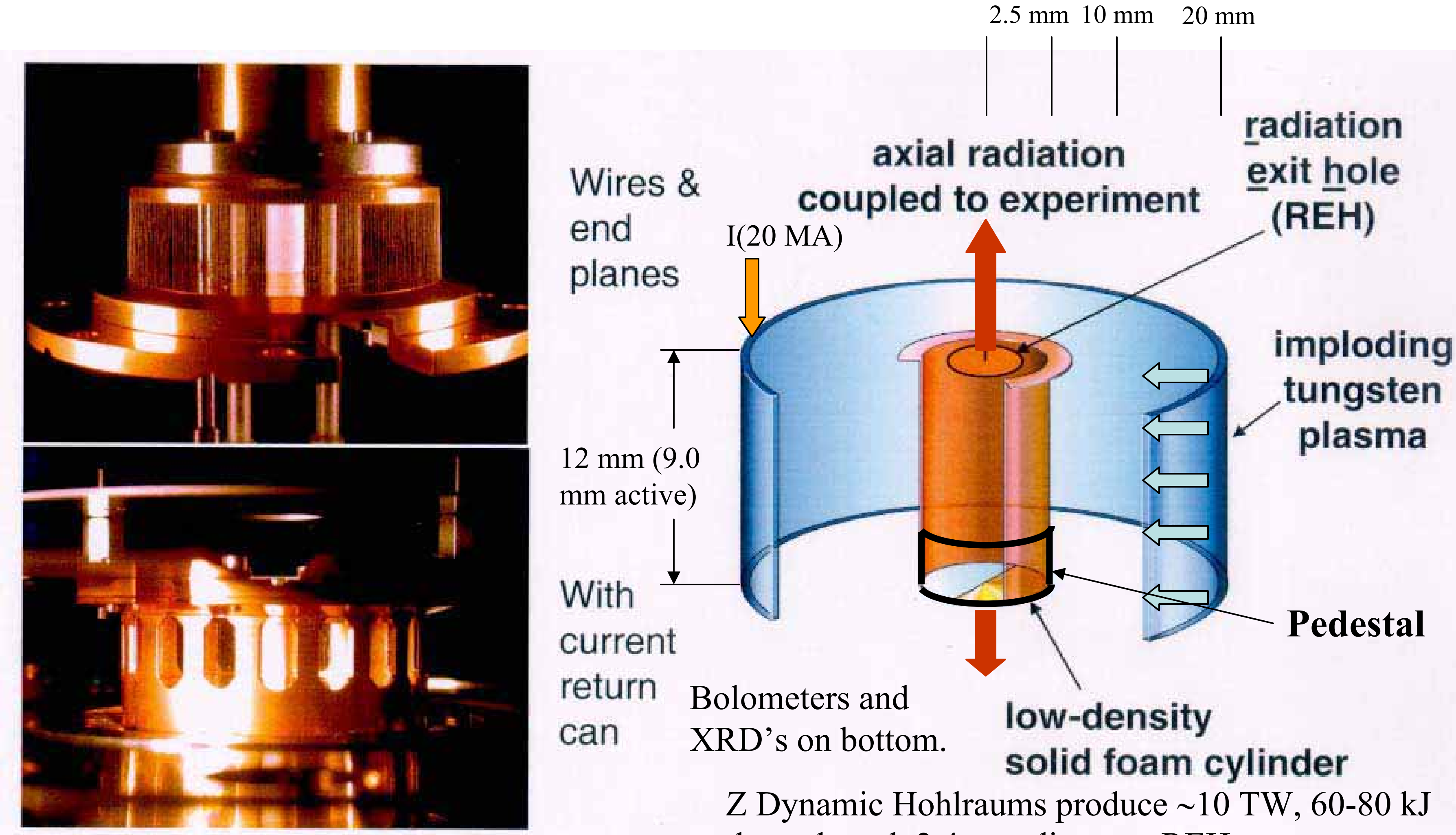

Z Dynamic Hohlraums produce ~10 TW, 60-80 kJ through each 2.4 mm diameter REH

Ionization fronts are observed in astrophysical systems

- Burst of UV photons from source (e.g. star, SN) ionizes medium - creates shock
- Shocked material emits photons
- Photons ionize medium ahead of shock.
- Ionization front is formed.
- Hot unshocked region is often referred as the precursor region.

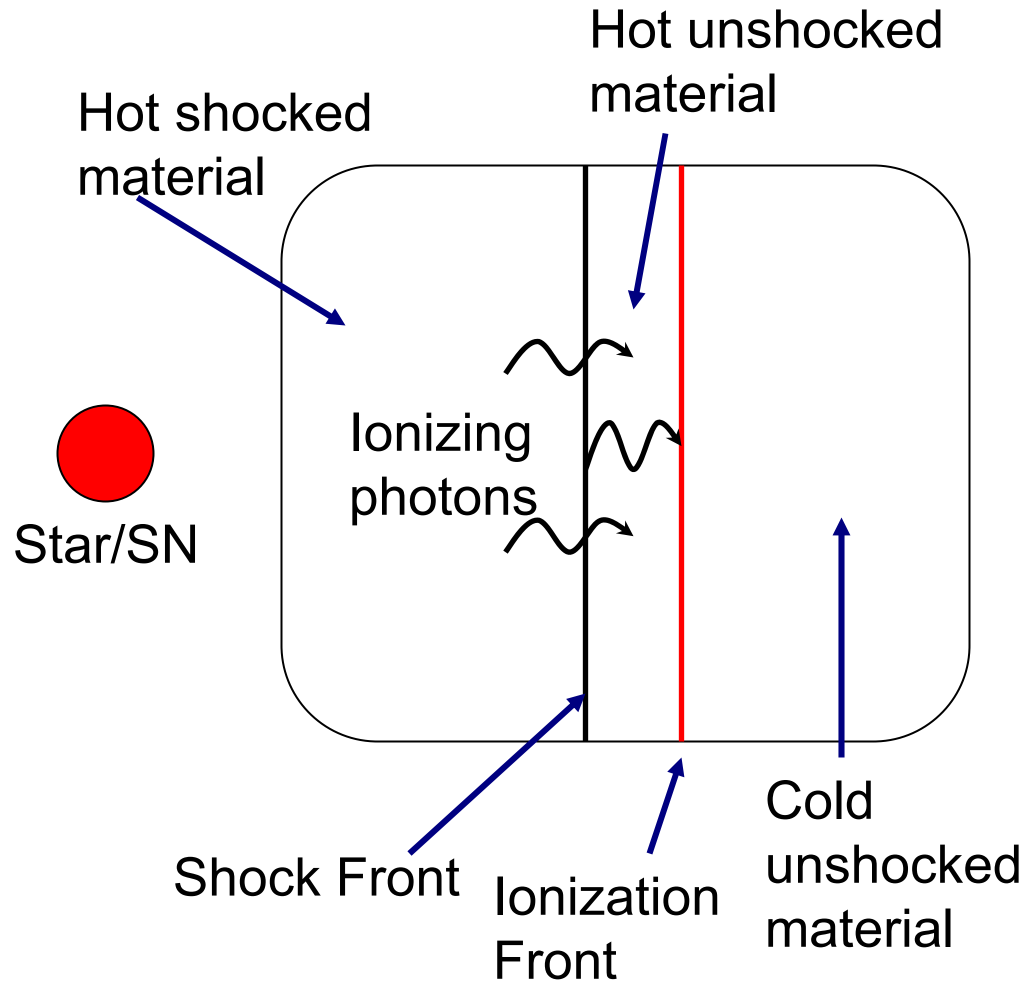

From Paul Keiter, et al.

Blast Waves Permit an Inference of the Energy Released in the Explosion

Tunguska Event, Siberia 1908

Z-1430, January 2005

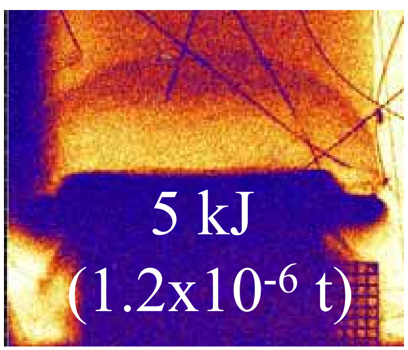

Shoemaker-Levy 9
Fragment G Striking Jupiter, 1994

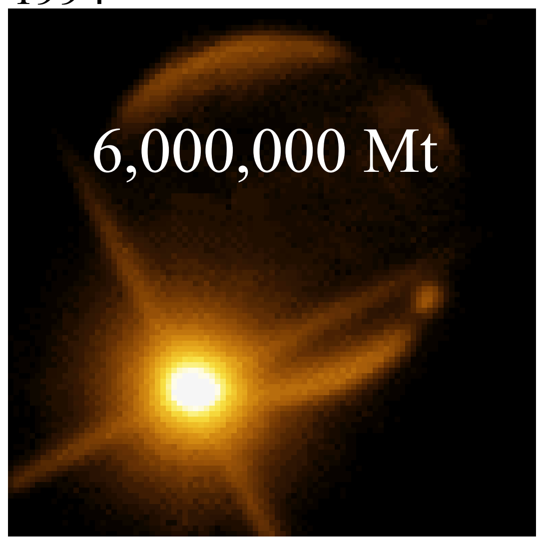

P.J. McGregor, P.D. Nicholson, and M.G. Allen, *Icarus*, 121, 361-388, 1996

Trinity, New Mexico
1945

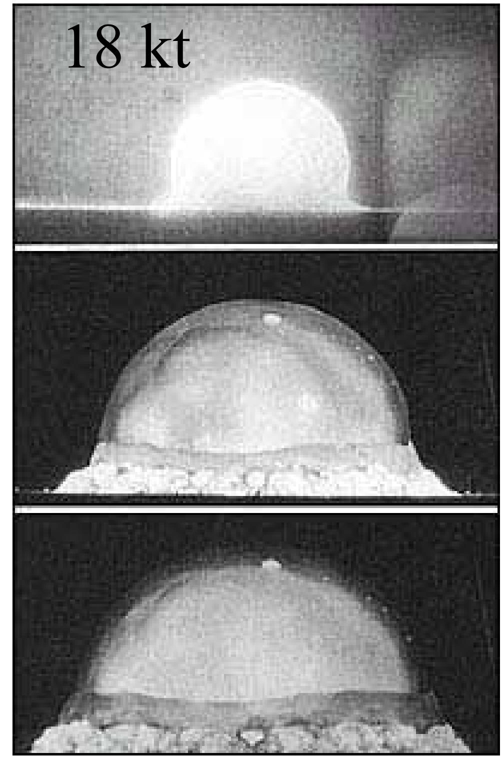

•Blast waves can be created in a planet’s atmosphere by meteors, comets, or other large explosions.

•They can also be created in laboratory plasmas (Z, NRL, LANL)

Z Blast Wave Experiment Using Dynamic Hohlraum Z-pinch Radiation Source

•**Position of Shock is a Sensitive to Drive Radiation Energy**

•Peak Radiation Drive Temperature ≈ 200 eV

•Radiation Transport is Supersonic Deep into the Foam.

•Measurement of Drive Radiation Fluence.

•One Experiment possible on Each Shot.

•Multiple Independent Radiation Power Measurements.

•Monochromatic Imaging of Mn Backlighter Radiation (D. Sinars, SNL) Produces High Quality Radiographs.

•Compare LASNEX simulations with experimental results.

– Tests radiation transport.

– Agreement in simple geometry allows us to move on to more complex problems.

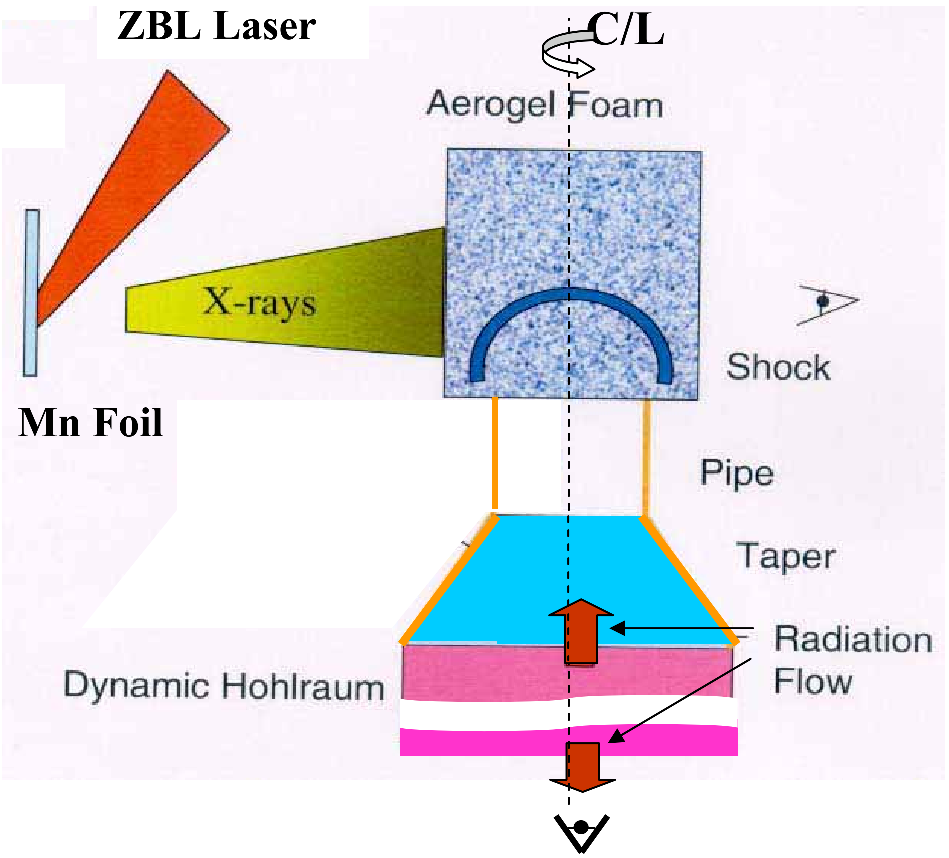

Transonic Radiation Wave in SiO_2 Foam Creates a Radiation-Drive Shock, Which Can be Radiographed.

•Radiation flows into the aerogel foam, initially as a supersonic, diffusive Marshak wave. The wave is moving faster than the foam can hydrodynamically respond to the pressure gradient applied at the radiation front.

•As the volume behind the Marshak front increases, the radiation temperature drops and the Marshak wave slows.

•Eventually, the Marshak wave slows to the speed of a shock in the foam. A radiation-driven shock is formed which is moving much slower than the initial Marshak wave and can be observed.

Observed Shock Position on Z1430 is Consistent with Radiation Power Observed Being Emitted from the Bottom of the DH

Pre-Shot Calculations

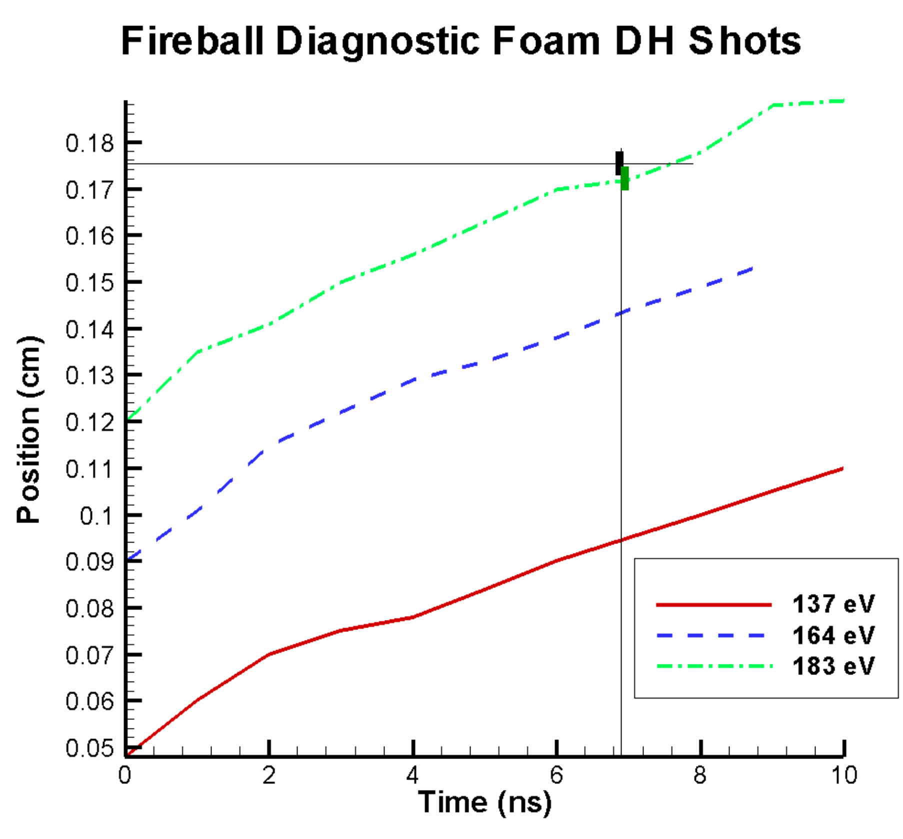

Power Measured at Bottom of DH Peaked at 176-183 eV.

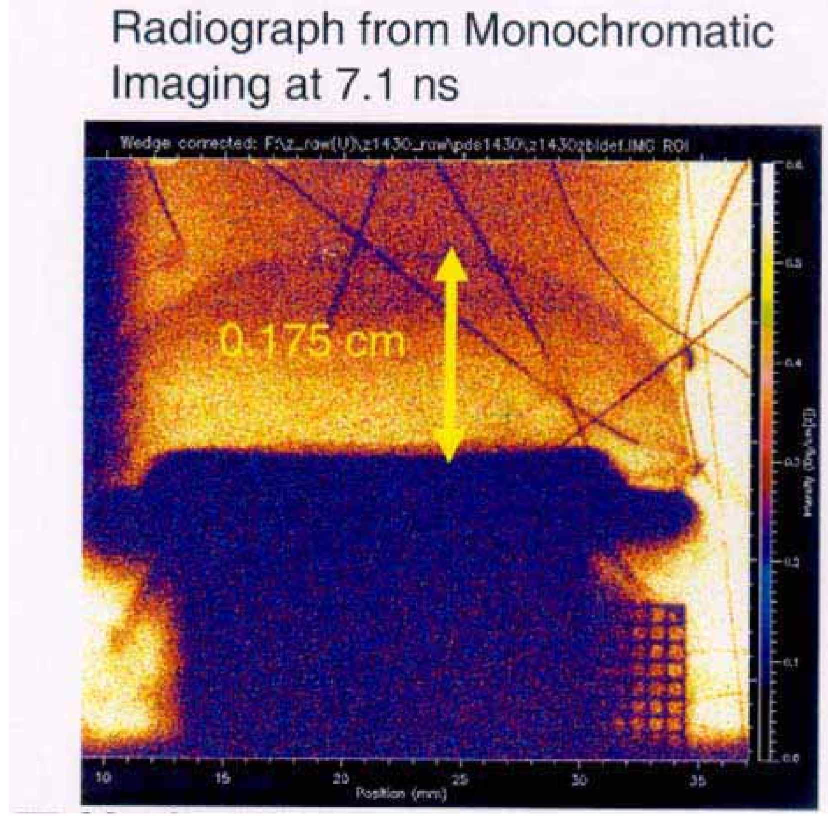

Width of ZBL x-ray pulse = 1 ns

Total uncertainty in shock position = 74 μm.

Z Foam Blast Wave Experiments Study Complex Radiation, Atomic and Atomic Physics, are an In-Situ Diagnostic of Radiant Power, and are a Platform for Other Experiments

- Blast wave experiments in SiO_2 foams on Z show the transition of a supersonic diffusive radiation wave into a sub-sonic fireball.
- Z shot 1430 showed that the position of a blast wave in a foam is a diagnostic of drive power.
- Blast wave experiments on Z provide a platform for additional physics experiments. (Opacity, Astrophysics, IFE Target Chambers)

Radiograph of Z Blast Wave Experiment Z1430

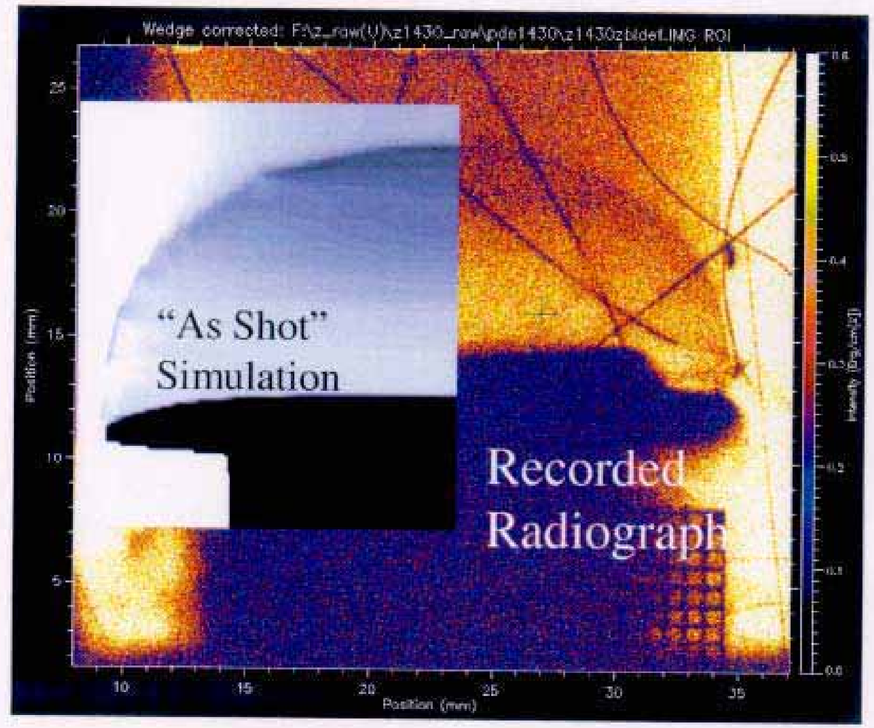

Shock Position is Sensitive to Drive Energy

- 1 eV change in drive causes a 16.6 μm change in shock position so the sensitivity as a drive temperature diagnostic is .06 eV/ μm.
- Other uncertainties in the experiment, such as variations in the foam density or drive pulse shape, have less effect.
- Calculations done with LASNEX.

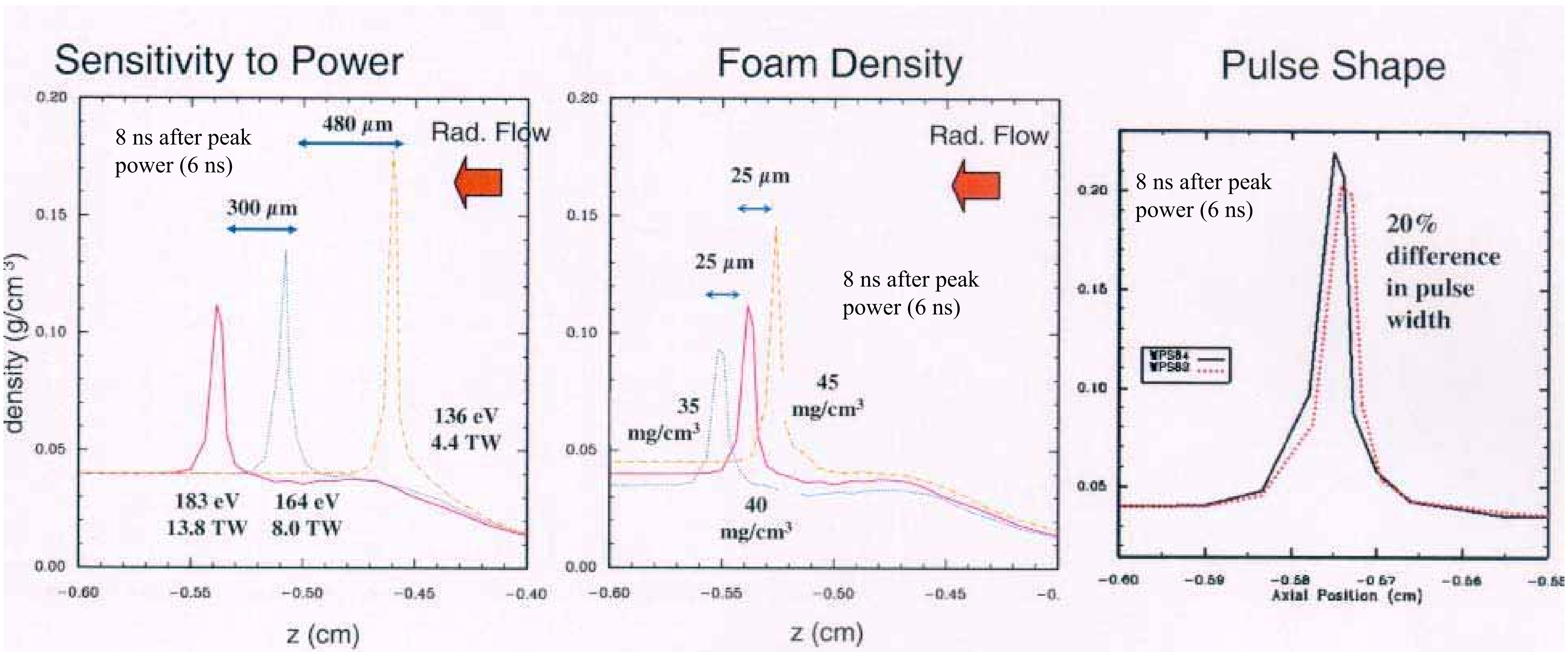

Expected Error in Z Blast Wave Experiments Will Allow Drive Fluence to be Inferred to 9%

Expected Uncertainties	Change in Shock Position (μm)
10 % change in drive fluence	83
2 mg/cc uncertainty in foam mass density	10
1 ns uncertainty in laser timing	52
Spatial resolution of radiograph (monochromatic imager)	12
10 % change in drive pulse width	10
Experimental Error (added in quadrature)	54
10 % uncertainty in SiO_2 opacity	25
10% uncertainty in Au opacity	25
5 % uncertainty in SiO_2 EOS	35
Calculational Error (added in quadrature)	50
Total uncertain excluding fluence	74

74 μm (Total Error) * 10%/83 μm = 9% Error in Drive Fluence

BUCKY Capsule Output Simulations of DH Z-pinch Reactor Target

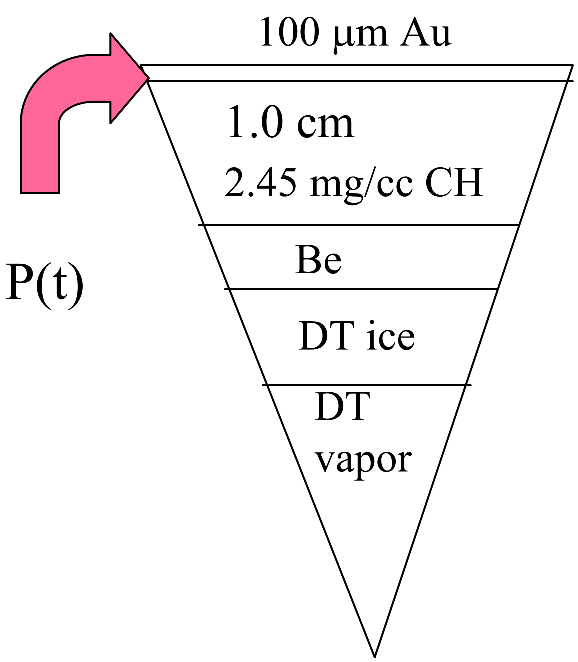

Capsule with Foam and Au Electrode

- Peak Radiation Power is 10^{18} W.
- Total Energy Radiated is 1.4 GJ.
- Radiated energy is 29 % of Yield.
- 5.5% of Yield in Debris

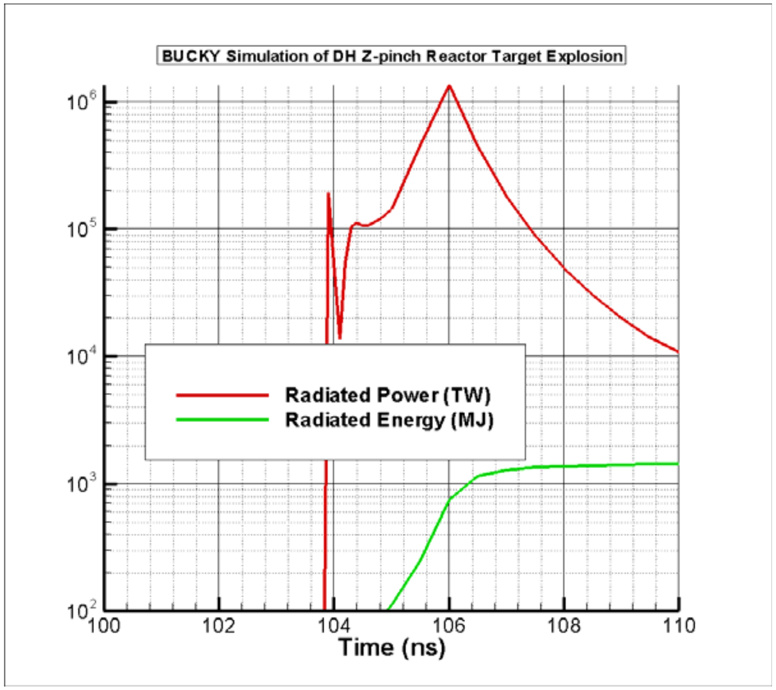

Target Ignites and Burns at about 104 ns, at about 108 ns the Capsule Collides with the Au Electrode

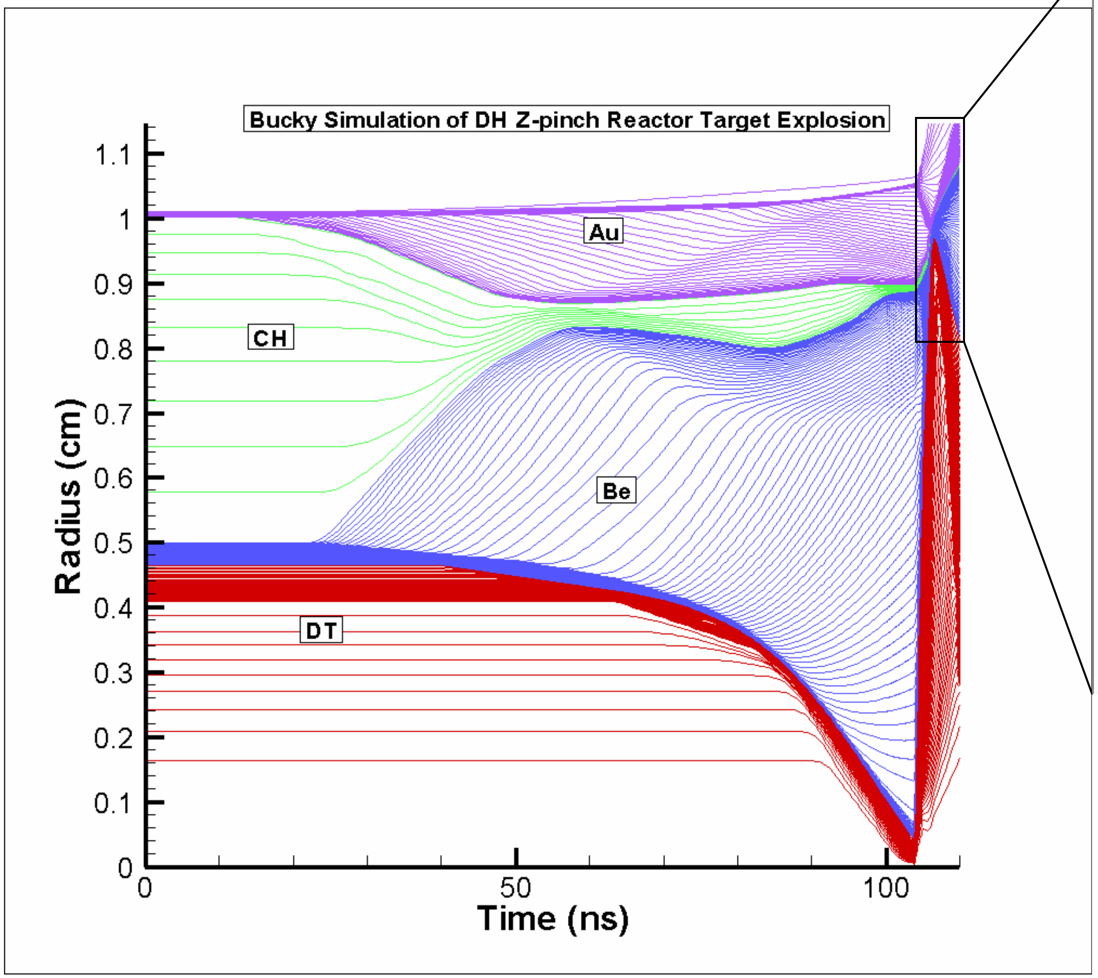

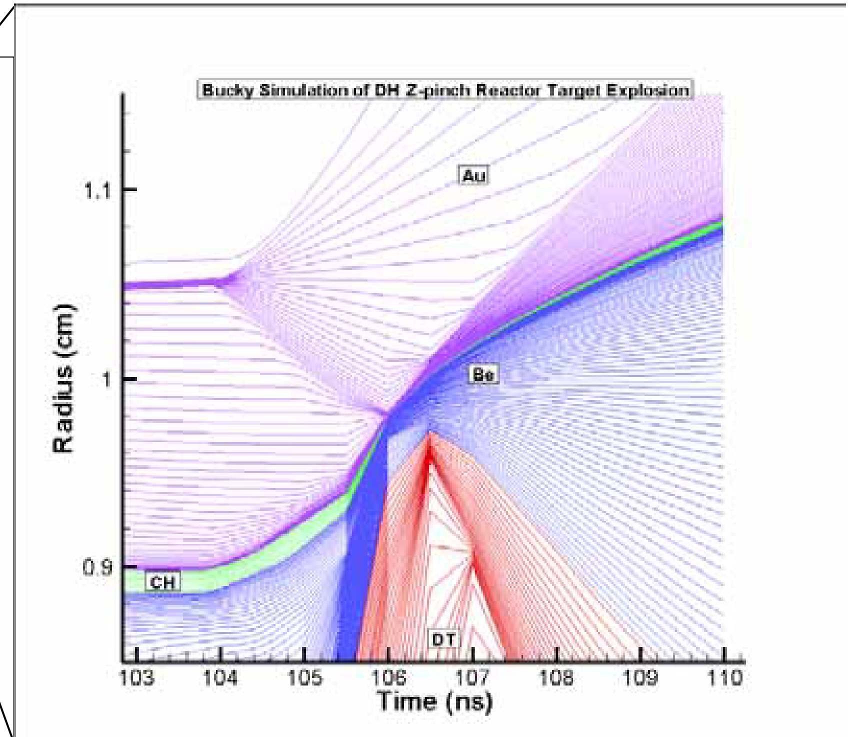

Collision between expanding capsule and electrode produces x-rays, but it is inherently 2-D.

Heated Tungsten Samples on Z, Dec 2003

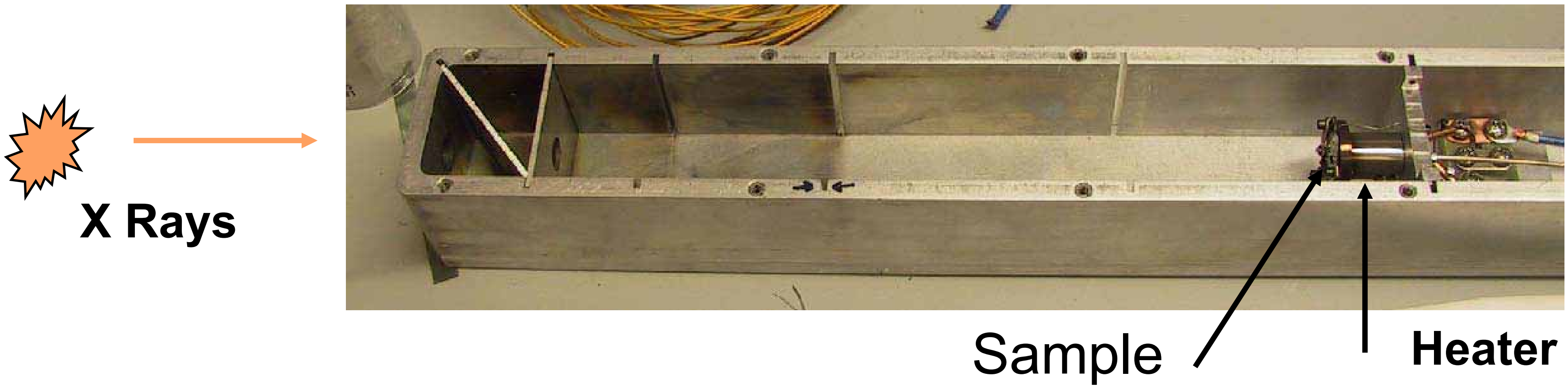

- CVD, powdered metal, and single crystal tungsten on each shot
- Samples mounted with TC in stainless shim stock in front of heaters
- Beryllium and Mylar filters plus distance to source used to adjust fluence
- 600-700 °C preheat temperature

T. Tanaka, SNL

RHEPP Ion Irradiation Experiments Mimic the Conditions of in IFE Target Chamber Walls and are a Test-bed for Material Science

RHEPP Ion Diode

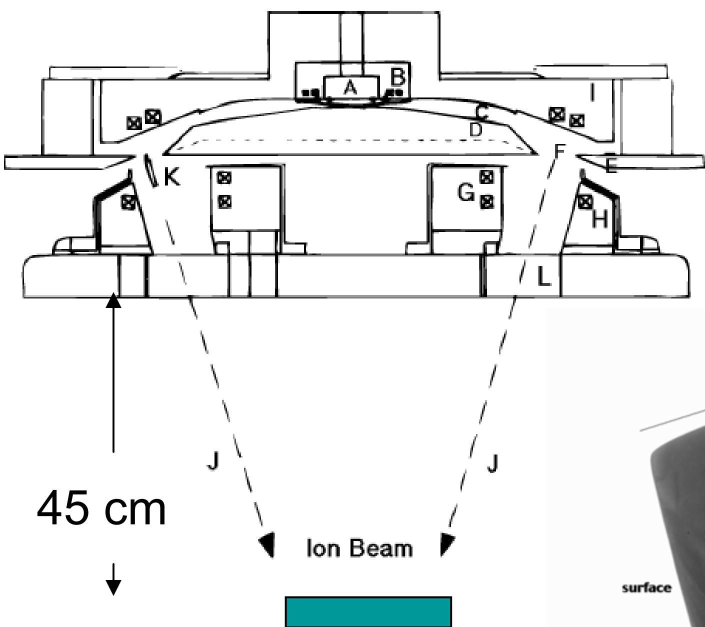

T. Renk, SNL

polycrystalline tungsten suffers fatigue cracking deep below surface after 1000 sub-melt pulses

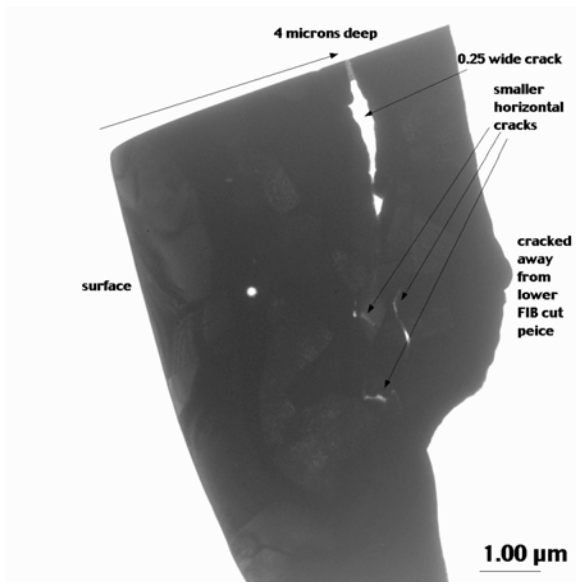

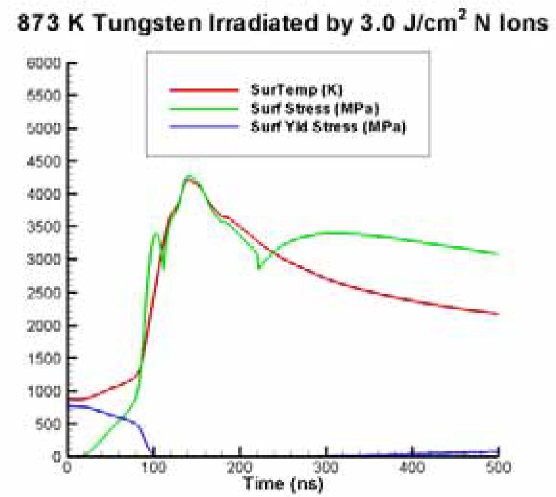

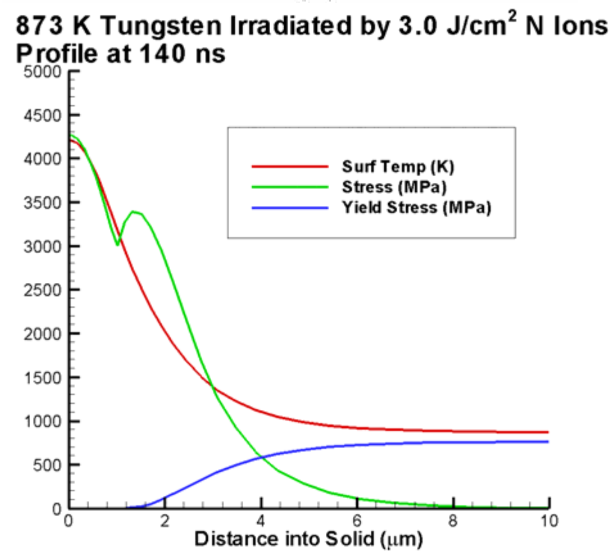

Opacity Experiments at Z Test Atomic Models

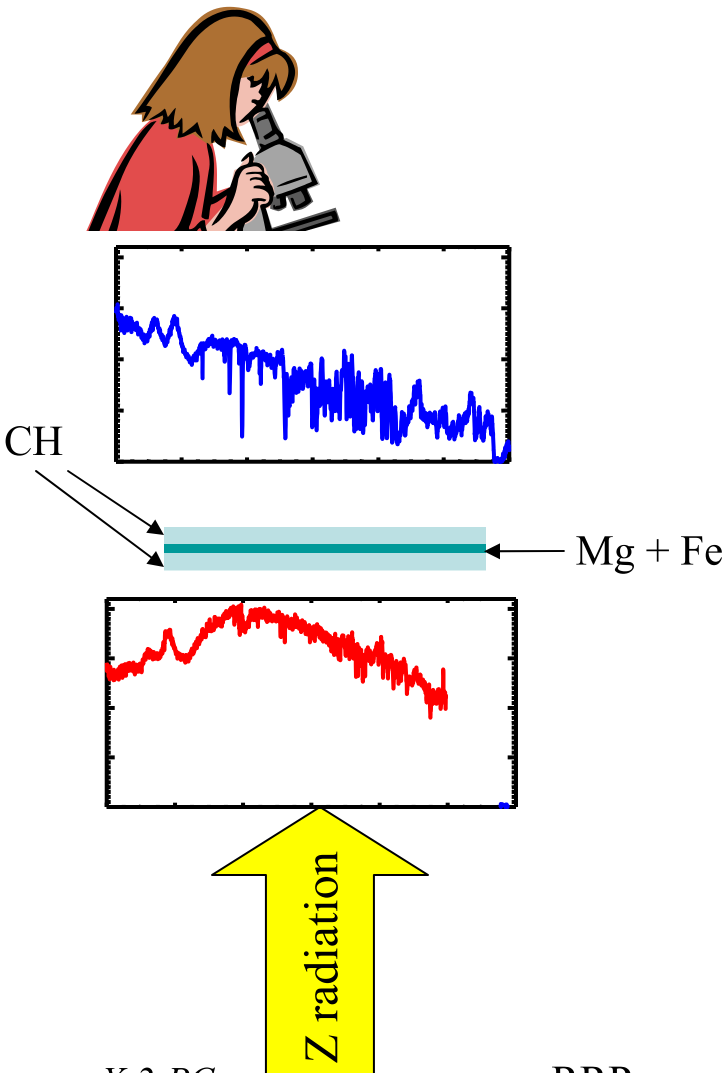

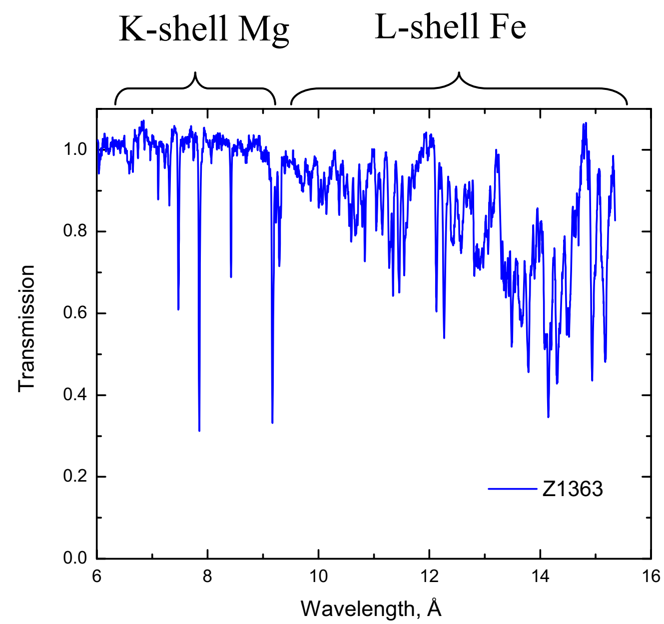

Shot Z1363
Fe + Mg transmission
Te ~ 160 eV, Ne ~ 10^{22} cm^{-3}

I. Golovkin, Prism

Astrophysically Relevant Calculations have been done with the RAGE Code

- Comet/meteor impacts with earth
- HED jet experiments
- Dynamics of objects near the black hole at center of our galaxy
- Mass accretion in binary stars
- Gravitational instabilities in inter-stellar media: star formation

Impact Models in RAGE: millimeter to kilometer scale, quantitative analysis (C. Plesko).

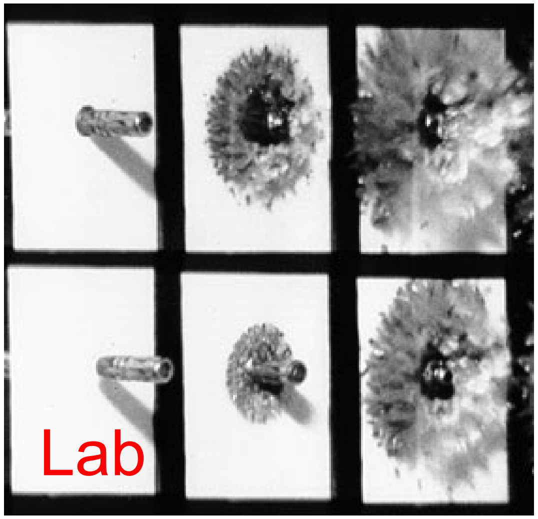

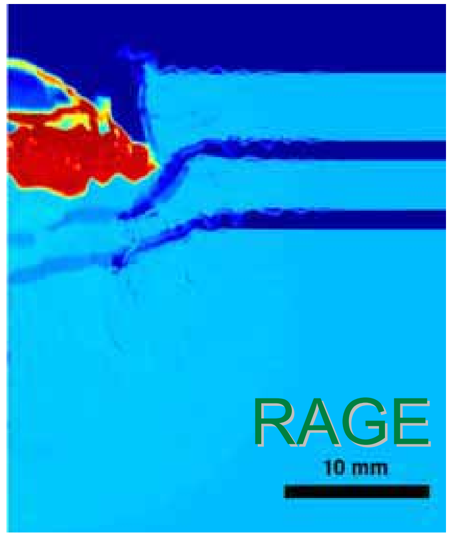

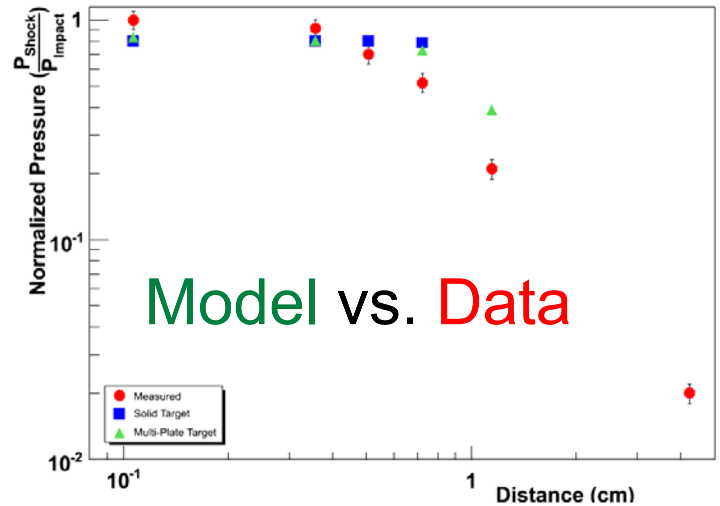

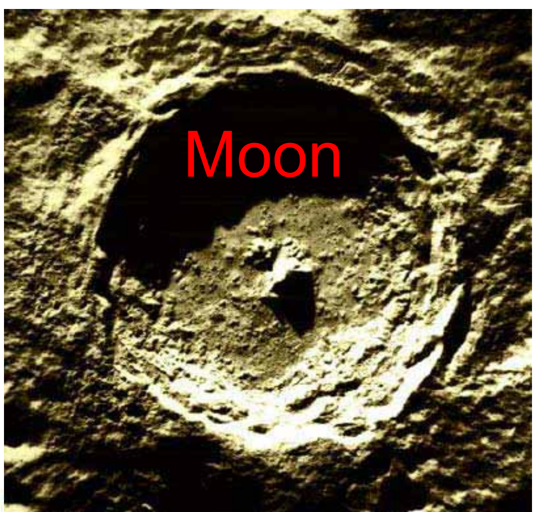

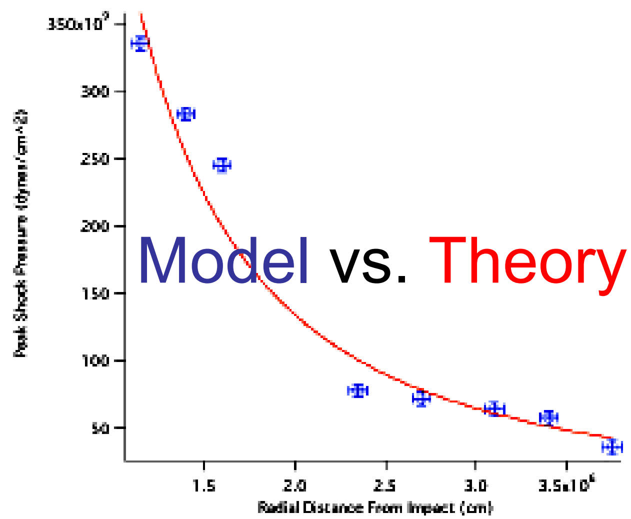

Galactic Center Models (R. Coker)

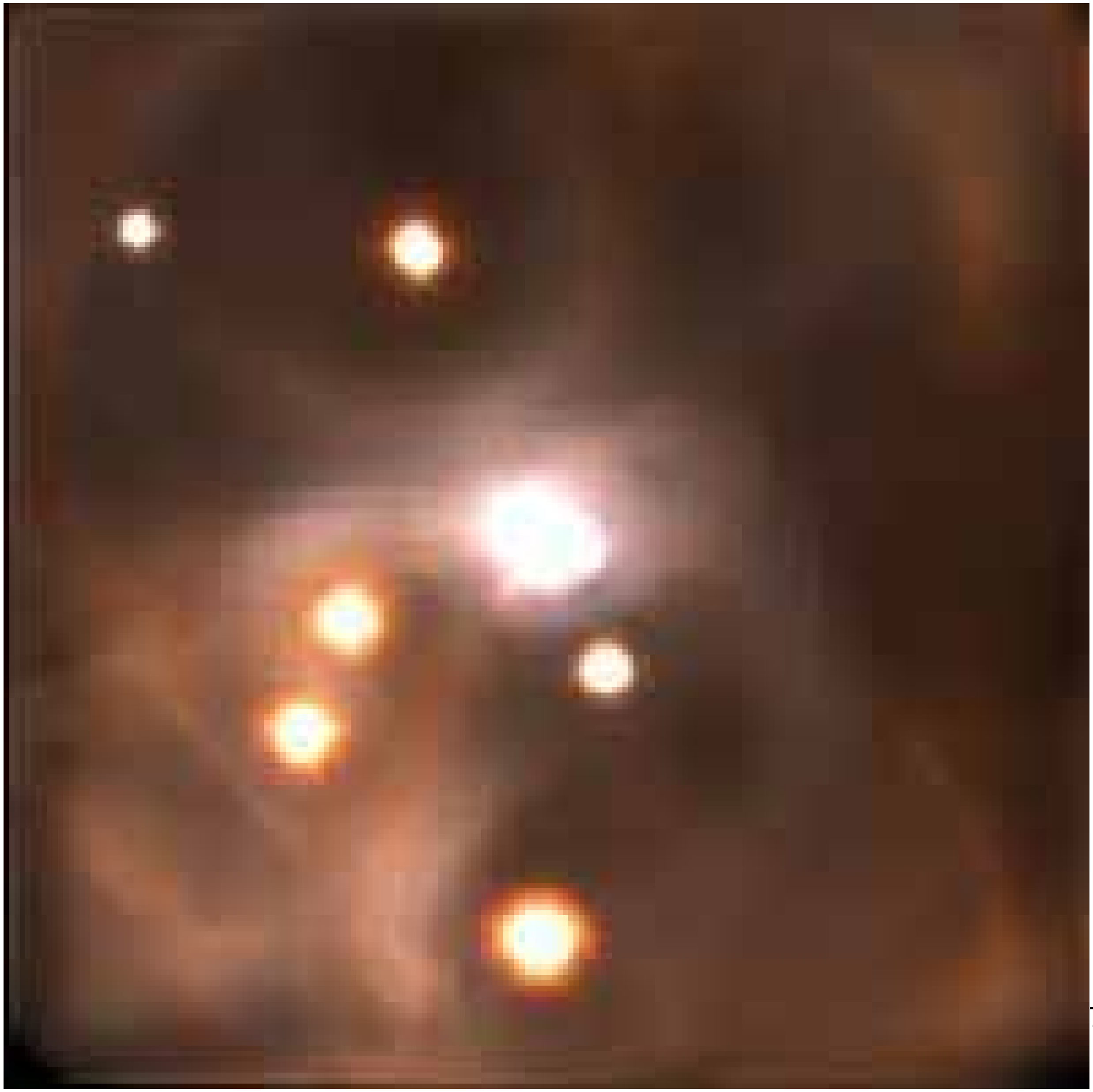

A synthetic X-ray image of Sgr A* (the black hole in the center of the Milky Way)

(Red is 2-3 keV emission and is likely to be partly absorbed due to the high extinction towards GC while green is 3-5 keV and blue is 5-10 keV.)

Conclusions

- Triad: physics models, HED experiments, codes.
- Present codes can be applied to IFE Targets and Chamber Dynamics.
- Present codes and models are being applied to a number of astrophysical problems.

Target Injection and Engagement

Ronald Petzoldt, Neil Alexander, Lane Carlson, Dan Goodin, Graham Flint, and Emanuil Valmianski

GENERAL ATOMICS

UCSD

Significant progress was achieved with high-speed gas gun

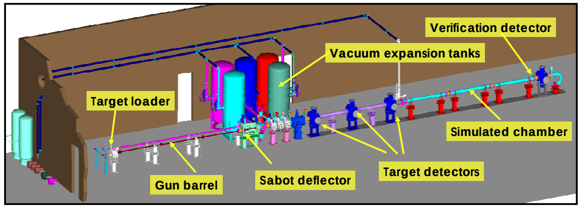

We demonstrated:

- Rep-rated operation (6 Hz, "burst" mode)
- Two-piece sabot separation and deflection
- Membrane support of target in sabot
- Injection velocity of ≥400 m/s with time "jitter" at chamber center of ~ 0.5 ms (KrF requirement of < 1 ms)
- Target placement accuracy standard deviation of 10 mm at 17 m

However, greater accuracy is needed.
- Two piece sabot removal and gas removal add to system complexity and reduce accuracy

The magnetic intervention concept allows removal of chamber protection gas and smaller chamber size

Substantially changes target injection requirements

- Target survival (> ~25 m/s injection velocity)
- Only one target in chamber at a time (> ~32 m/s at 5 Hz)
- We are evaluating ~50-100 m/s
  - 13-50 cm acceleration at 10,000 m/s^2
  - Opens door for other injection mechanisms (Mechanical, pneumatic, electric, etc.)
- Without gas in chamber, ±1 mm placement accuracy has been discussed - a challenge to be demonstrated
- Without sabot separation and with in-chamber tracking, the target flight distance could be reduced from 17 m to ~10 m

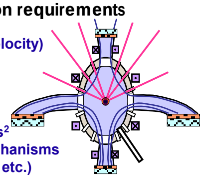

…Magnetic intervention should make target injection easier (i.e. slower)

Calculations indicate that plasma heating is dramatically reduced with lower gas density

- Radiation only reduces gas temperature to ~10,000 K between shots
- Mean free path << chamber radius for n>10^{13}/cm^3 (0.3 mTorr)
- Plasma does not quickly recombine without contacting surfaces
- Plasma transfers recombination energy to targets

⇒Gas density <~1 mTorr may be necessary for acceptably low target heating

Calculations for 10 m radius chamber

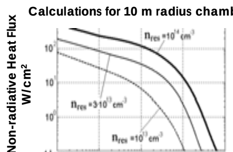

*Ref: Simulation of afterglow plasma evolution in an inertial fusion energy chamber, B.K. Frolov, A.Yu. Pigarov, S.I. Krasheninnikov, R.W. Petzoldt, D.T. Goodin, Journal of Nuclear Materials 337–339 (2005) 206–210

Work supported by Naval Research Laboratory thru contract N00173-06-C-60052

A single-shot mechanical injection device demonstrated improved injection accuracy

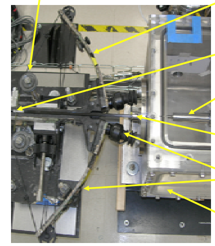

Injection method	Target Material	Mass	4 m, 1 σ accuracy	17 m, 1 σ Extrapolation
Gas gun best results ~10-20 mTorr	Solid Plastic	30 mg	NA	10 mm
Mechanical 10-20 mTorr with reduced static charge	Hollow plastic	1 mg	0.9 mm	3.8 mm

Mass of an IFE target is about 8 mg

Low-speed injectors can be built using a number of driving sources

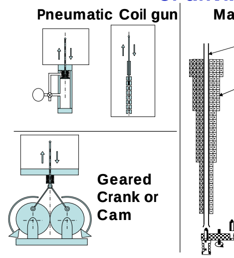

First step used two position measurements were previously used to predict final target position

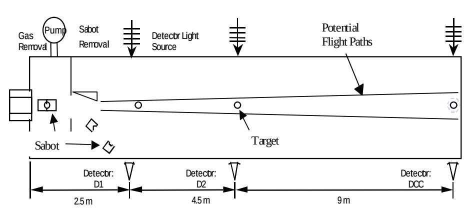

Currently use continuous transverse position measurement for early mirror steering

- The target is backlit throughout its trajectory
- Diffraction patterns from reference apertures are used to align the tracking beam
- Transverse position is measured using Poisson spot location
- Requires only one sensor for continuous 2 D tracking
- Requires clear beam path (e.g. electrostatic target acceleration)

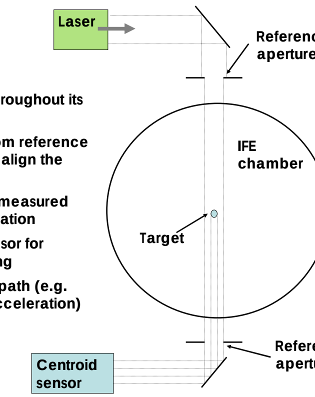

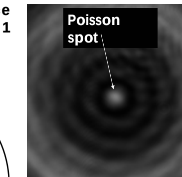

4 mm diameter target
4 m from detector
λ = 0.63 μm

The target itself provides a common reference point for final driver beam alignment and engagement

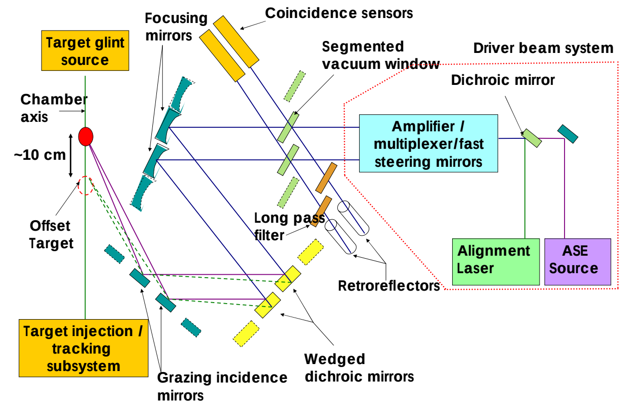

- The alignment beam is longer wavelength than the driver so goes through the long pass filter and retroreflector to the coincidence sensor.
- A "glint" off the target enters the coincidence sensors.
- Dichroic wedges compensate for target motion between the glint and driver beam arrival and also for the glint offset from target center.
- Differences between the glint and alignment beam positions on the coincidence sensor are corrected with fast steering mirrors.

Summary

- Higher accuracy demonstrated at reduced injection speed
- Magnetic intervention allows very low gas density
  - May be required to avoid excessive target heating
- Continuous target tracking is achieved by measuring Poisson spot motion from a backlit target
- Final beam-target alignment is facilitated by measuring position of a glint return off the target 1-2 ms prior to the shot.

IN FLIGHT TARGET STEERING TO IMPROVE INJECTION ACCURACY

Ronald Petzoldt, Neil Alexander, Lane Carlson, Dan Goodin, and Emanuil Valmianski

1 Introduction

- Driver beams must be steered to hit targets with 20 µm accuracy with target speed ~100 m/s.
- Target steering can;
  - Improve accuracy of target placement
  - Reduce steering distance and speed required for ~3000 drive beamlets.
  - Facilitate early FTF non-reprated operation with 50 cm standoff and no high-speed beam steering

2 Target Steering is Accomplished with Multiple Real Time Electric Field Corrections

- Electric charge is placed on the target
- Target passes between long electrodes
- Target transverse position is measured each 8 ms
- Electrode voltage is updated with each position measurement to provide desired steering correction

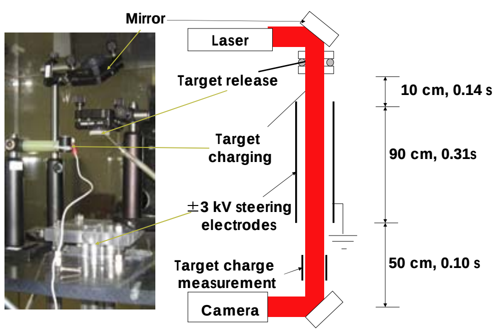

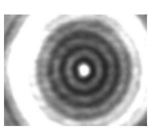
1) Capture image


2) Threshold pixels

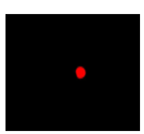
3) Particle filter

3 We Integrated In-Flight Steering with Real Time Trajectory Correction

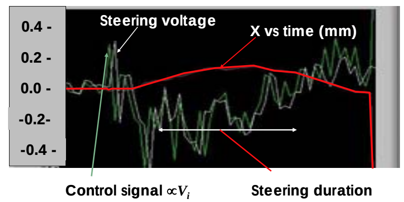

Steering voltage based on X position (Poisson spot's centroid) and velocity updates each ~8 ms

e.g.

$$V_i = -(2.4X_i + 60[X_i - X_{i-1}])\ \mathrm{kV}$$

4 Charge on Falling Sphere is Measured Indirectly

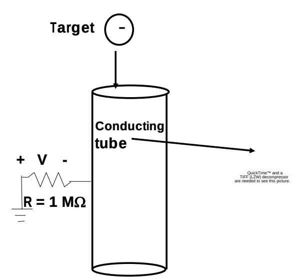

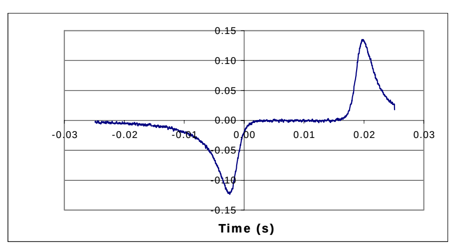

Charge is drawn onto target through 1 MΩ oscilloscope resistance

$$q = \int I dt = \int \frac{V}{R} dt = -0.74\ \mathrm{nC}$$

Standard deviation of charge is ~5 %

5 Two Axis Steering is Achieved with 4 Cylindrical Electrodes

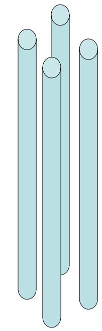

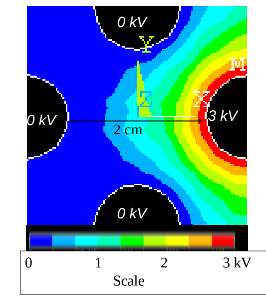

Electric field is less uniform with quadrupole steering electrodes than with parallel plates

We modified the steering algorithm to include this non-linearity

6 Placement Accuracy (2D) Improved from ~500 to ~50 µm (1σ)

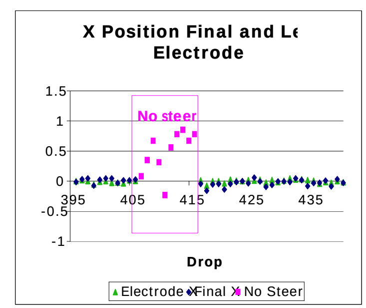

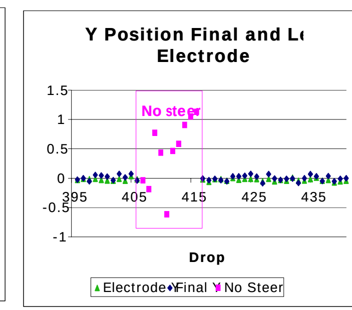

7 Summary and Conclusions

- Improved target placement accuracy reduces required beam steering
- 10X accuracy improvement with electrostatic steering demonstrated

Future work

- Move from steering solid spheres in air to hollow spheres in vacuum
- Increase position measurement update rate (8 ms to ~1 ms)
- Move from dropped targets to higher-speed injection

* Work supported by NRL contract N00173-06-C-2032

A Liquid Breeder Blanket for a Laser IFE Power Plant with Magnetic Intervention

A. R. Raffray (University of California, San Diego)
A. E. Robson (Consultant, Naval Research Laboratory)
M. E. Sawan (University of Wisconsin, Madison)
G. Sviatoslavsky (University of Wisconsin, Madison)
I. N. Sviatoslavsky (University of Wisconsin, Madison)
X. R. Wang (University of California, San Diego)

Inaugural IFE Science & Technology Strategic Planning Workshop

San Ramon, CA

April 24-27, 2007

Outline

- **Magnetic intervention as advanced option to reduce or eliminate ion threat on chamber wall**

- **Advanced chamber concept based on magnetic intervention**
  - **Self-cooled Pb-17Li or flibe with SiC_f/SiC**

The HAPL Program Aims at Developing IFE Based on Lasers, Direct Drive Targets and Solid Wall Chambers

- **Challenging to design dry wall armor to accommodate ion and photon threat spectra.**

- **For example, for baseline 350 MJ target (~24% of the energy is in ions and ~1% in photons), a large chamber (~10.75 m) is required to maintain W armor under a reasonable temperature.**

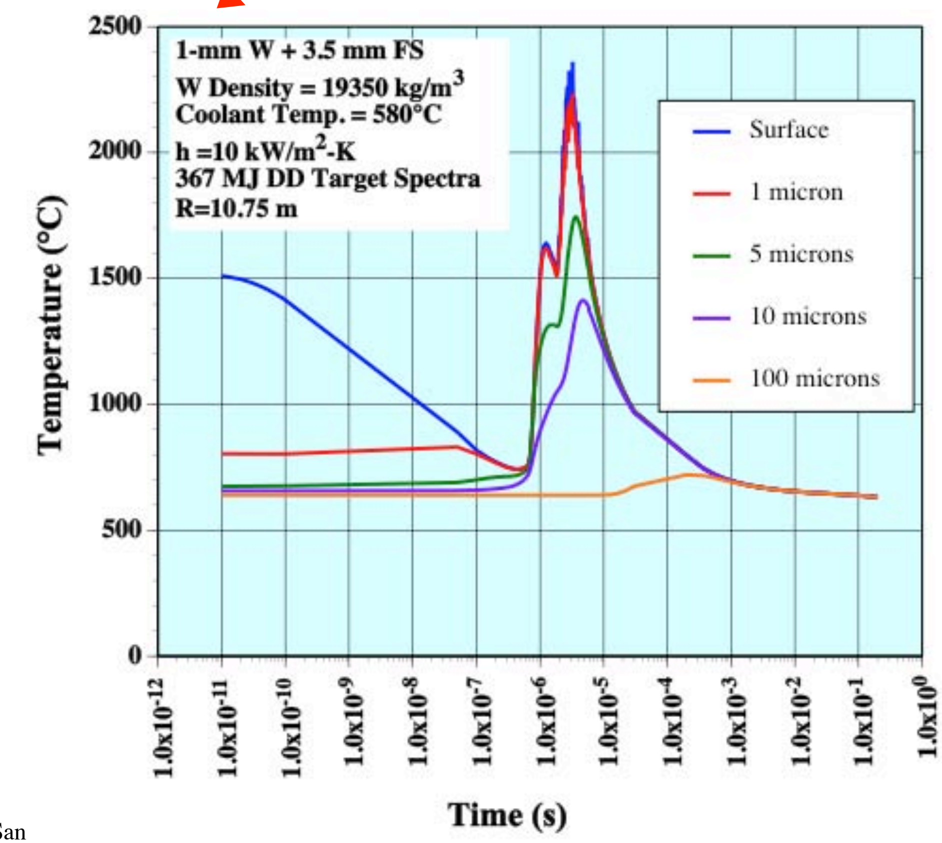

- **In addition, ion implantation (in particular He) can lead to exfoliation and premature failure of the armor .**

- **Maintain large chamber as baseline but look at advanced options that would reduce the ion threat spectra on the armor and allow for more compact chambers.**
  - **Magnetic intervention is such an option**

Magnetic Intervention: Utilizing a Cusp Field to Create a Magnetic Bottle Preventing the Ions from Reaching the Wall and Guiding them to Specific Locations at the Equator and Ends

- **Utilization of a cusp field for such magnetic diversion has been experimentally demonstrated previously.**
  - 1980 paper by R.E. Pechacek et al.,

- **Following the micro-explosion, the ions would compress the field against the chamber wall, the latter conserving the flux. Because of this flux conservation, the energetic ions would never get to the wall.**

- **One possibility would be to dissipate the magnetic energy resistively in the FW/blanket, which reduces the energy available to recompress the plasma and reduces the load on the external dumps.**
  - about 70% of ion energy dissipated in blanket
  - about 30% of ion energy in dump region

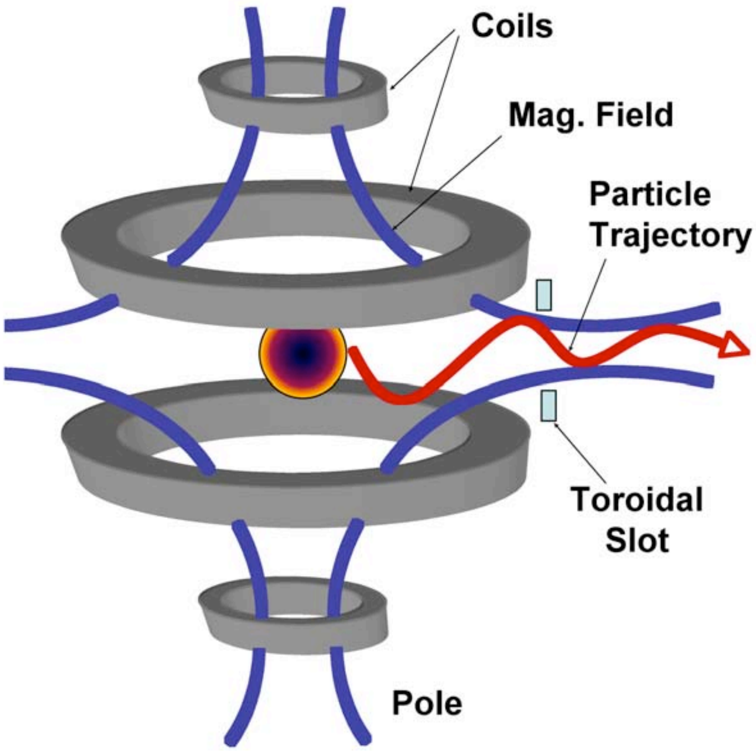

UC San Diego

Conical Chamber Well Suited to Cusp Coil Geometry and Utilizing SiC_f/SiC for Resistive Dissipation

- **Armored ion dumps could be inside the blanket chamber (as schematically shown) or outside, which is the preferred configuration allowing for easier maintenance.**

- **SiC_f/SiC blanket with liquid breeder .**

- **Water-cooled steel shield (~0.5 m thick) required to protect the coil (behind the blanket or around coil).**

- **Design provides for accommodation of laser ports.**

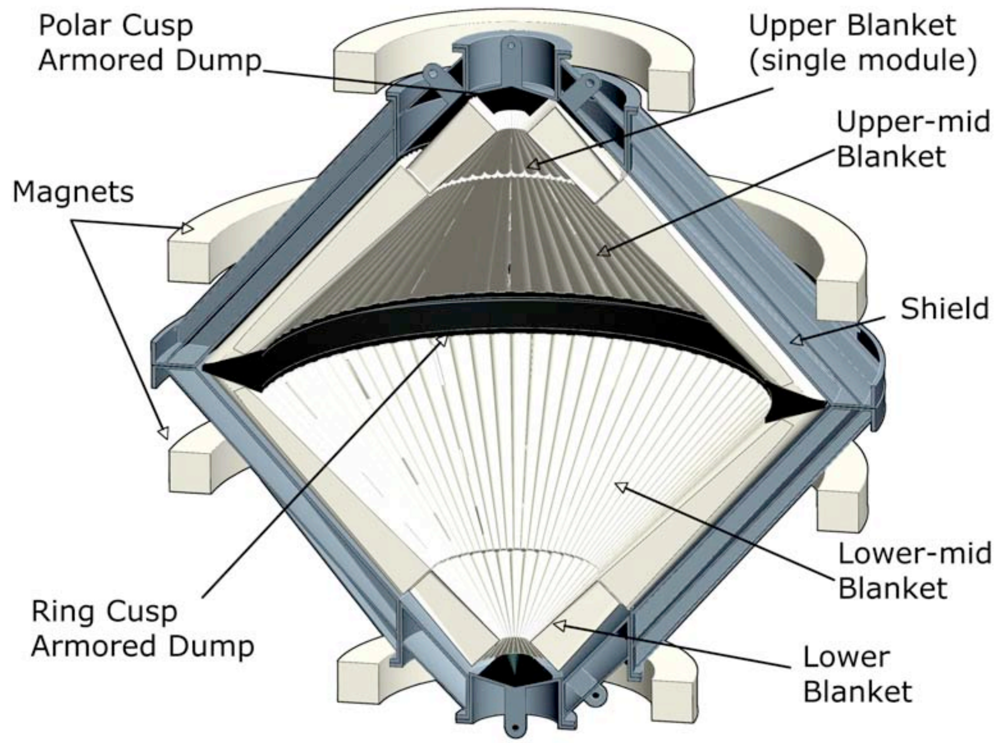

- **Preferred design includes an external vacuum vessel with maintenance performed from the top.**

Neutronics Analysis Indicates Acceptable Tritium Breeding and Blanket Module Lifetime

Angular Distribution of Neutron Wall Load in Chamber

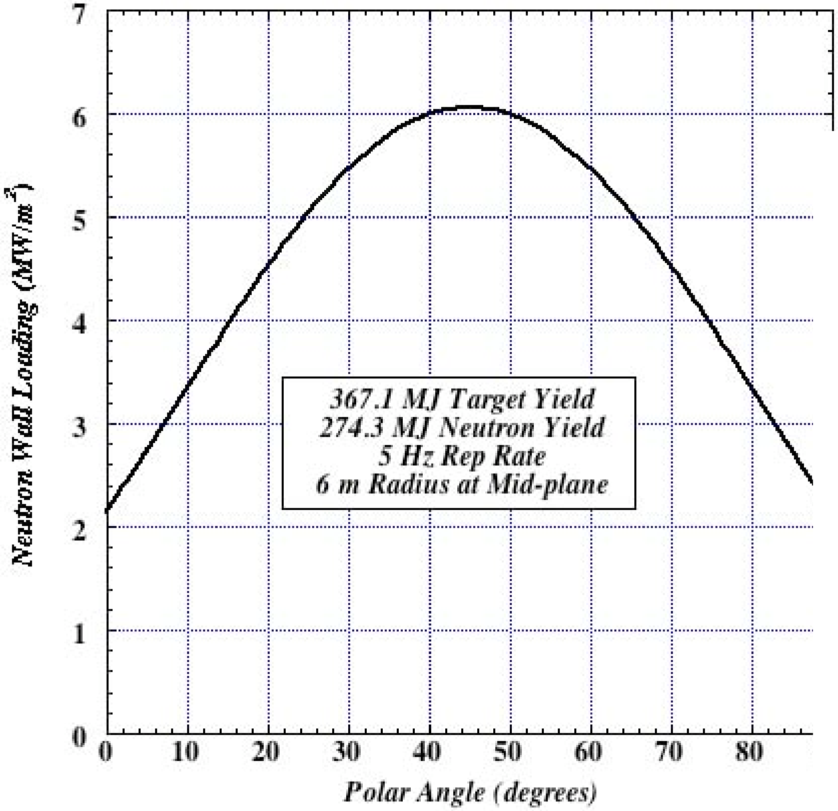

- Assuming a 3% burnup limit for SiC (corresponding to 260 dpa, 16,300 He appm, and 6,370 H appm), the blanket lifetime is 3.26 FPY .

Flexibility in setting TBR by adjusting ^{6}Li enrichment for different SiC$_f$/SiC FW thickness for Pb-17Li case

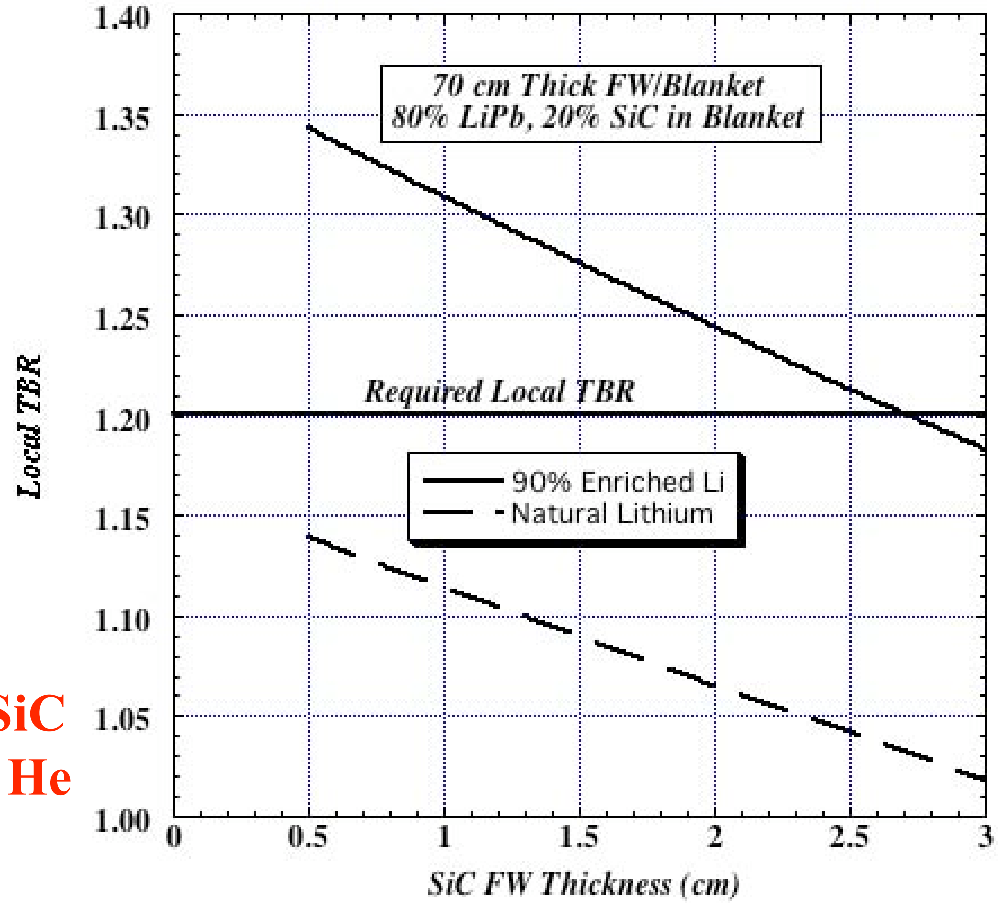

Self-Cooled Pb-17Li +SiC$_f$/SiC Blanket Optimized for High Cycle Efficiency

- **Simple annular submodule design builds on ARIES-AT concept.**
- **Pb-17Li flows in two-pass: first pass through the annular channel to cool the structure; and a slow second pass through the large inner channel where the Pb-17Li is self-heated.**
- **This allows for decoupling of the outlet Pb-17Li temperature from the maximum SiC$_f$/SiC temperature limit.**

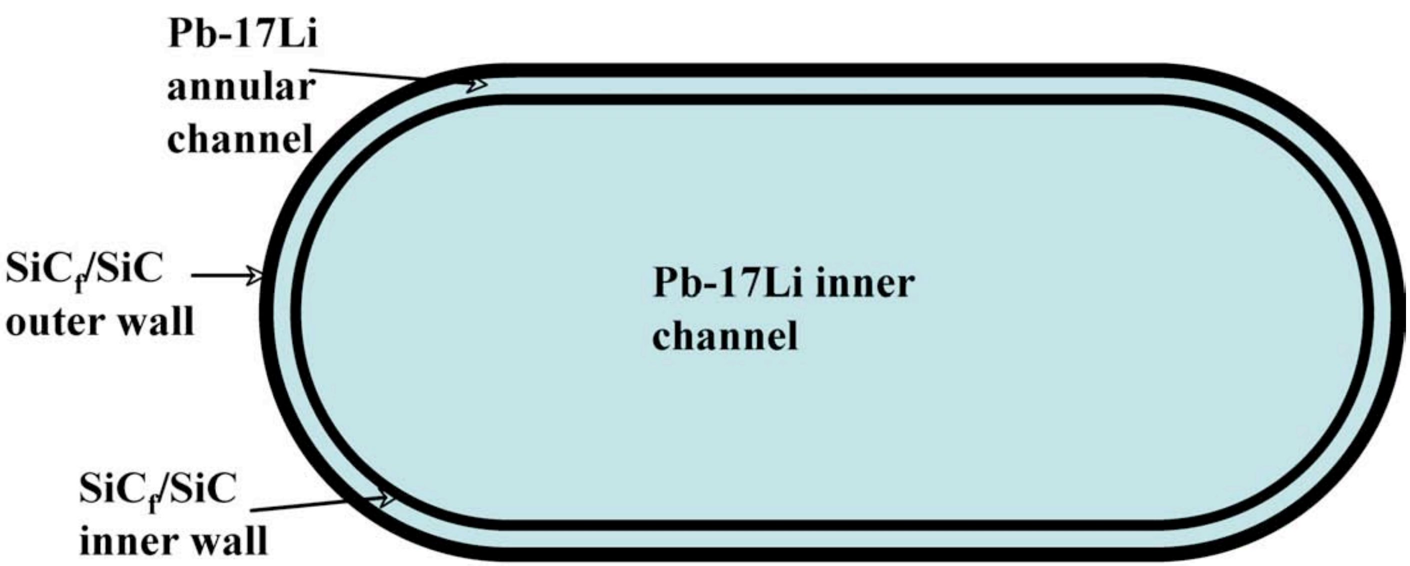

Submodule Configuration for Upper Mid-Blanket Region

- **Submodule cross-section changes because of conical geometry.**
- **Pb-17Li enters through annular channel at equator (C-C), turns at top (A-A), flows through inner channel and exits at A-A.**
- **5 submodules joined (e.g. by brazing) to form a modular unit for assembly and maintenance.**
- **Tight fit assembly so that all submodules are pressure-balanced by adjacent modules to avoid large stresses associated with long radial span (particularly at A-A).**

radial/toroidal dimensions:

A-A: 1.06/0.196 m

B-B: 0.88/0.33 m

C-C: 0.7/0.47 m

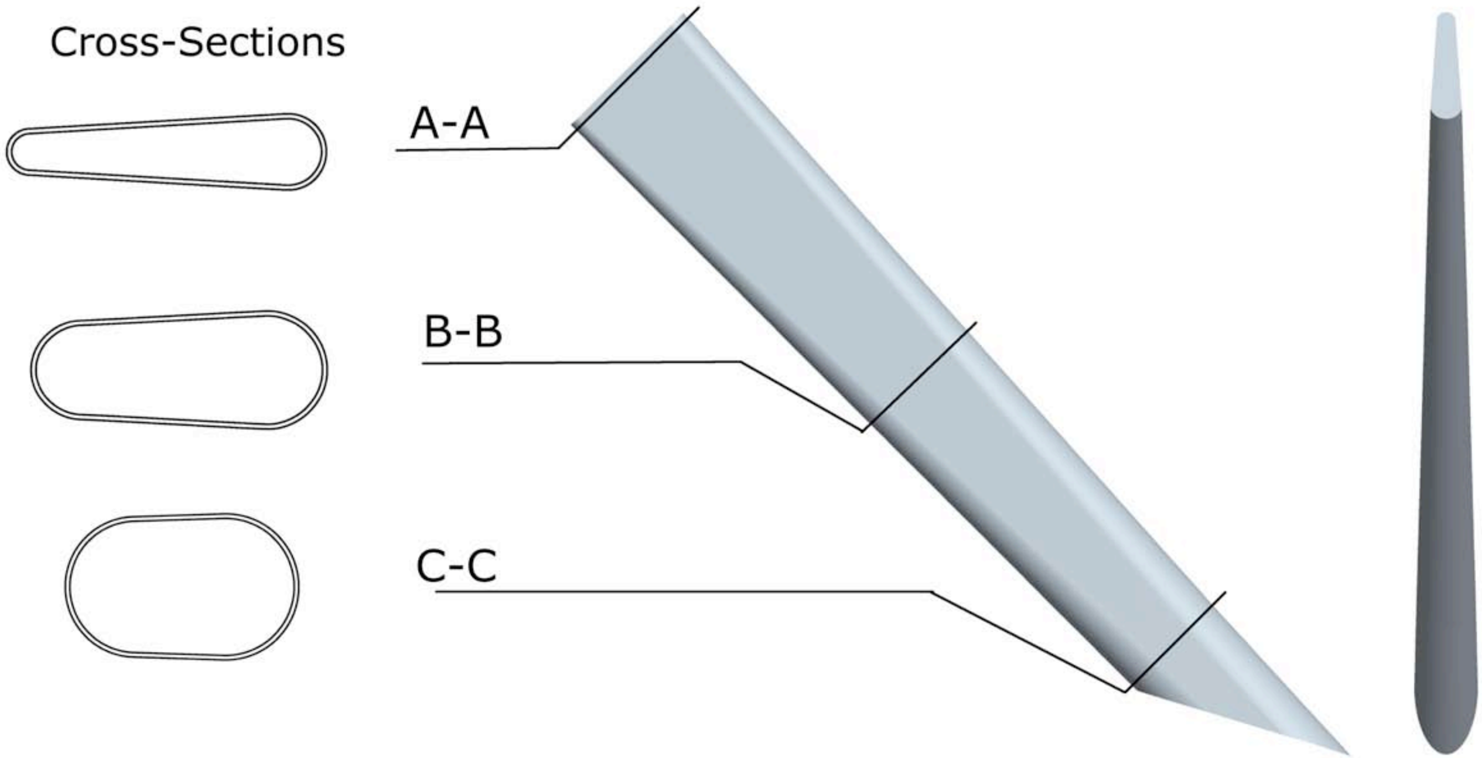

Submodules Shaped at Module End for Tight Fit Assembly and Pressure-Balancing of All Submodules

- **Concerns exist about the possible domino effect on all submodules in case of a catastrophic failure of a submodule.**

- **Possible solutions include isolating a limited number of modules by including structurally independent wedges and/or using pressure-sensitive valve system to drain and decompress the coolant in such an accident case.**

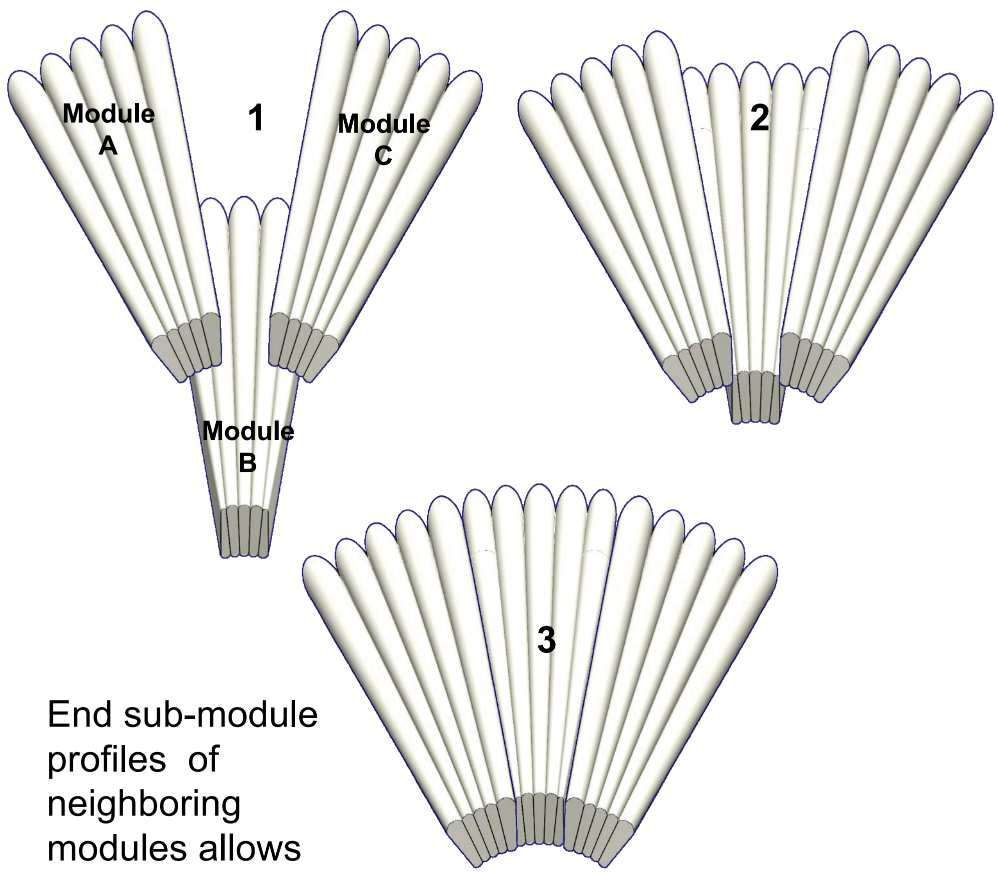

End sub-module profiles of neighboring modules allows natural fit

UC San Diego

2-D Stress Analysis of First Wall Performed with ANSYS

- At B-B, maximum heat loads: $q''=0.11\ MW/m^2$; $q_{SiC}''' = 31\ MW/m^3$.
- Pb-17Li pressure = 1 MPa (accounting for hydrostatic pressure ~0.33 MPa for ~4 m elevation, ΔP_{blkt} ~0.2 MPa and some margin).
- σ_{tot} increases sharply as the wall thickness is increased, indicating the dominating effect of the increasing $\sigma_{thermal}$ over the decreasing $\sigma_{pressure}$.
- For the present scoping design analysis, it seems reasonable to choose δ_{FW} ~5 mm; the corresponding σ_{tot} ~100 MPa for plane stress and ~230 MPa for plane strain , compared to an assumed limit of ~190 MPa for SiC_f/SiC.
- If more margin is needed in the future, a slightly thinner wall of larger chamber could be used.

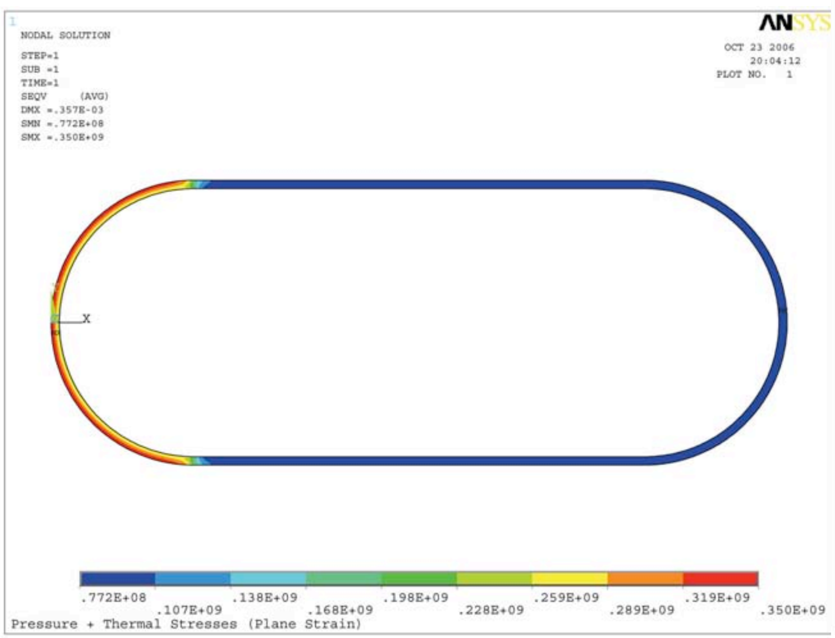

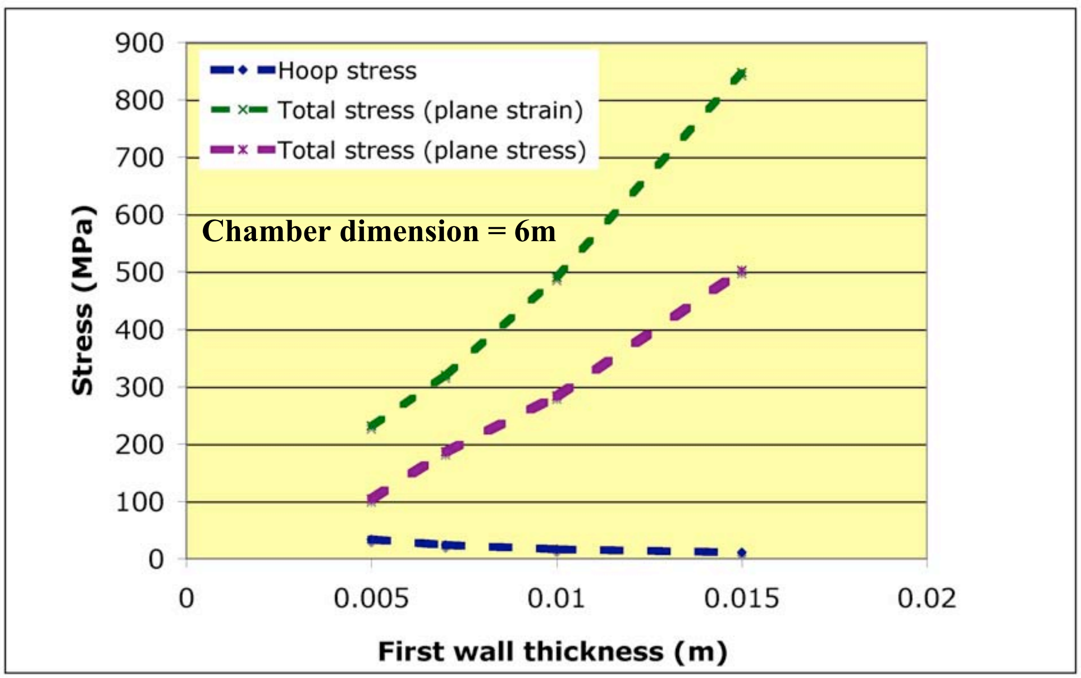

Possible Submodule Fabrication Method
(rectangular submodules shown for illustration)

Issue: Complex concentric walls prevent assembly of inner and outer channels

Solution: Expendable core form fabrication

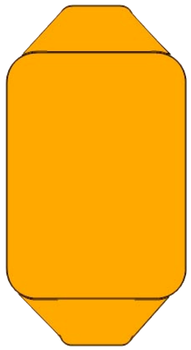

1. inner channel form

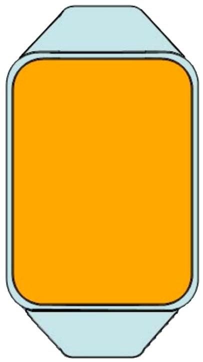

2. Lay-up & infiltrate inner channel

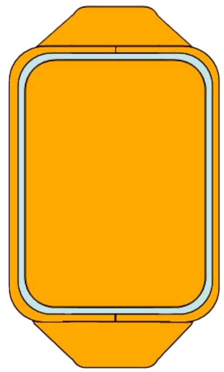

3. Two-piece form fitted over inner channel

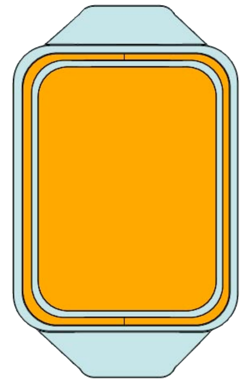

4. Lay-up & infiltrate outer channel

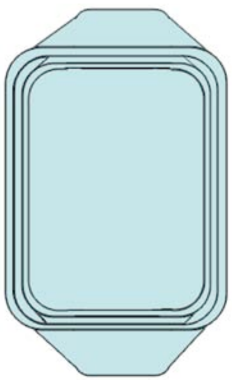

5. Consume both forms via chemical or thermal process

6. Braze end caps

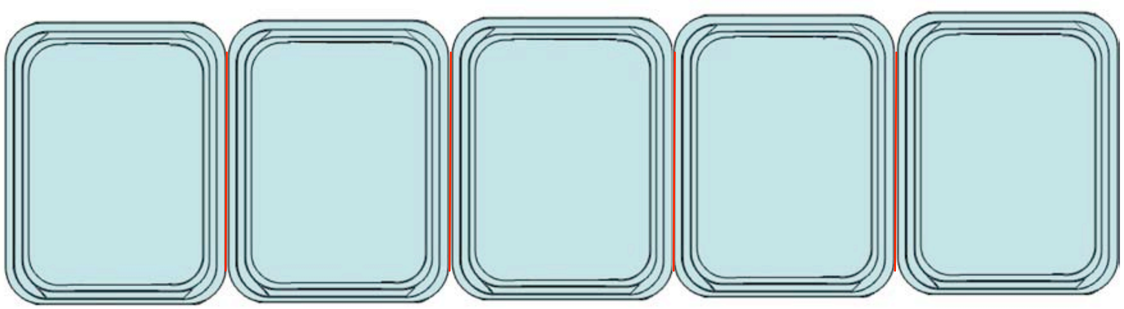

7. Braze 5 submodules together to form module

Self-Cooled Pb-17Li + SiC_f/SiC Blanket Coupled to a Brayton Cycle though a Pb-17Li/He HX

- 3 Compressor stages (with 2 intercoolers) + 1 turbine stage; $\Delta P/P \sim 0.05$; $1.5 < r_p < 3.5$
  - $\Delta T_{HX} \sim 30°C$
  - $\eta_{comp} = 0.89$
  - $\eta_{turb} = 0.93$
  - $\text{Effect.}_{recup} = 0.95$

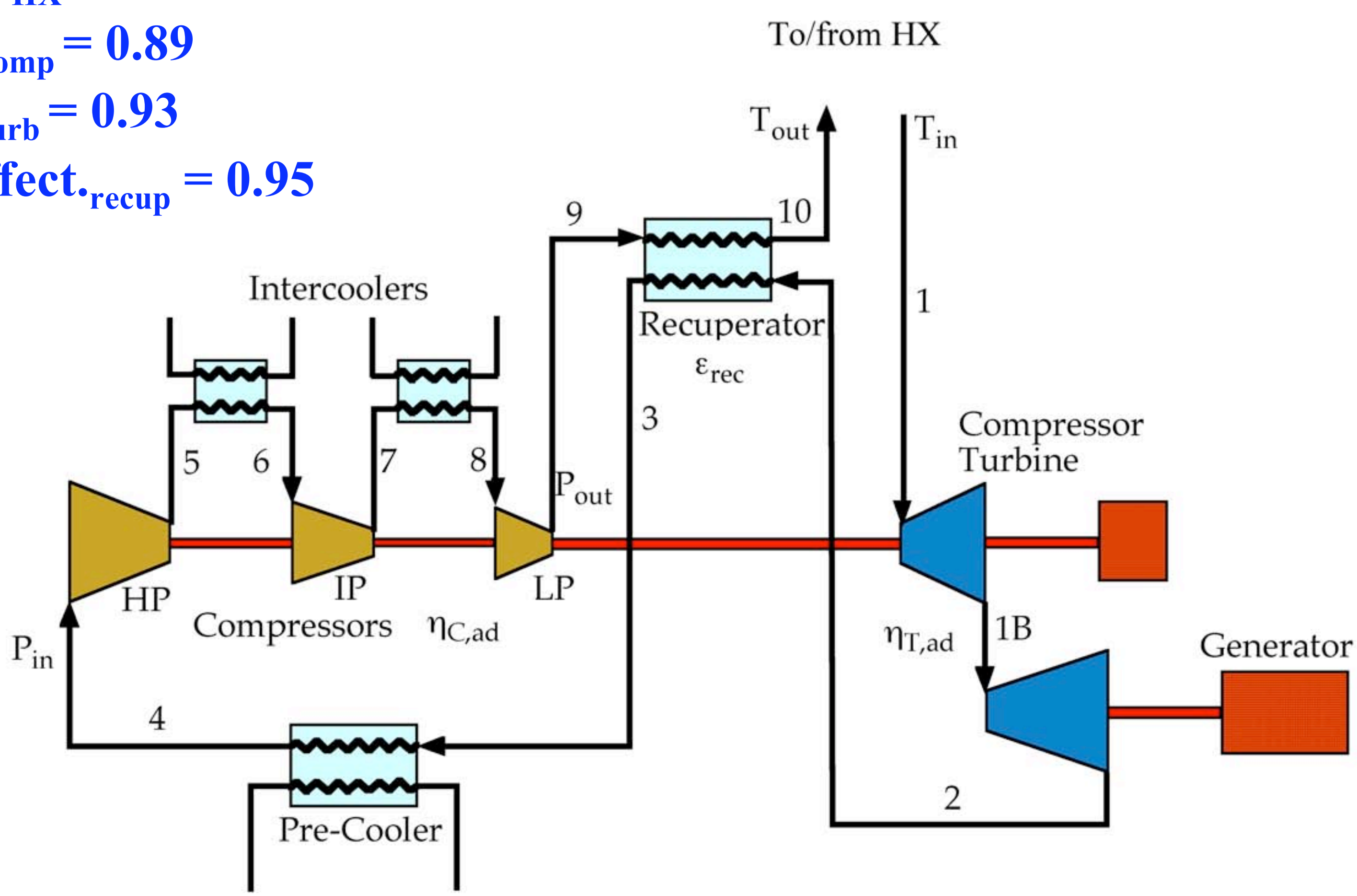

Thermal-Hydraulic Optimization Procedure

- **Set blanket design parameters.**
  - $SiC_f/SiC\ \delta_{FW}=0.5$ cm; $\delta_{annulus}=0.5$ cm
  - only the blanket length is adjusted based on the chamber size

- **Simple MHD assumption based on assumed 1 T field and flow laminarization with conduction only (probably conservative).**

- **For given chamber size and fusion power, calculate combination of inlet and outlet Pb-17Li temperatures that would maximize the cycle efficiency for given SiC_f/SiC temperature limit and/or Pb-17Li/SiC interface temperature limit.**
  - $SiC_f/SiC\ T_{max}<1000°C$
  - Pb-17Li/SiC $T_{max}<950°C$
  - Assume conservatively k=15 W/m-K for SiC_f/SiC

Target yield	367 MJ
Neutron/ion/photon energy partition	0.75/0.24/0.01
Rep rate	5
Fusion power	1837 MW
Energy multiplication factor	1.19
Total thermal power	2080 MW
Cone height/radius	6/6 m
Peak/avg. neutron wall load	6.1/4.3 MW/m^2
Peak power density in SiC	31 MW/m^3
Peak/avg. photon heat flux on first wall	0.11/0.08 MW/m^2

Brayton Cycle Efficiency as a Function of Cone-Shaped Chamber Size and Corresponding Outlet and Inlet Pb-17Li Temperatures

- **Pb-17Li/SiC T_{max} < 950°C is more constraining than SiC_f/SiC T_{max} <1000°C**
- **Both ΔP and P_{pump} show minima at a chamber dimension of 6 m corresponding to the largest ΔT between Pb-Li inlet and outlet temperatures (and lowest flow rate).**
- **For a 6 m chamber, Pb-17Li T_{out}~1125°C; $\eta_{Brayton}$ ~0.59**
- **Question about whether such a high Pb-17Li T_{out} can be handled in out of reactor annular piping and in heat exchanger.**

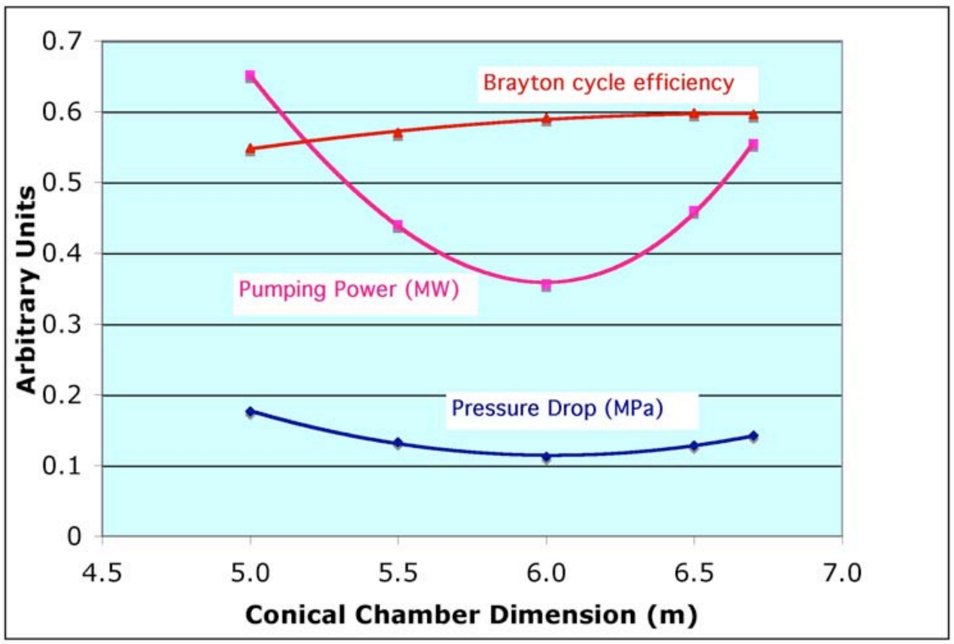

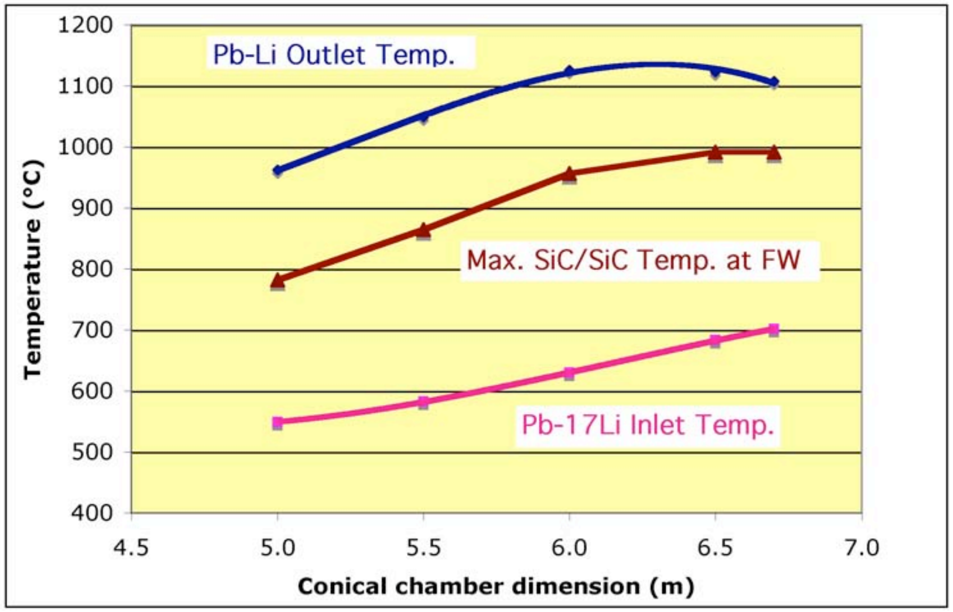

Effect of Varying the Pb-17Li/SiC Interface Temperature Limit

- **It is not clear what the allowable SiC/Pb-17Li T_{max} really is as it depends on a number of conditions.**
- **Earlier experimental results at ISPRA indicated no compatibility problems at 800°C, whereas more recent results indicate a higher limit.**
- **Decreasing the SiC/Pb-17Li T_{max} from 950°C to 800°C results in a marked reduction in cycle efficiency, from ~59% to ~50%.**
- **Interestingly, the pressure drop and pumping power minima correspond to an interface limit of 950°C, and both increase significantly as the interface temperature limit is decreased and an increased in flow rate is required.**

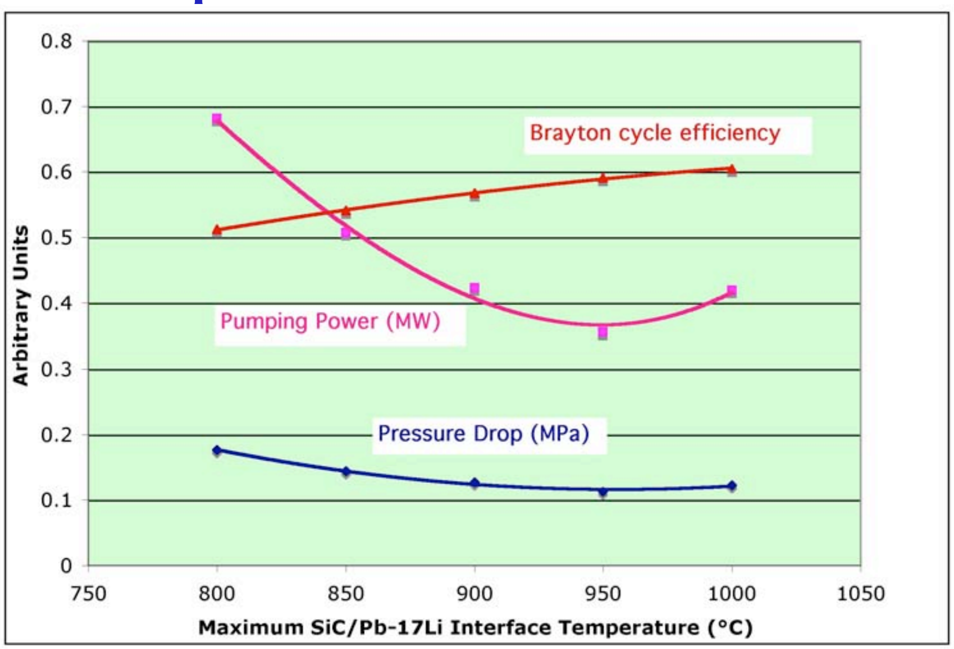

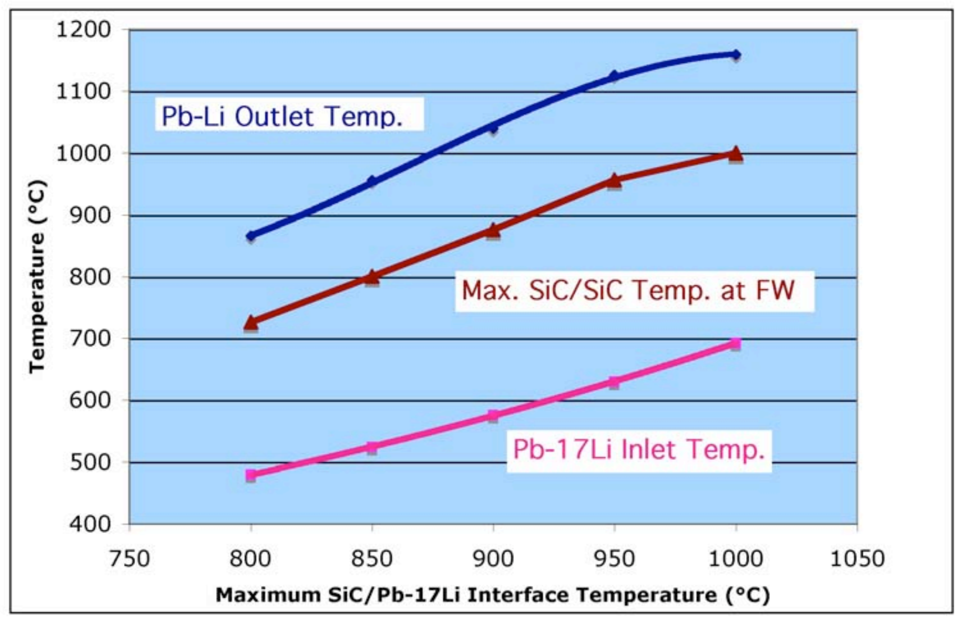

Adapting the Blanket for Flibe Requires a Be region for Tritium Breeding

- 1-1.5 cm Be region sufficient for TBR~1.1
- A Be plate can be included in the previous submodule design.
- Be also used for chemistry control of flibe.
- The flibe flows in two-pass: a first pass through the annular channel to cool the structure; and a slow second pass through the large inner channel where the flibe is self-heated.

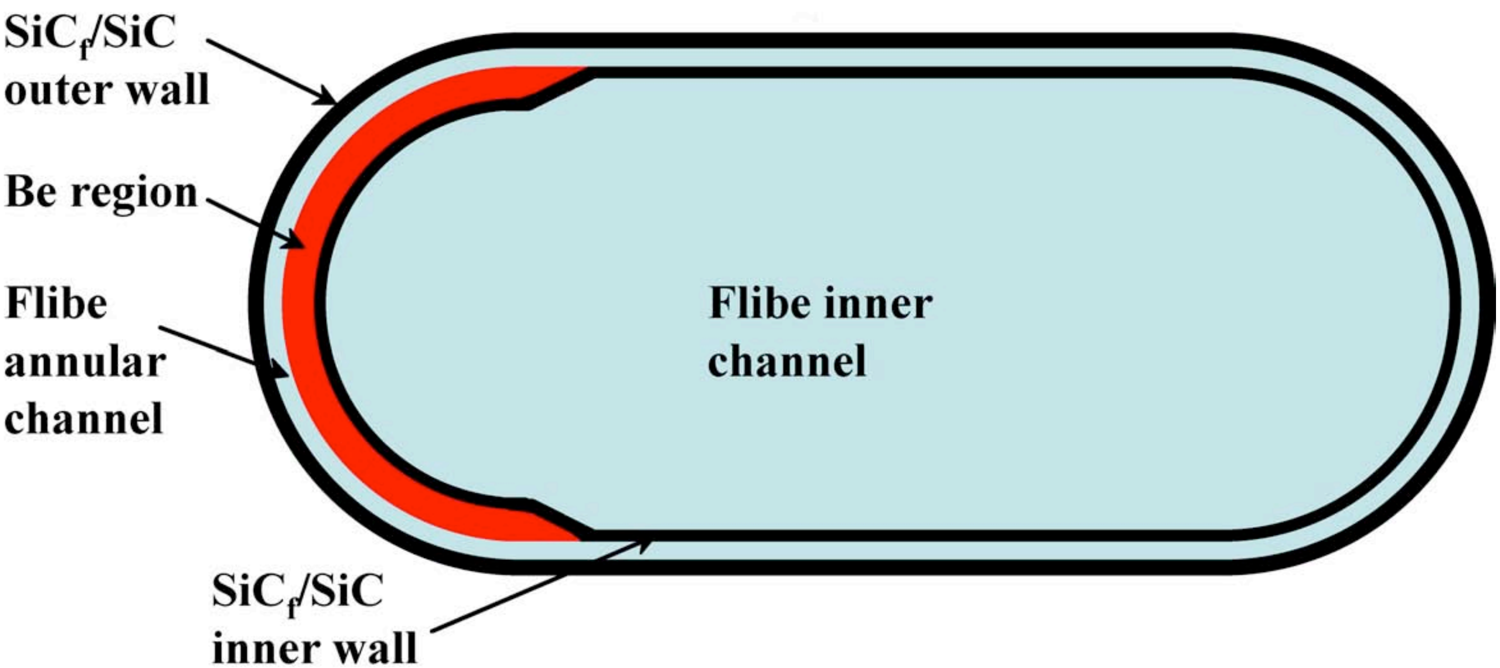

Effect of Varying the Flibe/SiC Interface Temperature Limit

- **Flibe T_{out} < Pb-17Li T_{out} mostly because of its poorer heat transfer properties.**

- **For 6 m conical chamber and 1000°C limit:**
  flibe Tin/Tout = 673/1000°C; Be T_{max} = 840 °C
  ΔP = 0.16 MPa; P_{pump} = 0.27 MW
  $\eta_{Brayton}$ = 0.57

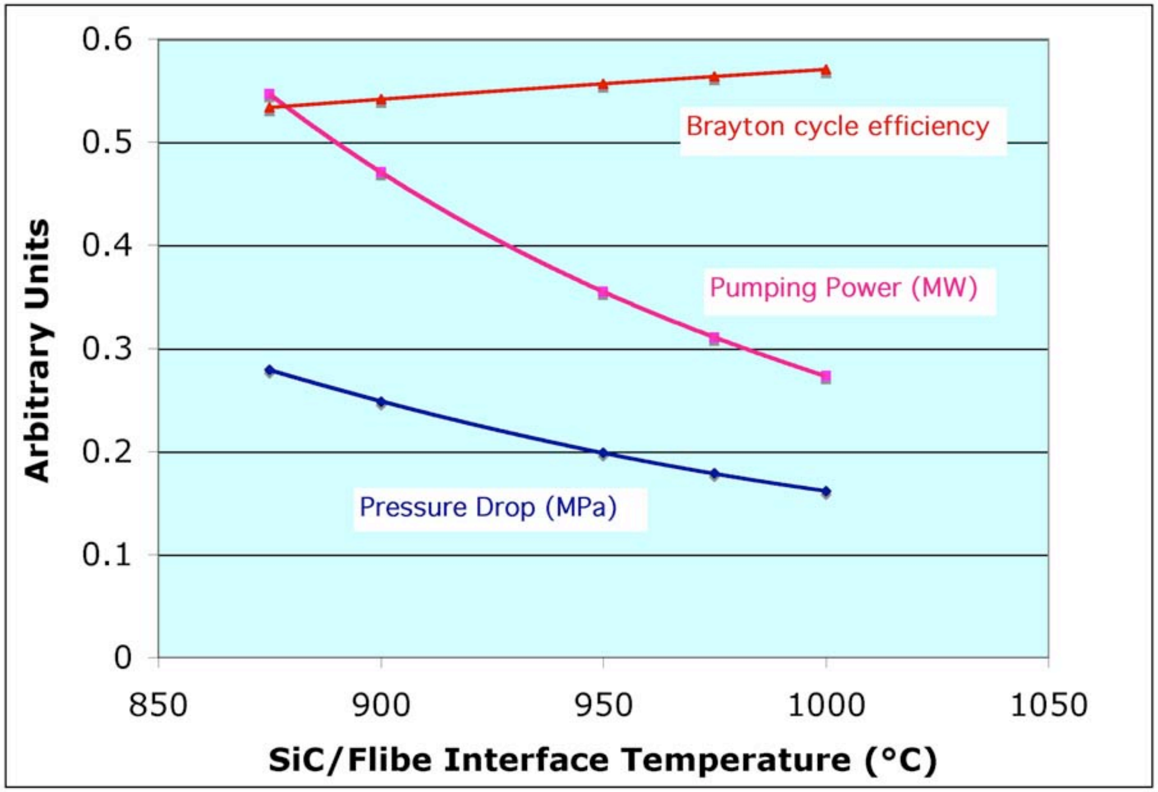

6 m chamber
SiC_f/SiC T_{max} < 1000°C:

UC San Diego

Summary

- A scoping design analysis has been performed of a self-cooled liquid breeder (Pb-17Li or flibe) + SiC_f/SiC blanket concept for use in the magnetic-intervention cone-shaped chamber geometry.
  - Simple geometry with ease of draining and accommodation of 40 rectangular laser ports with vertical aspect ratio .
  - Good performance, with the possibility of a cycle efficiency >50% depending on chamber size and SiC_f/SiC properties and temperature limits.
  - Submodule side walls are pressure-balanced; only the first wall and back wall are designed to accommodate the loads.
  - Must be noted that SiC_f/SiC is an advanced material requiring substantially more R&D than more conventional structural material (e.g. FS).
  - Submodule design can be adapted to flibe as breeder by adding a layer of Be to ensure a TBR of 1.1 and provide for chemistry control.
  - The high coolant temperatures result in high cycle efficiency and could also be used for H_2 production.
  - However, issues of what outside coolant tube and HX material(s) to use at these temperatures need to be further investigated.

UCRL-PRES-227874

Pressurized gas as a driver for Magnetized Target Fusion*

D.D. Ryutov
Lawrence Livermore National Laboratory, Livermore, CA 94551
Y.C. F. Thio
US Department of Energy, Germantown, MD 20874, USA

*(Presented at the ICC-07 Workshop, College Park, MD,
Skunkworks session, February 14, 2007)*

* Work performed for the U.S. DoE by UC LLNL under contract # W-7405-Eng-48.

THE SCOPE

• Magnetized Target Fusion (MTF) is a term designating a broad variety of approaches based on a unifying idea of adiabatic compression of a pre-formed magnetized β>1 plasma by a conducting liner

• MTF systems span a broad range of plasma parameters intermediate between magnetic confinement and inertial confinement

• We concentrate on a version of MTF that involves 3D implosions of a wall-confined plasma with the density in a compressed state ~ 10^{22} cm^{-3}, with energy in ~ 10-30 MJ and energy out ~ 300 MJ; the current ~ a few MA, current pulse-length ~ 5-10 μs.

*This fusion concept has a long history; a summary of the earlier work can be found in R.P. Drake, J.H. Hammer, C.W. Hartman, L.J. Perkins, D.D. Ryutov. "Submegajoule liner implosion of a closed field line configuration," Fusion Technology, **30**, 310, 1996.*

A variety of targets can be imploded in a 3D fashion by a liner of a varying thickness

Diffuse Z-pinch (toroidal field only)

FRC (poloidal field only)

Elongated spheromak (comparable toroidal and poloidal fields)

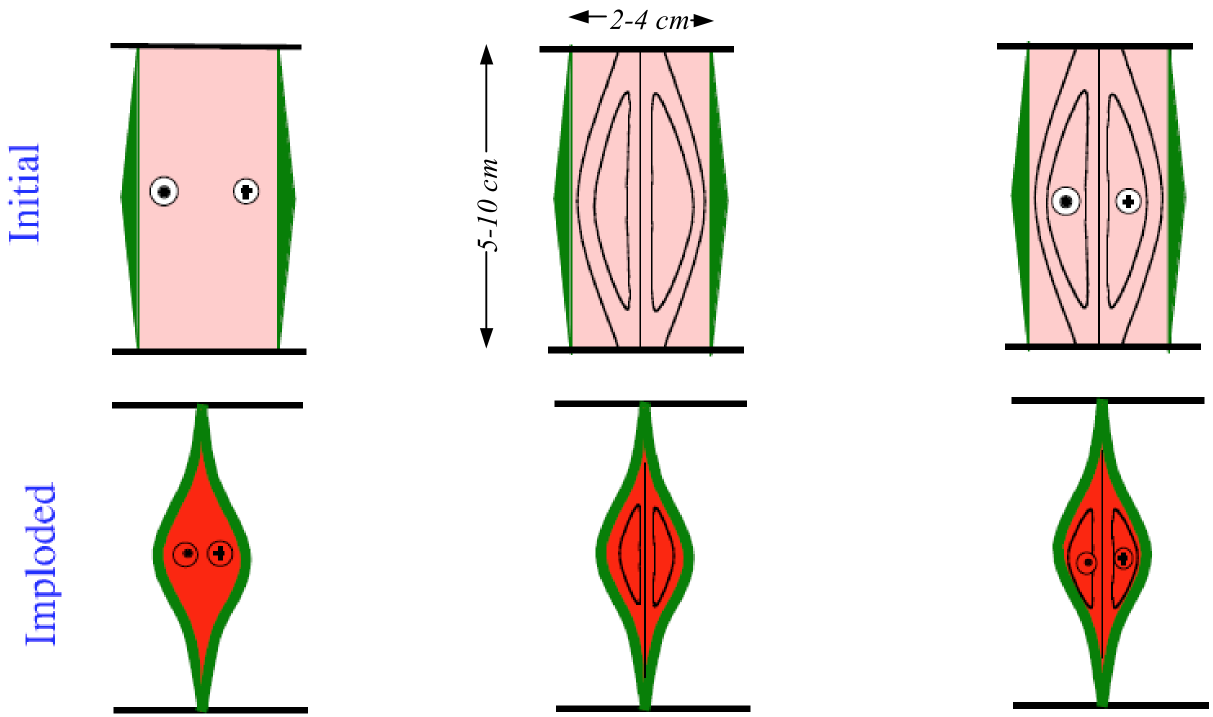

Initial configuration can be created *in situ*

FRC has to be created in a separate chamber and injected through a hole in the electrode (not shown)

Spheromak can be created in a "bubble-burst" fashion or *in situ*

We concentrate on a possible solution of the stand-off problem

An earlier work in this area:

Mechanical insertion of the target and disposable transmission line to a large chamber. (R.W. Moses, R.A. Krakowski, R.L. Miller. *"A conceptual design of the Fast-liner Reactor (FLR) for Fusion Power."* LANL report LA-7686-MS, February 1979)

Driving a magneto-cumulative generator by a fast projectile. (R.P. Drake, J.H. Hammer, C.W. Hartman, L.J. Perkins, D.D. Ryutov. *"Submegajoule liner implosion of a closed field line configuration,"* Fusion Technology, **30**, 310, 1996)

Delivering the current by a particle beam (inverse diode technique). (R.P. Drake, J.H. Hammer, C.W. Hartman, L.J. Perkins, D.D. Ryutov. *"Submegajoule liner implosion of a closed field line configuration,"* Fusion Technology, **30**, 310, 1996)

Using a set of converging, high Mach-number plasma jets. (Y.C.F. Thio, C.E. Knapp, R.C. Kirkpatrick, R.E. Siemon, P.J. Turchi. *"A physics exploratory experiment on plasma liner formation,"* J. Fusion Energy, **20**, 1, 2001; P.B. Parks, Y.C.F. Thio. *"The dynamics of Plasma Liners Formed by Merging of Supersonic Plasma Jets,"* Prepared for submittal to Phys. Plasmas)

Using a spherical liner made of high-Z plasma driven by subsonic thermal plasma. (D.D. Ryutov, Y.C.F. Thio. *"Plasma liner with an intermediate heavy shell and thermal pressure drive",* Fusion Sci. Technol., **49,** 39-55, 2006).

Using plasma streams as disposable electrodes. (D.D. Ryutov, Y.C.F. Thio. *"Solving the stand-off problem for Magnetized Target Fusion: plasma streams as disposable electrodes, together with a local spherical blanket."* Journal of Fusion Energy, http://dx.doi.org/10.1007/s10894-006-9050-5, 2006).

We consider the use of a pressurized gas as an energy source for MTF

This work is an extension of our previous studies of plasma liners

Pressurized gas has been considered earlier as a driver for liquid lithium liner in the LINUS concept (P.J. Turchi. *"A Compact-Toroid Fusion Reactor Design at 0.5 Megagauss, Based on Stabilized Liner Implosion Techniques,"* 3rd Int. Conf. on Megagauss Magn. Field, Novosibirsk, 1984, p.p.184-201)

This was a slow drive, ~ 1 ms time-scale

We consider a possibility of using the pressurized gas to drive the current pulse of ~ 10 μs duration suitable for the centimeter-size liner implosion in MTF

This is not an end-to-end analysis of a particular version of a fusion reactor, just some thoughts of pros and cons of a possible solution of the stand-off problem

The pressurized gas will be used to accelerate a heavy metal slug in a gas-gun configuration

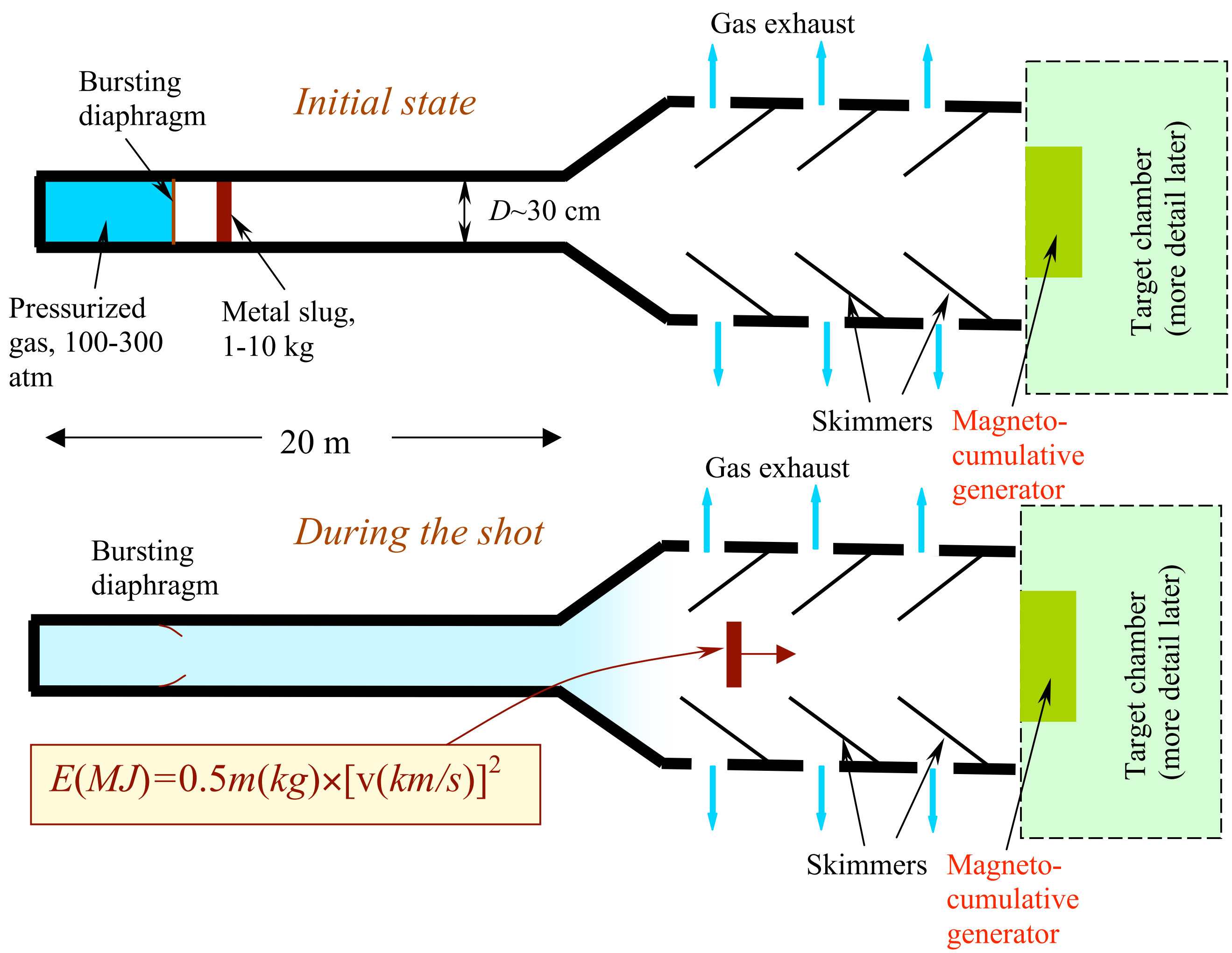

Accelerated slug will compress the bias magnetic field in the magneto-cumulative generator (MCG) and generate a 10-15 μs current pulse, suitable for driving the imploding liner.

A more detailed picture of a slug (expanded)

Using nitrogen (or even air) as a driving gas has a number of advantages:

Inexpensive

Relatively harmless

Can be exhausted back to the atmosphere
(after possible chemical cleaning and tests for the absence of radioactive substances)

Parameters of nitrogen

- Molecular weight M=28;
- Adiabatic index γ=7/5;
- Sound speed

$$s(m/s) = 350\sqrt{\frac{T(^oK)}{273}}$$

- Maximum expansion speed (very light slug)

$$\mathrm{v}_{\max} = \frac{2s}{\gamma - 1} = 5s$$

- Mass density $\rho(kg/m^3)=1.25\times p(atm)\times[273/T(^oK)]$
- Stored energy density $W(MJ/m^3) \approx 0.1\times p(atm)$

  W(MJ/kg)=0.082×[$T(^{o}\mathrm{K})$/273]

The performance would be significantly better for (a much more expensive) helium: higher slug velocities, higher efficiencies at the same pressure

Parameters of the acceleration system

- Acceleration efficiency η is determined by that the nitrogen gas has finite energy at the end of the pulse; it can be as low as ~ 0.5 for a properly chosen mass of the slug

- The achievable slug velocity: $v=0.5v_{max}=2.5s=0.875[T(K)/273]^{1/2}$ km/s (for a reasonable efficiency)

- Evaluate the gas volume: $V(m^3)\sim 10E(MJ)/\eta p(atm)$ [$V\sim 0.7$ m^3 for E=10 MJ, p=300 atm, η=0.5]

- The gun length ~ 10 m for the diameter ~ 30 cm.

- The achievable slug energy ($E=mv^2/2$):

  $E(MJ)=0.38m(kg)\times [T(^oK)/273]^{1/2}\sim 0.7$ m (kg) [a gas heated to ~ 500 ^{o}C].

- The slug parameters: r=15 cm, density ρ=10 g/cm^3, thickness h=2 cm (mass m=14 kg)

- Characteristic time of the energy delivery to MCG: ~ h/v=15 μs

A multistage magneto-cumulative generator would allow converting the slug energy into the energy of the current pulse*

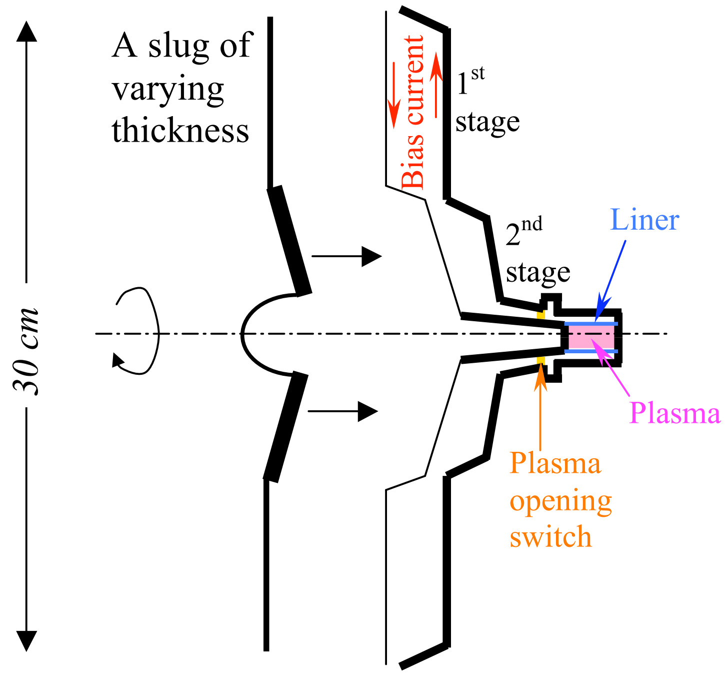

Additional opening switches can be used

Some parameters of MCG:

- Initial volume of the 1st stage 10 *l*
- Initial magnetic field 30 *kG*
- Initial volume of the second stage 3 *l*
- The magnetic field before the beginning of compression of the 2nd stage 150 kG
- The volume occupied by the magnetic field prior to the opening of POS 0.5 *l*
- The magnetic field 2 MG
- The pulse-width on the load 5 μs

---

* The MCGs have been a subject of detailed experimental and computational studies in 1980s-1990s; a lot of relevant information can be found in: J.H. Degnan, et al. Proc. 3rd Int. Conf. on Megagauss Magn. Field, Novosibirsk, 1984, p.p.352-358; C.M. Fowler, et al., ibid. p.p.282-291.

The magneto-cumulative generator can be built-in to the assembly that carries the MTF target and local spherical blanket.

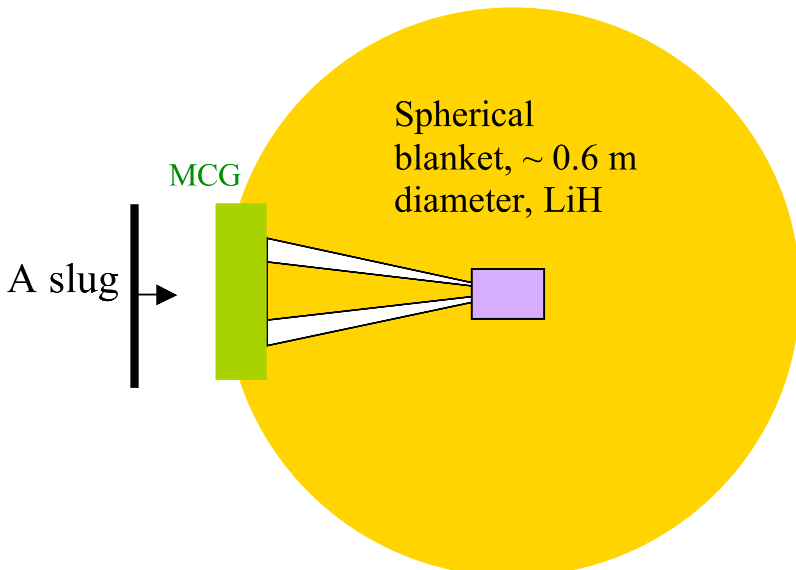

A local blanket (yellow) partly evaporated in every pulse. Breeds tritium and may beused as a working fluid (e.g., B.G. Logan. Fusion Engineering and Design, v. 22, p. 1953, 1993).

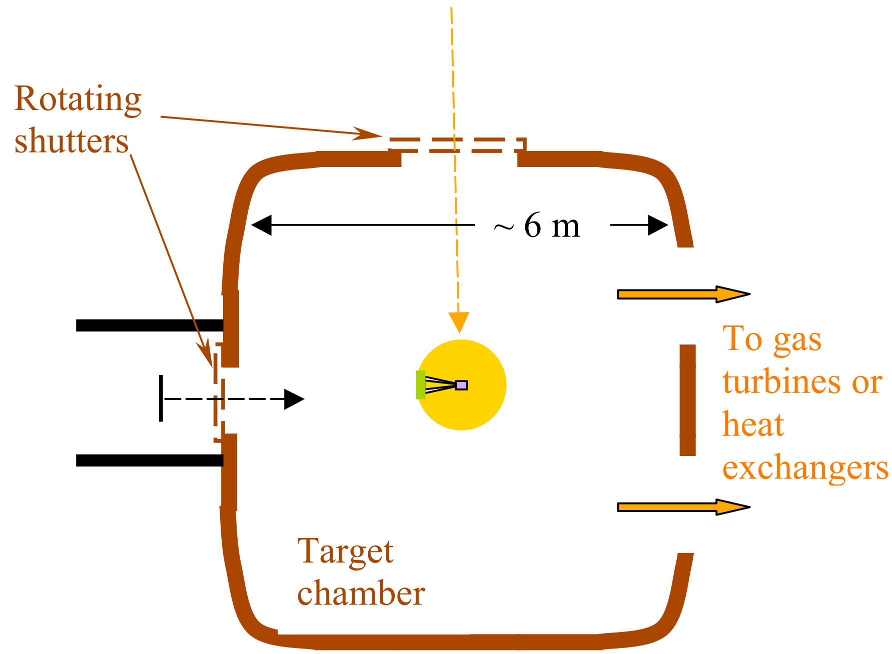

A possible general layout of a reaction chamber and a fast slug delivering energy to MCG (integrated with the spherical blanket)

SUMMARY

The pressurized nitrogen (helium) may become a simple and inexpensive energy source for MTF

Stored energy in the range of tens of megajoules is feasible for reasonable initial volumes

The metal slug with a mass of 10-30 kg can be accelerated to velocities ~ 1.5-2 km/s (2.5 – 3 km/s for helium) in a 20-m-long barrel

A hydrodynamic efficiency ~ 50% is feasible

Rep rate of a few Hz seems to be possible

Collision of a slug with a magneto-cumulative generator (MCG) can be used for converting its energy into the energy of a current pulse suitable for driving the MTF target

MCG can be integrated into the overall assembly that would be dropped into reaction chamber at a rate of a few Hz

Issues for the further analysis

Stable acceleration of a slug; possible use of a hydrodynamic stabilization

Preventing the evaporated blanket from bursting into acceleration/gas exhaust volume (rotating, non-vacuum-tight shutter followed by differential pumping system?)

The degree of contamination of the used driver gas

What happens to the slug? Can it melt (and evaporate) under the action of the neutron heating?

What techniques can be used for generating seed magnetic field in the MCG? Particle beams? Long-wavelength lasers? Disposable plasma electrodes?

Can the cost of every shot be made less than \$ 3 ?! (mass production?)

Three-Dimensional Nuclear Analysis for the Final Optics System of HAPL

Mohamed Sawan, Ahmad Ibrahim, Tim Bohm, Paul Wilson

Fusion Technology Institute - University of Wisconsin, Madison, WI

Baseline HAPL Optics Configuration with GIMM

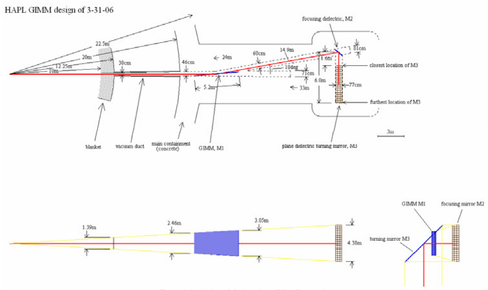

Provided by Malcolm McGeoch

Geometrical Model Used in 3-D Neutronics Analysis

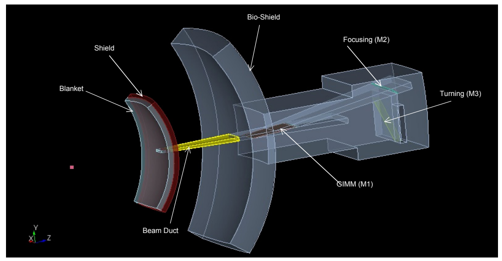

Fast Neutron Flux Distribution in Final Optics of HAPL

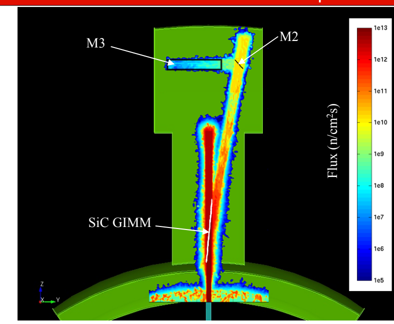

Objectives

- Determine nuclear environment at the GIMM (M1), focusing mirror (M2), and turning mirror (M3) final optics of HAPL
- Assess impact of GIMM design

Approach

- Used Monte Carlo code MCNPX-CGM with direct neutronics calculations in CAD model
- Continuous energy FENDL-2.1 nuclear data
- Modeled one beam with reflecting boundaries
- Neutron traps used behind GIMM and M2
- Two lightweight GIMM design options considered (SiC, AlBeMet)
- 1 cm thick Sapphire M2 and M3 mirrors
- Blanket/shield included in model
- Concrete containment building housing optics

Flux at Front Faceplate of GIMM

		Flux ($cm^{-2}.s^{-1}$)
SiC GIMM	Neutrons E>0.1 MeV	**1.39×10^{13}** (±2.1%)
	Total Neutrons	1.43×10^{13} (±2.1%)
	Total Gamma	1.57×10^{12} (± 5.5%)
AlBeMet GIMM	Neutrons E>0.1 MeV	1.21×10^{13} (±2.1%)
	Total Neutrons	1.30×10^{13} (±2.1%)
	Total Gamma	1.88×10^{12} (±4.4%)

Material choice and thickness slightly impacts peak flux in GIMM
Neutron spectrum softer for AlBeMet with 93% >0.1 MeV compared to 97% for SiC

Flux at Focusing Dielectric Mirror M2 Located @14.9 m from GIMM

		Flux ($cm^{-2}.s^{-1}$)	Fluence per full power year (cm^{-2})
SiC GIMM	Neutrons E>0.1 MeV	2.05×10^{10} (±4.0%)	6.46×10^{17}
	Total Neutrons	2.27×10^{10} (±4.0%)	7.15×10^{17}
	Total Gamma	0.88×10^{10} (±6.9%)	2.77×10^{17}
AlBeMet GIMM	Neutrons E>0.1 MeV	**3.18×10^{10}** (±3.9%)	**1.00×10^{18}**
	Total Neutrons	3.57×10^{10} (±3.8%)	1.12×10^{18}
	Total Gamma	1.35×10^{10} (±5.9%)	4.25×10^{17}

Neutron flux is a factor of ~1.6 higher with AlBeMet GIMM
Total neutron and gamma fluxes are more than two orders of magnitude lower than at GIMM
Neutron spectrum is hard with ~90% of neutrons @ E>0.1 MeV

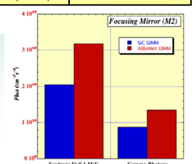

Peak Flux at Turning Mirror M3 Located @ 1.6-6 m from M2

		Peak Flux ($cm^{-2}.s^{-1}$)	Peak Fluence per full power year (cm^{-2})
SiC GIMM	Neutrons E>0.1 MeV	3.18×10^{8} (±7.3%)	1.00×10^{16}
	Total Neutrons	8.44×10^{8} (±8.2%)	2.66×10^{16}
	Total Gamma	7.51×10^{8} (±8.0%)	2.37×10^{16}
AlBeMet GIMM	Neutrons E>0.1 MeV	**5.14×10^{8}** (±7.6%)	**1.62×10^{16}**
	Total Neutrons	1.31×10^{9} (±8.8%)	4.13×10^{16}
	Total Gamma	1.01×10^{9} (±5.5%)	3.18×10^{16}

Neutron flux is a factor of ~1.6 higher with AlBeMet GIMM
Total neutron flux is about two orders of magnitude lower than at M2 with smaller gamma flux reduction
Neutron spectrum is softer with ~40% of neutrons @ E>0.1 MeV

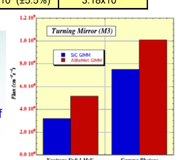

Peak Fast (E>0.1 MeV) Neutron Fluence per Full Power Year at Mirrors in Final Optics of HAPL

	Peak Fast Neutron Fluence per FPY (n/cm^2)	
	SiC GIMM	***AlBeMet GIMM***
GIMM (M1)	*4.38×10^{20}* (±2.1%)	*3.81×10^{20}* (±2.1%)
Focusing Mirror (M2)	*6.46×10^{17}* (±4.0%)	*1.00×10^{18}* (±3.9%)
Turning Mirror (M3)	*1.00×10^{16}* (±7.3%)	*1.62×10^{16}* (±7.6%)

The authors gratefully acknowledge the financial support of the HAPL program at the Naval Research Laboratory.

Findings and Conclusions

- 3-D neutronics calculation performed to determine nuclear environment in the HAPL final optics and compare impact of possible GIMM design options
- Neutron flux at dielectric mirrors is higher by a factor of ~1.6 with AlBeMet
- Neutron spectrum softens significantly at M3 (~40% >0.1 MeV vs. ~90% at M2)
- Peak fast (E>0.1 MeV) neutron fluence per FPY:
  - ***GIMM*** ***4.4×10^{20} n/cm²***
  - ***M2*** ***1.0×10^{18} n/cm²***
  - ***M3*** ***1.6×10^{16} n/cm²***
- Significant drop in nuclear environment occurs as one moves from the GIMM to dielectric focusing and turning mirrors
- Experimental data on radiation damage to metallic and dielectric mirrors are essential for accurate lifetime prediction
- For fluence limits of 10^{21} n/cm² (GIMM) and 10^{19} n/cm² (dielectric), expected GIMM lifetime is ~2 FPY, expected M2 lifetime is 10 FPY, and M3 is lifetime component

Modeling Ion Stopping for Warm Dense Matter Experiments

Peter Stoltz, Seth Veitzer
Tech-X Corporation, Boulder, CO

John Barnard
LLNL

Warm dense matter research can help answer important questions about EOS

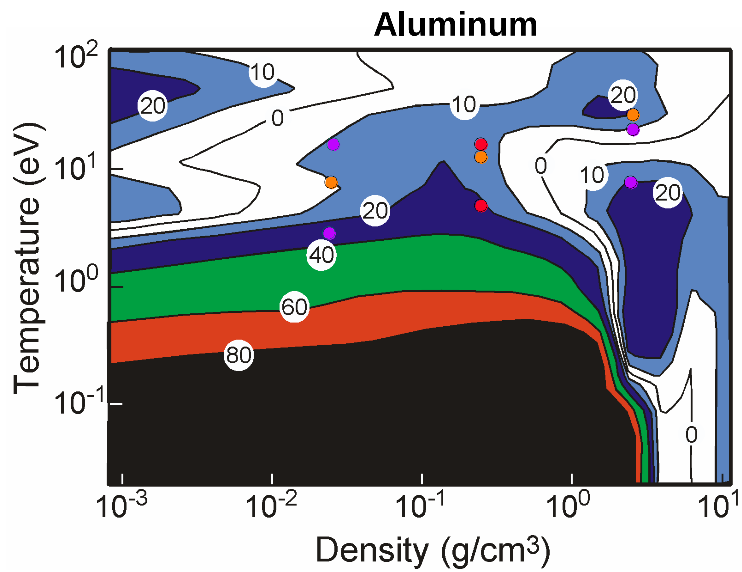

- Warm dense matter spans a regime that will help researchers distinguish between competing EOS models, but this requires accuracy (experiment or simulation) of a few percent

- The Hydra code is a well-benchmarked hydro code, but needs improved ion stopping to model ion driven WDM to the percent level

Ion beams can drive macroscopic targets to uniform temperatures for studying WDM states

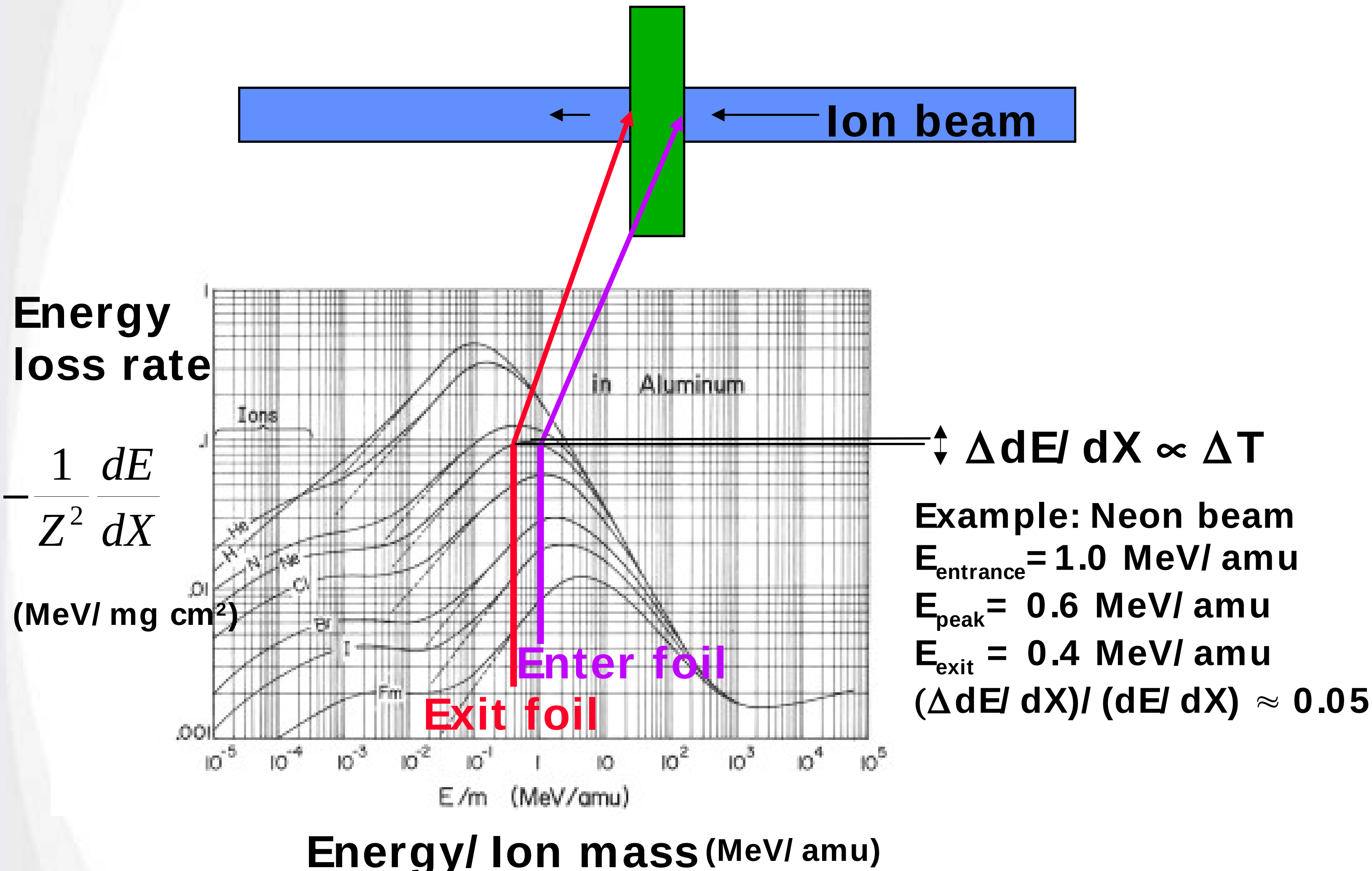

Tech-X and LBNL/LLNL collaborators are developing ion stopping models for WDM studies with the Hydra code

• Hydra will use TxPhysics, the new Tech-X algorithms

• Nuclear stopping in TxPhysics is an important new addition not presently available in Hydra

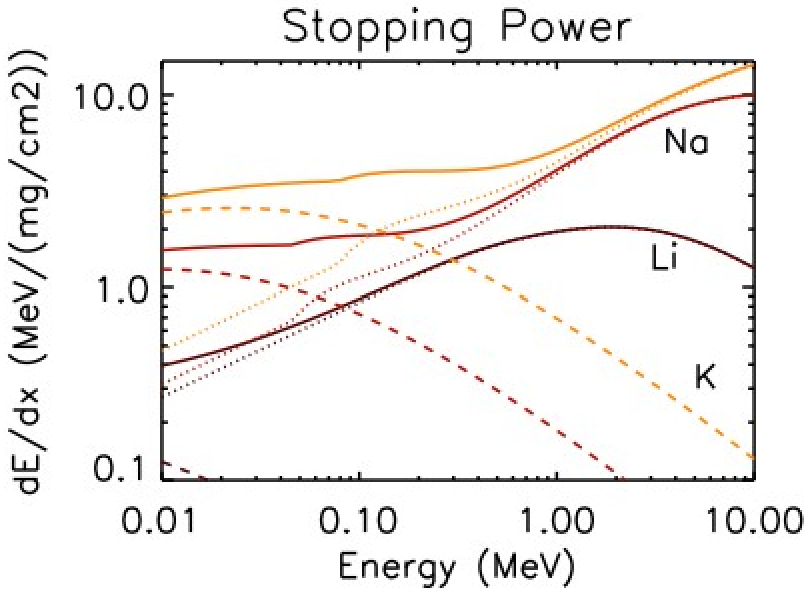

Dashed lines are nuclear stopping, dotted lines are electronic stopping, solid lines are total

SRIM and TxPhysics give the same result to within 10% for ions/targets relevant to WDM

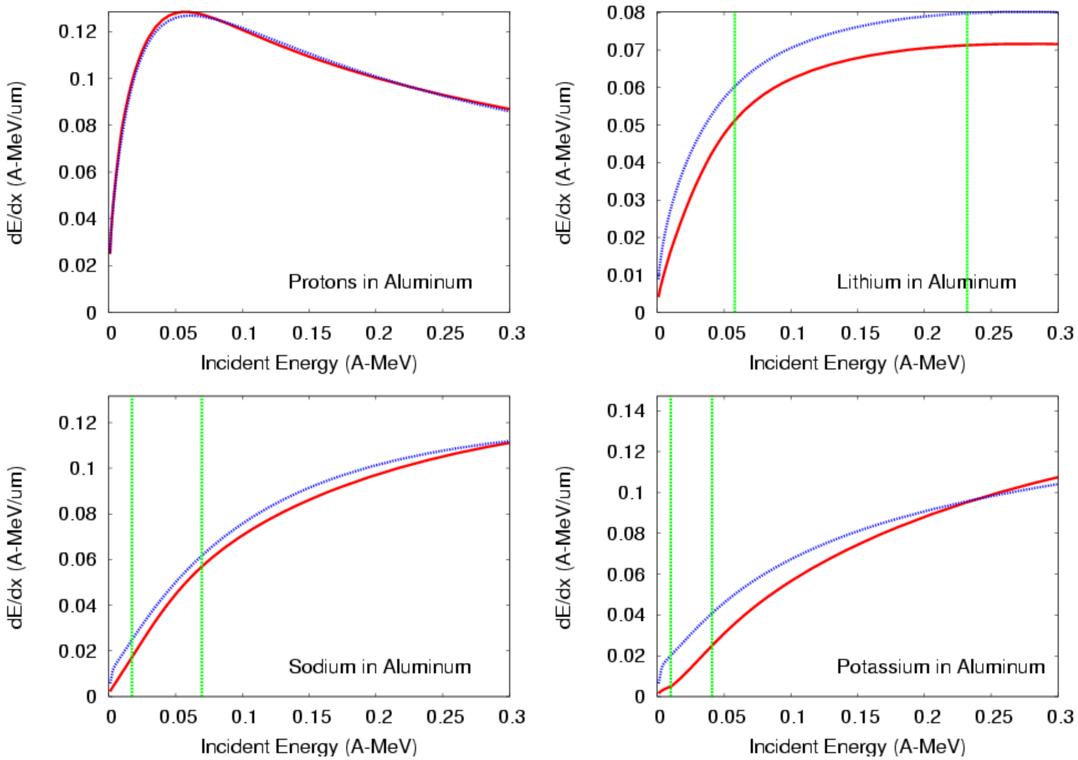

- Red is TxPhysics, blue is SRIM
- Green lines are 400 keV and 1.6 MeV (relevant to NDCX II)

With TxPhysics, user has access to ionization state, effective charge, etc, if needed

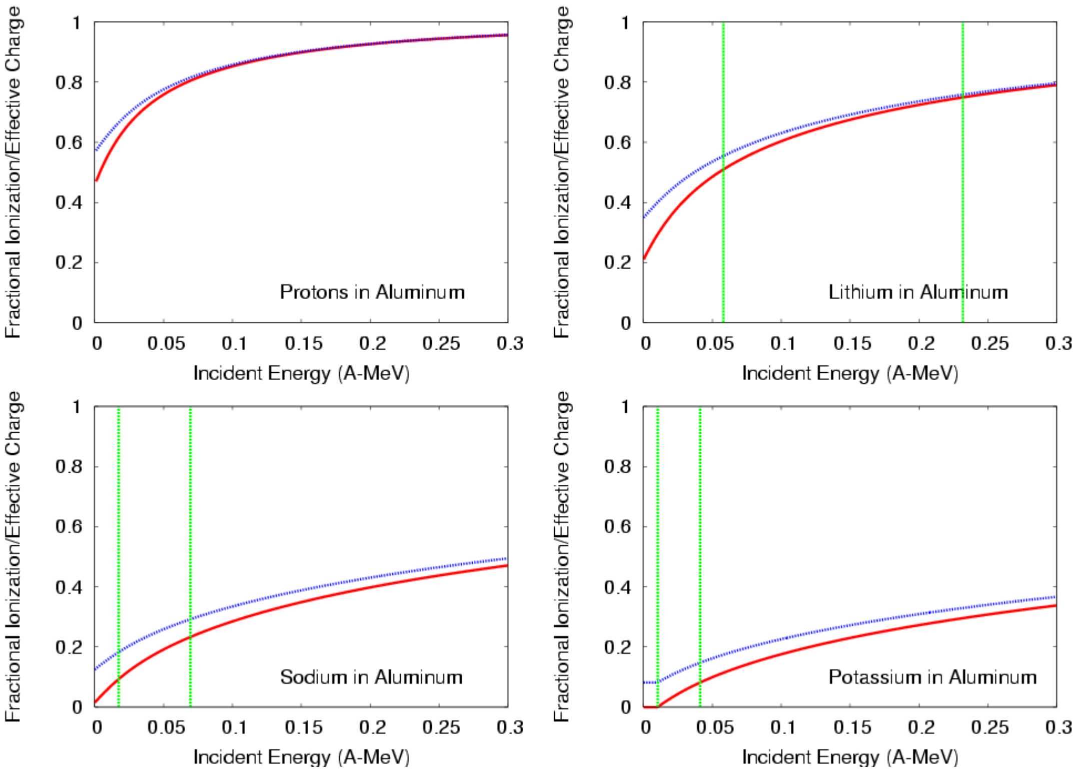

- Red is effective charge, blue is ionization state
- Green lines are 400 keV and 1.6 MeV

We have also implemented modifications for warm stopping based on Mehlhorn*

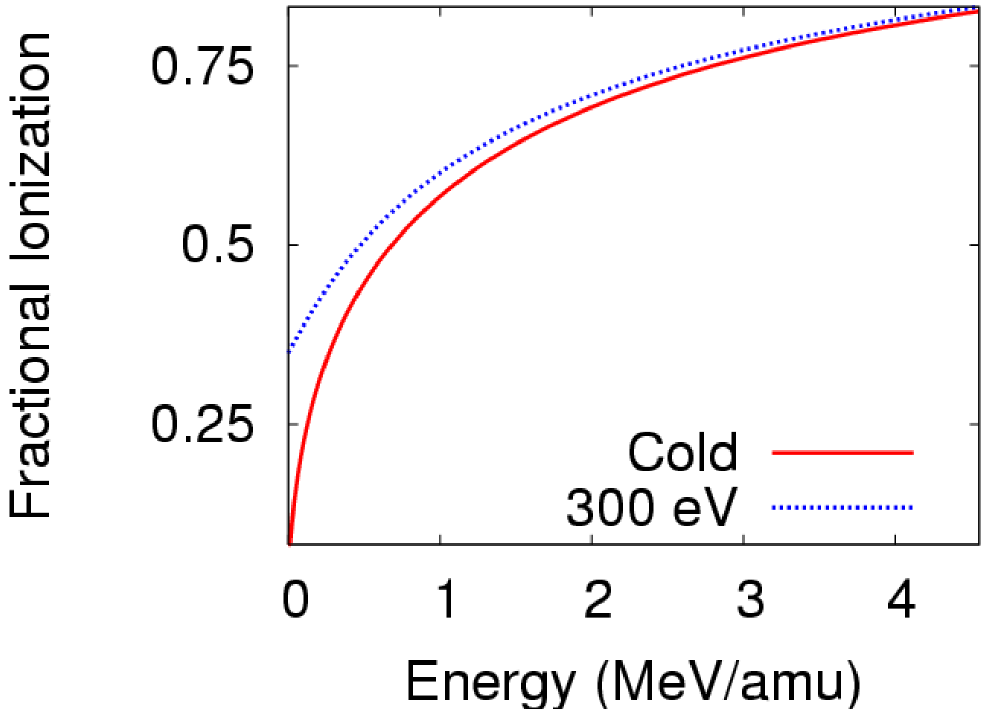

Projectile ionization as a function of velocity in a cold aluminum target (red) and a warm target (blue)

*MEHLHORN, T. (1981). A Finite Temperature Model For Ion Energy Deposition in Ion Driven Inertial Confinement Fusion Targets. J. Appl. Phys. 52, 6522

Simulation of Tungsten Surface Pores Formed by Low-Energy Helium Implantation

Akiyuki Takahashi[1], Shahram Sharafat[2], J. Kulcinski[3] and R. Radel[3], and Nasr Ghoniem[2]

[1]Tokyo University of Science, [2]University of California Los Angeles, [3]University of Wisconsin at Madison

1. Motivation

- Compelling experimental evidence: *Low energy He* ions implanted in W → unusual formation of oversized surface pores.
- The High Average Power Laser (*HAPL*) project is developing an IFE power with W-armored FW.
- Explain *UW-Madison IEC facility*, Low-E He implantation in W.
- Traditional *Rate-Theory* models are not suitable to simulate surface pore formation.
- New approach: Combine *KMC* techniques with Rate-Theory nucleation models.
- The new code: *MCMC*, which stands for Monte Carlo simulation of Migration and Coalescence.

Experimental Observations

730°C	990°C	1160°C
2.2×10^{15} He/cm²-s	8.8×10^{15} He/cm²-s	2.6×10^{16} He/cm²-s
30min	7.5min	2.5min

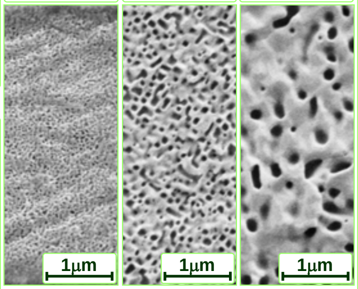

Implantation Rate & Surface Pore Size

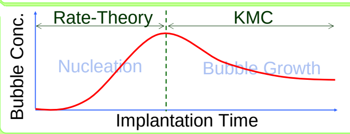

2. KMC Simulation Method

Possible events in the KMC simulation

1. He Implantation

$$\nu^{imp} = A\rho^{imp}$$

A: Surface area, ρ^{imp}: Implantation rate (He/cm²-s)

2. He Bubble Diffusion

$$D_b = \left(\frac{3\Omega^{4/3}}{2\pi r_i^4}\right) D_0 \exp\left(-\frac{E_s}{kT}\right)$$

Ω : Atomic volume, r_i: Bubble radius
D_0: Surface diffusion coe. ($10^{13}\delta^2/4$ /s)
E_s: Activation energy for surface diffusion(0.92 eV - 2.5 eV)

3. He Bubble Coalescence

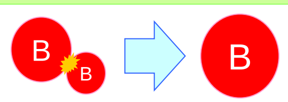

The bubble is immediately equilibrated

The bubble radius is determined by the equation of state.

4. Surface Pore Formation

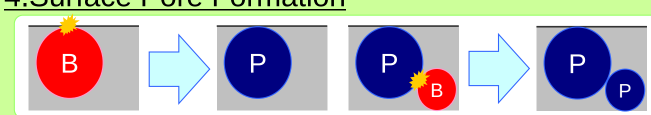

Note: He bubble nucleation saturates before M&C

3. Simulation Conditions

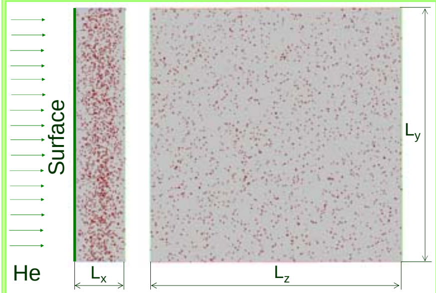

Bubble Density Evolution
HEROS Code (Rate Theory)

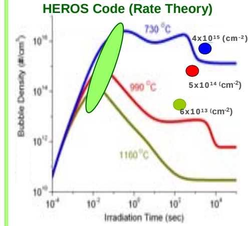

Helium bubble density in tungsten as a function of implantation time for E_{He} = 30 keV, fluence ~3×10^{22} He/m² (Filled symbols show experimental surface pore densities in cm⁻²).

1. Peak bubble nucleation densities are used as initial condition (taken from HEROS)
2. All He bubble diameters are initially same
3. The positions of He bubbles are given by a Gaussian distribution in the thickness (x) direction

	Temperature (°C)	Implantation Rate (He/cm²-s)	L_x (μm)	L_y (μm)	L_z (μm)
Model-1	730	2.2×10^{15}	0.2	1.0	1.0
Model-2	990	8.8×10^{15}	0.2	2.5	2.5
Model-3	1160	2.6×10^{16}	0.2	5.0	5.0

4. Evolution of He Bubbles and Pores

Snapshots of Model-1 (● : He bubble ● : Pore)

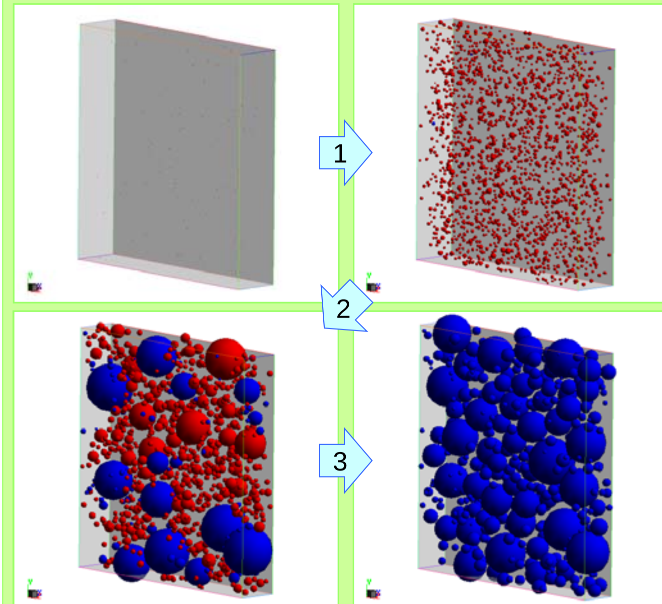

1. Growth of He bubbles (0-40 sec)
2. Surface pore formations (40-160 sec)
3. Only surface pores (160-1800 sec)

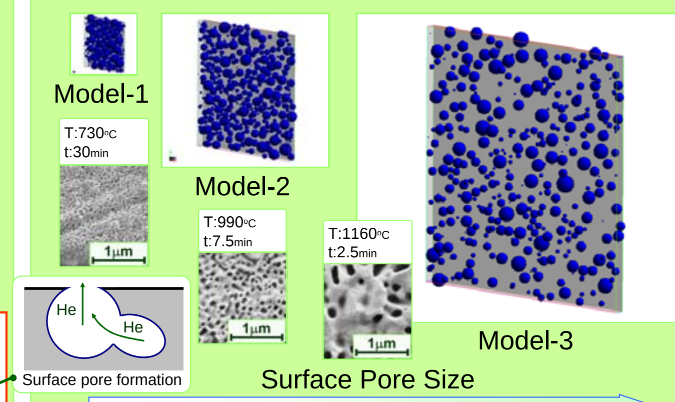

5. Comparison with Experimental Results

MCMC Results: Evolution of Average Surface Pore Diameter

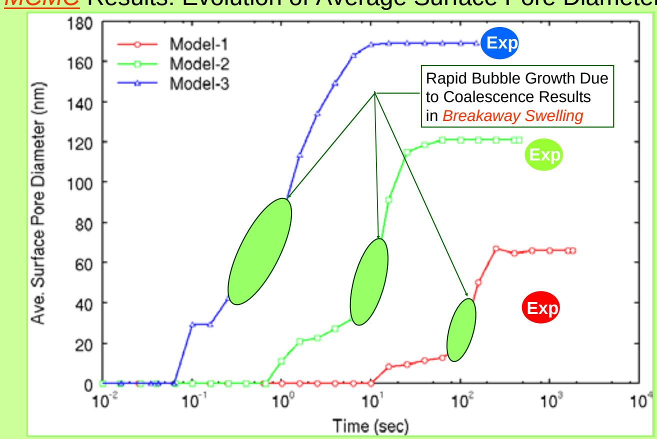

CONCLUSIONS:

- **Good Agreement between RT-KMC Simulation and Experiment**
- **Low Temperature Simulation Results are Lower than Data because T<0.3 T_m**
- ***MCMC* Code provides an *EXPLANATION* for the oversized Surface Pores**
- ***MCMC* Code development is continuing: *Pore THREADING***

High Velocity Dense Plasma Jets for MTF

F. Douglas Witherspoon, Andrew Case, Sarah J. Messer
Michael W. Phillips, Richard Bomgardner, David van Doren

HyperV Technologies Corp.
13935 Willard Road
Chantilly, VA 20151
703-378-4882

Poster presented at:

IFE Science & Technology Strategic Planning Workshop
San Ramon, California

April 24-27, 2007

High Velocity Dense Plasma Jets for MTF*

F. Douglas Witherspoon, Andrew Case, Sarah J. Messer,
Michael W. Phillips, Richard Bomgardner. David van Doren
HyperV Technologies Corp., Chantilly, VA

High velocity plasma jets are under development for a number of applications. The initial motivation for this line of research was Magneto-Inertial Fusion using high density, high velocity plasma jets as standoff drivers. Additional applications include reactor feuling, injection of angular momentum into centrifugally confined plasmas, HEDP, and others. The approach utilizes symmetrical pulsed injection of very high density plasma into the breech of a coaxial EM accelerator having a tailored cross-section geometry to prevent formation of the blow-by instability. Key to this approach is the mini-injectors used to produce the initial working plasma. We are following two parallel development paths to accomplish this initial injection. One uses a large number (ultimately up to 64) of electrothermal capillary discharges, while the second uses an even larger number of sparkgaps arranged in a toroidal configuration. Experiments are performed on two test fixtures; one is a 2pi configuration with 64 capillary injectors, and the second is a sparkgap array, which currently has 50 sparkgaps, but which is soon to be expanded to 112 in a new accelerator being fabricated using the sparkgap approach. Diagnostics used include Rogowski coils, Nikon D70s digital camera, a fast gated PI-Max camera, (which allows imaging of the plasma jets and their subsequent merging/interaction), and time resolved spectroscopy. Recent tests with a simple ballistic pendulum suggest the present half-scale prototype device is generating plasma jets with mass as high as 160 micrograms at 70 km/s.

*Research funded by the DOE Office of Fusion Energy Science through Grants DE-FG02-04ER83978, DE-FG02-05ER54810, DE-FG02-05ER84189

Plasma Liner Driven HEDLP and MIF

- Plasma liner provides an avenue for solving three major issues
  - Standoff delivery of imploding momentum
  - Repetitive operation
  - Liner fabrication and cost
- It is capable of faster compression if faster compression is desired
- It can form strongly coupled plasmas
- Remote current drive by lasers or particle beams is possible
- Diagnostics opportunities: Provide clear view of both the liner and the target, thus enhances the diagnostics access

Slide courtesy of F. Thio

Merging of high Mach number plasma (dusty plasma) jets to form plasma (microns) liners

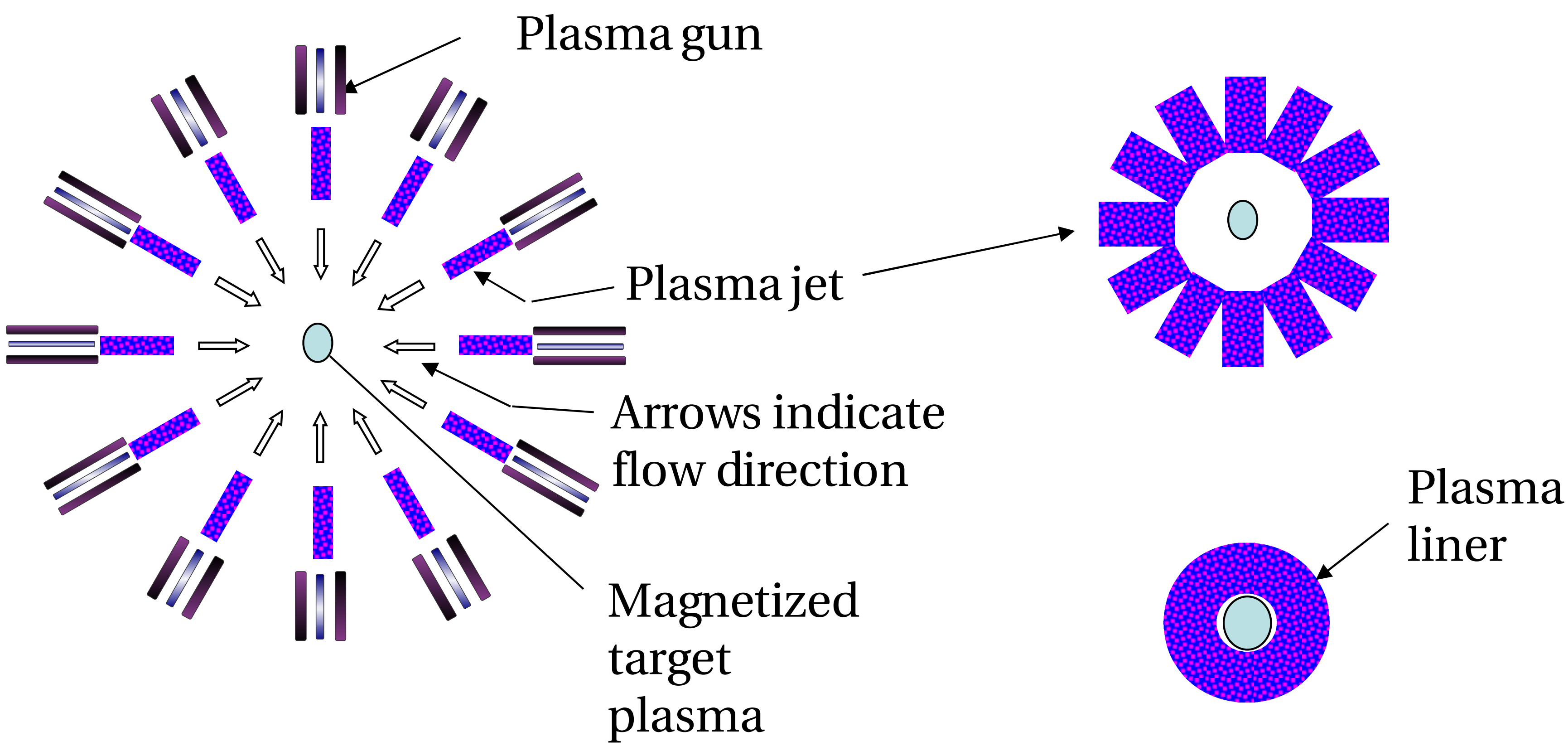

- An approximately spherical distribution of jets are launched towards a common center
- The jets merge to form a spheroidal shell (liner), imploding towards the center

Slide courtesy of F. Thio

TECHNICAL OBJECTIVE

Develop high density, high velocity plasma jets with:

$> 200\ km/s$ $> 100\ \mu g$ $10^{16} - 10^{17}\ cm^{-3}$ $> Mach\ 10$

TECHNICAL APPROACH

Refine Coaxial Plasma Accelerator Basic technology requires refinement and modification to provide additional controls over plasma macrodynamics.

Tailored Electrode Profiles To suppress blowby instability

High Density Electrothermal Plasma Injection using pulsed capillary discharges.

- Injection velocities of 10-20 km/s readily attainable
- Densities of 10^{19} cm^{-3} in capillary possible
- High degree of annular symmetry using large number of small pulsed jets
- Capillary discharge technology is relatively robust

Extensive Diagnostics and Computational Modeling

The Blowby Instability Limits Performance of a Classical Straight Coaxial Accelerator

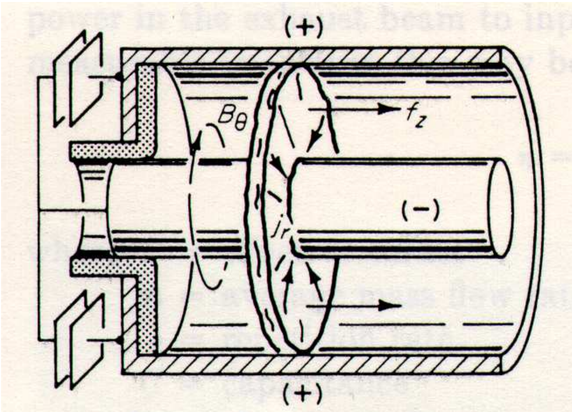

*From R.G. Jahn, "Physics of Electric Propulsion," 1st ed., New York, McGraw-Hill, 1968.

The classical straight coaxial accelerator* can attain the velocity needed (i.e. 200 km/s) but has difficulty accelerating all the mass due to occurrence of the blow-by instability which can bypass much of the plasma mass.

- $B = 1/r$
- higher $\vec{j} \times \vec{B}$ near inner electrode
- current distribution "runs away" leaving mass behind
- need to peak density profile near inner electrode

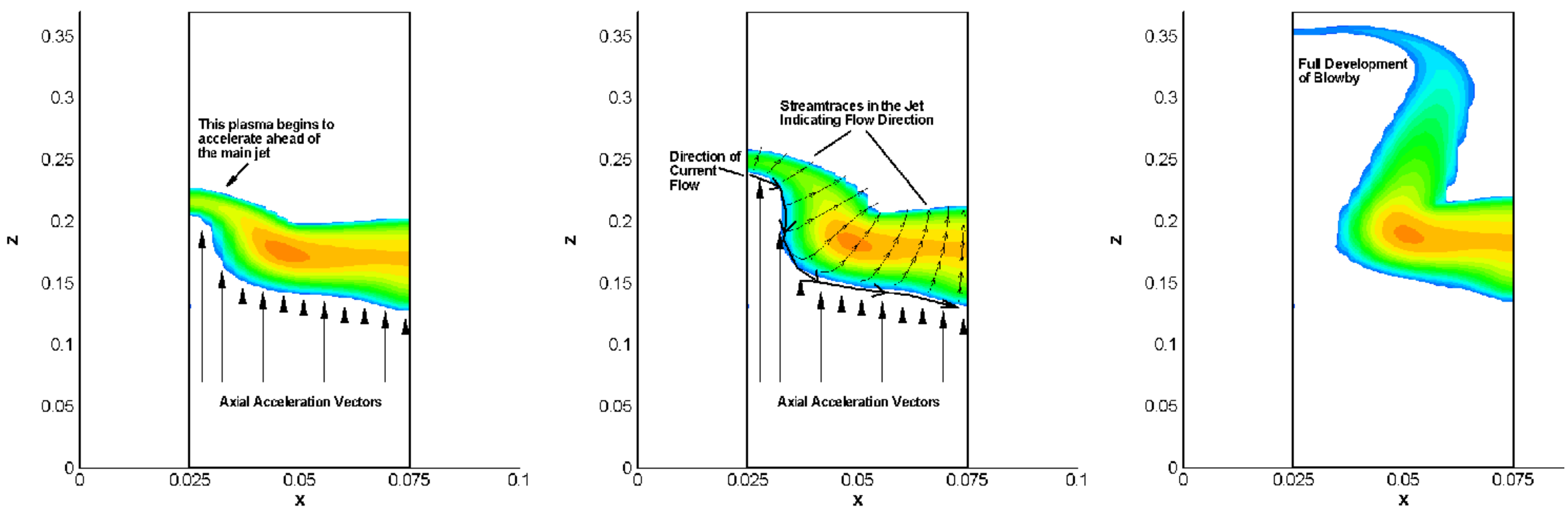

Mass density contour plots illustrate the blow-by instability in a straight coaxial accelerator. From Cassibry's PhD Dissertation referenced below.

Thio Suggested A New Methodology*

- No prefill is used. Operate at high vacuum. Any plasma to be accelerated is to be injected impulsively and nearly fully ionized with an initially high electrical conductivity. Electrothermal discharges were good possibilities.
- The main body of the plasma is sufficiently collisional so that the plasma behaves more like a fluid, to suppress the rich but undesirable particle kinetic effects.
- Taper the coaxial electrodes to provide some degree of macrodynamic control.

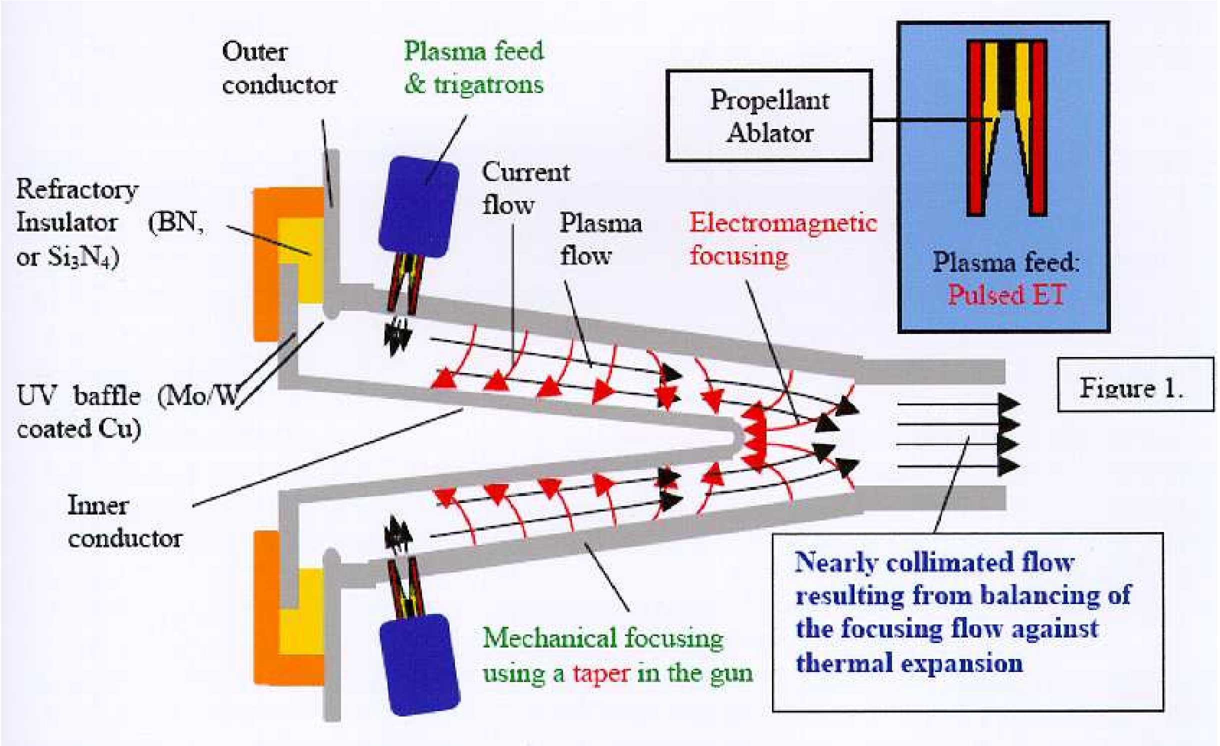

Cassibry and Thio also investigated exponentially tapered electrode profiles with encouraging results.**

*Y.C.F. Thio, J.T. Cassibry, and T.E. Markusic, "Pulsed Electromagnetic Acceleration of Plasmas," AIAA Joint Prop. Conf., Indianapolis, IN, July, 2002. Paper AIAA-2002-3803. **J.T. Cassibry, Numerical Modeling Studies of a Coaxial Plasma Accelerator as Standoff Driver for Magnetized Target Fusion, PhD Dissertation, University of Alabama in Huntsville, 2004.

Electrode Profile Tailoring Promises Greater Control of Plasma Macrodynamics

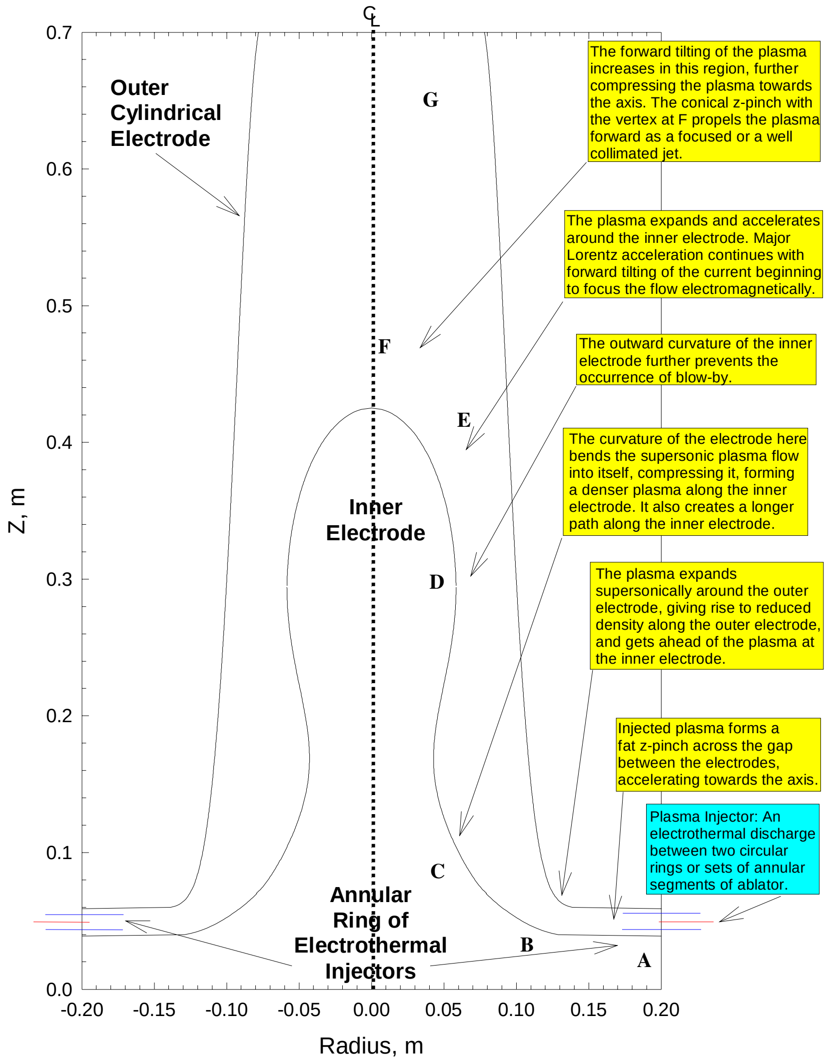

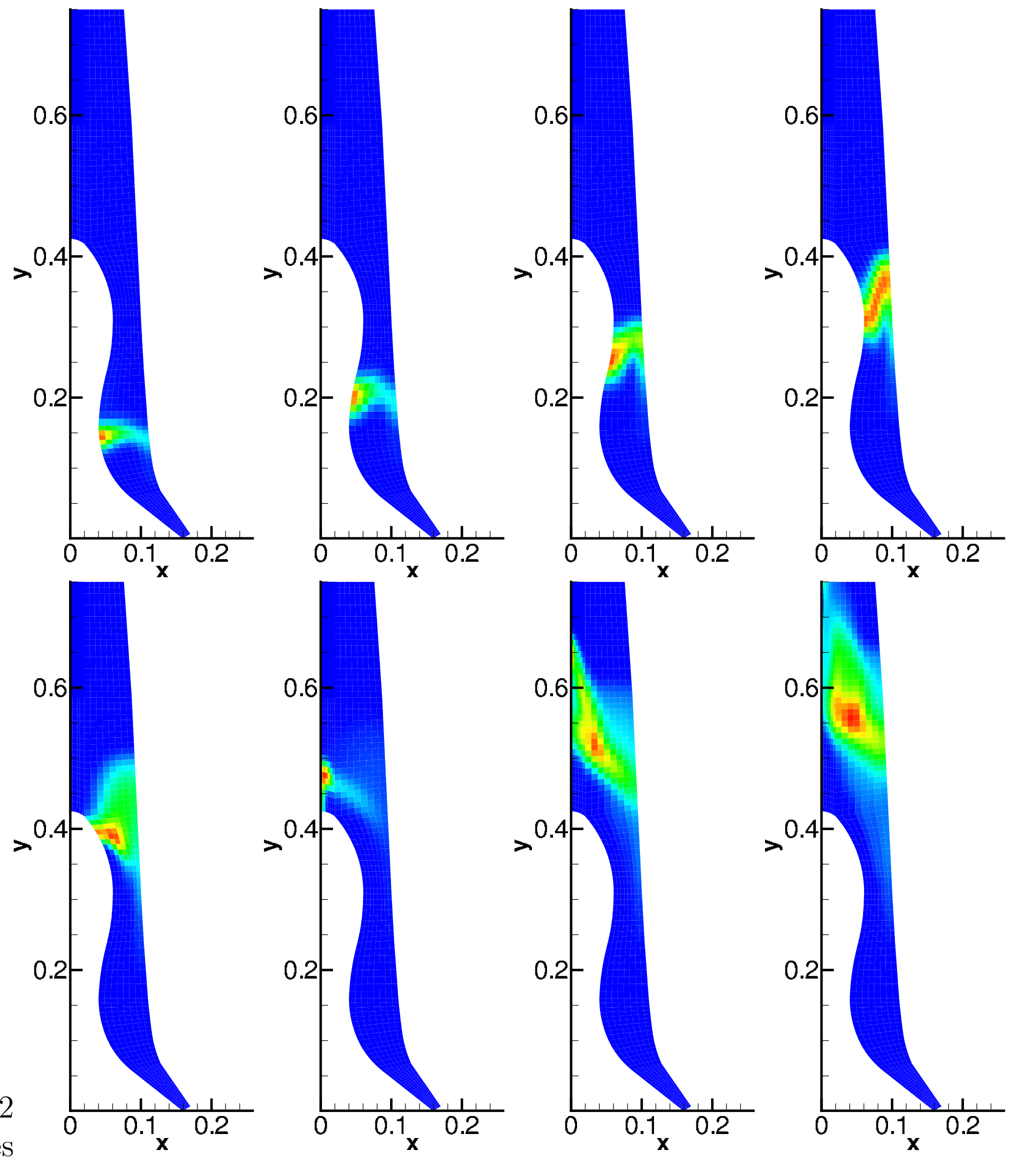

A 90 degree injection angle was originally proposed, but Mach2 modeling showed this needed to be reduced to about 45 degrees to ensure proper armature structure, as illustrated on right.

Plasma Injection is Accomplished Using Pulsed Electrothermal Capillary Discharges

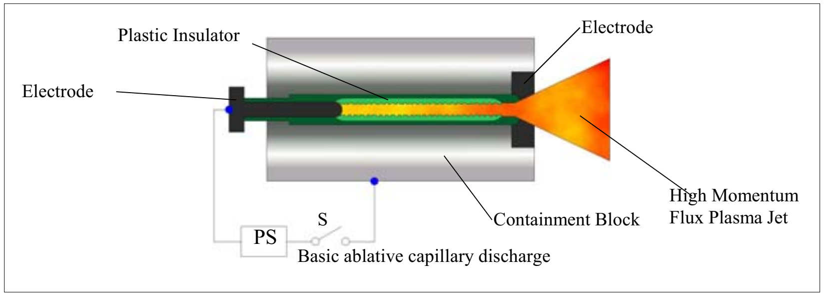

A capillary discharge can ablate large quantities of material off the wall, while controllably generating pressures up to several kilobars and temperatures of many eV. The exiting plasma jet can easily attain 10-30 km/s in vacuum.

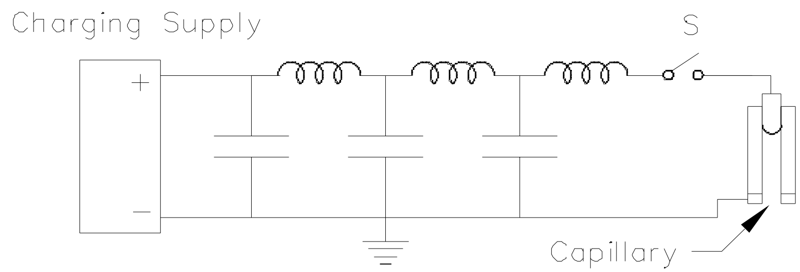

A typical circuit for a single capillary discharge.

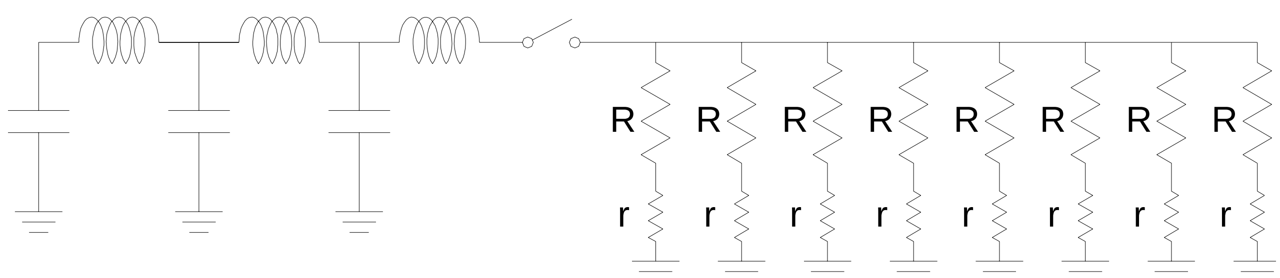

Driving capillaries in parallel requires large ballast resistance R in series with each capillary resistance r to ensure all capillaries will break down and then share current equally and stably.

Plasma Jet Accelerator System for MCX Injection

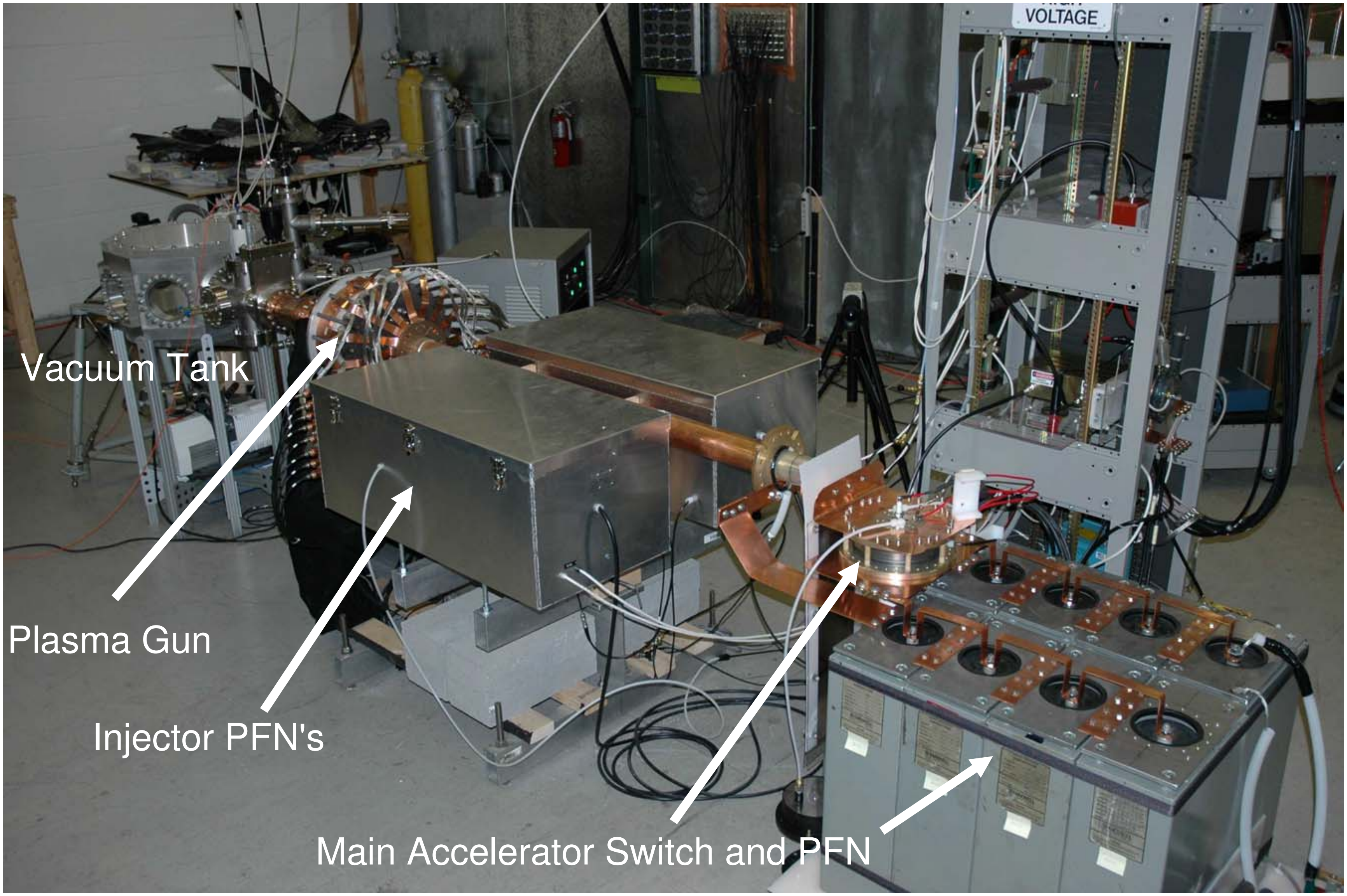

Plasma Jet Internal Structure

Visible Light

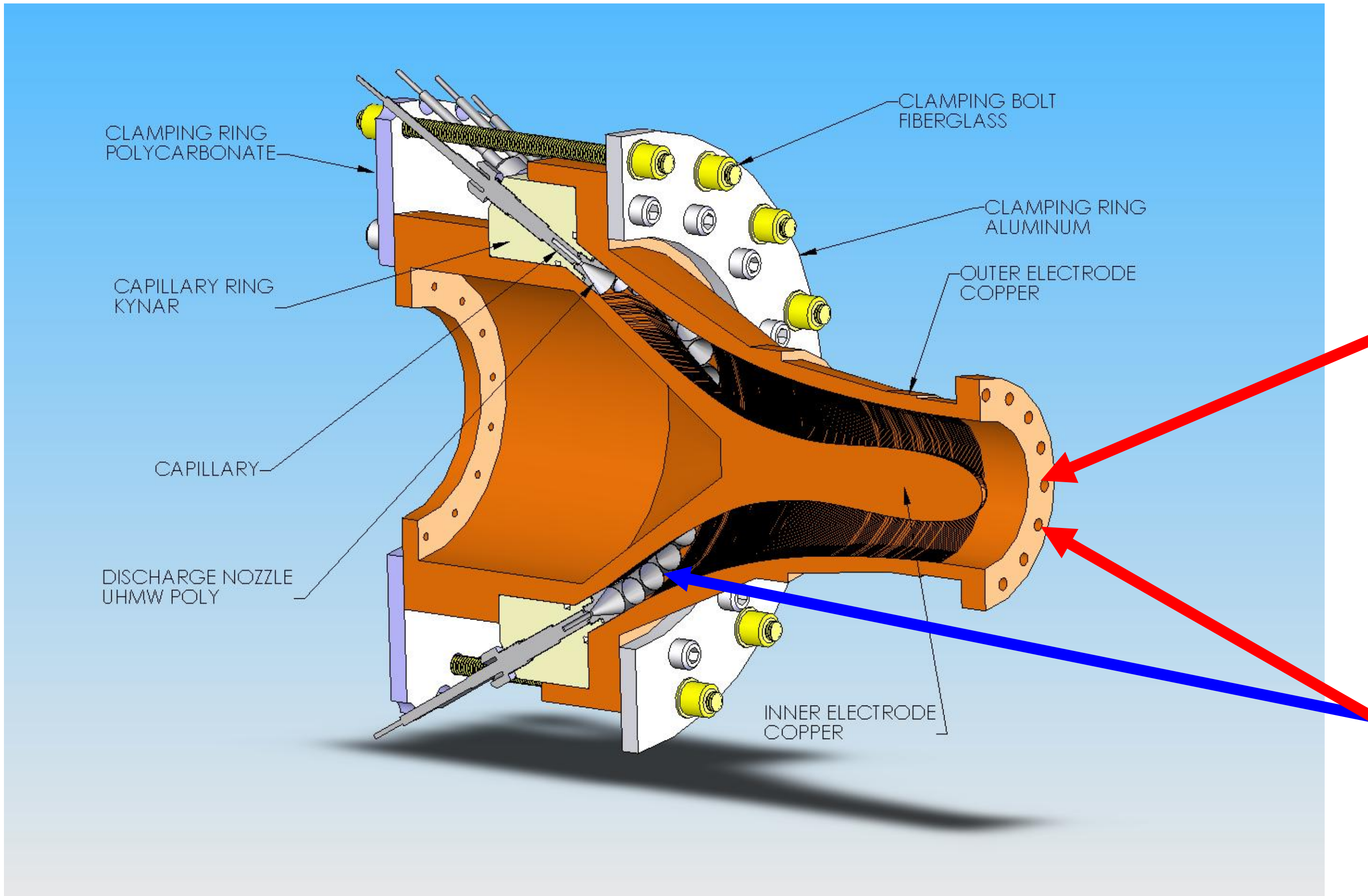

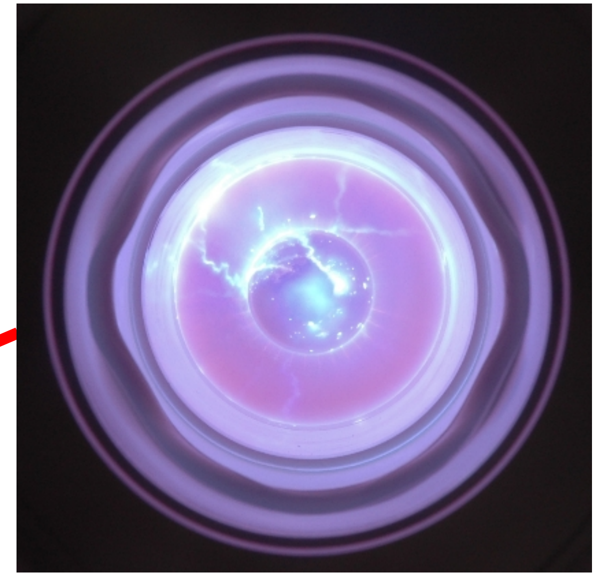

Main Current Pulse

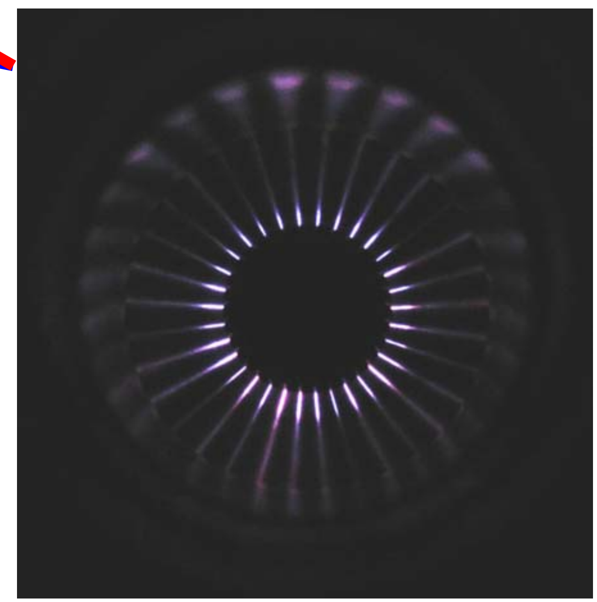

Capillaries Only

Cross-section of shaped main electrodes with 32 capillary discharge injectors.

Photos are end view time integrated exposures.

Capillary Discharge Units in the Main Gun

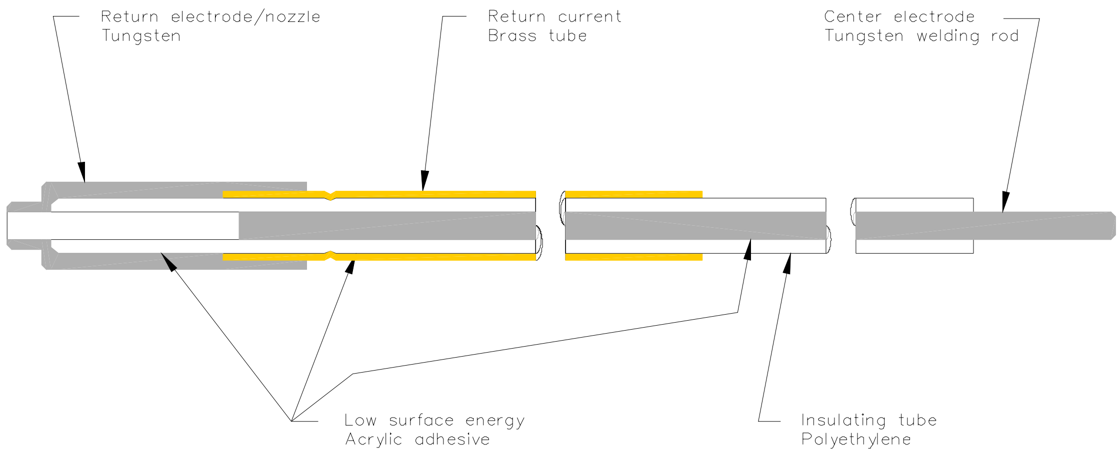

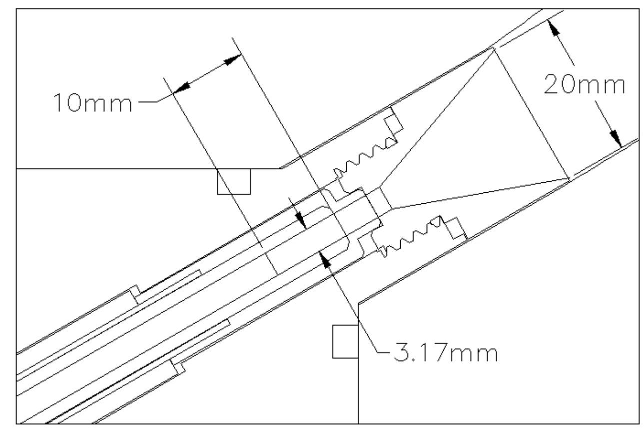

Detailed view of internal structure of capillary used in main accelerator. Except for the tungsten nozzle which requires machining, all components are commerical-off-the-shelf items simply cut to length. Internal vacuum seals are achieved using acrylic adhesives. Mounting details are shown on right.

HV Accelerator Circuit

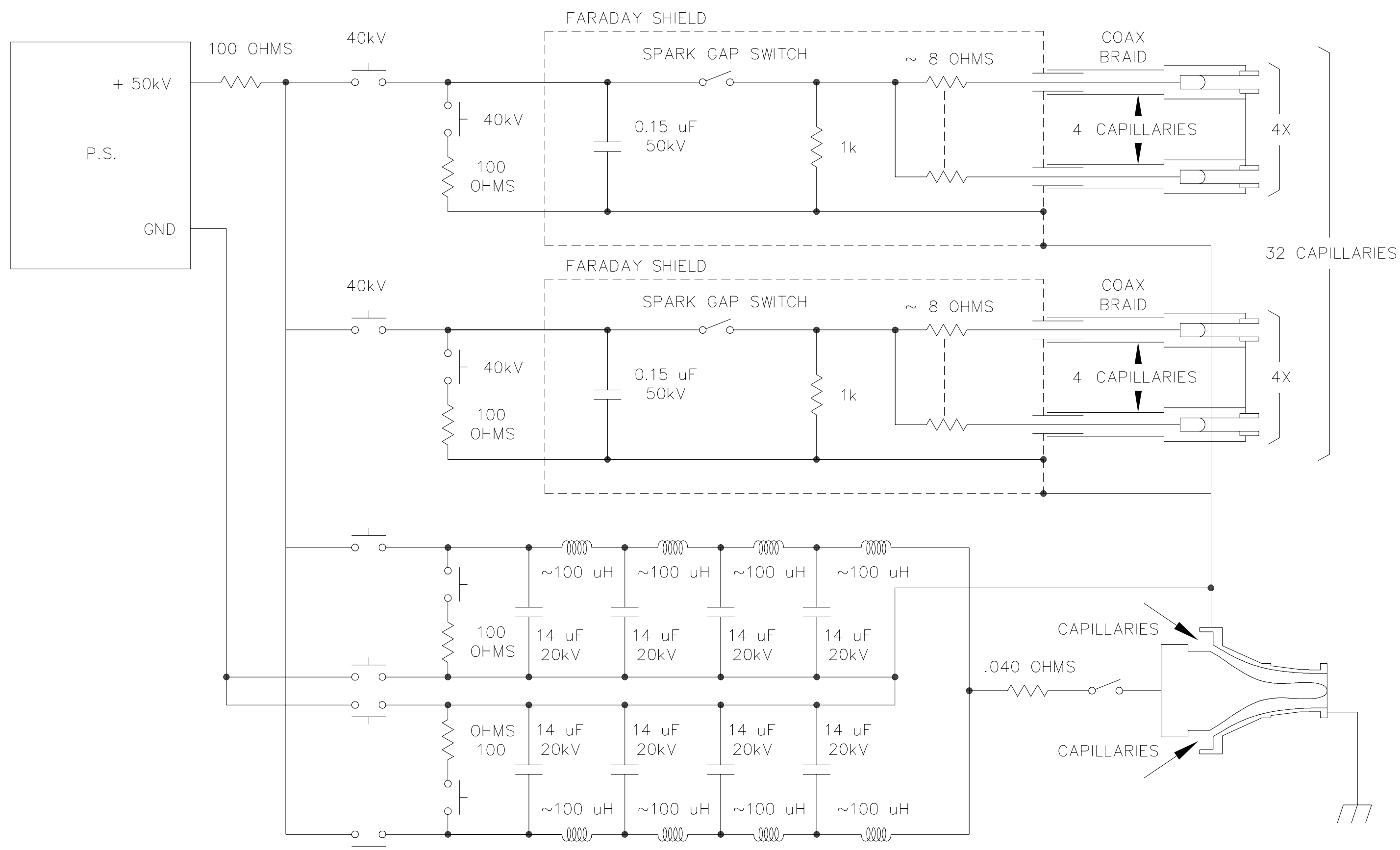

The High Voltage circuit for the capillary injectors utilizes two Titan 40624 sparkgap switches to drive 32 capillary discharges. Each switch drives four 0.15 μF Maxwell capacitors, each of which drives 4 capillaries in parallel with 8 ohms ballast in series with each capillary. The main electrode pfn has recently been upgraded as shown with eight 14 μF, 20 kV Maxwell capacitors arranged in two parallel legs. A 250 kA, 30 kV Beverly Associates spark gap switch Model SG-172C is used to switch voltage onto the rails after a typical 3 μs delay after the capillaries fire. This allows operation at higher voltages than previously attained with hot electrodes.

Gaussian Fits to Spectroscopy Doppler Data

Velocity Range is 50 - 100 km/s

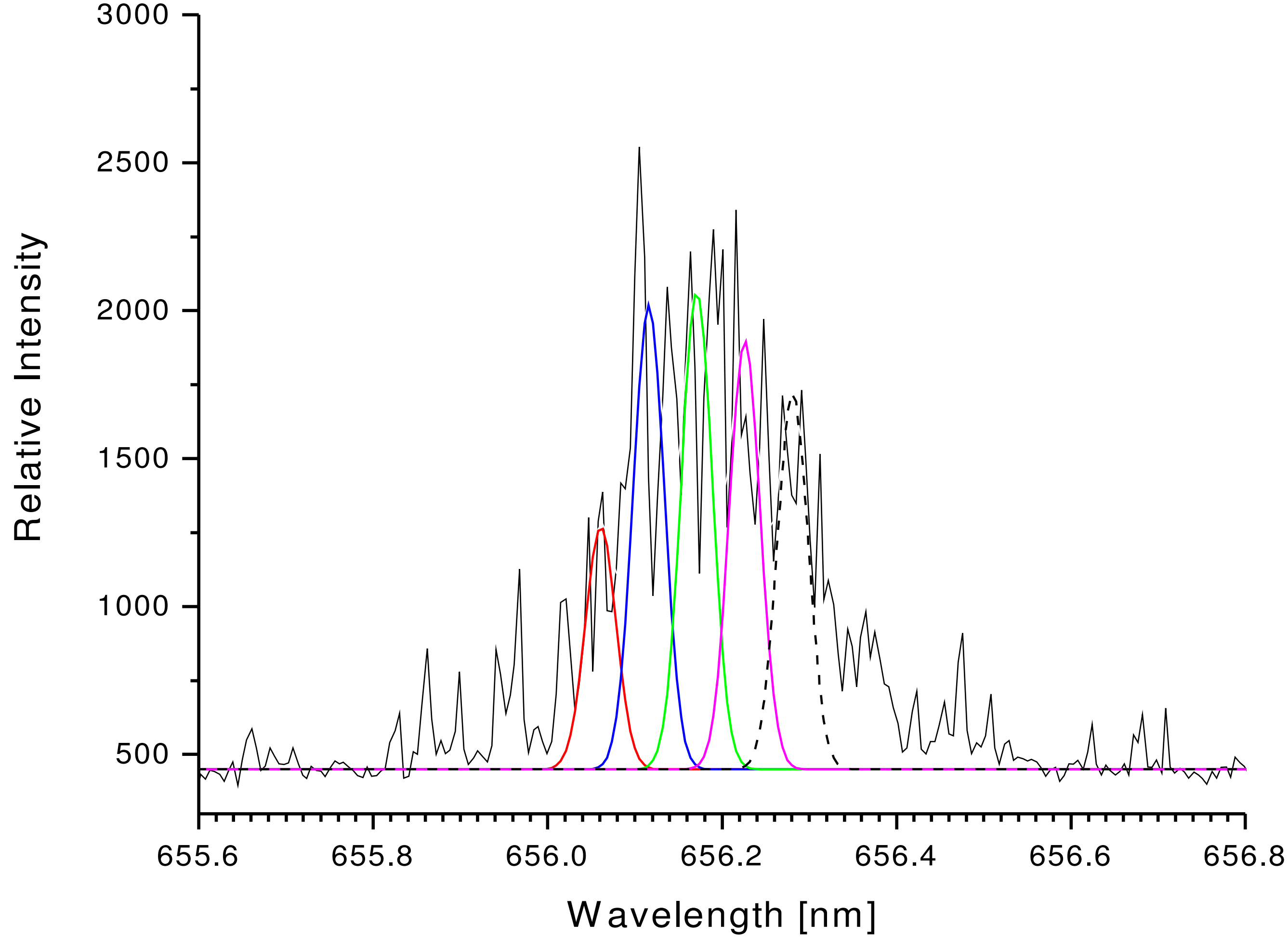

Five Gaussian fit to Doppler shifted H_α line. Fit is obtained by convolving the Gaussians with the known instrumental line profile to obtain a best fit to the data. The Gaussians are centered at wavelengths corresponding to (from right to left) 0 km/s, 24 km/s, 50 km/s, 75 km/s, and 100 km/s.

HyperV Plasma Jet – Mach2 Simulations

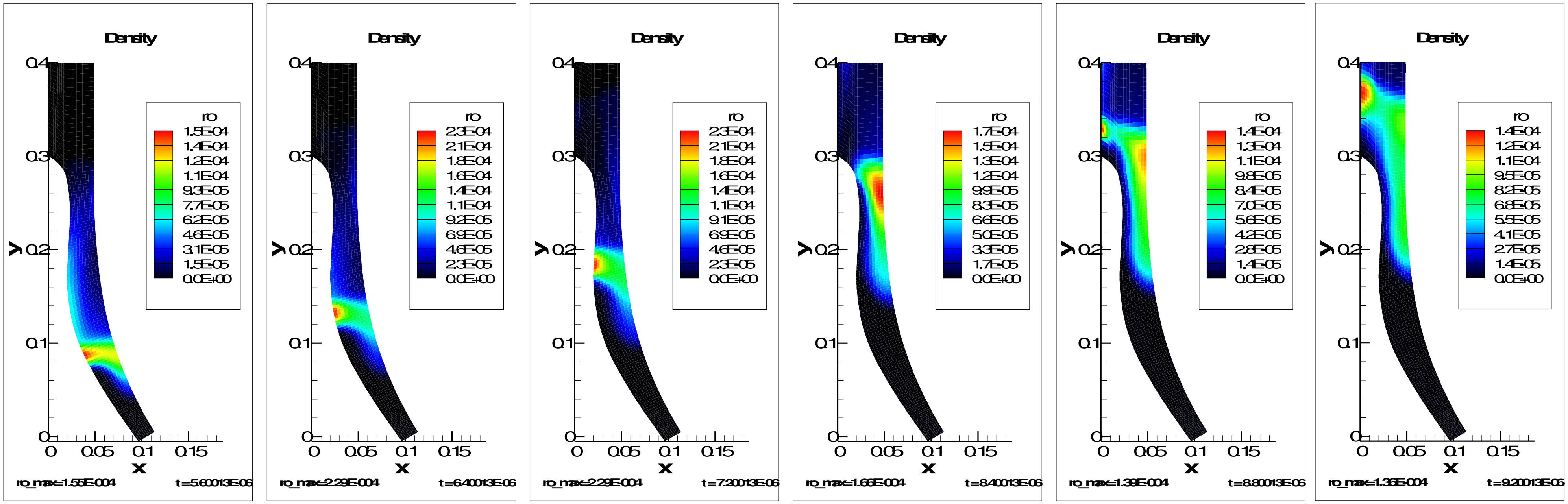

- Momentum and velocity follow rail gun scaling

Case above:

Mass = 87 gm

v_i = 5 km/sec

T_i = 5 eV

I_{max} = 187 kA

v_f = 88 km/sec

T_f = 131 eV

Momentum ~ I^2

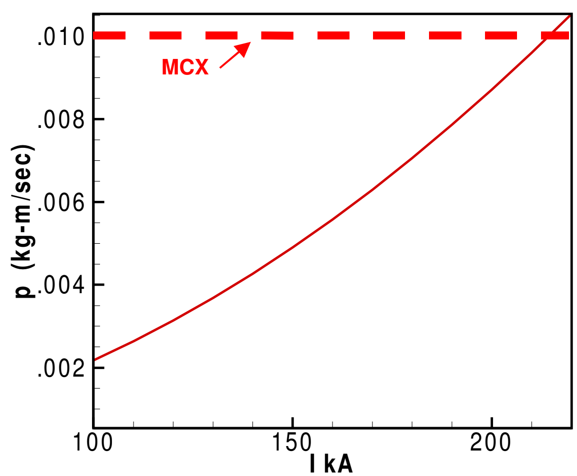

Exit velocity is mass dependent

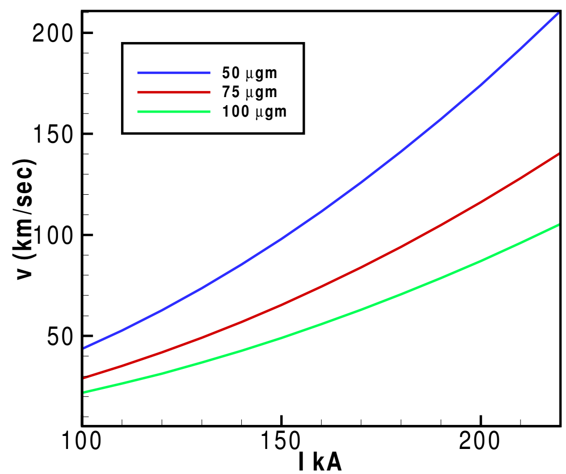

Ballistic Pendulum Tests

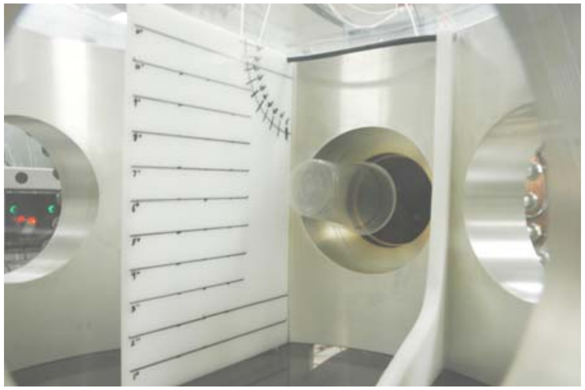

View of ballistic pendulum from angled port in vacuum tank.

The ballistic pendulum is constructed from a polyethylene support stand, using 100 micron tungsten wire, and 3 plastic drinking cups nested inside each other to obtain sufficient mass.

- Total combined cup mass = 12.75 gm
- Recoil velocity $\simeq$ 0.86 m/s
- Plasma velocity from Doppler shift $\simeq$ 70 km/s
- Calculated plasma mass $\simeq$ 157 μg

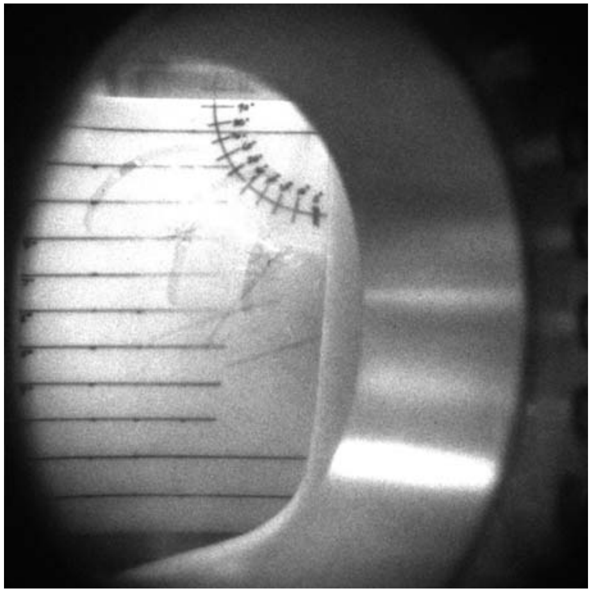

(a) Multi-gate exposure using PI-Max camera. 25 ms delay from main trigger. Five gates at 100 ms apart, 8 μs exposure.

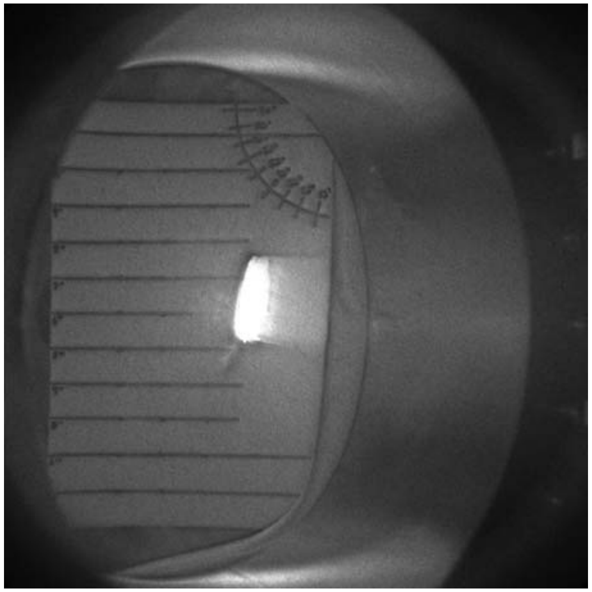

(b) Plasma stagnating on bottom inside of cup. From a PI-Max 50 ns exposure 18.5 μs after main trigger.

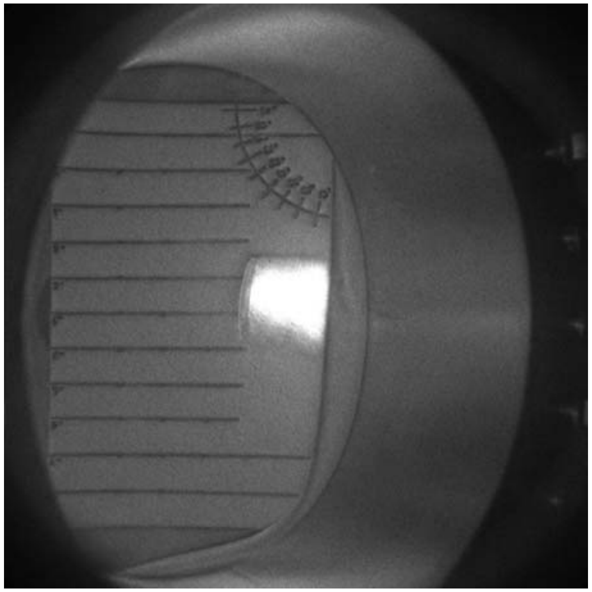

(c) Plasma expanding back to the right after impact at 28.5μs after main trigger.

The TwoPi Injector Test Fixture

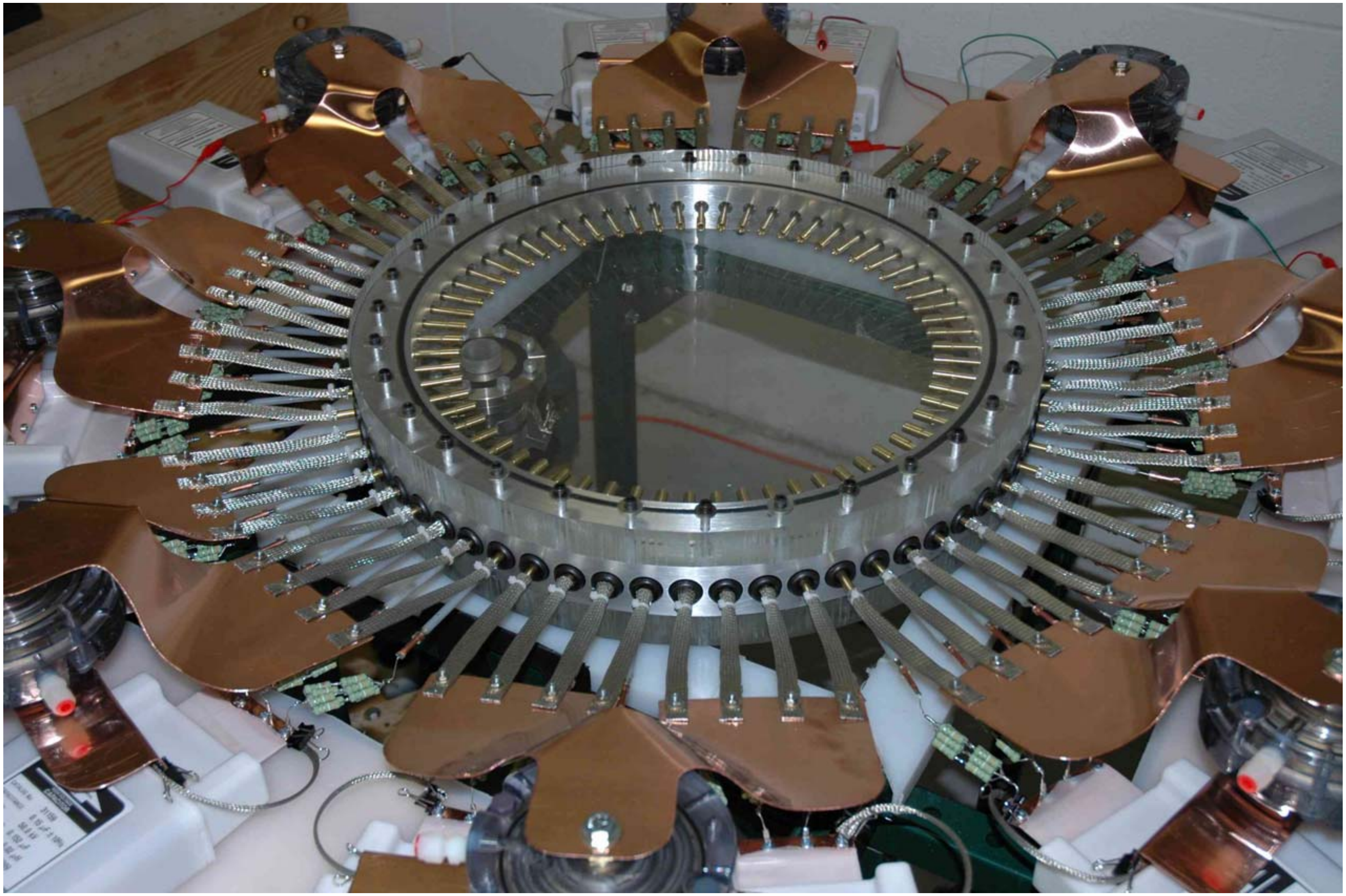

The 24 inch diameter 2π test fixture allows testing of up to 64 capillary jets under a variety of conditions and configurations. The vacuum chamber operates at 0.7 mTorr using a 70 l/s turbopump despite the large number of seals. This photo shows the recently upgraded system with simple RLC HV circuit using a 0.15 μF Maxwell capacitor for every 4 injector units operating in parallel. A ballast resistance of about 1.3 ohms is in series with each capillary providing a (usually) stable and equal distribution of current at charge voltages up to 38 kV. Breakdown reliability suffers below about 28 kV.

Symmetric Jet Merging in the TwoPi Fixture

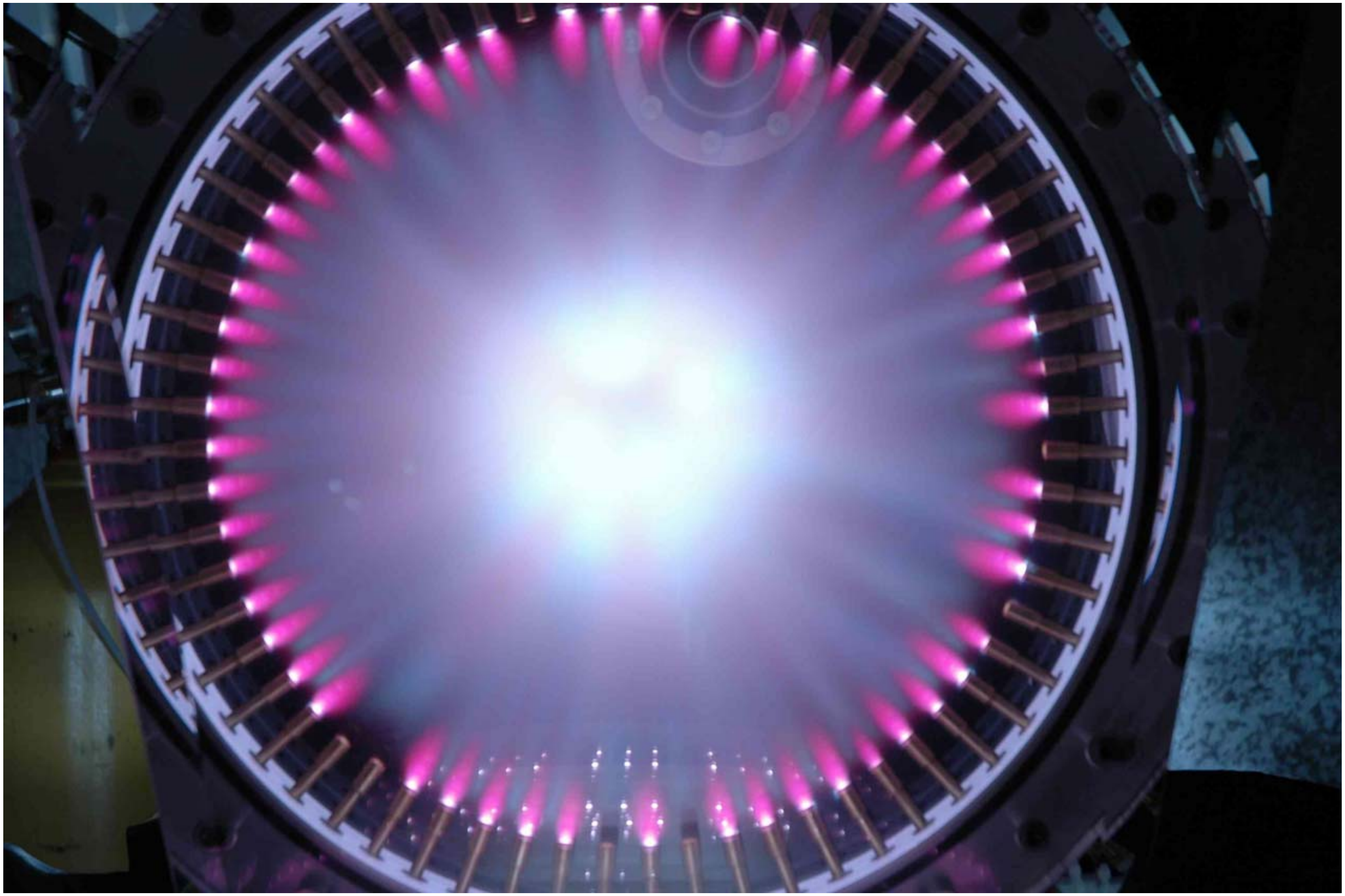

Implosion of almost 64 plasma injector jets. Diameter of aluminum vacuum chamber is about 24 inches.

Ion Implantation Effects on CVD SiC and Carbon-Carbon Velvet

Fusion Technology Institute, University of Wisconsin-Madison

S.J. Zenobia, G.L. Kulcinski, R.F. Radel, R.P. Ashley, D.R. Boris

Materials Irradiation Experiments and the UW-Madison IEC Device

Summary of Presented Experiments

- SRIM calculations have been used to estimate the range of He^+ in CVD silicon carbide (SiC) as well as the range of He^+ and D^+ in carbon-carbon velvet (CCV) and tungsten coated carbon-carbon velvet (CCV/W).
- CVD SiC samples (supplied by ORNL) were irradiated in the UW IEC device to 1×10^{18} and 1×10^{19} He^+/cm^2 at 850 and 950 °C.
- A partially masked SiC sample was irradiated to ~1.5×10^{19} He^+/cm^2 at 950 °C
- CCV and CCV/W samples were irradiated to 1×10^{19} He^+/cm^2 at 1150°C and a CCV sample was irradiated to 1×10^{19} D^+/cm^2
- SEM analysis has been performed to evaluate the surface damage on the CVD SiC, CCV, and CCV/W as functions of temperature and/or fluence.

Schematic of UW -IEC Device

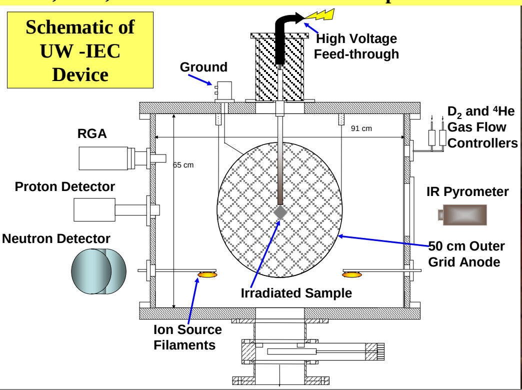

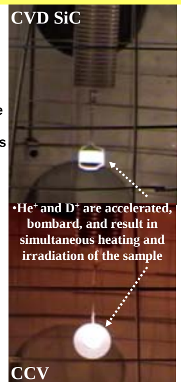

SRIM Range Calculations and Sample Setup

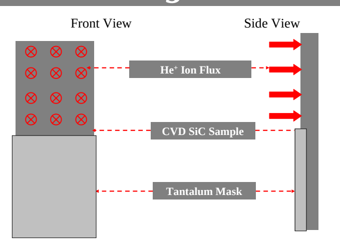

Sample Mount Schematic for masked CVD SiC Sample

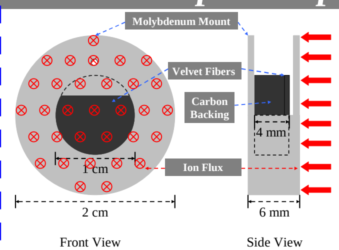

Molybdenum Irradiation Holster for CCV and CCV/W

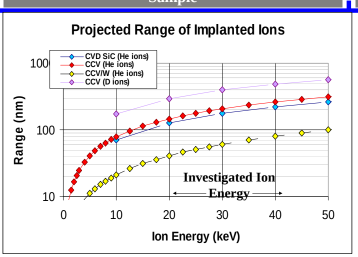

•To the left, ion ranges in CVD SiC, CCV, and CCV/W are shown as a function of the IEC ion energy. Investigated implantation energies are noted

•Helium ion range in the CVD SiC corresponds roughly to the flake thickness resultant from irradiation (a few microns).

•None of the calculated ion ranges correspond to the damage penetration depth observed in the velvet specimens.

He^+ Irradiation of CVD SiC

Irradiated @ 850 °C

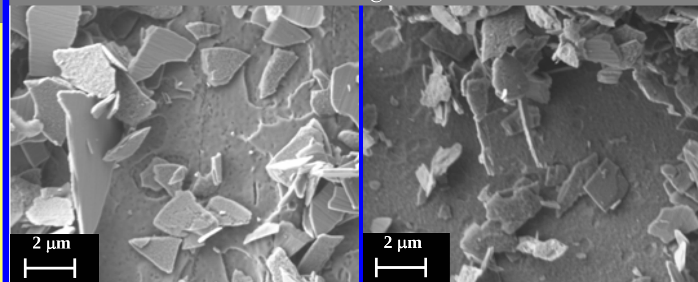

1×10^{18} He^+/cm^2 | 1×10^{19} He^+/cm^2

At 950 °C we notice flaking and pore formation in the 1×10^{18} He^+/cm^2 sample and an increased level of pore formation in the sample irradiated to 1×10^{19} He^+/cm^2

Irradiated @ 950 °C

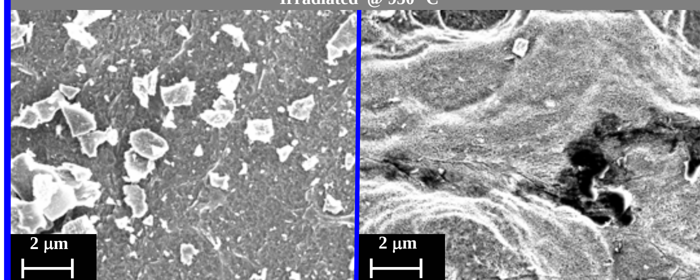

1×10^{18} He^+/cm^2 | 1×10^{19} He^+/cm^2

Once again excessive flaking is evident on both specimens, though the level of pore formation is not as high as the 1×10^{19} He^+/cm^2 and 950 °C specimen. These flakes appear to be approximately several microns in thickness.

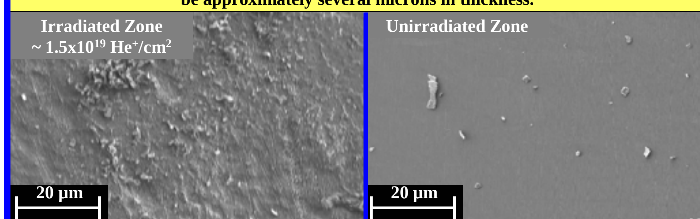

Lack of damage in the unirradiated zone confirms that the damage is due to helium ion fluence. The particles in the unirradiated zone are most likely a post-irradiation artifact.

SiC Conclusions

- Significant changes in SiC surface morphology occur at both 850 and 950 °C and fluences (1×10^{18} He^+/cm^2 to 1×10^{19} He^+/cm^2)
- At constant He^+ fluence, the characteristic damage of the sample is a function of the temperature at which the sample is irradiated
- However, ion fluence - NOT temperature, causes these surface morphology changes

The authors gratefully acknowledge the financial support of the HAPL program at the Naval Research Laboratory.

He^+ and D^+ Irradiation of CCV and CCV/W

Unirradiated Carbon-Carbon Velvet Specimen

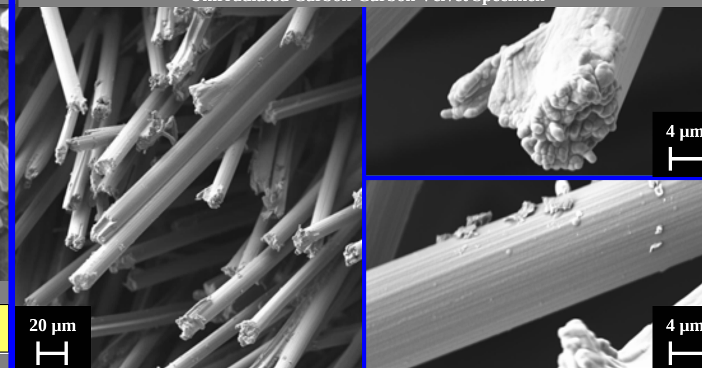

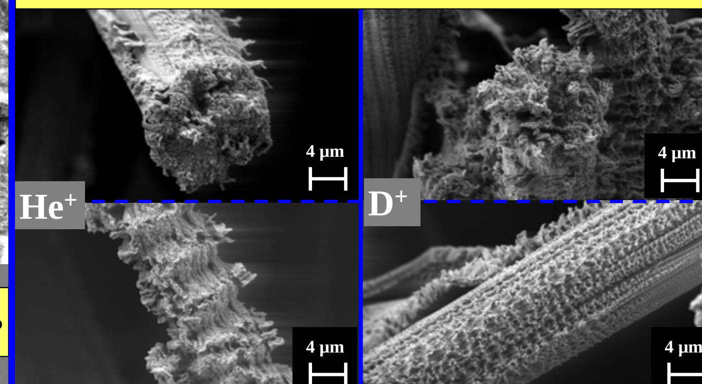

CCV irradiated with He^+ and D^+ to a fluence of 1×10^{19} ions/cm² at ~1150 °C

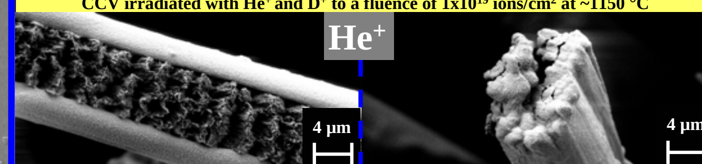

Tungsten-coated carbon-carbon velvet (CCV/W) irradiated with He^+ to a fluence of 1×10^{19} ions/cm² at ~1150 °C

CCV and CCV/W Conclusions

- Both He^+ and D^+ irradiation of carbon-carbon velvet specimens cause fiber shaft corrugation, though He^+ irradiated samples have a more pronounced effect.
- Both He^+ and D^+ irradiation of carbon-carbon velvet specimens causes fiber shaft corrugation, though He^+ irradiated samples have a more pronounced effect
- Some W-coated carbon fiber shafts incur rupturing, in addition to increased W surface roughness after He^+ irradiation